FUEL MOTION IN LOSS-OF-FLOW ACCIDENTS

A THESIS

Presented to

The Faculty of the Division of Graduate Studies

By

Dhunjishaw Lal

In Partial Fulfillment

of the Requirements for the Degree

Doctor of Philosophy

in the School of Nuclear Engineering

Georgia Institute of Technology

October, 1977

FUEL MOTION IN LOSS-OF-FLOW ACCIDENTS

Approved:

Roger W. Carlson, Chairman

J. H. Rust

J. N. Davidson

P. V. Desai

W. Z. Black

Date approved by Chairman Oct. 18, 1977

ACKNOWLEDGMENTS

Through the course of this work, a number of people have contributed to its successful completion. I wish to express my appreciation to all of them.

I owe a debt of gratitude to my advisor, Dr. Roger Carlson, for his constant encouragement and guidance. His support, during the good times and the not-so-good times, has meant a lot to me. I would like to thank the members of my reading committee, Dr. James Rust, Dr. Narl Davidson, Dr. Prateen Desai, Dr. William Black, and Dr. Stephen Demko, for their suggestions and comments. I must also thank Dr. William Ames for his advice on numerical methods.

Project funding was provided by the Energy Research and Development Administration and I appreciate the cooperation of Dr. Harry Alter, Mr. Sam Berk, and Mr. Michael Tanzio. I also thank Dr. Walter Deitrich (Argonne National Laboratory), and Dr. John Travis and Dr. Anthony Amsden (Los Alamos Scientific Laboratory) for their assistance in answering questions and supplying needed information.

The progress of this research was significantly aided by the use of the Civil Engineering computational facility. I am most grateful to Dr. Leroy Emkin for his generosity in allowing me the use of the facility.

My heartfelt thanks go out to the wonderful secretaries, who through the past several months have helped prepare progress reports of this research. Mrs. Florence Bigham, Mrs. Kim Franklin and Mrs.

Lydia Geeslin showed great determination in typing their way through the unmanageable equations. Mrs. Janie Griffith and Mrs. Ruth Salley did a superb job in preparing the final report.

I have benefited from the many fruitful discussions with my fellow students, particularly Shahid Khan and Robert Kim.

I thank my parents for their love and encouragement through the years, and I am beholdent to dear God for all that He has done.

TABLE OF CONTENTS

TABLE OF CONTENTS (continued)

LIST OF ILLUSTRATIONS

LIST OF ILLUSTRATIONS (continued)

LIST OF ILLUSTRATIONS (continued)

LIST OF ILLUSTRATIONS (continued)

LIST OF ILLUSTRATIONS (continued)

LIST OF ILLUSTRATIONS (concluded)

SUMMARY

Fuel motion is studied in both one [axial] and two [radial and axial] dimensions in the pre-disassembly stage of a loss-of-flow accident in a liquid metal fast breeder reactor. The analysis is based on a model channel, consisting of an isolated single fuel pin with cladding and associated subassembly containment structure.

A mathematical model is set up to describe the motion of the seven materials of interest: liquid fuel, liquid steel, solid fuel, solid steel, vapor fuel, vapor steel and gaseous fission products. The multi-field approach is used, avoiding the usual lumping of multiple fluids into a single fluid with average properties. The materials are treated as distinct fields, each with its own equations of density, momentum and energy transport. The various fields are linked together via binary exchange functions for mass, momentum and energy transfer. These exchange functions can be manipulated to give any desired degree of linkage between two fields.

The cylindrical region is zoned into a mesh of fixed cells, and the differential equations are approximated by finite difference representations in these cells. The implicitly formulated difference expressions for density and momentum transport are solved iteratively for the density, velocity and pressure distributions. The explicit formulation for energy transport then permits the direct calculation of the internal energy corresponding to these distributions.

This numerical scheme has been programmed into the PLOFA computer code, designed for the efficient solution of multi-field confined flow problems. Results for a loss-of-flow accident are presented for single and multi-dimensional calculations. It is observed that an axial analysis is insufficient to predict the phenomena occurring in the initiation phase. The addition of a radial dimension is found to be vitally necessary for realistic accident modeling.

CHAPTER I

INTRODUCTION

1.1 Objective

Never before has the need for energy been as great as it is today, and with each passing day the world community becomes increasingly aware that all sources of power are finite. The breeder reactor, long held to be a potential cornerstone of U. S. energy supply, has now been downgraded in the scheme of energy priorities; but to abandon such a viable energy source without further examination of its drawbacks and seeking possible solutions, appears wasteful. It is in keeping with the spirit of scientific inquiry about the safety of the breeder, that this research was undertaken to study the dynamics of fuel motion, contributing to the continuing refinement of the overall safety effort.

The main factors affecting the reactivity changes in a liquid metal fast breeder reactor (LMFBR) are control rod motion, the doppler effect in U^{238}, the voiding and possible re-entry of sodium coolant, and fuel motion. Fuel motion influences reactivity in several ways. The most obvious is the effect of dynamic core geometry changes while the fuel is mobile: any configuration that leads to a more dense fuel distribution adds reactivity. The simplest case of fuel motion in an accident situation is slumping under the action of gravitational forces, this occurring usually in fresh fuel. In general it is more energetic due to built up fission gas pressure, or fuel or clad vapor pressure.

Fuel motion substantially affects the future course of an accident. A suitable fuel motion model, exchanging information with a concurrent kinetics model, is thus vitally important to the prediction of the accident sequence in any safety analysis. Prior computer analysis of fuel motion has been one dimensional (axial) in nature. This is appropriate only for a limited version of fresh fuel slumping under gravity. The radial flux distribution would need to be fairly constant for the assumption of simultaneous radial melting at a given axial location. In the usual reactor operational situation there is a distinctly non-uniform radial temperature distribution in the fuel. This might well cause centerline melting while substantial portions of the remainder of the fuel are still solid. One dimensional modeling is unable to treat this commonplace situation. In addition, the presence of vapors and fission gas cause radial velocity distributions, and attempting to neglect this only leads to an erroneous picture of the system's fluid dynamics.

In view of the need for a more accurate description of fuel motion, the objective of this research is to provide a means for the two dimensional (radial and axial) fluid dynamics analysis of fuel motion in an LMFBR during the pre-disassembly phase of a loss-of-flow accident (LOFA), and to compare the results of this two dimensional analysis with those which might be obtained by using only axial calculations. The accident modeling offers an improvement over prior one dimensional research, not only by the addition of a new dimension, but also by a multi-field treatment it avoids the usual lumping of multiple fluids into a single fluid with average properties.

1.2 Background

It is difficult to find any large-scale industrial operation which can match the excellent safety record of the nuclear power industry. This form of energy production has, on the one hand, the potential of supplying a large part of today's energy requirements, and on the other, the potential of causing "significant" environmental damage and loss of human life. But the term "significant loss of human life" applied to the nuclear power industry, refers to a mortality rate far below the normal rates for other fatalities. For example, the Rasmussen Report[1] predicts that a fairly serious accident might lead to a total of about 50,000 fatalities from latent cancers over a thirty year period. These 50,000 deaths in an accident which might occur once in a million reactor years are small compared to the more than 300,000 annual fatalities in the U. S. from cancers due to other causes. On an average annual basis, the nuclear figure is several orders of magnitude lower. In a journal article[2] discussing common objections to nuclear power, the Nobel laureate, Hans Bethe, estimates the average risk for the entire U. S. population as two fatalities per year from all types of reactor accidents.

Low mortality rates, of course, do not tell the entire story. The public's concern about nuclear safety has a geniune basis in some instances. Responding to this public concern, governmental regulatory commission pressure, and its own firm belief that risks to the general public must be kept as low as possible and much below those associated with other industries, the nuclear power industry has placed, and will continue to place, safety as one of the most important factors in its

plans. The U. S. now spends about seventy million dollars annually on improving reactor safety. Proper design and construction is emphasized in order to produce an inherently safe and reliable reactor, and protection systems are provided to ensure that any abnormal condition can be detected and stopped or safely accommodated.

In spite of designing against any anticipated situation that might pose a threat to public safety, it is possible that extremely unlikely or unforeseen circumstances arise that could endanger the public. Safety analysts must consider what special features would be required to provide an additional margin of public protection in such cases. Hence, it is necessary to study the damage that might be caused by a variety of extremely unlikely situations.

One remote possibility is the hypothetical core disruptive accident (HCDA), so called because it is not a real accident, but can be hypothesized as occurring with some minute probability. The mechanistic approach is used in the study of such an accident, i.e. the accident sequence is analyzed beginning with some initiating event and proceeding through to a conclusion using a step-by-step cause and effect relationship. The initiating event is a postulated failure of some part of the power plant's protection system.

Three[3] types of accidents, dealing with a wide range of consequences, have received major attention. In the first of these, the transient overpower accident (TOP), the reactor fails to scram when reactivity is added at a fixed rate which is chosen to represent specific phenomena or faults that could contribute positive reactivity. The reactivity addition rate might also be selected for evaluating damage by

some unforeseen initiating event. The second type of accident, the unprotected loss-of-flow accident (LOFA) is initiated by a loss of power of the coolant pumps. The resulting flow coastdown, coupled with a failure of the plant's protective system to shut the reactor, develops into an accident situation. Yet another type of accident is that which might be caused by the propagation of local fault conditions from fuel-pin to fuel-pin or subassembly to subassembly.

The accident sequence can be analyzed in four major stages to allow for the different techniques necessary to study the changing reactor conditions: initiation, disassembly, damage evaluation and post-accident heat removal. The accident initiation phase deals with core neutronics and thermal behavior up to the point of loss of subassembly integrity. The prompt critical excursion that is induced at this point leads to the disassembly stage, in which the rapid heating and vaporization of the fuel produce high pressures that disassemble the core. The potential damage the excursion can do to the system is studied in the damage evaluation phase by calculating the rate at which thermal energy released in the transient is converted to work, this work being in the form of expansion of the core materials or the vaporization and expansion of sodium coolant interacting with these materials. The final stage of the accident analysis involves a study of the long term decay heat removal from the fuel, to determine a terminal configuration which can be permanently cooled.

Proper analysis of the initiation phase is important in assessing later stage of the accident. The analysis treats phenomena such as transient thermal-hydraulics, fuel pin mechanics and failure, and

cladding and fuel motion. A typical sequence[3] in the accident initiation phase, taking the example of a LOFA without scram for a FFTF (Fast Flux Test Facility) type of reactor, begins with a flow coastdown followed by boiling of the liquid sodium coolant, cladding dryout about a second later, cladding melting and motion in another two or three seconds, and finally fuel melting and motion in about two more seconds.

The reactor power strongly influences the timing of events after boiling initiation. At boiling inception the reactor might operate around 65-75% of its full power, but cladding motion and relocation out of the middle core region could add a dollar or two of reactivity and raise the power (to perhaps twice the nominal power) by the time fuel motion begins. As the fuel becomes more mobile, slumping in the hottest channels might lead to an initial power burst peaking at between five and thirty times the nominal operating power. These initial high intensity bursts terminate very quickly by a combination of several strong negative reactivity effects like doppler and axial expansion feedbacks, and fuel dispersal caused by fission gas and fuel/steel vapor pressures. The rapid energy generation in the burst (typically of the order of one full power-second) creates a domino effect, initiating fuel motion in channels which are near melting. Fuel dispersal eventually causes subassembly rupture, when sufficiently high pressures and temperatures are reached, leading into the transition or disassembly stage of the accident.

The reactivity in the transient accident initiation phase is affected by the changing configurations of the density, pressure, velocity and temperature distributions of the fuel and the material associated with it. The core configuration of an LMFBR is such that redistribution

of the fuel to a more dense state results in reactivity addition. These reactivity changes, in turn, govern the fuel motion, and hence, the future course of the accident. A suitable fuel motion model, exchanging information with a concurrent kinetics model, is thus vitally necessary to the prediction of the accident sequence in any LOFA analysis.

The importance of fuel motion in accident analysis has caused it to receive much attention in recent years. Prominent in this area are the large scale experimental programs that have been undertaken by the Argonne National Laboratory[4,5] and the Hanford Engineering Development Laboratory.[6]

Fuel melting laboratory studies at HEDL were conducted to describe the response to rapid heating of both unirradiated UO_2 and mixed oxide fuel irradiated in EBR-II (Experimental Breeder Reactor). Thermal Transients were applied to fuel samples in a resistively heated tungsten tube. The system was designed to allow for continuous gamma radiography of the sample, as well as pressure and temperature measurements. The research has centered on fuel material behavior and the determination of input parameters needed for fuel motion models.

The Fuel Dynamics Program at ANL has included extensive tests on fresh and irradiated Fast Test Reactor (FTR) fuel in its TREAT System. Topics of prime importance include prefailure fuel movement, cladding failure threshold, the nature and location of initial and secondary cladding failure, coolant dynamics, fuel-coolant interactions, and post-failure fuel motion. The tests have provided valuable and formerly unavailable data for testing and improving accident analysis models.

To compliment the experimental programs, several computer codes have

been written to analyze reactor accidents. Well known in the United States is the SAS LMFBR Accident Analysis Code System[7] (Current version SAS3A) developed at the Argonne National Laboratory. This code includes models which allow an integral treatment of both transient overpower and loss-of-flow unprotected accident sequences through fuel pin disruption and up to the point of subassembly disruption.

Fuel motion in SAS is modeled by the SLUMPY[8] Module. The fuel motion is initiated following the satisfaction of three criteria.

(i) channel sodium voiding has occurred

(ii) the cladding has melted, and

(iii) a specified fuel temperature is exceeded at a specified radial node at any axial position or a specified fraction of molten fuel is reached at any axial node.

The voided channel volume of the initial axial nodes which meet fuel slumping requirements are assumed filled by radial expansion due to the pressure of retained fission or fill gas in the fuel or any fission gas in a central void. The fuel motion analysis considers three regions: a middle slumped region, an upper falling segment, and a lower stationary segment. The middle slumped region moves according to area-dependent one dimensional (axial) compressible Lagrangian hydrodynamics. As more fuel melts, SLUMPY calculations include the new nodes using conservation of mass, momentum and energy.

In view of the importance of fuel geometry on reactivity in a Fast Reactor System, it is necessary to include the reality of radial fuel motion. The research detailed here studies two dimensional fuel motion in the pre-disassembly stage of a loss-of-flow accident. This allows

more realistic hydrodynamic modeling by eliminating the need for the radial uniformity that is inherent in a one dimensional axial calculation. By virtue of its two dimensional nature, the new modeling handles situations that cannot be modeled in a one dimensional case. These include fuel motion within a strong clad, and partial melting of fuel above a usual "one dimensional slumped region." In addition, it yields useful field variable distributions such as the pressure distribution in the growing molten region that begins to develop around the central axis of the fuel pin in the early stages of the transient. This pressure distribution can be used to calculate the stresses acting on the surrounding solid shell, and thus provide data for the formulation of a mechanical criterion in addition to the present solely thermal criterion used in initiating motion in one dimensional fuel motion codes. This improved picture of fuel relocation paves the way for a more accurate spatial reactivity calculation, leading to increased confidence in the accident analysis.

1.3 Research Overview

This research analyzes the fluid dynamics in the pre-disassembly stage of a loss-of-flow accident, paving the way for improved spatial reactivity calculations, thus enhancing the development of overall safety codes. The fuel motion analysis is based on model channel consisting of an isolated single fuel pin with cladding and associated subassembly containment structure. It is assumed that a calculation performed on this single pin is representative of all pins in the entire subassembly. The core of an LMFBR can be mocked up by a number of these channels, with

each channel representing one or more subassemblies with similar power, flow and irradiation conditions. Thus a multi-channel time, position and temperature dependent representation of the accident sequence is possible, with inter-channel non-coherence. The accident can be analyzed up to the point of channel disruption, when a switch to a disassembly code must be made.

Equations of motion and energy transfer have to be formulated to describe the material motion in a channel. The formulation of these mathematical equations is entirely dependent on the flow model. This flow model could be simplified to consist merely of solid and liquid regions, where the liquid region is assumed to be a single representative homogeneous fluid. This single liquid concept considerably simplifies the solution, but is a far cry from the actual phenomenon. It must be realized that in the course of an accident, the two main materials of interest (fuel and steel) could be in a solid, liquid or vapor form, while the third material (fission products) is essentially gaseous. These different phases and components exist in various proportions and at different temperatures and pressures throughout the channel. The assumption of average properties thus results in a considerable loss of information.

On the other hand, the various phases and components could be treated as distinct materials, each with its own density, velocity, pressure and internal energy. Proper boundary conditions could then be applied to determine the change in the field variables at an interface. This method, while aligning itself with the real situation, would be perhaps impossible to solve because of the substantial mixing of the phases

and components in the entire channel.

A compromise needs to be reached between the single fluid concept and the entirely distinct fluids method. It is important to preserve component and phase distinction, but the impracticability of applying boundary conditions at interfaces must be realized. Accordingly, distinction between the various materials is allowed, but the interaction between them is treated via exchange functions. These exchange functions are based on the interaction between an essentially discrete medium placed in a continuous medium. The flexibility afforded by these exchange functions permits manipulation to achieve any desired degree of linkage between two materials. The material interface positions cannot be described exactly, but the proportions of the various materials in any region are known, as are the distinct field variables.

The seven materials (referred to as fields in the discussion) in the channel are lqiuid fuel, liquid steel, solid fuel, solid steel, vapor fuel, vapor steel and gaseous fission products. The equations of motion and energy transfer for these distinct fields are discussed in the next chapter, along with the forms of the mass, momentum and energy exchange functions.

The mathematical model is far too complex to yield a direct analytical solution; meaningful results can only be achieved by numerical methods. A numerical scheme must address itself to the problems of choosing a suitable mesh to zone the region of interest, locating the field variables in this mesh, approximating the differential equations of motion and energy transport by finite difference equations with the desired accuracy, analyzing the stability of the difference equations, and formulating an iterative scheme to solve the difference equations. The numerical scheme chosen

follows the multi-field approach of Harlow and Amsden,[9,10] based on an extension of the implicit continuous fluid, Eulerian (ICE) technique.[11]

The cylindrical region is zoned into a mesh of fixed cells, and the finite difference approximations of the equations of density and momentum transport are iteratively solved in each cell by an implicit treatment of velocity and pressure. The energy equation is then solved explicitly. Appropriate boundary conditions are applied at container boundaries and certain material interfaces, such as between a substantial solid region and a liquid or a vapor region. Details of the numerical scheme are presented in Chapter III.

This numerical scheme has been programmed for use on the CDC Cyber 70/Model 74 available at the Georgia Institute of Technology. The program, written in FORTRAN 4 and named PLOFA, is designed for the efficient solution of multi-field confined flow problems. A description of PLOFA along with results for a rather severe accident initiation phase appear in Chapter IV.

Conclusions are presented in Chapter V, along with recommendations for future refinement and development of PLOFA.

CHAPTER II

FUEL MOTION MODEL

The problem of interest is the modeling of fuel motion within a cylindrical channel consisting of an isolated single fuel pin with cladding and the associated subassembly containment structure. In the course of a LOFA, the nuclear fuel and steel cladding could be in a solid, liquid or vapor phase, while the fission products are assumed always to be in a gaseous form. One is thus faced with an unsteady, multi-phase, multi-component, two dimensional, confined flow problem in the presence of nuclear reactions.

The flow analysis of this complex mixture can be approached in several different ways, depending on the degree of simplification desired. Associated with each simplifying assumption there is naturally a loss of reality from the actual phenomenon. This model, while ensuring a satisfactory solution in a reasonable amount of time, dispenses with the need for complete homogeneity in the flow field, thus avoiding the necessity of the average densities, velocities and temperatures that are often used in multi-component flows.

The analysis follows the multi-field approach of Harlow and Amsden,[9,10] at Los Alamos. This multi-field approach is an extension of the implicit, continuous fluid, Eulerian (ICE) technique,[11] which by an implicit treatment of the pressure in the numerical scheme, allows for the analysis of flow speeds ranging from Mach numbers of zero (the

incompressible limit) to infinity (the hypersonic limit).

The seven distinct fields in the problem are:

	Field	Phase	Component	Type of Material
1.	liquid fuel	liquid	fuel	almost incompressible
2.	liquid steel	liquid	steel	almost incompressible
3.	vapor fuel	vapor	fuel	compressible
4.	vapor steel	vapor	steel	compressible
5.	fission gas	vapor	gaseous fission products	compressible
6.	solid fuel	solid	fuel	incompressible
7.	solid steel	solid	steel	incompressible

Each field is characterized by its own equations of mass, momentum and energy transport. An equation of state is also needed to relate the density to the internal energy and the pressure (if applicable). For the totally compressible vapor fields, density is affected by both the internal energy and the pressure. On the other hand, the density of a less compressible liquid field is dominated mostly by its internal energy, while the density of a solid field is assumed to be independent of the pressure and is affected only by temperature changes.

The presence of multiple fields is accounted for by equilibrating the pressures of the compressible materials, and linking all fields by mass, momentum and energy exchange functions. Boundary conditions in the usual sense are not applied at the interfaces between different fields, because the high degree of interpenetration and mixing in this confined flow problem makes it impossible in practice to keep track of the material interfaces. A Lagrangian approach is better suited to handle

interfaces, but keeping the materials distinct in this complex mixture would require a high degree of resolution and introduce substantial rezoning errors.

An Eulerian mesh of fixed cells is chosen, and boundary conditions applied at the container boundaries, and at the interfaces between a substantial solid region and a liquid or a vapor region. All other interfacing is done via the exchange functions. These binary exchange functions are based on a discrete field in an essentially continuous material. There is thus some sacrifice of the continuum assumption on which the equations of motion are based. However, the flexibility afforded by treating the various materials as distinct fields partially offsets this lack of resolution. In addition, the exchange functions can be manipulated to give whatever degree of linkage is desired between any two fields.

2.1 Fundamental Equations

Each field has density, momentum and internal energy transport equations which can be described in vector form as

$$\frac{\partial \rho}{\partial t} + \nabla\cdot(\rho \underset{\sim}{u}) = S \tag{1}$$

$$\frac{\partial \rho \underset{\sim}{u}}{\partial t} + \nabla\cdot(\rho \underset{\sim}{u}\underset{\sim}{u}) = N - \alpha\nabla p + \nabla\cdot\underset{\sim}{\tau} + \rho \underset{\sim}{g} + D(\bar{\underset{\sim}{u}} - \underset{\sim}{u}) \tag{2}$$

$$\frac{\partial \rho I}{\partial t} + \nabla\cdot(\rho \underset{\sim}{u} I) = - p\nabla\cdot(\alpha \underset{\sim}{u}) + Q + H(\bar{T} - T) + \nabla\cdot(k\alpha\nabla T)$$

$$+ \mu\Phi + \Lambda \tag{3}$$

The equation of state, describing the microscopic properties of each field is

$$p = f(\rho', I). \tag{4}$$

The terms in these equations are:

ρ = macroscopic density

$= \alpha \rho'$

ρ' = microscopic density

α = volume fraction of that field

$\underset{\sim}{u}$ = velocity vector

$\bar{\underset{\sim}{u}}$ = representative velocity vector for other fields

p = pressure

$\underset{\sim}{g}$ = acceleration due to gravity

I = specific internal energy

k = thermal conductivity (function of temperature)

T = temperature

$\bar{T}$ = representative temperature of other fields

μ = viscosity (function of temperature).

Included in the transport equations are various source and exchange functions.

1. **S is a source function for the density transport equation, It generally arises from phase transitions, but can also arise (as in the case of the fission gas) from nuclear reactions and release from solid fuel.**
2. $\Delta \cdot \underset{\sim}{\tau}$ is the rate of momentum gain by viscous transfer.
3. **N is a source function for the momentum transport equation, arising because of the S function in the density equation.**

4. D is a drag function to account for the drag between various fields.
5. Q is a source function for the energy transport equation, arising from such processes as phase transitions and nuclear reactions.
6. H is an exchange function to the mean exchange temperature for a field.
7. Δ is a dissipative term. It represents the rate of internal energy production as a result of momentum exchange.
8. $\mu\Phi$ is the heat term due to viscous dissipation.

It may be noted here that the density and momentum transport equations are in conservative form, while the equation for the transport of specific internal energy is not. The energy equation could have been made conservative by transporting the total energy, rather than the specific internal energy. But, in fully conservative form, slight fluctuations of velocity at high speeds could result in large temperature fluctuations. This does not occur in the internal energy formulation, compensating for the slight non-conservation of energy.

These fundamental equations of motion and energy transport now need to be considered in detail for a particular field.

2.2 Density Transport Equation

$$\frac{\partial \rho}{\partial t} + \frac{1}{r}\frac{\partial}{\partial r}(\rho u r) + \frac{\partial}{\partial z}(\rho v) = S$$

Considering field 1, for example, the source function is

$$S_1 = S_{31} + S_{61} - S_{13} - S_{16},$$

where the notation S_{31}, for example, denotes the mass per unit time per unit volume that is changing from field 3 (fuel vapor) to field 1 (liquid fuel).

The source function for the density equation can arise from phase changes or (in the case of fission gas) by gas release from solid fuel.

(1) Phase Changes

Phase changes arise only for the fuel and steel components. The fission products are always assumed to be in a gaseous form. We need to consider phase changes between (a) vapor and liquid fields, and (b) liquid and solid fields.

(a) Vapor-Liquid Interchange

(i) If there is substantially more of the liquid phase then use the following relation[12] based on kinetic theory.

$$S_{1\to g} = \frac{3\,\sigma_{1_e}\,\alpha_g}{r_g\sqrt{2\pi R}}\,\frac{p^*_1}{\sqrt{T_1}},$$

where 1 indicates the liquid phase

g indicates the vapor phase

σ_{1_e} = evaporation coefficient

R = gas constant

p^*_1 = saturation pressure corresponding to the liquid temperature T_1

r_g = radius of vapor bubble

α_g = volume fraction of vapor.

$$S_{g\to l} = \frac{3\sigma_{g_c}\,\alpha_g}{r_g\sqrt{2\pi R}}\,\frac{p_g}{\sqrt{T_g}}$$

where σ_{g_c} = condensation coefficient (normally equal to σ_{l_e})

p_g = gas pressure.

(ii) If there is substantially more vapor than liquid, use

$$S_{l\to g} = \frac{3\sigma_{l_e}\,\alpha_l}{r_l\sqrt{2\pi R}}\,\frac{p^*_l}{\sqrt{T_l}}\,,$$

and $$S_{g\to l} = \frac{3\sigma_{g_c}\,\alpha_l}{r_l\sqrt{2\pi R}}\,\frac{p}{\sqrt{T_g}}$$

(b) Solid Liquid Interchange

A solid is assumed to melt when its internal energy exceeds that which is required for melting at that particular temperature and pressure.

(2) Gas Release from Solid Fuel

The rate of release of fission gas from solid fuel is dependent on its concentration in the fuel. Thus,

$$\frac{\partial \rho}{\partial t} = -a\rho = S\,,$$

where a is a suitably chosen time constant.

2.3 Momentum Transport Equation

In component form the momentum transport equation is

(i) radial direction momentum equation

$$\frac{\partial \rho u}{\partial t} + \frac{1}{r}\frac{\partial}{\partial r}(r\rho uu) + \frac{\partial}{\partial z}(\rho uv)$$

$$= N_r - \alpha \frac{\partial p}{\partial r} + D(\bar{u} - u) + V_r$$

where u = radial component of velocity

v = axial component of velocity

V_r = radial component of the viscous term.

The various source and exchange functions are

1. N_r is the radial component of the momentum source function, arising from the S function in the density transport equation.

   Taking the liquid fuel (field 1) as an example,

$$N_{r_1} = u_3 S_{31} + u_6 S_{61} - u_1(S_{13} + S_{16}).$$

2. D is the drag term accounting for the momentum exchange between the different fields. Again considering field 1,

$$D_1 = \sum_{\substack{n \\ n \neq 1}} D_{1n} = D_{12} + D_{13} + D_{14} + D_{15} + D_{16} + D_{17}$$

and

$$D_1 \bar{u} = \sum_{\substack{n \\ n \neq 1}} D_{1n} u_n .$$

In general, the binary drag term between fields m and n is given by[10]

$$D_{mn} = \frac{3}{2} \alpha_m \alpha_n \left(\frac{1}{r_m} + \frac{1}{r_n} \right)^2 \left\{ \frac{3\mu_m \mu_n}{\mu_m + \mu_n} \frac{C_{D_{mn}} \rho'_m \rho'_n \left| \underset{\sim}{u}_m - \underset{\sim}{u}_n \right| r_m r_n}{4(r_n \rho'_m + r_m \rho'_n)} \right\} ,$$

$$\underset{\sim}{u}_m - \underset{\sim}{u}_n = \left\{ (u_m - u_n)^2 + (v_m - v_n)^2 \right\}^{\frac{1}{2}} ,$$

where r_m = radius of m^{th} field particles

r_n = radius of n^{th} field particles

$C_{D_{mn}}$ = coefficient of drag between the m^{th} and n^{th} fields.

This binary drag formula will not be used to evaluate the drag between the two liquid fields. Rather, the liquid-liquid drag term will be set to a very high number to account for the fact that when these two liquid fields intermix, they are fairly well tied to each other.

3. V_r is the radial component of the momentum gain due to viscous transfer. For a compressible Newtonian fluid this is readily shown to be

$$V_r = \frac{1}{r} \frac{\partial}{\partial r} \left[2\mu r \frac{\partial u}{\partial r} - \frac{2}{3} \mu \frac{\partial}{\partial r} (ru) - \frac{2}{3} \mu r \frac{\partial v}{\partial z} \right]$$

$$- \frac{2\mu u}{r^2} + \frac{2}{3}\frac{\mu}{r^2}\frac{\partial}{\partial r}(ru) + \frac{2}{3}\frac{\mu}{r}\frac{\partial v}{\partial z}$$

$$+ \frac{\partial}{\partial z}\left[\mu\left(\frac{\partial v}{\partial r} + \frac{\partial u}{\partial z}\right)\right].$$

It must be noted that the mass exchange terms prevent the reduction of this expression to the standard incompressible form of the viscous term for the essentially incompressible liquid fields. Hence the compressible form of the viscous term is used for both the vapor and liquid fields.

(ii) axial direction momentum equation

$$\frac{\partial \rho v}{\partial t} + \frac{1}{r}\frac{\partial}{\partial r}(r\rho uv) + \frac{\partial}{\partial z}(\rho vv)$$

$$= N_z - \alpha\frac{\partial p}{\partial z} + D(\bar{v} - v) + V_z + \rho g.$$

The axial momentum source function is of the same form as its radial counterpart, with the radial velocity components changed to the corresponding axial velocity components.

The axial viscosity term for a compressible fluid is

$$V_z = \frac{1}{r}\frac{\partial}{\partial r}\left[\mu r\left(\frac{\partial v}{\partial r} + \frac{\partial u}{\partial z}\right)\right] + \frac{\partial}{\partial z}\left\{\mu\left[\frac{4}{3}\frac{\partial v}{\partial z} - \frac{2}{3r}\frac{\partial}{\partial r}(ru)\right]\right\}$$

2.4 Internal Energy Transport Equation

$$\frac{\partial \rho I}{\partial t} + \frac{1}{r}\frac{\partial}{\partial r}(r\rho uI) + \frac{\partial}{\partial z}(\rho vI)$$

$$= -\frac{p}{r}\frac{\partial}{\partial r}(\alpha ur) - p\frac{\partial}{\partial z}(\alpha v) + Q$$

$$+ H(\bar{T} - T) + \frac{1}{r}\frac{\partial}{\partial r}(rk\alpha\frac{\partial T}{\partial r})$$

$$+ \frac{\partial}{\partial z}(k\alpha\frac{\partial T}{\partial z}) + \mu\Phi + \Lambda .$$

The various source and exchange functions are

1. Φ is the viscous dissipation term, and for a Newtonian fluid is given in standard textbooks such as Bird[13] as

$$\Phi = 2\left[(\frac{\partial u}{\partial r})^2 + (\frac{u}{r})^2 + (\frac{\partial v}{\partial z})^2\right] + (\frac{\partial u}{\partial z} + \frac{\partial v}{\partial r})^2$$

$$- \frac{2}{3}\left[\frac{1}{r}\frac{\partial}{\partial r}(ru) + \frac{\partial v}{\partial z}\right]^2 .$$

2. Λ is also a dissipative term, representing the rate of internal energy production as a result of momentum exchange. The total rate for all fields is

$$\Lambda_t = \frac{1}{2}\sum_n\sum_m D_{nm}\left[(u_m - u_n)^2 + (v_m - v_n)^2\right].$$

For the m^{th} field,

$$\Lambda_m = \lambda_m \Lambda_t ,$$

where the λ_m's are weighing coefficients such that $\sum_m \lambda_m = 1$.

3. H is the energy exchange function between the various fields. For the example of field 1,

$$H_1 = \sum_{\substack{n \\ n \neq 1}} H_{1n},$$

and $$H_1 \bar{T}_1 = \sum_{\substack{n \\ n \neq 1}} H_{1n} T_n.$$

The different binary energy exchange functions that must be considered are liquid-vapor, liquid-solid, vapor-solid, liquid-liquid, vapor-vapor, and solid-solid.

(i) Liquid-vapor:

For low Reynold's number, the energy exchange function for liquid droplets in a continuous vapor is shown by Soo[14] to be

$$H_{g1} = \left(\frac{\alpha_1}{\alpha_g}\right) \frac{3k_g}{r_1^2},$$

where subscript g indicates the vapor

subscript 1 indicated the liquid

r_1 = radius of liquid droplet

k_g = thermal conductivity of the gas.

(ii) Liquid-solid:

$$H_{1s} = h_{1s} \frac{4\pi r_s^2}{\frac{4}{3}\pi r_s^3} = \frac{3\, h_{1s}}{r_s},$$

where h_{ls} = heat transfer coefficient between the solid particle and the liquid (the particle is assumed spherical)

$$= \frac{N_{Nu}\, k_l}{2r_s}$$

$$N_{Nu} = 2 + 0.6\, N_{Pr}^{\frac{1}{3}}\, N_{Re}^{\frac{1}{2}}$$

(the Rantz - Marshall Relationship)[15]

$$N_{pr} = \frac{\mu_l\, c_{p_l}}{k_l}$$

$$N_{Re} = \frac{\rho_l \left| \sqrt{(u_l - u_s)^2 + (v_l - v_s)^2} \right| 2r_s}{\mu_l}$$

(iii) Vapor-solid:

This can be treated analogous to the liquid-solid case, by replacing the liquid parameters by the corresponding vapor parameters.

(iv) Liquid-Liquid:

The liquid-liquid energy exchange function is set to a very high value because the substantial intermixing of the two liquid fields brings them thermally close together.

(v) Vapor-vapor:

This is also set to a high value because of substantial mixing between the vapor fields.

(vi) Solid-Solid:

When there is substantial solid present, this exchange function will be in the form of a heat contact conductance between the two stationary solid fields. Some fraction of this contact conductance is used between small solid particles in motion, to account for the decreased contact area.

4. Q is a source function for the internal energy transport equation, arising from phase transitions and nuclear reactions.

$Q = Q_{phase} + Q_{nuclear}$.

We need to consider two types of phase changes

(i) liquid-vapor[12]:

$$Q_{\substack{phase \\ liq}} = S_{g\to l}\, I_l\,(T_g) - S_{l\to g}\, I_l\,(T_l)$$

$$- \frac{\rho_l\, c_l}{\rho_l\, c_l + \rho_g\, c_{p_g}} \left[S_{l\to g}\, h_{fg}\,(T_l) - S_{g\to l}\, h_{fg}\,(T_g) \right]$$

$$Q_{\substack{\text{phase} \\ \text{vap}}} = S_{l \to g} \left[I_g\,(T_l) + p_g\, v_{fg}\,(T_l) \right]$$

$$- S_{g \to l} \left[I_g\,(T_g) + p_g\, v_{fg}\,(T_g) \right]$$

$$- \frac{\rho_g\, c_{p_g}}{\rho_l\, c_l + \rho_g\, c_{p_g}} \left[S_{l \to g}\; h_{fg}\,(T_l) - S_{g \to l}\; h_{fg}\,(T_g) \right],$$

where

$Q_{\substack{\text{phase} \\ \text{liq}}}$ = source function (in the energy equation for the liquid) due to a liquid-vapor phase interchange

$Q_{\substack{\text{phase} \\ \text{vap}}}$ = source function (in the energy equation for the vapor) due to a liquid-vapor phase interchange

$I_l(T_g)$ = internal energy of the liquid at the gas saturation temperature T_g

$I_g(T_l)$ = internal energy of the gas at the liquid saturation temperature T_l

$h_{fg}(T_l)$ = latent heat of vaporization at the liquid saturation temperature T_l

$h_{fg}(T_g)$ = latent heat of vaporization at the gas saturation temperature T_g

$v_{fg}(T_l)$ = change in specific volume due to evaporation at the liquid saturation temperature T_l

$v_{fg}(T_g)$ = change in specific volume due to condensation at the gas saturation temperature T_g.

In these expressions, the work terms due to phase changes have been assigned entirely to the vapor. The heat of vaporization required for the phase change is drawn from each phase in proportion to its heat capacity per unit volume of the mixture.

(ii) liquid-solid:

$$Q_{\substack{\text{phase} \\ \text{liq}}} = S_{s\to l}\, I_l\,(T_s) - S_{l\to s}\, I_l\,(T_l)$$

$$- \frac{\rho_l\, c_l}{\rho_l\, c_l + \rho_s\, c_s}\left[S_{s\to l}\, h_{ls}\,(T_s) - S_{l\to s}\, h_{ls}\,(T_l)\right]$$

$$Q_{\substack{\text{phase} \\ \text{sol}}} = S_{l\to s}\, I_s\,(T_l) - S_{s\to l}\, I_s\,(T_s)$$

$$- \frac{\rho_s\, c_s}{\rho_l\, c_l + \rho_s\, c_s}\left[S_{s\to l}\, h_{ls}\,(T_s) - S_{l\to s}\, h_{ls}\,(T_l)\right]$$

where

$I_l\,(T_s)$ = internal energy of the liquid at the melting temperature of the solid T_s

$I_s\,(T_l)$ = internal energy of the solid at the solidification temperature of the liquid T_l

$h_{ls}(T_s)$ = latent heat of fusion at temperature T_s

$h_{ls}(T_l)$ = latent heat of fusion at temperature T_l.

The source term due to nuclear heating, $Q_{nuclear}$, is based on the reactivity worth of the fuel in a particular configuration.

CHAPTER III

NUMERICAL APPROXIMATION

The complex equations of motion and energy transfer are impossible to solve analytically, necessitating the formulation of a numerical solution. This requires a numerical scheme which can be programmed for use on a large computer so as to achieve meaningful results in a reasonable amount of calculational time.

Analytical methods yield solutions to differential equations at every point in the domain, while numerical solutions are applicable only at discrete points. Thus, basic to any numerical scheme is the choice of a mesh and the location of variables in this mesh. A fixed set of cells is chosen to zone the region of interest as shown in Figure 1. Each of these cells is a cylindrical annulus of width δr and height δz. The total number of cells will be based on computational time, available computer memory and desired accuracy. Within a cell, the radial velocity components are indexed on the sides of the cell, the axial velocity components on the top and bottom, and the scalar variables like density, pressure and internal energy at the cell center as in Figure 2. This placement[16] of field variables is based on its ability to achieve conservation without the necessity of involving cells which are not the immediate neighbors of the calculational cell. The use of distant cells would add to the complexity of the solution procedure and might introduce considerable error.

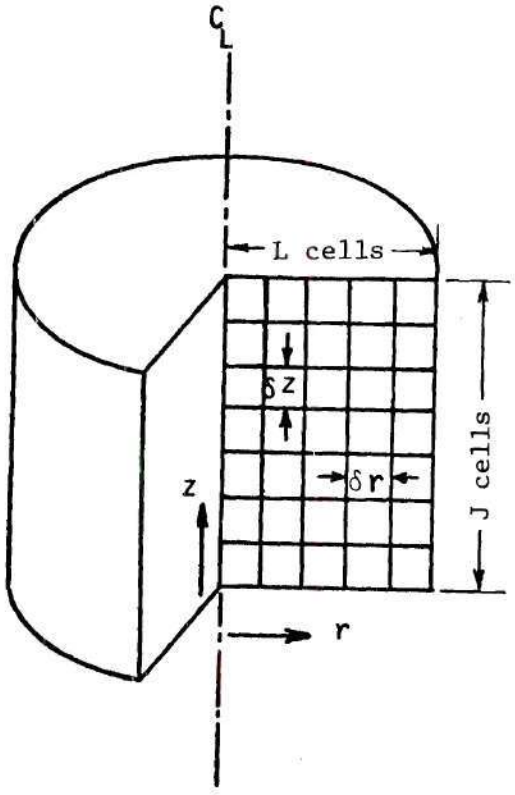

FIGURE 1. Axisymmetric Two Dimensional Computing Mesh

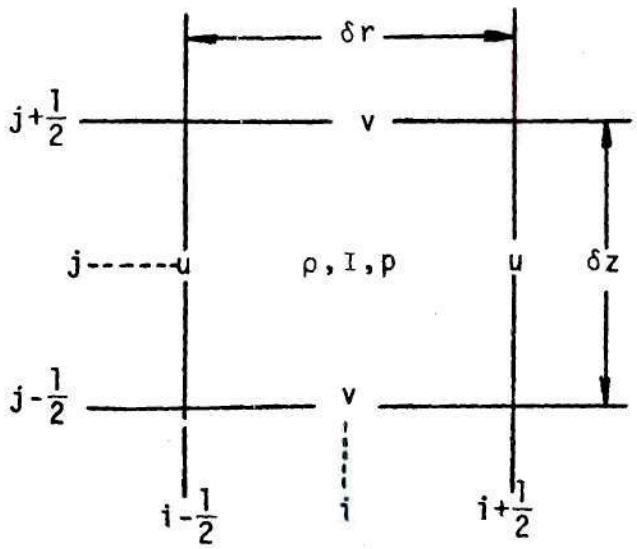

FIGURE 2. Location of Variables and Indices

The equations of motion and energy transfer can now be solved for each cell by replacing the differential equations with finite difference approximations, and choosing an iterative scheme to proceed through the difference equations. However, for this solution to depict a particular flow situation, the variables must satisfy certain physical constraints (in the form of boundary conditions) at container boundaries and at some material interfaces (for example, between a substantial solid region and a liquid or a vapor region).

The rest of this chapter is devoted to these aspects of the numerical scheme. The finite difference approximations to the equations of density, momentum and energy transport are presented in Sections 3.1, 3.2 and 3.3. Section 3.4 details the solution procedure for these difference approximations, the stability analysis is discussed in Section 3.5, and some boundary conditions for the velocity and temperature are listed in Section 3.6.

3.1 Density Transport Equation

The differential equation of density transport is given by

$$\frac{\partial \rho}{\partial t} + \frac{1}{r}\frac{\partial}{\partial r}(\rho u r) + \frac{\partial}{\partial z}(\rho v) = S,$$

where ρ = macroscopic density

$= \alpha\rho'$

ρ' = microscopic density

α = volume fraction of a field

u = radial component of velocity

v = axial component of velocity

S = density source function.

This differential equation can be replaced by a finite difference approximation which is first order accurate in time, and second order in space. Thus, for cell i, j we have

$$\frac{1}{\delta t}\left[{}^{n+1}\rho_i^j - \rho_i^j\right] + \frac{1}{r_i \delta r}\left[{}^{n+1}\langle \rho u r\rangle_{i+\frac{1}{2}}^{j} - {}^{n+1}\langle \rho u r\rangle_{i-\frac{1}{2}}^{j}\right]$$

$$+ \frac{1}{\delta z}\left[{}^{n+1}\langle \rho v\rangle_{i}^{j+\frac{1}{2}} - {}^{n+1}\langle \rho v\rangle_{i}^{j-\frac{1}{2}}\right] = S_i^j,$$

where i = radial coordinate index

j = axial coordinate index

n = time step index

δt = time step.

All quantities not time indexed are evaluated at the n^{th} time step. The source function, S, is readily obtained by evaluating, for cell i, j, the parameters in the S expression of Chapter II.

The difference approximation must deal with convective fluxes of cell centered quantities, such as ρ_i^j. This convective flux is the product of the normal velocity component and that quantity. Thus the convective flux of density across the right hand face of cell i, j is $(u\rho)^j_{i+\frac{1}{2}}$. But this flux is based on the concentrations of the specified quantity in the two cells (the donor cell and the centered cell) which form the interface. The properties of both centered and donor-cell are combined in the partial donor-cell technique[9] to yield a flux expression of the form

$$\langle u\rho \rangle^j_{i+\frac{1}{2}} = u^j_{i+\frac{1}{2}} \left[\left(\frac{1+\xi}{2}\right)\rho^j_i + \left(\frac{1-\xi}{2}\right)\rho^j_{i+1} \right],$$

where ξ depends on the parameters β_o and θ_o as

$$\xi = (\beta_o u^j_{i+\frac{1}{2}} \delta t)/\delta r + \theta_o \text{ sign } (u^j_{i+\frac{1}{2}}).$$

The input coefficients β_o and θ_o can take on a range of values between 0 and 0.5, assuming that $|u_{max}|\delta t/\delta r < \frac{1}{2}$ everywhere. The simplest choice of $\theta_o = \beta_o = o$ ($\xi = o$) leads to a purely space centered flux which is readily shown[17] to be numerically unstable unless counteracted by an added diffusion process.

Selecting $\theta_o = 0.5$ and $\beta_o = o$ reverts to the standard donor-cell differencing method where, for example,

$$\langle \rho \rangle^{j}_{i+\frac{1}{2}} = \begin{cases} \rho^{j}_{i} & \text{if } u^{j}_{i+\frac{1}{2}} \geq 0 \\ \rho^{j}_{i+1} & \text{if } u^{j}_{i+\frac{1}{2}} < 0 \end{cases}$$

On the other hand, this standard donor-cell differencing is omitted entirely by choosing $\theta_o = o$ and $\beta_o = 0.5$ (a fully interpolated donor-cell form). In the more general case, one chooses both θ_o and β_o to be non-zero which provides some control on truncation errors without the need for explicit diffusion.

The convective flux terms for the finite difference representation of the density transport equation are given by

$$^{n+1}\langle \rho ur \rangle^{j}_{i+\frac{1}{2}} = {}^{n+1}u^{j}_{i+\frac{1}{2}}\, r_{i+\frac{1}{2}} \left[(\tfrac{1}{2} + \xi)\, {}^{n+1}\rho^{j}_{i} + (\tfrac{1}{2} - \xi)\, {}^{n+1}\rho^{j}_{i+1} \right],$$

where

$$\xi = (\beta_o\, {}^{n+1}u^{j}_{i+\frac{1}{2}}\, \delta t)/\delta r + \theta_o \operatorname{sign}({}^{n+1}u^{j}_{i+\frac{1}{2}}),$$

and

$$^{n+1}\langle \rho v \rangle^{j+\frac{1}{2}}_{i} = {}^{n+1}v^{j+\frac{1}{2}}_{i} \left[(\tfrac{1}{2} + \xi)\, {}^{n+1}\rho^{j}_{i} + (\tfrac{1}{2} - \xi)\, {}^{n+1}\rho^{j+1}_{i} \right],$$

where

$$\xi = (\beta_o\, {}^{n+1}v^{j+\frac{1}{2}}_{i}\, \delta t)/\delta z + \theta_o \operatorname{sign}({}^{n+1}v^{j+\frac{1}{2}}_{i}).$$

3.2 Momentum Transport Equation

(1) radial direction momentum equation

$$\frac{\partial \rho u}{\partial t} + \frac{1}{r}\frac{\partial}{\partial r}(r\rho uu) + \frac{\partial}{\partial z}(\rho uv)$$

$$= N_r - \alpha \frac{\partial p}{\partial r} + D(\bar{u} - u) + V_r$$

In this equation,

N_r = radial component of momentum source function

p = pressure

D = drag term

$\bar{u}$ = representative radial velocity component for other fields.

The radial component of the viscous term, denoted by V_r, is

$$V_r = \frac{1}{r}\frac{\partial}{\partial r}\left[2\mu r \frac{\partial u}{\partial r} - \frac{2}{3}\mu \frac{\partial}{\partial r}(ru) - \frac{2}{3}\mu r \frac{\partial v}{\partial z}\right]$$

$$- \frac{2\mu u}{r^2} + \frac{2}{3}\frac{\mu}{r^2}\frac{\partial}{\partial r}(ru) + \frac{2}{3}\frac{\mu}{r}\frac{\partial v}{\partial z}$$

$$+ \frac{\partial}{\partial z}\left[\mu\left(\frac{\partial v}{\partial r} + \frac{\partial u}{\partial z}\right)\right].$$

The differential equation for radial momentum transport can then be approximated at the point $i + \frac{1}{2}$, j by

$$\frac{1}{\delta t}\left[{}^{n+1}(\rho u)^{j}_{i+\frac{1}{2}} - (\rho u)^{j}_{i+\frac{1}{2}}\right] + \frac{1}{r_{i+\frac{1}{2}}\delta r}\left[\langle \rho uur\rangle^{j}_{i+1} - \langle \rho uur\rangle^{j}_{i}\right]$$

$$+ \frac{1}{\delta z}\left[\langle \rho uv \rangle^{j+\frac{1}{2}}_{i+\frac{1}{2}} - \langle \rho uv \rangle^{j-\frac{1}{2}}_{i+\frac{1}{2}} \right]$$

$$= (N_r)^{j}_{i+\frac{1}{2}} - {}^{n+1}\alpha^{j}_{i+\frac{1}{2}} \left[{}^{n+1}p^{j}_{i+1} - {}^{n+1}p^{j}_{i} \right] / \delta r$$

$$+ D^{j}_{i+\frac{1}{2}} \left[{}^{n+1}\bar{u}^{j}_{i+\frac{1}{2}} - {}^{n+1}u^{j}_{i+\frac{1}{2}} \right] + (V_r)^{j}_{i+\frac{1}{2}} \quad ,$$

where all non-time indexed terms are evaluated at the n^{th} time step. The radial momentum source function (N_r) and the drag term (D) are readily obtained by evaluating, at the point $i + \frac{1}{2}$, j, the parameters in the N_r and D expressions of Chapter II. Quantities to be evaluated at points in between those at which they are indexed in the mesh are obtained by simple linear interpolation. For example, $u^{j}_{i} = \frac{1}{2}(u^{j}_{i-\frac{1}{2}} + u^{j}_{i+\frac{1}{2}})$.

The convective and viscous terms in the finite difference expression are calculated as follows.

$$\text{(i)} \quad \langle \rho uur \rangle^{j}_{i} = u^{j}_{i}\, r_i \left[(\tfrac{1}{2} + \xi)(\rho u)^{j}_{i-\frac{1}{2}} + (\tfrac{1}{2} - \xi)(\rho u)^{j}_{i+\frac{1}{2}} \right]$$

$$\text{where } \xi = (\beta_o\, u^{j}_{i}\, \delta t)/\delta r + \theta_o \text{ sign } (u^{j}_{i})$$

$$u^{j}_{i} = \frac{1}{2}(u^{j}_{i-\frac{1}{2}} + u^{j}_{i+\frac{1}{2}}).$$

It may be noted here that in a momentum convective flux expression, the ρu term must not be thought of as a density flux term and evaluated by another convective flux expression. Rather, it is directly obtained from the solution of the momentum equation at the previous time step.

$$\text{(ii)} \quad \langle \rho uv \rangle^{j+\frac{1}{2}}_{i+\frac{1}{2}} = v^{j+\frac{1}{2}}_{i+\frac{1}{2}} \left[\left(\tfrac{1}{2} + \xi\right)(\rho u)^{j}_{i+\frac{1}{2}} + \left(\tfrac{1}{2} - \xi\right)(\rho u)^{j+1}_{i+\frac{1}{2}} \right]$$

$$\text{where} \quad \xi = \left(\beta_o \, v^{j+\frac{1}{2}}_{i+\frac{1}{2}} \, \delta t\right)/\delta z + \theta_o \, \text{sign} \left(v^{j+\frac{1}{2}}_{i+\frac{1}{2}}\right)$$

$$v^{j+\frac{1}{2}}_{i+\frac{1}{2}} = \frac{1}{2}\left[v^{j+\frac{1}{2}}_{i} + v^{j+\frac{1}{2}}_{i+1} \right]$$

$$\text{(iii)} \quad (V_r)^{j}_{i+\frac{1}{2}} = \frac{2}{r_{i+\frac{1}{2}} \delta r} \left\{ \mu^{j}_{i+1} \, r_{i+1} \left[u^{j}_{i+\frac{3}{2}} - u^{j}_{i+\frac{1}{2}} \right] \right\} /\delta r$$

$$- \mu^{j}_{i} \, r_i \left[u^{j}_{i+\frac{1}{2}} - u^{j}_{i-\frac{1}{2}} \right] /\delta r$$

$$- \frac{1}{3} \mu^{j}_{i+1} \left[u^{j}_{i+\frac{3}{2}} \, r_{i+\frac{3}{2}} - u^{j}_{i+\frac{1}{2}} \, r_{i+\frac{1}{2}} \right] /\delta r$$

$$+ \frac{1}{3} \mu^{j}_{i} \left[u^{j}_{i+\frac{1}{2}} \, r_{i+\frac{1}{2}} - u^{j}_{i-\frac{1}{2}} \, r_{i-\frac{1}{2}} \right] /\delta r$$

$$- \frac{1}{3} \mu^{j}_{i+1} \, r_{i+1} \left[v^{j+\frac{1}{2}}_{i+1} - v^{j-\frac{1}{2}}_{i+1} \right] /\delta z$$

$$+ \frac{1}{3}\mu_i^j\, r_i \left[v_i^{j+\frac{1}{2}} - v_i^{j-\frac{1}{2}} \right]/\delta z \Bigg\}$$

$$-2(\mu u)^j_{i+\frac{1}{2}}/(r^2)_{i+\frac{1}{2}} + \frac{2}{3}\,\mu^j_{i+\frac{1}{2}} \left[u^j_{i+1}\, r_{i+1} - u^j_i\, r_i \right]/(\delta r)(r_{i+\frac{1}{2}})^2$$

$$+ \frac{2}{3}\,\mu^j_{i+\frac{1}{2}} \left[v^{j+\frac{1}{2}}_{i+\frac{1}{2}} - v^{j-\frac{1}{2}}_{i+\frac{1}{2}} \right]/(\delta z)(r_{i+\frac{1}{2}})$$

$$+ \frac{1}{\delta z}\Bigg\{ \mu^{j+\frac{1}{2}}_{i+\frac{1}{2}} \left[\left(v^{j+\frac{1}{2}}_{i+1} - v^{j+\frac{1}{2}}_{i} \right)/\delta r + \left(u^{j+1}_{i+\frac{1}{2}} - u^{j}_{i+\frac{1}{2}} \right)/\delta z \right]$$

$$- \mu^{j-\frac{1}{2}}_{i+\frac{1}{2}} \left[\left(v^{j-\frac{1}{2}}_{i+1} - v^{j-\frac{1}{2}}_{i} \right)/\delta r + \left(u^{j}_{i+\frac{1}{2}} - u^{j-1}_{i+\frac{1}{2}} \right)/\delta z \right] \Bigg\},$$

where the interpolated terms are

$$u^j_i = \frac{1}{2}\left(u^j_{i-\frac{1}{2}} + u^j_{i+\frac{1}{2}} \right)$$

$$v^{j\pm\frac{1}{2}}_{i+\frac{1}{2}} = \frac{1}{2}\left(v^{j\pm\frac{1}{2}}_i + v^{j\pm\frac{1}{2}}_{i+1} \right)$$

$$\mu^j_{i+\frac{1}{2}} = \frac{1}{2}\,(\mu^j_i + \mu^j_{i+1})$$

$$\mu^{j\pm\frac{1}{2}}_{i+\frac{1}{2}} = \frac{1}{4}\left(\mu^j_i + \mu^j_{i\pm1} + \mu^{j\pm1}_i + \mu^{j\pm1}_{i\pm1} \right)$$

(2) axial direction momentum equation

$$\frac{\partial \rho v}{\partial t} + \frac{1}{r}\frac{\partial}{\partial r}(r\rho uv) + \frac{\partial}{\partial z}(\rho vv)$$

$$= N_z - \alpha\frac{\partial p}{\partial z} + D(\bar{v} - v) + V_z + \rho g.$$

In this equation,

N_z = axial component of momentum source function

$\bar{v}$ = representative axial velocity component

The axial component of the viscous term, denoted by V_z, is

$$V_z = \frac{1}{r}\frac{\partial}{\partial r}[\mu r(\frac{\partial v}{\partial r} + \frac{\partial u}{\partial z})] + \frac{\partial}{\partial z}\{\mu[\frac{4}{3}\frac{\partial v}{\partial z} - \frac{2}{3r}\frac{\partial}{\partial r}(ru)]\}.$$

The differential equation for axial momentum transport can then be approximated at the point i, $j + \frac{1}{2}$ by

$$\frac{1}{\delta t}\left[{}^{n+1}(\rho v)_i^{j+\frac{1}{2}} - (\rho v)_i^{j+\frac{1}{2}}\right] + \frac{1}{r_i\,\delta r}\left[\langle\rho uvr\rangle_{i+\frac{1}{2}}^{j+\frac{1}{2}} - \langle\rho uvr\rangle_{i-\frac{1}{2}}^{j+\frac{1}{2}}\right]$$

$$+ \frac{1}{\delta z}\left[\langle\rho vv\rangle_i^{j+1} - \langle\rho vv\rangle_i^{j}\right]$$

$$= (N_z)_i^{j+\frac{1}{2}} - {}^{n+1}\alpha_i^{j+\frac{1}{2}}\left[{}^{n+1}p_i^{j+1} - {}^{n+1}p_i^{j}\right]/\delta z$$

$$+ D_i^{j+\frac{1}{2}}\left[{}^{n+1}\bar{v}_i^{j+\frac{1}{2}} - {}^{n+1}v_i^{j+\frac{1}{2}}\right] + (V_z)_i^{j+\frac{1}{2}}$$

$$+ \quad \rho_i^{n+1} \; g^{j+\frac{1}{2}}.$$

Again, all non-time indexed terms are evaluated at the n^{th} time step, and the axial momentum source function (N_z) is readily obtained by evaluating, at the point i, $j + \frac{1}{2}$, the parameters in the N_z expression of Chapter II. Quantities to be evaluated at points in between those at which they are indexed in the mesh are obtained by simple linear interpolation.

The convective and viscous terms in the finite difference expression are calculated as follows.

$$\text{(i)} \quad \langle \rho uvr \rangle_{i+\frac{1}{2}}^{j+\frac{1}{2}} = u_{i+\frac{1}{2}}^{j+\frac{1}{2}} \; r_{i+\frac{1}{2}} \left[(\tfrac{1}{2} + \xi)(\rho v)_i^{j+\frac{1}{2}} + (\tfrac{1}{2} - \xi)(\rho v)_{i+1}^{j+\frac{1}{2}} \right]$$

$$\text{where } \xi = (\beta_o \; u_{i+\frac{1}{2}}^{j+\frac{1}{2}} \; \delta t)/\delta r + \theta_o \; \text{sign} \; (u_{i+\frac{1}{2}}^{j+\frac{1}{2}})$$

$$u_{i+\frac{1}{2}}^{j+\frac{1}{2}} = \tfrac{1}{2}(u_{i+\frac{1}{2}}^{j} + u_{i+\frac{1}{2}}^{j+1})$$

$$\text{(ii)} \quad \langle \rho vv \rangle_i^j = v_i^j \left[(\tfrac{1}{2} + \xi)(\rho v)_i^{j-\frac{1}{2}} + (\tfrac{1}{2} - \xi)(\rho v)_i^{j+\frac{1}{2}} \right]$$

$$\text{where } \xi = (\beta_o \; v_i^j \; \delta t)/\delta z + \theta_o \; \text{sign} \; (v_i^j)$$

$$v_i^j = \tfrac{1}{2}(v_i^{j-\frac{1}{2}} + v_i^{j+\frac{1}{2}})$$

(iii)

$$(V_z)_i^{j+\frac{1}{2}} = \frac{1}{r_i\,\delta r}\left\{\mu_{i+\frac{1}{2}}^{j+\frac{1}{2}} r_{i+\frac{1}{2}}\left[\left(v_{i+1}^{j+\frac{1}{2}} - v_i^{j+\frac{1}{2}}\right)/\delta r + \left(u_{i+\frac{1}{2}}^{j+1} - u_{i+\frac{1}{2}}^{j}\right)/\delta z\right]\right.$$

$$\left. - \mu_{i-\frac{1}{2}}^{j+\frac{1}{2}} r_{i-\frac{1}{2}}\left[\left(v_i^{j+\frac{1}{2}} - v_{i-1}^{j+\frac{1}{2}}\right)/\delta r + \left(u_{i-\frac{1}{2}}^{j+1} - u_{i-\frac{1}{2}}^{j}\right)/\delta z\right]\right\}$$

$$+ \frac{1}{\delta z}\left\{\mu_i^{j+1}\left[\frac{4}{3}\left(v_i^{j+\frac{3}{2}} - v_i^{j+\frac{1}{2}}\right)/\delta z - \frac{2}{3r_i}\left(r_{i+\frac{1}{2}}\, j_{i+\frac{1}{2}}^{j+1} - r_{i-\frac{1}{2}}\, u_{i-\frac{1}{2}}^{j+1}\right)/\delta r\right]\right.$$

$$\left. - \mu_i^{j}\left[\frac{4}{3}\left(v_i^{j+\frac{1}{2}} - v_i^{j-\frac{1}{2}}\right)/\delta z - \frac{2}{3r_i}\left(r_{i+\frac{1}{2}}\, u_{i+\frac{1}{2}}^{j} - r_{i-\frac{1}{2}}\, u_{i-\frac{1}{2}}^{j}\right)/\delta r\right\}\right.$$

where $\mu_{i\pm\frac{1}{2}}^{j+\frac{1}{2}} = \frac{1}{4}\left(\mu_{i\pm1}^{j+1} + \mu_i^{j+1} + \mu_{i\pm1}^{j} + \mu_i^{j}\right)$

3.3 Internal Energy Transport Equation

The transport of specific internal energy is given by

$$\frac{\partial \rho I}{\partial t} + \frac{1}{r}\frac{\partial}{\partial r}(r\rho uI) + \frac{\partial}{\partial z}(\rho vI)$$

$$= -\frac{p}{r}\frac{\partial}{\partial r}(\alpha ur) - p\frac{\partial}{\partial z}(\alpha v) + Q$$

$$+ H(\bar{T}-T) + \frac{1}{r}\frac{\partial}{\partial r}\left(rk\alpha\frac{\partial T}{\partial r}\right)$$

$$+ \frac{\partial}{\partial z}\left(k\alpha\frac{\partial T}{\partial z}\right) + \mu\Phi + \Delta,$$

where Q = internal energy source function

H = energy exchange function

$\bar{T}$ = representative temperature of other fields

T = temperature of field

k = thermal conductivity

Δ = internal energy production due to momentum exchange.

The viscous dissipation term, ϕ, is given by

$$\Phi = 2\left[\left(\frac{\partial u}{\partial r}\right)^2 + \left(\frac{u}{r}\right)^2 + \left(\frac{\partial v}{\partial z}\right)^2\right]$$

$$+ \left(\frac{\partial u}{\partial z} + \frac{\partial v}{\partial r}\right)^2 - \frac{2}{3}\left[\frac{1}{r}\frac{\partial}{\partial r}(ru) + \frac{\partial v}{\partial z}\right]^2$$

An explicit form of the finite difference representation of the energy equation at the point i, j is

$$\frac{1}{\partial t}\left[{}^{n+1}(\rho I)_i^j - {}^{n}(\rho I)_i^j\right] + \frac{1}{r_i \delta r}\left[\langle \rho Iur\rangle_{i+\frac{1}{2}}^{j} - \langle \rho Iur\rangle_{i-\frac{1}{2}}^{j}\right]$$

$$+ \frac{1}{\delta z}\left[\langle \rho Iv\rangle_i^{j+\frac{1}{2}} - \langle \rho Iv\rangle_i^{j-\frac{1}{2}}\right]$$

$$= \frac{-p_i^j}{r_i \delta r}\left[r_{i+\frac{1}{2}} (\alpha u)^j_{i+\frac{1}{2}} - r_{i-\frac{1}{2}} (\alpha u)^j_{i-\frac{1}{2}} \right]$$

$$- \frac{p_i^j}{\delta z}\left[(\alpha v)_i^{j+\frac{1}{2}} - (\alpha v)_i^{j-\frac{1}{2}} \right] + Q_i^j + H_i^j \left[\bar{T}_i^j - T_i^j \right]$$

$$+ \frac{1}{r_i \delta r}\left\{ r_{i+\frac{1}{2}} (k\alpha)^j_{i+\frac{1}{2}} (T^j_{i+1} - T^j_i)/\delta r - r_{i-\frac{1}{2}} (k\alpha)^j_{i-\frac{1}{2}} (T^j_i - T^j_{i-1})/\delta r \right\}$$

$$+ \frac{1}{\delta z}\left\{ (k\alpha)_i^{j+\frac{1}{2}} (T_i^{j+1} - T_i^j)/\delta z - (k\alpha)_i^{j-\frac{1}{2}} (T_i^j - T_i^{j-1})/\delta z \right\}$$

$$+ (\mu\Phi)^j_i + \Delta^j_i$$

The new internal energy value can be obtained directly from this explicit formulation. However, the density and momentum transport equations, which have been written in an implicit fashion, must be solved simultaneously by iteration. The solutions of these implicit equations are carried out before proceeding to the explicit energy equation. Hence, the latest known values of the density, pressure, volume fraction and velocity components can be used in the energy equation, except in the time term, ${}^n(\rho I)^j_i$, which must be evaluated at the n^{th} time step. The convective terms are also calculated with the old values of the density and internal energy.

The source and exchange functions are readily obtained by evaluating, at the point i, j, the parameters for these functions in Chapter II. Linear interpolation is used for quantities at points in between those at which they are indexed in the mesh.

The convective and viscous dissipation terms in the finite difference expression are calculated as follows

(i) $$\langle \rho I u r \rangle^{j}_{i+\frac{1}{2}} = r_{i+\frac{1}{2}}\, u^{j}_{i+\frac{1}{2}} \left\{ (\tfrac{1}{2} + \xi)(\rho I)^{j}_{i} + (\tfrac{1}{2} - \xi)(\rho I)^{j}_{i+1} \right\}$$

where

$$\xi = (\beta_o u^{j}_{i+\frac{1}{2}}\, \delta t)/\delta r + \theta_o \ \text{sign}\ (u^{j}_{i+\frac{1}{2}})$$

(ii) $$\langle \rho I v \rangle^{j+\frac{1}{2}}_{i} = v^{j+\frac{1}{2}}_{i} \left\{ (\tfrac{1}{2} + \xi)(\rho I)^{j}_{i} + (\tfrac{1}{2} - \xi)(\rho I)^{j+1}_{i} \right\}$$

where

$$\xi = (\beta_o v_i^{\,j+\frac{1}{2}}\, \delta t)/\delta z + \theta_o \ \text{sign}\ (v^{j+\frac{1}{2}}_{i})$$

(iii) $$\Phi^{j}_{i} = 2 \left\{ \left[(u^{j}_{i+\frac{1}{2}} - u^{j}_{i-\frac{1}{2}})/\delta r \right]^2 + (u^{j}_{i}/r_i)^2 + \left[(v^{j+\frac{1}{2}}_{i} - v^{j-\frac{1}{2}}_{i})/\delta z \right]^2 \right\}$$

$$+ \left\{ (u^{j+\frac{1}{2}}_{i} - u^{j-\frac{1}{2}}_{i})/\delta z + (v^{j}_{i+\frac{1}{2}} - v^{j}_{i-\frac{1}{2}})/\delta r \right\}^2$$

$$- \frac{2}{3} \left\{ \frac{1}{r_i \delta r} (r_{i+\frac{1}{2}}\, u^{j}_{i+\frac{1}{2}} - r_{i-\frac{1}{2}}\, u^{j}_{i-\frac{1}{2}}) + (v^{j+\frac{1}{2}}_{i} - v^{j-\frac{1}{2}}_{i})/\delta z \right\}$$

where

$$u^{j}_{i} = \tfrac{1}{2} (u^{j}_{i+\frac{1}{2}} + u^{j}_{i-\frac{1}{2}})$$

$$u^{j\pm\frac{1}{2}}_{i} = \tfrac{1}{4} (u^{j}_{i+\frac{1}{2}} + u^{j}_{i-\frac{1}{2}} + u^{j\pm1}_{i-\frac{1}{2}} + u^{j\pm1}_{i-\frac{1}{2}})$$

$$v^{j}_{i+\frac{1}{2}} = \tfrac{1}{4} (v^{j+\frac{1}{2}}_{i} + v^{j-\frac{1}{2}}_{i} + v^{j+\frac{1}{2}}_{i+1} + v^{j-\frac{1}{2}}_{i+1}).$$

3.4 Solution Procedure

The finite difference representations of the equations of density and momentum transport in the preceding sections are in an implicit formulation, necessitating a simultaneous iterative solution. The iterative procedure follows the multi-field approach of Harlow and Amsden[10]. Once the solutions to the equations of motion are known at a given time step, the explicit energy equation can be solved directly using the new velocity, pressure and density distributions.

The solutions of the finite difference equations are carried through successive time steps, making use at each time level of quantities evaluated at the previous level. Thus, the momentum equations can be rewritten in the form

$$ {}^{n+1}(\rho u)^{j}_{i+\frac{1}{2}} = (X_r)^{j}_{i+\frac{1}{2}} + D^{j}_{i+\frac{1}{2}}\,\delta t\left[{}^{n+1}\bar{u}^{\,j}_{i+\frac{1}{2}} - {}^{n+1}u^{\,j}_{i+\frac{1}{2}} \right] $$

$$ + \; {}^{n+1}\alpha^{j}_{i+\frac{1}{2}}\,\delta t\left[{}^{n+1}p^{\,j}_{i} - {}^{n+1}p^{\,j}_{i+1} \right]/\delta r, $$

$$ \text{and} \quad {}^{n+1}(\rho v)^{j+\frac{1}{2}}_{i} = (X_z)^{j+\frac{1}{2}}_{i} + D^{j+\frac{1}{2}}_{i}\,\delta t\left[{}^{n+1}\bar{v}^{\,j+\frac{1}{2}}_{i} - {}^{n+1}v^{\,j+\frac{1}{2}}_{i} \right] $$

$$ + \; {}^{n+1}\alpha^{j+\frac{1}{2}}_{i}\,\delta t\left[{}^{n+1}p^{\,j}_{i} - {}^{n+1}p^{\,j+1}_{i} \right]/\delta z $$

$$ + \; {}^{n+1}\rho^{j+\frac{1}{2}}_{i}\, g\, \delta t, $$

where X_r and X_z are those terms of the radial and axial momentum equations which are evaluated at the preceding time step. Thus,

$$(X_r)^j_{i+\frac{1}{2}} = (\rho u)^j_{i+\frac{1}{2}} + \frac{\delta t}{r_{i+\frac{1}{2}}\,\delta r}\left[\langle \rho uur\rangle^j_i - \langle \rho uur\rangle^j_{i+1}\right]$$

$$+ \quad \frac{\delta t}{\delta z}\left[\langle \rho uv\rangle^{j-\frac{1}{2}}_{i+\frac{1}{2}} - \langle \rho uv\rangle^{j+\frac{1}{2}}_{i+\frac{1}{2}}\right]$$

$$+ \quad (N_r)^j_{i+\frac{1}{2}}\,\delta t + (V_r)^j_{i+\frac{1}{2}}\,\delta t,$$

and $$(X_z)^{j+\frac{1}{2}}_i = (\rho v)^{j+\frac{1}{2}}_i + \frac{\delta t}{r_i \delta r}\left[\langle \rho uvr\rangle^{j+\frac{1}{2}}_{i-\frac{1}{2}} - \langle \rho uvr\rangle^{j+\frac{1}{2}}_{i+\frac{1}{2}}\right]$$

$$+ \quad \frac{\delta t}{\delta z}\left[\langle \rho vv\rangle^j_i - \langle \rho vv\rangle^{j+1}_i\right]$$

$$+ \quad (N_z)^{j+\frac{1}{2}}_i\,\delta t + (V_z)^{j+\frac{1}{2}}_i\,\delta t.$$

A test of the convergence of the iteration scheme is to see how well the density transport equation is satisfied. Therefore, let

$${}^{n+1}B^j_i = \left[{}^{n+1}\rho^j_i - \rho^j_i\right]/\delta t$$

$$+ \quad \left[{}^{n+1}\langle \rho ur\rangle^j_{i+\frac{1}{2}} - {}^{n+1}\langle \rho ur\rangle^j_{i-\frac{1}{2}}\right]/(r_i \delta r)$$

$$+ \quad \left[{}^{n+1}\langle \rho v\rangle^{j+\frac{1}{2}}_i - {}^{n+1}\langle \rho v\rangle^{j-\frac{1}{2}}_i\right]/\delta z$$

$$- \quad S^j_i.$$

Then, the iteration scheme for solving the implicit equations of motion converges when B is sufficiently close to zero.

The solution procedure at each time step consists of an explicit part and an implicit part described in detail below.

1. Explicit Calculation

At the beginning of a time step, the values of the field variables are known in all the cells. Begin each time cycle by using the equation of state for each field to calculate a new pressure based on the latest known values of the density and internal energy. Then initialize the velocity components by a simple reformulation of the momentum equations, recognizing that all quantities are from the previous time step, except the new pressures. Thus,

$$\tilde{u}^{j}_{i+\frac{1}{2}} = \left\{ (X_r)^{j}_{i+\frac{1}{2}} + \alpha^{j}_{i+\frac{1}{2}}\,\delta t \left[\tilde{p}^{j}_{i} - \tilde{p}^{j}_{i+1} \right] /\delta r \right.$$

$$\left. + \quad (\bar{Du})^{j}_{i+\frac{1}{2}}\,\delta t \right\} \Big/ \left\{ \rho^{j}_{i+\frac{1}{2}} + D^{j}_{i+\frac{1}{2}}\,\delta t \right\} ,$$

$$\text{and} \quad \tilde{v}^{j+\frac{1}{2}}_{i} = \left\{ (X_z)^{j+\frac{1}{2}}_{i} + \alpha^{j+\frac{1}{2}}_{i}\,\delta t \left[\tilde{p}^{j}_{i} - \tilde{p}^{j+1}_{i} \right] /\delta z \right.$$

$$\left. + \quad (\bar{Dv})^{j+\frac{1}{2}}_{i}\,\delta t + \rho^{j+\frac{1}{2}}_{i}\, g\,\delta t \right\} \Big/ \left\{ \rho^{j+\frac{1}{2}}_{i} + D^{j+\frac{1}{2}}_{i}\,\delta t \right\} .$$

In these and subsequent equations, a tilde above a quantity indicates an unconverged value at the current time step.

The new velocity components yield the new density as

$$\tilde{\rho}_i^j = \rho_i^j + \delta t \left\{ \left[\langle \rho \tilde{u} r \rangle_{i-\frac{1}{2}}^{j} - \langle \rho \tilde{u} r \rangle_{i+\frac{1}{2}}^{j} \right] / (r_i \delta r) \right.$$

$$\left. + \left[\langle \rho \tilde{v} \rangle_i^{j-\frac{1}{2}} - \langle \rho \tilde{v} \rangle_i^{j+\frac{1}{2}} \right] / \delta z - S_i^j \right\} .$$

When the velocity and density calculations are completed for all the fields in a cell, determine the new volume fractions of the less compressible fields (liquid and solid fields) by

$$\tilde{\alpha}_i^j = \tilde{\rho}_i^j / \rho' ,$$

where ρ' is the microscopic density at the temperature and pressure of the previous time step. This microscopic density is expected to remain fairly constant.

Thus far in the explicit part of the solution procedure, all calculations have been done independently for each field. However, the vapor fields, which are highly compressible, now need to be equilibrated in pressure (following the method described in Appendix A) such that their volume fractions add up to the volume fraction not occupied by the liquid and solid fields. This pressure equilibration yields both a new pressure for the vapor fields and a set of volume fractions corresponding to the equilbrium pressure.

Having obtained a new set of velocity, pressure, density and volume fraction distributions for all the fields in all

cells, one can begin the implicit part of the calculation and iterate toward the final values for this time step.

2. Implicit Calculation

The implicit part of the solution procedure consists of an iterative process dependent on the magnitude of the discrepancy, B, in the density transport equation. New pressures, densities and velocities are calculated based on the value of B, and the iteration continued until B is sufficiently small.

At the start of each iteration, one knows the velocity, pressure and density distributions for all the fields, either from the previous iteration or the initialization process. B can then be calculated from the density transport equation. For the vapor fields, which are highly compressible, B is given by

$$\tilde{B}_i^j = \left[\tilde{\rho}_i^j - \rho_i^j \right] / \delta t$$

$$+ \left[\langle \tilde{\rho}\tilde{u}r \rangle_{i+\frac{1}{2}}^{j} - \langle \tilde{\rho}\tilde{u}r \rangle_{i-\frac{1}{2}}^{j} \right] / (r_i \delta r)$$

$$+ \left[\langle \tilde{\rho}\tilde{v} \rangle_{i}^{j+\frac{1}{2}} - \langle \tilde{\rho}\tilde{v} \rangle_{i}^{j-\frac{1}{2}} \right] / \delta z$$

$$- S_i^j .$$

In the case of the essentially incompressible liquid and solid fields, the total derivative of the density can be taken to be zero, leading to a simpler expression for B as

$$\tilde{B}_i^j = \tilde{\rho}_i^j \left\{ \left[\tilde{u}_{i+\frac{1}{2}}^j r_{i+\frac{1}{2}} - \tilde{u}_{i-\frac{1}{2}}^j r_{i-\frac{1}{2}} \right] /(r_i \delta r) \right.$$

$$\left. + \left[\tilde{v}_i^{j+\frac{1}{2}} - \tilde{v}_i^{j-\frac{1}{2}} \right] /\delta z \right\} - S_i^j .$$

The pressures of each field are then incremented by a relaxation technique as

$$\delta \tilde{p}_i^j = -\omega \left(\frac{\partial \tilde{B}_i^j}{\partial \tilde{p}_i^j} \right)^{-1} \tilde{B}_i^j ,$$

where the derivative term is obtained by differentiating the density transport equation with respect to the pressure as shown in Appendix B. Since this is an iterative process, the derivative can be simplified for computational ease, as long as the convergence rate is not significantly retarded.

The equations of state are now used to calculate the microscopic densities related to the new pressures. These microscopic densities and the volume fractions from the previous iteration then yield the new macroscopic densities for the compressible fields.

For the less compressible fields the macroscopic density is evaluated as

$$\tilde{\rho}_i^j = \rho_i^j + \delta t \left\{ \left[\langle \rho \tilde{u} r \rangle_{i-\frac{1}{2}}^j - \langle \rho \tilde{u} r \rangle_{i+\frac{1}{2}}^j \right] /(r_i \delta r) \right.$$

$$\left. + \left[\langle \rho \tilde{v} \rangle_i^{j-\frac{1}{2}} - \langle \rho \tilde{v} \rangle_i^{j+\frac{1}{2}} \right] /\delta z - S_i^j \right\} .$$

All calculations thus far in the implicit part of the solution procedure have been essentially independent for each field. At this stage, then, the pressures of the compressible fields are equilibrated keeping their macroscopic densities constant, as described in Appendix A of this report. The process yields both an equilibrium pressure, and a new set of volume fractions corresponding to this pressure. The sum of the volume fractions of the compressible fields is the same before and after the equilibration. If the total volume fraction of the compressible fields is above a specified minimum value, the equilibrium pressure also serves as the pressure for the less compressible fields.

The new pressures, densities and volume fractions can now be used to calculate the velocity components independently for each field as

$$\tilde{u}^{j}_{i+\frac{1}{2}} = \left\{ (X_r)^{j}_{i+\frac{1}{2}} + \tilde{\alpha}^{j}_{i+\frac{1}{2}} \, \delta t \left[\tilde{p}^{j}_{i} - \tilde{p}^{j}_{i+1} \right] / \delta r \right.$$

$$\left. + \quad (D\tilde{d})^{j}_{i+\frac{1}{2}} \, \delta t \right\} \Big/ \left\{ \tilde{\rho}^{j}_{i+\frac{1}{2}} + D^{j}_{i+\frac{1}{2}} \, \delta t \right\} ,$$

and

$$\tilde{v}^{j+\frac{1}{2}}_{i} = \left\{ (X_z)^{j+\frac{1}{2}}_{i} + \tilde{\alpha}^{j+\frac{1}{2}}_{i} \, \delta t \left[\tilde{p}^{j}_{i} - \tilde{p}^{j+1}_{i} \right] / \delta z \right.$$

$$\left. + \quad (\tilde{Dv})^{j+\frac{1}{2}}_{i} \, \delta t + \tilde{\rho}^{j+\frac{1}{2}}_{i} \, g \, \delta t \right\} \Big/ \left\{ \tilde{\rho}^{j+\frac{1}{2}}_{i} + D^{j+\frac{1}{2}}_{i} \, \delta t \right\} .$$

In these expressions the velocities of the other fields used in the drag terms are the velocities from a previous iteration, i.e. they are changed only between iterations and the velocity of a just calculated field is not substituted in another field's calculation during an iteration. Once the new velocities are obtained for all the fields, the

value of B is calculated and the iteration repeated until B is sufficiently close to zero.

When this condition is reached, the densities are recalculated as

$$\tilde{\rho}_i^j = \rho_i^j + \delta t \left\{ \left[\langle \rho \tilde{u} r \rangle_{i-\frac{1}{2}}^j - \langle \rho \tilde{u} r \rangle_{i+\frac{1}{2}}^j \right] / (r_i \delta r) \right.$$

$$\left. + \left[\langle \rho \tilde{v} \rangle_i^{j-\frac{1}{2}} - \langle \rho \tilde{v} \rangle_i^{j+\frac{1}{2}} \right] / \delta z - S_i^j \right\} ,$$

with the volume fractions of the less compressible fields then being obtained from

$$\tilde{\alpha}_i^j = \tilde{\rho}_i^j / \rho' .$$

The compressible fields are equilibrated in pressure to yield a new pressure for the vapor fields and a set of volume fractions corresponding to the equilibrium pressure.

The equations of density and momentum transport have now been solved for that particular time step and one can proceed to the internal energy equation. Since the energy equation is in explicit form, it can be solved immediately using the latest known velocity, pressure and density distributions as explained in Section 3.3. The new temperatures are obtained from the internal energies using the specific heats. The microscopic densities of the compressible fields are updated at the new temperatures, and the corresponding macroscopic densities are evaluated using the volume fractions. The pressures of these compressible fields are then equilibrated to get an equilibrium pressure and a set of volume fractions corresponding to the new temperatures. This then results in a final set of values for the densities, pressures, internal energies and

velocities for each field for that time step.

The solution of the equations of motion and energy transfer can now be advanced through subsequent time steps by repeating the procedure described in this section. In this manner, the solution is carried through the desired length of time.

3.5 Stability Analysis

The finite difference schemes presented in the preceding sections for the equations of motion and energy transfer need to be examined for stability, to preclude diverging or oscillatory solutions. Linear difference equations, with constant coefficients, can be analyzed for stability using a well known Fourier method proposed by von Neuman[19]. However, the equations of interest are nonlinear with variable coefficients, and no standard method exists for their stability analysis. Some idea of their stability can be obtained from a modified analysis of a linear approximation of the equations, but this could be seriously in error.

Heuristic methods must be resorted to in order to gain an idea of the stability of these nonlinear equations. One such method proposed by Hirt[17] consists of reducing a finite difference equation to a differential equation by expanding each of its terms in a Taylor series. The lowest order terms in the expansion must represent the approximated differential equation. All higher order terms are truncation errors associated with the finite difference approximation. By comparison with known linear examples and test problems, Hirt demonstrates that stability conditions can be obtained from an examination of these truncation errors.

In the case of the equations of fluid mechanics, this truncation error technique requires that the coefficients of diffusion-like terms be positive for stability. The methods suggested by Hirt[17] and Warming[18] were carried out for the finite difference representations of the preceding sections. The process is too cumbersome to be detailed here, but is detailed in Appendix C. Only the final modified equations are presented here for the equations of density, momentum and energy transport. In each case, the coefficients of the diffusion-like terms on the right hand side of the equations must be positive for stability.

(i) density transport equation

$$\frac{\partial \rho}{\partial t} + \frac{1}{r}\frac{\partial}{\partial r}(\rho u r) + \frac{\partial}{\partial z}(\rho v) = S$$

$$+\left\{\frac{\delta t}{2}\left(u^2 + \frac{\partial p}{\partial \rho'}\right) + \frac{\delta t}{2}\left(\frac{\xi_1-\xi_2}{1+\delta t\,\frac{\partial S}{\partial \rho}}\right)\left[(\xi_1-\xi_2-1)\,u^2 + (\xi_1+\xi_2)\,\frac{\delta r}{2}\,u\,\frac{\partial u}{\partial r}\right]\right.$$

$$\left. + (\xi_1-\xi_2-1)\,\frac{(\delta r)^2}{4}\,\frac{\partial u}{\partial r} + \frac{\delta r}{2}\,(\xi_1+\xi_2)\,u\right\}\frac{\partial^2 \rho}{\partial r^2}$$

$$+\left\{\frac{\delta t}{2}\left[u^2 - \left(\frac{\xi_1-\xi_2}{1+\delta t\,\frac{\partial S}{\partial \rho}}\right)u^2 + \frac{\partial p}{\partial \rho'}\right] + (\xi_1-\xi_2-1)\frac{(\delta r)^2}{4}\,\frac{\partial u}{\partial r} + \frac{\delta r}{2}\,(\xi_1+\xi_2)\,u\right\}\frac{1}{r}\,\frac{\partial \rho}{\partial r}$$

$$+\left\{\frac{\delta t}{2}\left(v^2 + \frac{\partial p}{\partial \rho'}\right) + \frac{\delta t}{2}\left(\frac{\xi_3-\xi_4}{1+\delta t\,\frac{\partial S}{\partial \rho}}\right)\left[(\xi_3-\xi_4-1)\,v^2 + (\xi_3+\xi_4)\,\frac{\delta z}{2}\,v\,\frac{\partial v}{\partial z}\right]\right.$$

$$\left. + (\xi_3-\xi_4-1)\,\frac{(\delta z)^2}{4}\,\frac{\partial v}{\partial z} + \frac{\delta z}{2}\,(\xi_3+\xi_4)\,v\right\}\frac{\partial^2 \rho}{\partial z^2},$$

where

$$\xi_1 = \left(\beta_0 \frac{\delta t}{\delta r}\right) {}^{n+1}u^{j}_{i+e} + \theta_0 \, \text{sign}\left({}^{n+1}u^{j}_{i+e}\right)$$

$$\xi_2 = \left(\beta_0 \frac{\delta t}{\delta r}\right) {}^{n+1}u^{j}_{i-e} + \theta_0 \, \text{sign}\left({}^{n+1}u^{j}_{i-e}\right)$$

$$\xi_3 = \left(\beta_0 \frac{\delta t}{\delta z}\right) {}^{n+1}v^{j+e}_{i} + \theta_0 \, \text{sign}\left({}^{n+1}v^{j+e}_{i}\right)$$

$$\xi_4 = \left(\beta_0 \frac{\delta t}{\delta z}\right) {}^{n+1}v^{j-e}_{i} + \theta_0 \, \text{sign}\left({}^{n+1}v^{j-e}_{i}\right)$$

$$e = 1/2.$$

(ii) radial direction momentum transport equation

$$\frac{\partial \rho u}{\partial t} + \frac{1}{r}\frac{\partial}{\partial r}(\rho u u r) + \frac{\partial}{\partial z}(\rho u v) = N_r - \alpha \frac{\partial p}{\partial r} + D(\bar{u}-u)$$

$$+\left\{\frac{2}{3r}\left[\mu \frac{\partial v}{\partial z} - u \frac{\partial \mu}{\partial r} - 2\frac{\mu u}{r}\right] + \frac{4}{3}\frac{\partial \mu}{\partial r}\frac{\partial u}{\partial r} + \frac{\partial \mu}{\partial z}\frac{\partial u}{\partial z} - \frac{2}{3r}\frac{\partial}{\partial r}\left(\mu r \frac{\partial v}{\partial z}\right) + \frac{\partial}{\partial z}\left(\mu \frac{\partial v}{\partial r}\right)\right\}$$

$$+\left\{\frac{\delta t}{2}\left(\frac{\rho}{\rho + D\delta t}\right)(1-\xi_1+\xi_2)\left[\delta t D u^2 + (\xi_1-\xi_2-1)\rho u^2\right.\right.$$

$$\left. + (\xi_1+\xi_2)\frac{\delta r}{2}\left(3u^2\frac{\partial \rho}{\partial r} + \rho u \frac{\partial u}{\partial r}\right)\right] + \frac{\delta t}{2}\rho \frac{\partial p}{\partial \rho'} + \frac{4}{3}\mu$$

$$\left. + (\delta r)^2 (\xi_1-\xi_2-1)\left[\frac{3}{4}u\frac{\partial \rho}{\partial r} + \frac{1}{2}\rho\frac{\partial u}{\partial r}\right] + \frac{\delta r}{2}(\xi_1+\xi_2)\rho u\right\}\frac{\partial^2 u}{\partial r^2}$$

$$+\left\{\frac{\delta t}{2}\left(\frac{\rho}{\rho+D\delta t}\right)\left[\delta t D u^2 + (\xi_1-\xi_2-1)\rho u^2 + (\xi_1+\xi_2)\frac{\delta r}{2}\left(3u^2\frac{\partial \rho}{\partial r} + \rho u \frac{\partial u}{\partial r}\right)\right]\right.$$

$$+ \frac{\delta t}{2}\rho\frac{\partial p}{\partial \rho'} + \frac{4}{3}\mu + (\delta r)^2(\xi_1-\xi_2-1)\left[\frac{3}{4}u\frac{\partial \rho}{\partial r} + \frac{1}{4}\rho\frac{\partial u}{\partial r}\right]$$

$$\left. + \frac{\delta r}{2}(\xi_1+\xi_2)\rho u\right\}\frac{1}{r}\frac{\partial u}{\partial r}$$

$$+\left\{\frac{\delta t}{2}\left(\frac{\rho}{\rho+D\delta t}\right)(1-\xi_3+\xi_4)\left[(\xi_3-\xi_4-1)\,\rho v^2+(\xi_3+\xi_4)\frac{\delta z}{2}\left(2v^2\frac{\partial\rho}{\partial z}+\rho v\frac{\partial v}{\partial z}\right)\right]\right.$$

$$\left.+\mu+(\delta z)^2(\xi_3-\xi_4-1)\left[\frac{1}{2}v\frac{\partial\rho}{\partial z}+\frac{1}{4}\rho\frac{\partial v}{\partial z}\right]+\frac{\delta z}{2}(\xi_3+\xi_4)\rho v\right\}\frac{\partial^2 u}{\partial z^2}\,.$$

where

$$\xi_1=\left(\beta_0\frac{\delta t}{\delta r}\right)^n u_{i+1}^j+\theta_0\,\mathrm{sign}\left({}^n u_{i+1}^j\right)$$

$$\xi_2=\left(\beta_0\frac{\delta t}{\delta r}\right)^n u_{i}^j+\theta_0\,\mathrm{sign}\left({}^n u_{i}^j\right)$$

$$\xi_3=\left(\beta_0\frac{\delta t}{\delta z}\right)^n v_{i+e}^{j+e}+\theta_0\,\mathrm{sign}\left({}^n v_{i+e}^{j+e}\right)$$

$$\xi_4=\left(\beta_0\frac{\delta t}{\delta z}\right)^n v_{i+e}^{j-e}+\theta_0\,\mathrm{sign}\left({}^n v_{i+e}^{j-e}\right)\,.$$

(iii) <u>axial direction momentum transport equation</u>

$$\frac{\partial\rho v}{\partial t}+\frac{1}{r}\frac{\partial}{\partial r}(\rho uvr)+\frac{\partial}{\partial z}(\rho vv)=N_z-\alpha\frac{\partial p}{\partial z}+D(\bar{v}-v)+\rho g$$

$$+\left\{\frac{\partial\mu}{\partial r}\frac{\partial v}{\partial r}+\frac{4}{3}\frac{\partial\mu}{\partial z}\frac{\partial v}{\partial z}+\frac{1}{r}\left[\frac{\partial}{\partial r}\left(r\mu\frac{\partial u}{\partial z}\right)-\frac{2}{3}\frac{\partial}{\partial z}\left(\mu\frac{\partial}{\partial r}(ur)\right)\right]\right\}$$

$$+\left\{\frac{\delta t}{2}\left(\frac{\rho}{\rho+D\delta t}\right)(1-\xi_1+\xi_2)\left[(\xi_1-\xi_2-1)\,\rho u^2+(\xi_1+\xi_2)\frac{\delta r}{2}\left(2u^2\frac{\partial\rho}{\partial r}+\rho u\frac{\partial u}{\partial r}\right)\right]\right.$$

$$\left.+\mu+(\delta r)^2(\xi_1-\xi_2-1)\left(\frac{1}{2}u\frac{\partial\rho}{\partial r}+\frac{1}{4}\rho\frac{\partial u}{\partial r}\right)+\frac{\delta r}{2}(\xi_1+\xi_2)\rho u\right\}\frac{\partial^2 v}{\partial r^2}$$

$$+\left\{\frac{\delta t}{2}\left(\frac{\rho}{\rho+D\delta t}\right)\left[(\xi_1-\xi_2-1)\,\rho u^2+(\xi_1+\xi_2)\frac{\delta r}{2}\left(2u^2\frac{\partial\rho}{\partial r}+\rho u\frac{\partial u}{\partial r}\right)\right]\right.$$

$$\left.+\mu+(\delta r)^2(\xi_1-\xi_2-1)\left(\frac{1}{2}u\frac{\partial\rho}{\partial r}+\frac{1}{4}\rho\frac{\partial u}{\partial r}\right)+\frac{\delta r}{2}(\xi_1+\xi_2)\rho u\right\}\frac{1}{r}\frac{\partial v}{\partial r}$$

$$+\left\{\frac{\delta t}{2}\left(\frac{\rho}{\rho+D\delta t}\right)(1-\xi_3+\xi_4)\left[(Dv^2-\rho gv)\,\delta t + (\xi_3-\xi_4-1)\,\rho v^2\right.\right.$$

$$\left.+(\xi_3+\xi_4)\,\frac{\delta z}{2}\left(3v^2\,\frac{\partial\rho}{\partial z}+\rho v\,\frac{\partial v}{\partial z}\right)\right]+\frac{\delta t}{2}\,\rho\,\frac{\partial p}{\partial \rho'}+\frac{4}{3}\,\mu$$

$$\left.+(\delta z)^2\,(\xi_3-\xi_4-1)\left(\frac{3}{4}\,v\,\frac{\partial\rho}{\partial z}+\frac{1}{2}\,\rho\,\frac{\partial v}{\partial z}\right)+\frac{\delta z}{2}\,(\xi_3+\xi_4)\,\rho v\right\}\frac{\partial^2 v}{\partial z^2}\,,$$

where

$$\xi_1 = \left(\beta_0\,\frac{\delta t}{\delta r}\right)^{n}u_{i+e}^{j+e} + \theta_0\,\mathrm{sign}\left(^{n}u_{i+e}^{j+e}\right)$$

$$\xi_2 = \left(\beta_0\,\frac{\delta t}{\delta r}\right)^{n}u_{i-e}^{j+e} + \theta_0\,\mathrm{sign}\left(^{n}u_{i-e}^{j+e}\right)$$

$$\xi_3 = \left(\beta_0\,\frac{\delta t}{\delta z}\right)^{n}v_{i}^{j+1} + \theta_0\,\mathrm{sign}\left(^{n}v_{i}^{j+1}\right)$$

$$\xi_4 = \left(\beta_0\,\frac{\delta t}{\delta z}\right)^{n}v_{i}^{j} + \theta_0\,\mathrm{sign}\left(^{n}v_{i}^{j}\right)\,.$$

(iv) internal energy transport equation

$$\frac{\partial\rho I}{\partial t}+\frac{1}{r}\,\frac{\partial}{\partial r}\,(\rho u I r)+\frac{\partial}{\partial z}\,(\rho v I) = -\,\frac{p}{r}\,\frac{\partial}{\partial r}\,(\alpha u r)-p\,\frac{\partial}{\partial z}\,(\alpha v)+Q$$

$$+H\,(\bar{T}-T)+\mu\Phi+\Lambda+\frac{\partial}{\partial r}\,(k\alpha)\,\frac{\partial T}{\partial r}+\frac{\partial}{\partial z}\,(k\alpha)\,\frac{\partial T}{\partial z}$$

$$+\left\{\frac{\delta t}{2}\,(1-\xi_1+\xi_2)\left[(\xi_1-\xi_2-1)\,\rho u^2+(\xi_1+\xi_2)\,\frac{\delta r}{2}\left(2u^2\,\frac{\partial\rho}{\partial r}+\rho u\,\frac{\partial u}{\partial r}\right)\right]\right.$$

$$\left.+k\alpha\,\frac{\partial T}{\partial I}+(\xi_1-\xi_2-1)\,(\delta r)^2\left(\frac{1}{2}\,u\,\frac{\partial\rho}{\partial r}+\frac{1}{4}\,\rho\,\frac{\partial u}{\partial r}\right)+\frac{\delta r}{2}\,(\xi_1+\xi_2)\,\rho u\right\}\frac{\partial^2 I}{\partial r^2}$$

$$+\left\{\frac{\delta t}{2}\left[(\xi_1-\xi_2-1)\,\rho u^2+(\xi_1+\xi_2)\,\frac{\delta r}{2}\left(2u^2\,\frac{\partial\rho}{\partial r}+\rho u\,\frac{\partial u}{\partial r}\right)\right]+k\alpha\,\frac{\partial T}{\partial I}\right.$$

$$+ (\xi_1-\xi_2-1)\ (\delta r)^2\left(\frac{1}{2}\ u\ \frac{\partial \rho}{\partial r} + \frac{1}{4}\ \rho\ \frac{\partial u}{\partial r}\right) + \frac{\delta r}{2}\ (\xi_1+\xi_2)\ \rho u\Bigg\}\frac{1}{r}\ \frac{\partial I}{\partial r}$$

$$+\Bigg\{\frac{\delta t}{2}\ (1-\xi_3+\xi_4)\left[(\xi_3-\xi_4-1)\ \rho v^2 + (\xi_3+\xi_4)\ \frac{\delta z}{2}\left(2v^2\ \frac{\partial \rho}{\partial z} + \rho v\ \frac{\partial v}{\partial z}\right)\right]$$

$$+ k\alpha\ \frac{\partial T}{\partial I} + (\xi_3-\xi_4-1)\ (\delta z)^2\left(\frac{1}{2}\ v\ \frac{\partial \rho}{\partial z} + \frac{1}{4}\ \rho\ \frac{\partial v}{\partial z}\right) + \frac{\delta z}{2}\ (\xi_3+\xi_4)\ \rho v\Bigg\}\frac{\partial^2 I}{\partial z^2}\ ,$$

where

$$\xi_1 = \left(\beta_0\ \frac{\delta t}{\delta r}\right)^n u_{i+e}^j + \theta_0\ \text{sign}\left({}^n u_{i+e}^j\right)$$

$$\xi_2 = \left(\beta_0\ \frac{\delta t}{\delta r}\right)^n u_{i-e}^j + \theta_0\ \text{sign}\left({}^n u_{i-e}^j\right)$$

$$\xi_3 = \left(\beta_0\ \frac{\delta t}{\delta z}\right)^n v_i^{j+e} + \theta_0\ \text{sign}\left({}^n v_i^{j+e}\right)$$

$$\xi_4 = \left(\beta_0\ \frac{\delta t}{\delta z}\right)^n v_i^{j-e} + \theta_0\ \text{sign}\left({}^n v_i^{j-e}\right)\ .$$

3.6 Boundary Conditions

A variety of boundary conditions can be applied to the fuel motion model. In this Section are presented some conditions for the velocity and temperature at the container boundaries for a confined flow problem. The implicit treatment of the pressure and velocity, as detailed in Section 3.4, despenses with the need for pressure boundary conditions.

Boundary conditions also need to be used within the container itself, as for example, between a substantial solid region and a liquid or a vapor region. These conditions are similar to those at the container boundaries, and the method of numerical application is analogous.

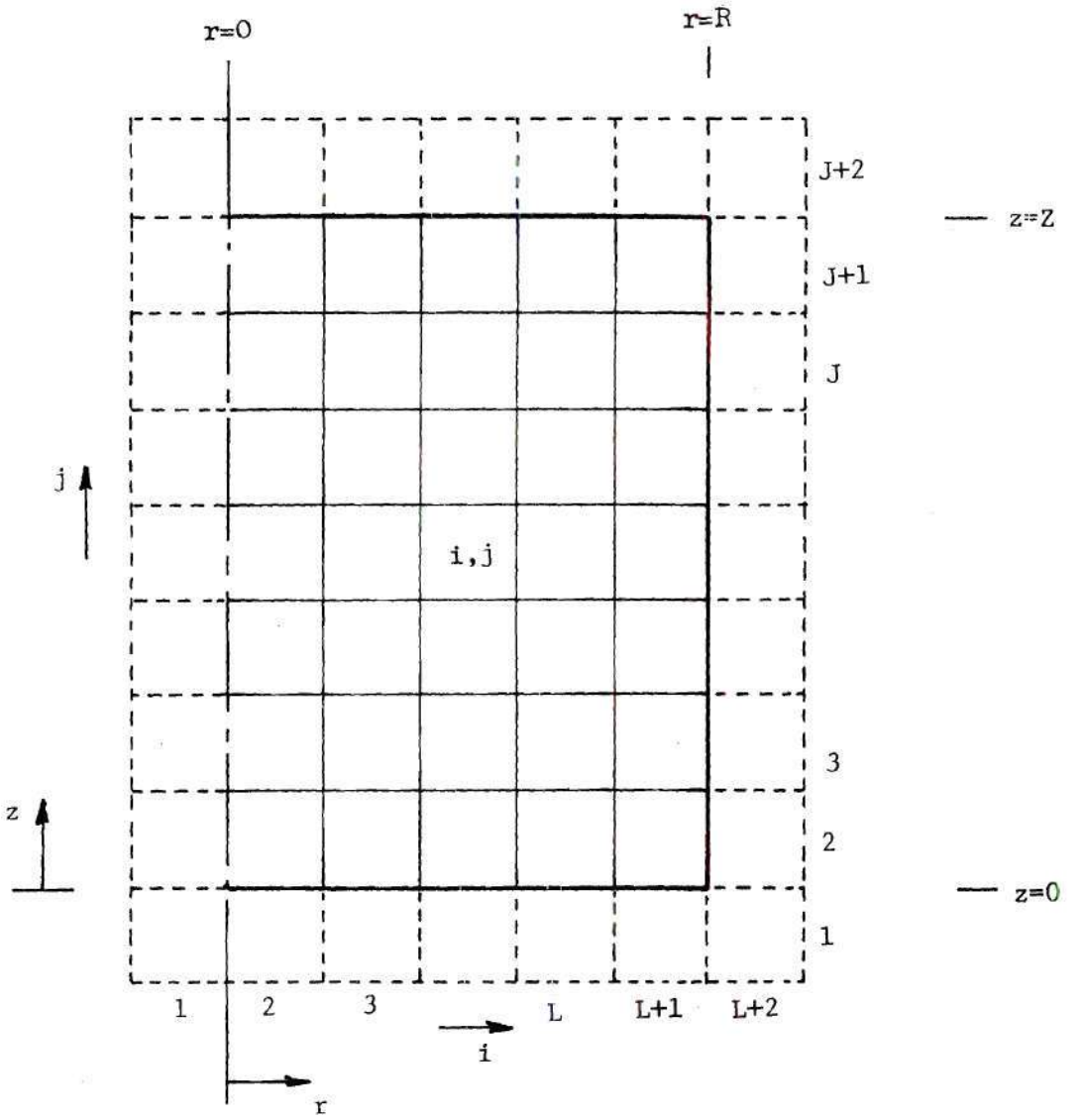

FIGURE 3. Cell Numbering

The numerical application of boundary conditions at the container boundaries is greatly simplified by the introduction of a fictitious band of cells on all four sides of the mesh, as shown in the planar view in Figure 3. In this case, the real mesh consists of J cells in the axial direction and L cells along the radius, indexed as indicated.

The transport equations require two boundary conditions in r and two in z for the temperature and both velocity components. These boundary conditions and their numerical forms are presented below.

1. radial velocity

Along r: $$\left.\frac{\partial u}{\partial r}\right|_{r = 0} = 0$$

$$u\Big|_{r = R} = 0$$

Along z: $$u\Big|_{z = 0} = u\Big|_{z = Z} = 0 \quad \text{[no slip for solids and liquids]}$$

or

$$\left.\frac{\partial u}{\partial z}\right|_{z = 0} = \left.\frac{\partial u}{\partial z}\right|_{z = Z} = 0 \quad \text{[free slip for vapor]}$$

In numerical form these conditions become

Along r: $$u^{j}_{1-\frac{1}{2}} = u^{j}_{2+\frac{1}{2}}$$

$$u^{j}_{L+\frac{3}{2}} = 0$$

Along z:

$$u^{1}_{i+\frac{1}{2}} = -\,u^{2}_{i+\frac{1}{2}}$$

$$u^{J+2}_{i+\frac{1}{2}} = -\,u^{J+1}_{i+\frac{1}{2}}$$

} no slip

$$u^{1}_{i+\frac{1}{2}} = u^{2}_{i+\frac{1}{2}}$$

$$u^{J+2}_{i+\frac{1}{2}} = u^{J+1}_{i+\frac{1}{2}}$$

} free slip

2. axial velocity

Along r: $v\big|_{r = R} = 0$ [no slip]

or

$$\left.\frac{\partial v}{\partial r}\right|_{r = R} = 0$$ [free slip]

and $$\left.\frac{\partial v}{\partial r}\right|_{r = 0} = 0$$

Along z: $v\big|_{z = 0} = 0$

$$v\big|_{z = Z} = 0$$

In numerical form these conditions become

Along r:

$$v^{j+\frac{1}{2}}_{L+2} = -\,v^{j+\frac{1}{2}}_{L+1}$$ [no slip]

or

$$v^{j+\frac{1}{2}}_{L+2} = v^{j+\frac{1}{2}}_{L+1}$$ [free slip

and

$$v_1^{j+\frac{1}{2}} = v_2^{j+\frac{1}{2}}$$

Along z:

$$v_i^{1+\frac{1}{2}} = 0$$

$$v_i^{J+\frac{3}{2}} = 0.$$

3. temperature (energy)

$$\left.\frac{\partial T}{\partial r}\right|_{r = 0} = 0.$$

At the other three boundaries specify

(i) constant T

or (ii) heat transfer coefficient and environment temperature. For example, the other three boundary conditions could be

$$T\Big|_{z = 0} = T_o$$

$$T\Big|_{z = Z} = T_Z$$

$$-k \left.\frac{\partial T}{\partial r}\right|_{r = R} = h \left[T\Big|_{r = R} - T_e \right]$$

where k = thermal conductivity

h = heat transfer coefficient

T_e = environment temperature.

In numerical form the first three conditions become

$$T_2^j = T_1^j$$

$$T_i^1 = 2T_o - T_i^2$$

$$T_i^{J+2} = 2T_Z - T_i^{J+1}$$

The last boundary condition, involving the heat transfer coefficient, takes the form

$$-k\left[T_{L+2}^j - T_{L+1}^j\right]/\delta r = h\left[\frac{1}{2}(T_{L+2}^j + T_{L+1}^j) - T_e\right]$$

which can be rearranged to give

$$T_{L+2}^j = \left\{\left(1 + \frac{h\ \delta r}{k}\right) T_{L+1}^j + \left(\frac{h\ \delta r}{k}\right) T_e\right\} / \left(1 + \frac{h\ \delta r}{k}\right).$$

CHAPTER IV

RESULTS

The numerical scheme for analyzing fuel motion has been programmed for use on the CDC Cyber 70/Model 74 at the Georgia Institute of Technology. This program, written in FORTRAN 4 and named PLOFA, is designed for the efficient solution of multi-field confined flow problems. Though geared for a seven material loss-of-flow problem, PLOFA has been designed to allow the inclusion of additional materials without substantial difficulty, and it can be modified for use in a wide variety of flow situations. The basic PLOFA setup is described in Section 4.1, while Section 4.2 summarizes previously documented tests of PLOFA. Two dimensional and one dimensional calculations of a multi-field case, beginning with a solid and proceeding through melting and liquid vaporization is presented in Section 4.3.

4.1 Basic PLOFA Setup

The program begins by requesting input data describing the mesh, material properties and specifications, and output frequencies. Material information is input region-wise, rather than cell-wise, where a region is defined as being a rectangular region (in the radial-axial cross section) comprising an integer number of cells with non-varying material data.

Once the input data processing is completed, the code begins the hydrodynamics by calculating the explicit terms in the momentum transport equations. Velocity fields are then initialized, the macroscopic densities are computed from the density transport equations, followed by volume fractions and pressures corresponding to these densities. The implicit part of the calculations is now begun and an iterative solution obtained to the momentum and density transport equations. The specific internal energy is then directly obtained from an explicit solution of the energy transport equation.

At the end of a cycle, if the problem time matches an output request time, output processing takes place and the user is supplied with printed and/or graphic output as desired.

The calculational cycles have been written to minimize mathematical operations that require longer processor times, and transform them into ones which require shorter processor times. All subroutines are without arguments, thus considerably decreasing the processor time involved in a CALL statement. Information transfer is achieved via COMMON and EQUIVALENCE blocks, which also serve to reduce computer core requirements. Each subroutine has multiple entry points, which further contribute to programming efficiency.

While the motion studied is two dimensional, and it might therefore seem appropriate to have doubly dimensioned variables, the use of multiply dimensioned variables in a high level language such as FORTRAN appears to be a needless drain on processor time. PLOFA reduces all multiply dimensioned variables to singly dimensioned variables, without

sacrificing the increased readability associated with multiple indices. This is done by using meaningful representations for the single indices, and computing all neighboring indices in terms of a single cell index. Also, half indices, required by the vector velocity fields, are handled by the same cell index as for the scalar fields. The program automatically picks the correct position (cell center or cell edge) depending on the variable.

In spite of the tremendous care taken to reduce PLOFA's memory requirements, it has always been realized that cases can very easily be reached where execution of PLOFA would necessitate using a very high fraction of available computer core, causing unnecessarily slow processing in the multi-processing environment of most large computers. Further, it might require more core than is available on a university type computer with tight budgetary restrictions. PLOFA has therefore been designed to run either in the standard form (where core requirements are dictated by the problem being run) or in a limited small size core. The latter option (which can be selected via the input data) is achieved by keeping in core only the row of cells being processed, its immediate lower neighbor and its immediate upper two neighbors. When the current row calculation has ended, its lower neighbor which is now no longer needed is stored on disk and a single new row of data is entered in its place. By a dexterous handling of the cell and row indices, PLOFA eliminates any need for reshuffling data when a new row is read in. Sequential files are used for this type of information transfer between disk and core. However, the output plot processing

requires data from cells in a non-regular fashion (unlike the hydrodynamics calculations) which would be highly inefficient with sequential files. Random access files, with proper indexing, are used in such cases to achieve efficient use of processor time.

4.2 Prior PLOFA Tests

It is essential in the formation of a complex computer program that constant tests be made to check the accuracy of the programming and determine the workability of the program. This philosophy has been basic to the development of PLOFA. Included in the experimentation have been comparisons with the results of (1) a computer program written at the Los Alamos Scientific Laboratory, (2) an analytical solution, (3) an approximate analytical solution, and (4) results presented at a technical review meeting. All of these cases have been described in previous reports[21,22,25] and are summarized in this section.

Early in its development, a simple version of PLOFA was compared with the two field KACHINA[20] fluid flow program. In this test case, documented in Reference 21, a vapor-liquid mixture initially at rest and nonuniformly distributed in a closed cylinder was studied as a function of time. PLOFA's calculations of the behavior of this mixture compared well with KACHINA calculations.

Comparison with an analytical solution of a fluid dynamics problem was performed by testing PLOFA against the exact starting flow solution of Szymanski[23]. Here, fluid which is initially at rest in a long pipe of circular cross section is suddenly subjected to a constant

pressure gradient. The fluid begins to move under the influence of viscous and inertial forces, with the velocity profile asymptotically approaching the parabolic distribution in Hagen-Poiseuille flow. Essentially perfect agreement[22] was obtained with the published results of Szymanski[23].

In yet another test, PLOFA was used to calculate the flow in an internal natural convection problem. A closed circular cylinder is completely filled with fluid which is initially in a stably-stratified state of rest. The temperature of the container walls is then impulsively changed, such that the upper half of the wall is heated with a linearly increasing temperature distribution, and the bottom half cooled with a linearly decreasing distribution. PLOFA results for the flow that develops are documented in Reference 22. An approximate analytical solution to this problem has been obtained by Jischke and Doty[24]. PLOFA calculations do not agree quantitatively with this solution because of the many approximations made by Jischke and Doty in attempting to derive an analytical solution to a complex flow problem. However, qualitative predictions made by both models are in unison.

A totally compressible mixture of fission gas and fuel vapor, initially at rest and non-uniformly distributed in a closed cylinder, formed the basis for another problem studied by PLOFA. The transient distributions of velocity, volume fraction, density, pressure and temperature that develop have been described in a previous report[25]. These results were also presented and discussed at a technical review

meeting attended by internal ERDA reviewers and external invited reviewers from the Los Alamos Scientific Laboratory, Argonne National Laboratory, Hanford Engineering and Development Laboratory, and General Electric.

4.3 One and Two Dimensional Loss-of-Flow Accident Results

This section presents the results of the initiation phase of an LMFBR loss-of-flow accident using a two dimensional fluid dynamics model, and compares these calculations with one dimensional modeling. At the start of the accident the fuel is enclosed in solid steel cladding. Both materials are undergoing a temperature increase because of the cessation of sodium coolant flow to the model channel as a result of some catastrophic event. The steel melts first, followed by center line fuel melting which proceeds radially outward. Eventually, partial fuel vaporization occurs in the center of the channel. The accident initiation phase is ended soon thereafter, to give way to whole core treatment during the core disruption state.

The accident analysis described in this section lacks direct reactivity feedback due to fuel motion. This is because PLOFA was designed with the objective of being part of an overall safety analysis system of codes. In such a system, the fuel motion module would receive neutronic feedback from the reactivity modules in the code. The effect of the neutronic coupling would be to increase the disuniformity in the power generation, adding further to the need for two dimensional modeling of fuel motion.

(a) Two Dimensional Results

The closed cylindrical region, constituting the model channel, is divided into 6 equal radial cells and 7 axial cells. The mesh spacing was chosen from past experience with similar problems, wherein it was observed that this choice of a mesh could accurately represent the derivatives that had been numerically approximated in the finite difference equations, without wasting valuable computer core storage. The cylinder is zoned into four PLOFA regions [each region being an annular region comprising an integer number of cells with non-varying material data], as shown in the half cylinder of Figure 4.

Region 1 is a solid fuel [80%] region with confined fission gas [20%]. It encompasses the first 5 cells radially, and all cells axially. As shown in Figure 87, a parabolic temperature distribution is imposed both axially and radially, with a 300°K axial temperature difference between the mid-axial region and the two ends of the cylinder, and about 700°K temperature difference radially. The hottest temperature of 2500°K is on the centerline at the mid-axial location, while the minimum temperature, 1560°K is at the top and bottom right extremity of the region. The pressure of the enclosed fission gas, assumed to be in thermal equilibrium with the fuel, is set at 1 atmosphere and its density calculated from its equation of state.

The last radial column is divided into three PLOFA regions: 2,3, 4. Region 3 contains solid steel [60%] and fission gas [40%], while regions 2 and 4 contain 90% solid steel and 10% fission gas. As indicated in Figure 90, an axially symmetric parabolic temperature distribution, with a temperature difference of 100°K is imposed on this

steel column. The highest temperature of 1600°K is at mid-height. The pressure of the enclosed fission gas, assumed to be in thermal equilibrium with the steel, is set at 1 atmosphere and its density calculated from its equation of state.

Starting with this configuration, an initial heating rate of 100 watts per gram is applied to the fuel to account for nuclear heating effects in the initial stages of the loss-of-flow accident prior to fuel melting. This energy generation is distributed parabolically, both radially and axially; the radial variation being 10% and the axial variation 5%. The only mode of heat transfer in this early stage of the accident is via conduction in the fuel, and by contact conductance between fuel and steel. After 2.049 seconds the steel has entirely melted in region 3, whereupon the heat generation rate is increased by a factor of 10^3 to account for the expected increase in accident severity as a result of material motion. This increase in the heating rate is probably higher, by a factor of 5 or 10, than what might be expected in a typical accident situation. The high value is chosen here to represent a severe accident, in which fuel vaporization occurs within a short period of time, so that the effect of vapor formation on subsequent motion might be studied. The heat generation term now dominates other terms in the internal energy equation for the short time [3.15 milliseconds] left in the problem.

As the accident progresses, fuel also begins to melt in Region 1. Eventually all fuel has melted except for the single radial annulus adjacent to the steel. The heat generated is sufficient to cause partial fuel vaporization in the hottest cell (located at the mid-

axial region along the centerline). The accident is allowed to continue approximately 0.07 milliseconds, at which time conditions indicate the initiation phase is essentially complete, and whole core analysis needs to be applied in the next part of the accident, the core disruption stage. During this transient stage of vapor formation, a high pressure develops in the center, forcing material out toward the lower pressure regions. The problem time steps are reduced at this stage to handle the severe transient. During this very short period of time the fuel vapor is driven at high velocities into neighboring regions, but has little opportunity to reach thermal equilibrium with the other materials in those regions. The continued generation of vapor maintains the high pressure in the hot cell, and almost all the fission gas initially there is rapidly pushed out into neighboring cells.

At problem termination time [2.052 seconds] the cylinder contains molten steel and fission gas in the outer-most radial annulus, with the top and bottom cells in this annulus still containing solid steel at the fusion temperature, but not having received enough heat in the short transient to equal the latent heat of fusion. Adjacent to the steel column is a column of solid fuel and trapped fission gas, again at the fusion temperature but lacking enough heat for complete melt-through. The rest of the cylinder contains molten fuel and fission gas, with vapor fuel being generated in the center and driven under high pressures towards the neighboring regions.

The results of the two dimensional calculations as the problem progresses through time till problem termination at 2.052 seconds are shown in Figures 5 through 92. Velocities are plotted vectorially in

the half cylinder, with arrows denoting both direction and relative magnitudes. Three dimensional scalar plots are made for the volume fraction, macroscopic density, pressure and temperature of each field.

Velocity plots are shown in Figures 5 through 26. The velocities are averaged at the center of each cell, with the direction of an arrow indicating the direction of flow and the length indicating the relative magnitude of the velocity in that cell compared to the other cells. Steel and fission gas velocities are shown both after steel melting and after fuel vaporization, while fuel velocities appear only after fuel vaporization.

Figures 5 through 9 present the liquid fuel velocities shortly after fuel vaporization. Prior to this, the liquid fuel had been moving in a downward direction under the action of gravitational forces. Fuel vaporization in the hottest cell creates a high pressure region, and this pressure differential forces liquid to move outward from that region. Thus, there is very substantial radial motion at the mid-axial location, and part of the downward motion just above this location has actually turned around because of the high pressure. The velocities in regions further away are much smaller than the central velocities.

Liquid steel velocities are shown in Figure 10 just after steel melting, and in Figures 11 through 15 after fuel vaporization. The steel is still separated from the liquid and vapor fuel by a column of solid fuel, and so is unaffected by fuel vaporization at the center. It retains its downward velocity throughout the problem.

The vaporization of fuel in the hot cell creates a large pressure build-up in this cell, and the pressure differential forces material

towards the low pressure regions. This is well demonstrated in Figures 16 through 20 which show the convection of vapor fuel into regions further away from the center as time progresses. The large pressure difference results in high velocities, on the order of 100 metres per second. Motion is very substantial radially as material is forced away from the central high pressure region.

Figure 21 shows the fission gas velocity slightly after steel melting, while Figures 22 through 26 depict the velocities after fuel vaporization. Along the outer boundary of the cylinder (the steel region) the velocity of the fission gas is downward at first, due to initial drag by the molten steel, but then moves slowly upward because of buoyancy effects. This velocity is not discernible after fuel vaporization, since its magnitude is negligible compared to the high velocity in the center. In the inner region the fission gas is rapidly pushed away from the hot cell, which is almost immediately devoid of fission gas, and travels into the lower pressure regions surrounding the center.

Scalar property distributions appear in Figures 27 through 92. These are three dimensional representations, with the maximum value normalized to 1.0 in each non-zero plot. Values are again plotted at the center of each cell. The ratio of the height to the width of a cell is taken to be 1.0 for plotting purposes only, so that radial differences may be viewed more clearly. Plotting times are at the start of the problem (0.0 seconds), slightly after steel melting (2.04889 seconds), and the end of the problem (2.05204 seconds).

Volume fractions of the various fields are shown in Figures 27 through 44. Figures 27 through 29 depict the liquid fuel volume fraction.

There is no fuel at the beginning of the problem and slightly after steel melting. Only later, when the heat generated is sufficient to melt the fuel, does the volume fraction become non-zero. By the time of fuel vaporization, the fuel has melted everywhere it was initially present except for a single annulus immediately adjacent to the steel. Thus the final plot (Figure 29) at the end of the problem shows liquid fuel in all the first 4 radial annuli. There is a small dip in the center because of partial vaporization.

Liquid steel volume fractions are shown in Figures 30 through 32. No liquid exists at the start, but after two seconds the solid steel melts in the inner 5 axial regions as shown in Figure 31, and remains this way till the end of the calculations, there being no further steel melting and no vaporization.

Figures 33 through 35 present the volume fraction of the vapor fuel, which is produced late in the accident sequence. Figure 35 shows the distribution at the end of the problem. The volume fraction is maximum in the hot cell, and declines in the 3 radial and 2 upper axial and 2 lower axial neighboring cells into which it has convected.

Fission gas volume fractions are shown in Figures 36 through 38. The initial distribution (Figure 36) is uniform in the fuel region, higher in the inner steel region and lower in the outermost axial steel regions. The distribution just after steel melting is unchanged. By the end of the problem, the distribution in the steel region is still relatively unchanged, but the fuel region has undergone substantial change. Fission gas has been forced out of the hot cell by the high

pressure due to fuel vaporization and pushed into the neighboring cells, leading to the large dip in Figure 38.

Figures 39 through 41 show the solid fuel volume fraction. It is uniform initially, and slightly after steel melting. However, by the time of fuel vaporization it has melted in all cells except the single radial annulus adjacent to the steel region, and remains this way till the end of the problem as depicted in Figure 41.

The solid steel volume fractions are pictured in Figures 42 through 44. Steel is initially present in a single radial annulus at the boundary, with more of it concentrated at the top and bottom as shown in the fortress wall like structure of Figure 42. After about 2 seconds the steel in the inner axial regions has melted by heat transferred from the fuel. Only the top and bottom axial cells are solid, as shown in Figure 43, and the situation is essentially unchanged at the end of the problem time (Figure 44).

The macroscopic densities of the various fields are shown in Figures 45 through 62. These distributions resemble the volume fractions, but whereas the volume fractions are initially uniform in a specified region, the densities are non-uniform because they are also dependent on the initially non-uniform temperature distributions.

Figures 63 through 74 depict the pressure distributions of the various fields. Liquid fuel pressures are shown in Figures 63 through 65. There is no molten fuel until substantially after steel melting, and by the end of the problem the liquid fuel pressure distribution takes the configuration of Figure 65. The center is at a much higher

pressure than the rest of the cylinder because of the vaporization of some of the liquid fuel. The high pressure forces material away from this region into the lower pressure regions which are closer in pressure to one another.

Liquid steel pressures are shown in Figures 66 through 68. Initially no liquid steel is present, but after two seconds the steel melts. The uniform pressure distribution that develops, and remains that way for the few milliseconds left in the problem, is depicted in Figures 67 and 68.

Figures 69 through 71 present the vapor fuel pressure distributions. Vapor fuel does not develop until near the end of the problem, when liquid in the center partially vaporizes, leading to a substantial pressure increase in this central cell. The large pressure differential between this cell and its neighbors forces material to flow outwards and dissipate in the lower pressure regions. The pressure in the neighboring regions can equilibrate since no vapor is being generated there. However, the continual generation of vapor in the hot cell maintains the high pressure in this cell as shown in Figure 71.

Fission gas pressures appear in Figures 72 through 74. Initially, the confined fission gas is set at a uniform pressure everywhere in the cylinder. As the fuel and steel heat up, the fission gas pressure changes. Since the gas is still relatively immobile, pressure equilibration cannot take place, resulting in the non-uniform distribution of Figure 73 just after steel melting. When the fuel begins to melt, the greater mobility of the gas allows for pressure equilibration in the molten regions. Later, as fuel vaporizes in the hot cell, the high

pressure and continued generation of vapor forces out most of the fission gas from that cell and pushes it into neighboring lower pressure regions. This is shown in Figure 74, where the hot cell is essentially devoid of any fission gas and the pressure in the rest of the molten region is fairly uniform. There is a lower pressure of gas where it is confined in the solid fuel column adjacent to the steel, and finally, the lowest pressure exists in the cooler steel region.

The temperature distributions of the various fields are shown in Figures 75 through 92. The mode of heat transfer is by conduction until the steel melts, after which it is by conduction and convection. The rapid heat generation that is introduced after the steel melts dominates other terms in the internal energy equation in the few milli-seconds left in the problem. Liquid fuel temperatures are pictured in Figures 75 through 77. There is no liquid fuel at the start of the problem and at the time of steel melting. Liquid fuel only forms later in the problem, and by termination time assumes the distribution shown in Figure 77. The distribution is still parabolic, with the hottest temperature in the center.

Liquid steel temperatures are shown in Figures 78 through 80. Initially there is no liquid steel, but after about 2 seconds, the steel in the inner axial regions melts by heat transferred from the hotter fuel. Solid steel is left only at the extreme top and bottom axial regions. The parabolic steel temperature distribution is relatively unchanged in the few milliseconds left in the problem, as indicated in Figures 79 and 80.

Figures 81 through 83 depict the vapor fuel temperature distributions. There is no vapor fuel initially, nor when the steel melts. Fuel vaporizes in the hot cell very late in the problem. The high pressure that is created forces vapor fuel into surrounding areas. Because of the rapid heat generation, and the short time remaining in the problem (about 0.07 milli-seconds), the vapor fuel has little opporutnity to achieve thermal equilibrium with other materials. As a result, its temperature in neighboring regions to which it has been driven is only slightly lower than its temperature at birth. This is indicated in Figure 83, where the temperature distribution is fairly flat, except for a very small rise in the center.

Fission gas temperatures are shown in Figures 84 through 86. At the start, the trapped fission gas is set to be in thermal equilibrium with the fuel and steel. Thus the initial temperature distribution is parabolic, in accordance with the fuel and steel temperatures. This distribution loses some of its curvature by the time the steel melts, as indicated in Figure 85. Finally, it takes the shape shown in Figure 86 at the end of the problem. The hot cell is devoid of fission gas, accounting for the dip shown in the figure. The gas is hotter in the inner regions, and cools off as one gets into the solid fuel region surrounding the steel, and finally into the cooler steel region itself.

Figures 87 through 89 picture the solid fuel temperature distributions. Solid fuel is initially present everywhere except for the last radial annulus which contains steel. A parabolic temperature distribution is imposed as shown in Figure 87. Heat is conducted across the fuel and into the cooler steel. After about 2 seconds the steel has melted

in the inner axial regions, leaving the fuel with the distribution shown in Figure 88. Later in the problem, the fuel melts in all but the single radial column adjacent to the steel. Thus, at the end of the problem there is only one annulus of solid fuel with the fairly uniform distribution of Figure 89.

Solid steel temperatures are shown in Figures 90 through 92. Steel is initially present in the outermost radial annulus with the temperature distribution of Figure 90. After 2.049 seconds it melts in the inner axial locations by gaining heat from the fuel. Only the top and bottom cells remain solid as in Figure 91. Their temperatures are still at the fusion point when the problem is terminated 3 milliseconds later, as indicated in Figure 92.

(b) One Dimensional Results

The two dimensional problem described earlier in this Section was repeated with the same input data but with one dimensional calculations, to determine the differences that arise by assuming radial uniformity. Input data was averaged across the radial cross section at each axial location, to get appropriate one dimensional starting values. The treatment is similar to that followed in the SLUMPY module of the SAS[7] code, but the multi-field approach is still used.

The simultaneous presence of fuel and steel leads to a difficulty with the initial material configuration, in that the steel at any axial location would melt much earlier than the fuel because of the large difference in melting points. This problem is circumvented in SLUMPY [where the fuel and steel are treated as a single material with averaged

properties] by assuming clad to be mixed with fuel only if fuel melting has occurred at the same time or before clad melting; otherwise only pure fuel is considered. The problem worsens with a multi-field approach since one would have molten, and eventually some vapor, steel enclosed in still solid fuel. In the PLOFA model, except for fission gas diffusion, no motion is allowed in a cell until all the solid has melted. Therefore, to avoid the unrealistic conditions that would be created by trapping the molten and vapor steel, a SLUMPY type assumption has to be used. Rather than ignoring the steel, as SLUMPY does, it is treated as fuel in the input data, but with no internal heat generation. Thus, at a given axial location there is solid fuel and fission gas, with initial properties averaged over the radius, and steel added as non-heat generating fuel.

The solid fuel density is the radial average of the fuel and steel densities,

$$\bar{\rho} = \frac{\sum_r \rho V}{\sum_r V} \quad ,$$

where V indicates the volume of each radial annulus, ρ the corresponding fuel or steel macroscopic density, and the summation is carried out over all radial annuli. A similar calculation yields the average fission gas density.

$$\bar{T} = \frac{\sum_r \rho c_p T V}{\sum_r \rho c_p V} \quad ,$$

where T is the fuel or steel temperature in an annulus. The specific heat, c_p, is calculated at the temperature T using the c_p formulation for fuel.

The fission gas temperature is set equal to this fuel temperature.

An average microscopic density, $\bar{\rho}'$, is calculated for the fuel, using the density-temperature relationship evaluated at the average fuel temperature, $\bar{T}$. This then yields an average volume fraction for fuel as

$$\bar{\alpha} = \bar{\rho}/\bar{\rho}' \ .$$

The fission gas volume fraction is merely the difference between 1.0 and $\bar{\alpha}$ [i.e., the fission gas occupies the remaining space]. Knowing the average fission gas density, volume fraction and temperature at each axial location, one can then use its equation of state to calculate its pressure at that location.

The heat generation rate is the product of the two dimensional heat generation rate and the ratio of fuel volume to fuel + steel volume.

The one dimensional calculations are begun with these average values for fuel and fission gas. After 2.049 seconds the heat generation is increased by a factor of 10^3 in conformance with the two dimensional case. No melting has occurred at this time because there is no steel to melt at a low temperature, but rather fuel which melts at a much higher temperature. The calculations continue with this rapid energy generation, and fuel finally begins to melt, initially at the mid-axial region, around 2.051 seconds. By the time the problem is terminated 0.6 milli-seconds later at 2.052 seconds [the end of the two dimensional calculations] fuel has melted at all but the extreme axial locations. However, no vapor has formed anywhere in the container, because, unlike the two dimensional case, there is no hot cell close to the center to permit vaporization in a localized region.

The results of the one dimensional calculations as the problem progresses through time, until termination at 2.052 seconds, are shown in Figures 93 through 133. Velocities are plotted vectorially, while three dimensional plots are made of the scalar variables.

Velocity vectors appear in Figures 92 through 100. These plots cover the last 0.4 milliseconds of the problem from 2.05164 to 2.05204 seconds. As the fuel heats up, it melts first in the mid-axial region and then at increasing distances from it. The liquid fuel velocities are shown in Figures 93 through 96. In the absence of other significant forces, the liquid moves down under the action of gravitational forces. Three axial locations are shown being mobile in Figure 93, while the remaining plots show melting and motion in two more axial locations. The extreme top and bottom rows remain solid throughout the problem.

Figures 97 through 100 display the fission gas velocities. The fission gas moves downward at first (Figure 97), due to drag by the liquid fuel. It then begins to turn around and move upward because of buoyancy. In Figure 98 it has turned around partially, while Figures 99 and 100 show it moving upward everywhere.

Scalar property distributions are shown in Figures 101 through 133. Plotting times are the same as those in the two dimensional case, viz., 0.0, 2.04889 and 2.05204 seconds.

The volume fractions of the various fields are depicted in Figures 101 through 109. Figures 101 through 103 show the liquid fuel volume fractions. There is no liquid fuel present till late in the problem when the solid fuel melts in all but the extreme axial locations, as in Figure 103 which shows an essentially uniform distribution in the molten region.

Fission gas volume fractions are shown in Figures 104 through 106. Initially, the fission gas has a uniform volume fraction distribution in the inner axial region, and is slightly lower at the extreme top and bottom as in Figure 104 because there was more steel in these locations in the two dimensional problem (hence more non-heat generating fuel in this case). The distribution is the same in Figure 105 with no melting, and is only slightly changed at the end of the problem in Figure 106.

Figures 107 through 109 show the solid fuel volume fraction. It is uniform in the inner axial region, and is slightly higher at the extreme top and bottom because the increased amount of steel that was present in these locations in the two dimensional case is now added as non-heat generating fuel. The distribution is the same in Figure 108 with no melting. By the end of the problem, the solid has melted through in all but the extreme top and bottom locations, and these are the only non-zero values in Figure 109.

Macroscopic density distributions for the individual fields appear in Figures 110 through 118. These resemble the volume fraction representations, but whereas the volume fractions were specified to be initially uniform in a given region, the macroscopic densities [which also depend on the non-uniform temperature distributions] are initially non-uniform. The flat surfaces of the volume fractions become slightly curved surfaces for the initial density distributions.

Figures 119 through 124 portray the individual pressure distributions. Liquid fuel pressures are shown in Figures 119 through 121. No liquid is present until late in the problem, as in Figure 121 which

indicates a fairly uniform distribution for the downward flowing liquid.

Fission gas pressures are shown in Figures 122 through 124. The initial pressure is lower in the extreme top and bottom regions. In the inner axial regions, the combination of a concave density surface and a convex temperature surface have combined, through the equation of state, to give a barely discernible concave surface for the pressure distribution. The same distribution holds in Figure 123, with no melting. Figure 124 shows the pressure distribution at the end of the problem. The higher temperatures have raised the pressure everywhere.

Temperature distributions for the individual fields are pictured in Figures 125 through 133. Liquid fuel temperatures are shown in Figures 125 through 127. By initiation phase termination, the fuel has melted in all the inner axial regions and the temperature distribution is parabolic as in Figure 127.

Fission gas temperatures are shown in Figures 128 through 130. The initial distribution is parabolic. It is similar in Figure 129, but with temperatures higher everywhere. The final temperature distribution in Figure 130 is more uniform throughout.

Figures 131 through 133 picture the solid fuel temperature distributions. The initial distribution is parabolic as shown in Figure 131. In Figure 132 it is still parabolic, but slightly flatter because of conduction between the layers. Later in the problem, the fuel melts in all but the extreme top and bottom locations, and these have the only non-zero values in Figure 133.

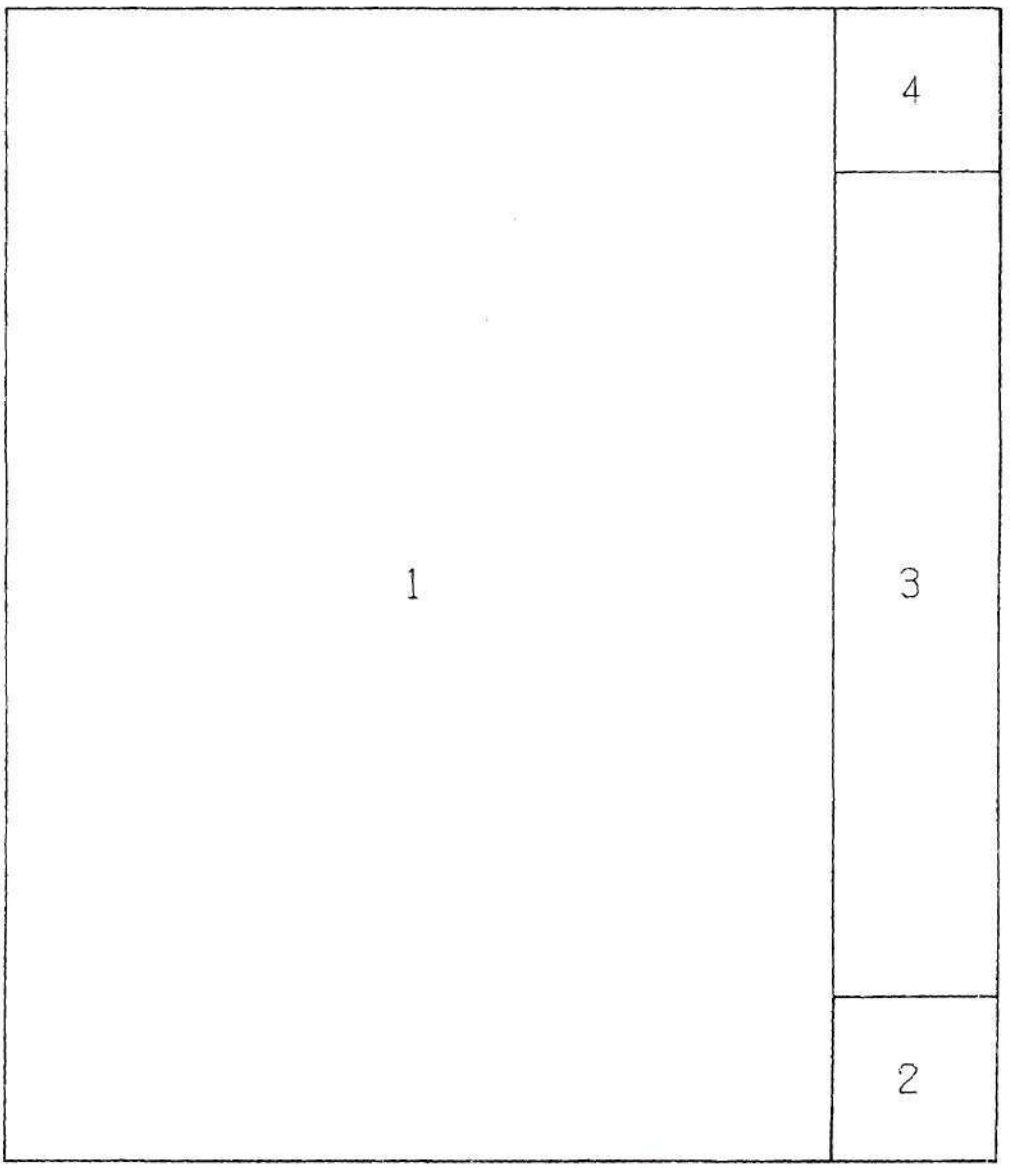

Figure 4: Input Material Regions

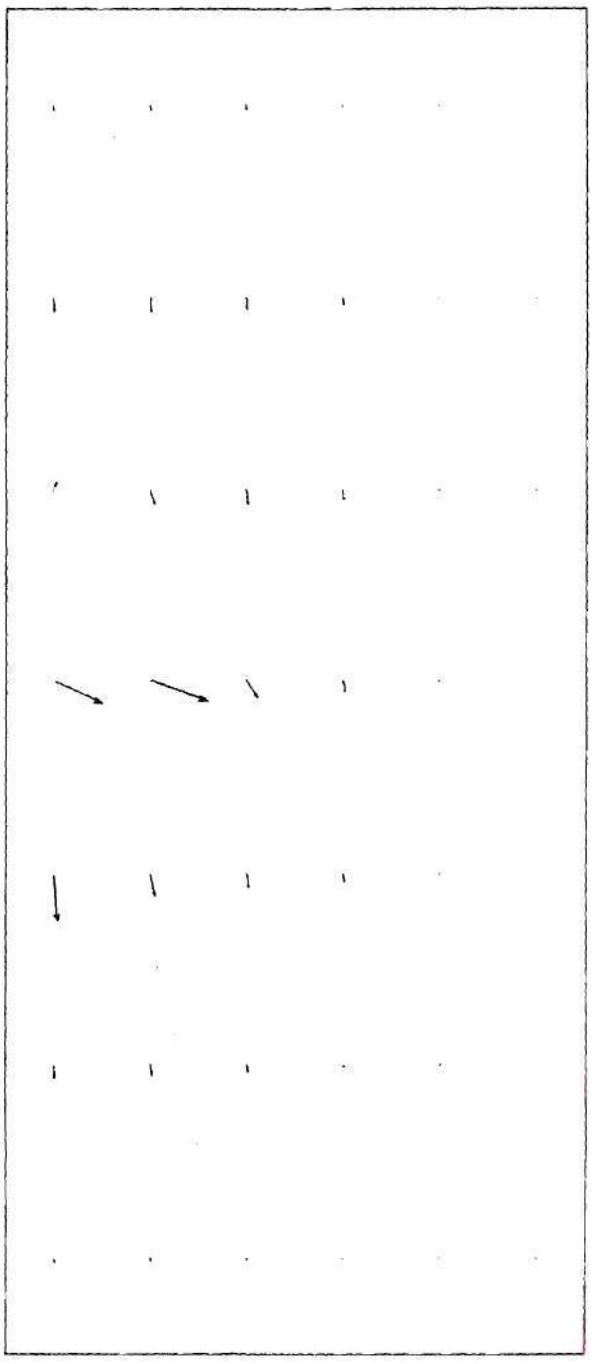

Figure 5: Liquid Fuel Velocity [T = 2.05197 sec]

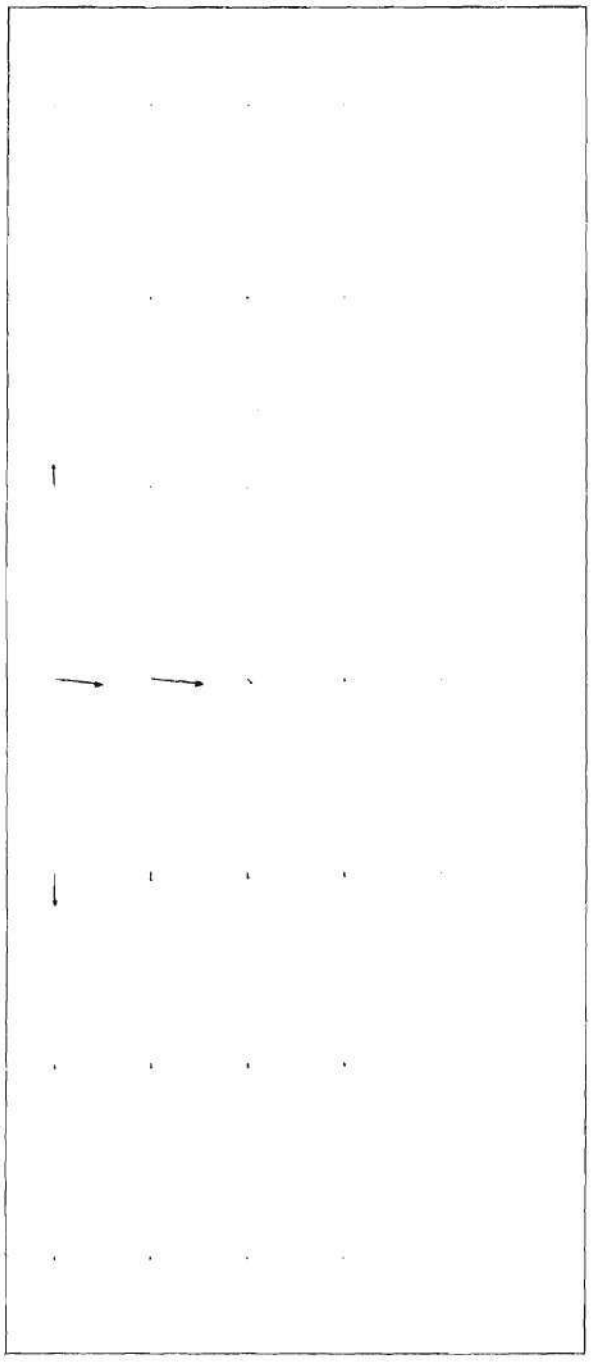

Figure 6: Liquid Fuel Velocity [T = 2.05198 sec]

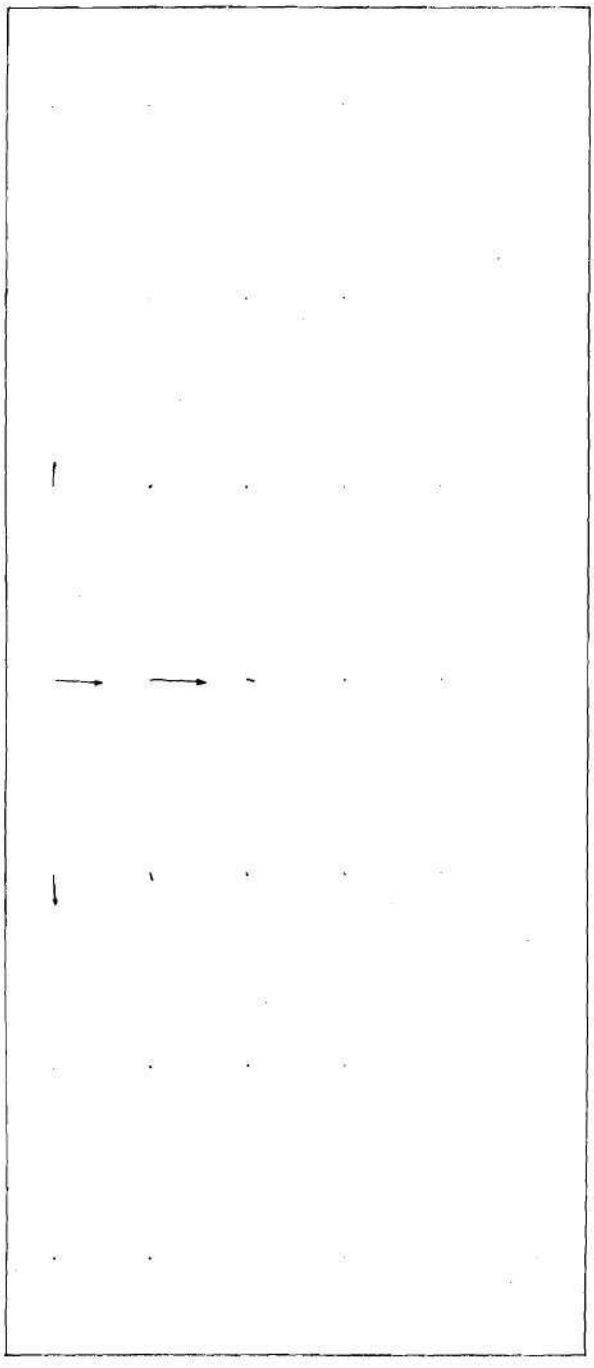

Figure 7: Liquid Fuel Velocity [T = 2.05200 sec]

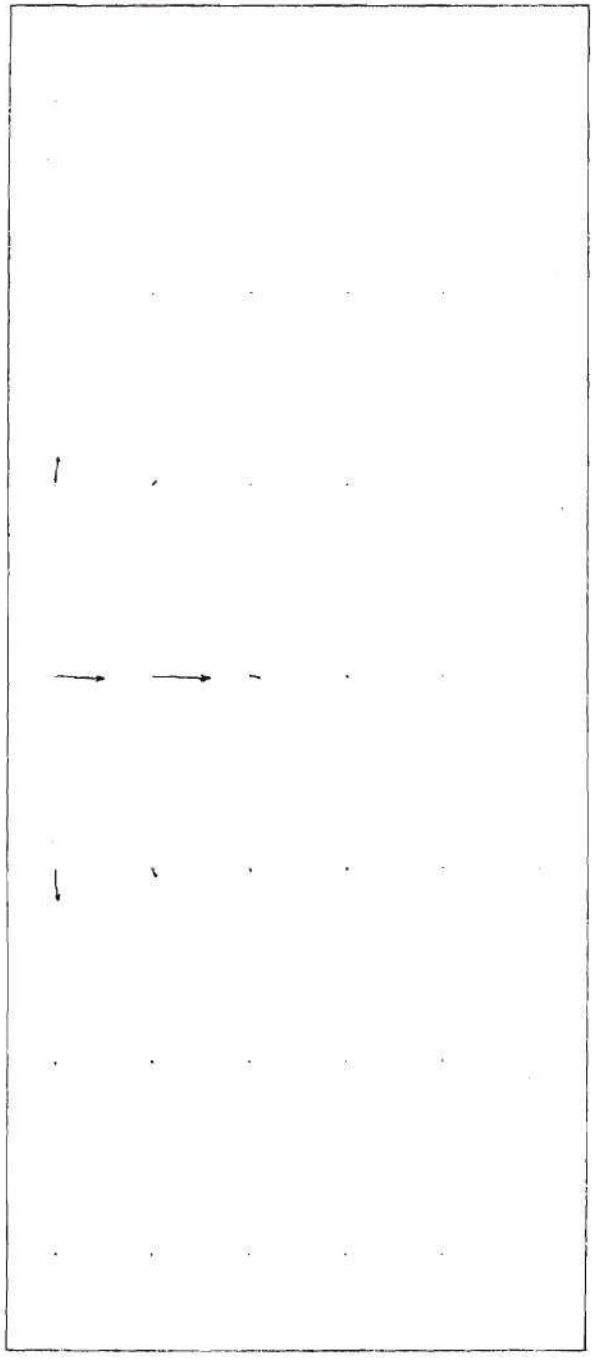

Figure 8: Liquid Fuel Velocity [T = 2.05202 sec]

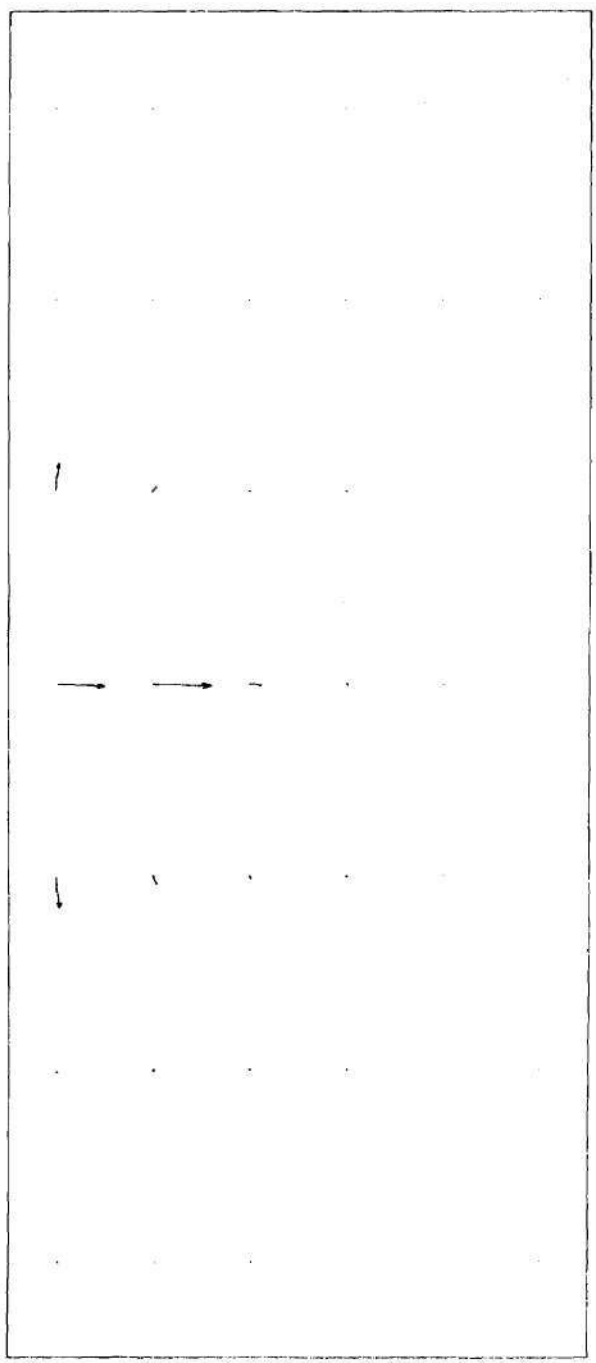

Figure 9: Liquid Fuel Velocity [T = 2.05204 sec]

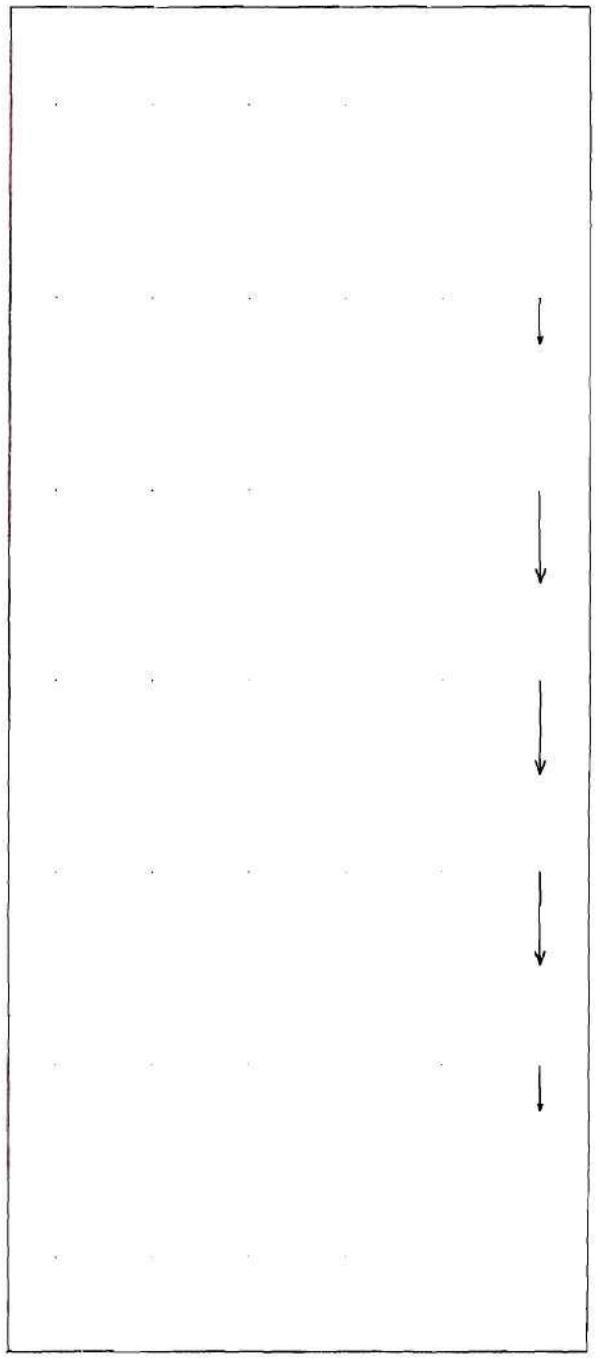

Figure 10: Liquid Steel Velocity [T = 2.04889 sec]

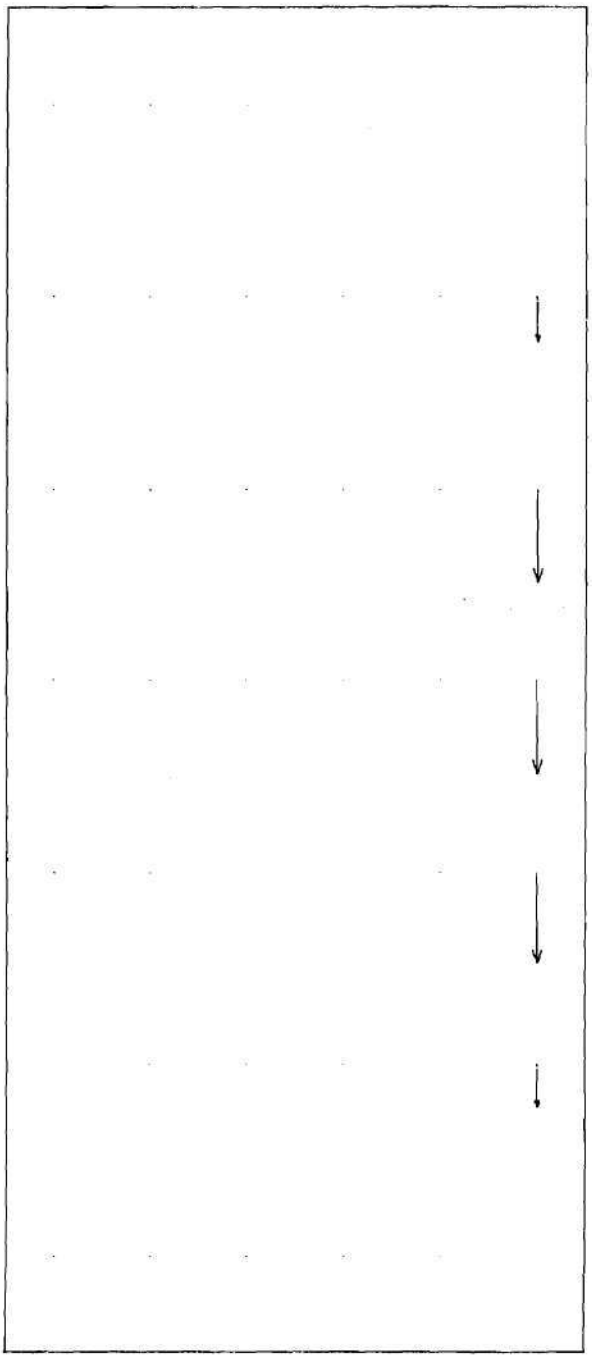

Figure 11: Liquid Steel Velocity [T = 2.05197 sec]

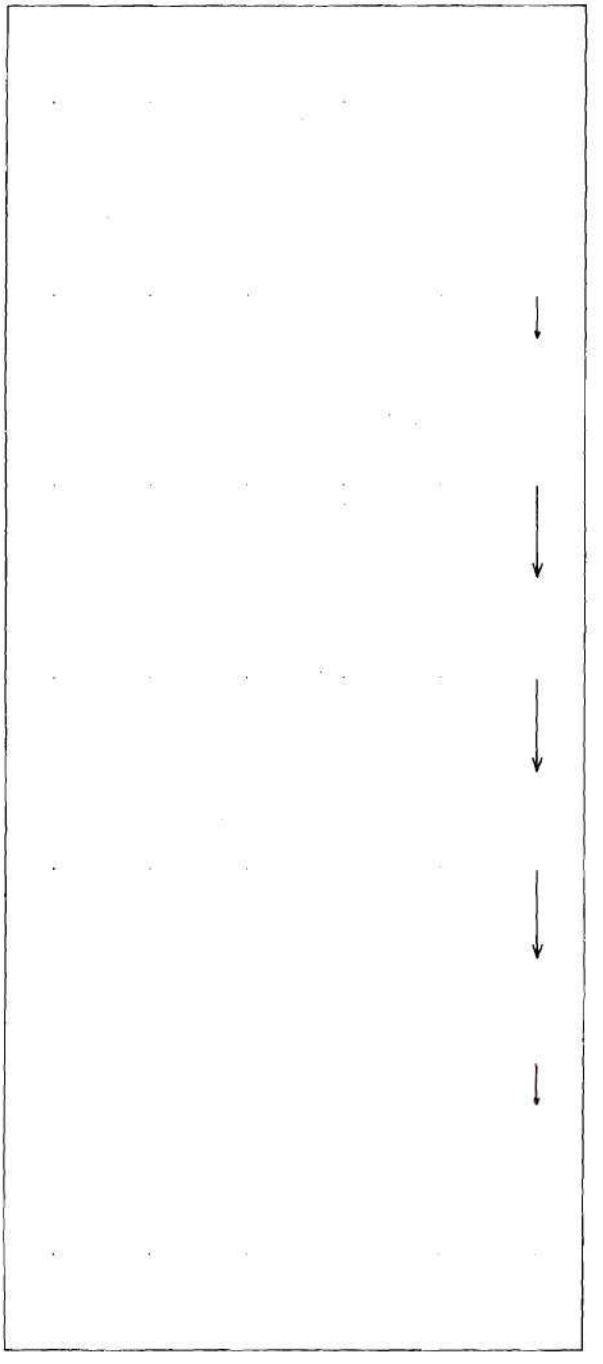

Figure 12: Liquid Steel Velocity [T = 2.05198 sec]

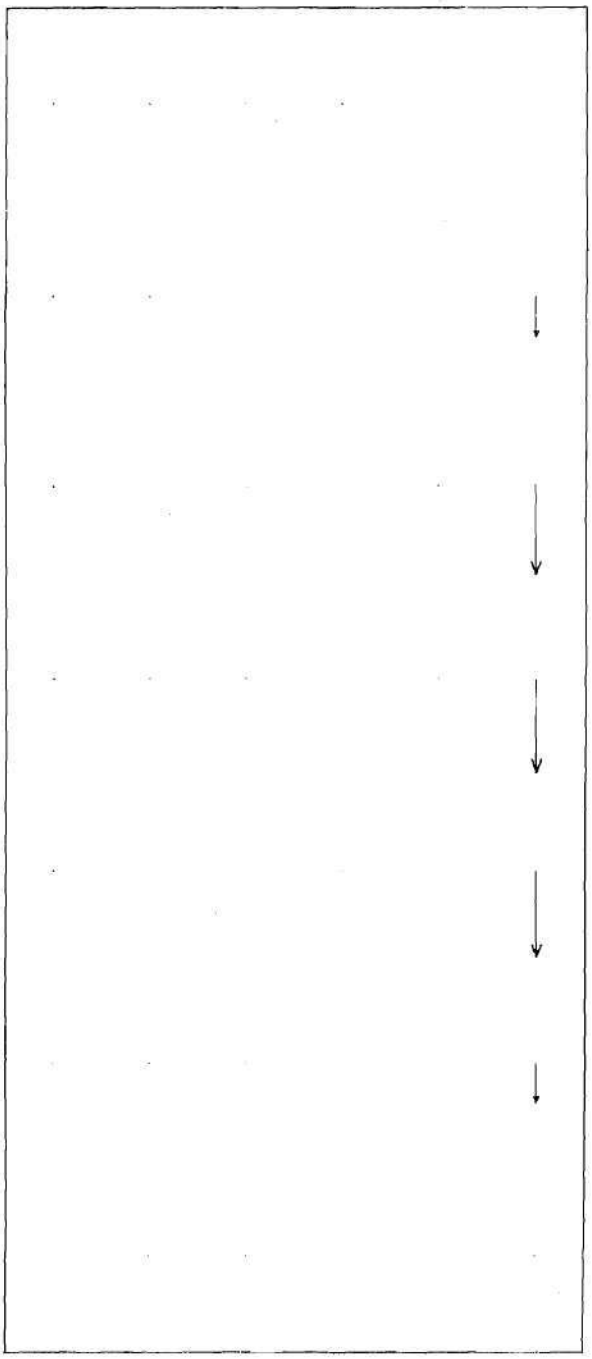

Figure 13: Liquid Steel Velocity [T = 2.05200 sec]

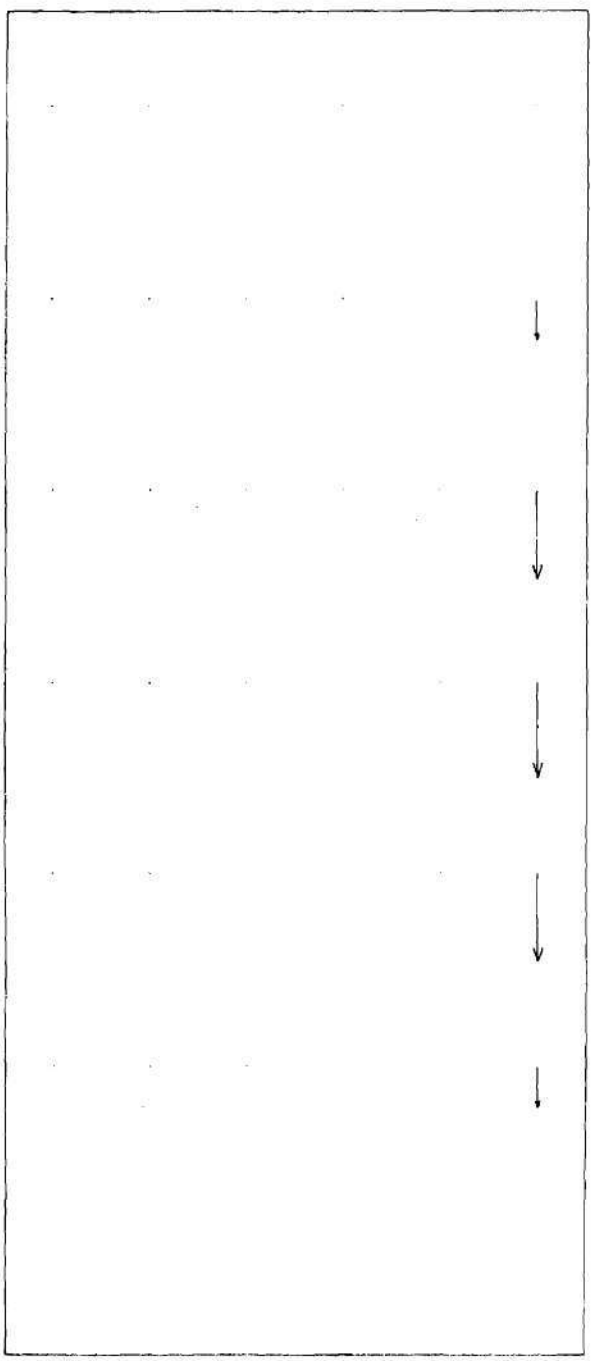

Figure 14: Liquid Steel Velocity [T = 2.05202 sec]

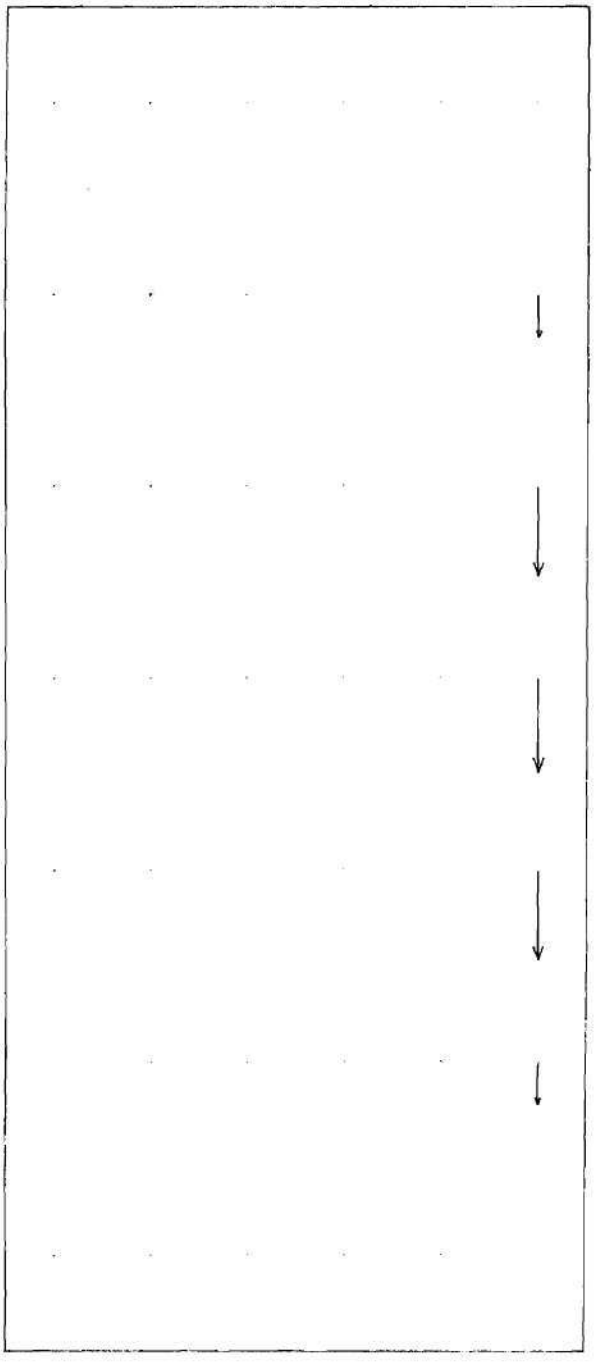

Figure 15: Liquid Steel Velocity [T = 2.05204 sec]

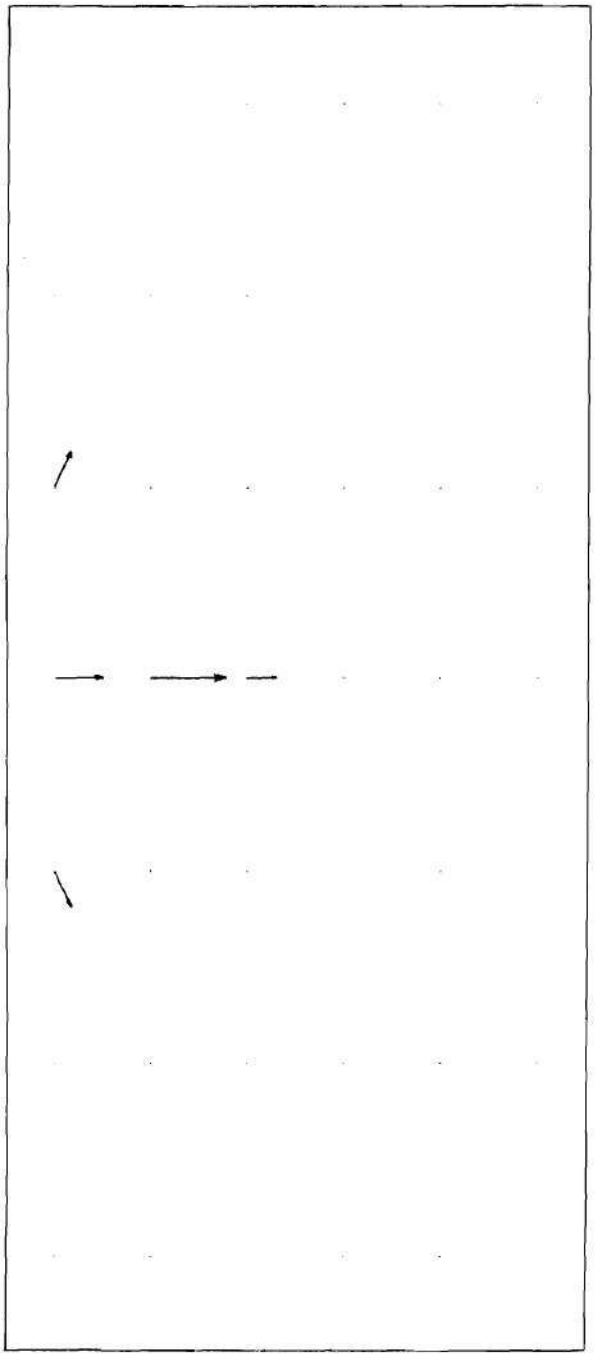

Figure 16: Vapor Fuel Velocity [T = 2.05197 sec]

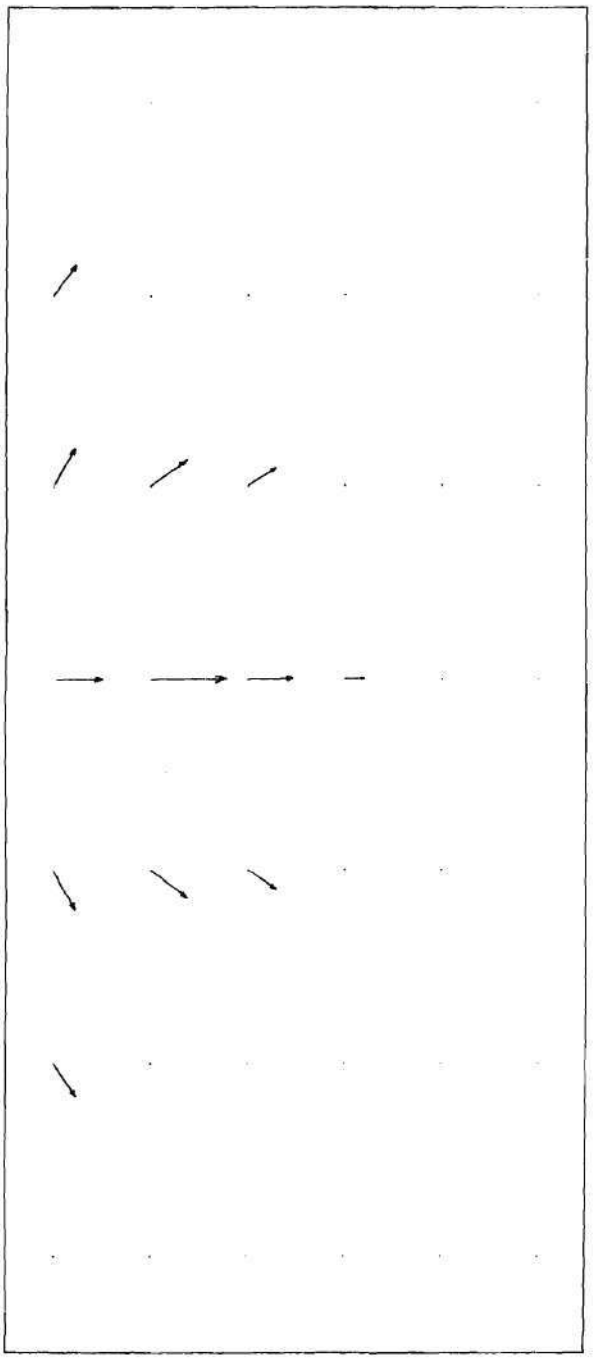

Figure 17: Vapor Fuel Velocity [T = 2.05198 sec]

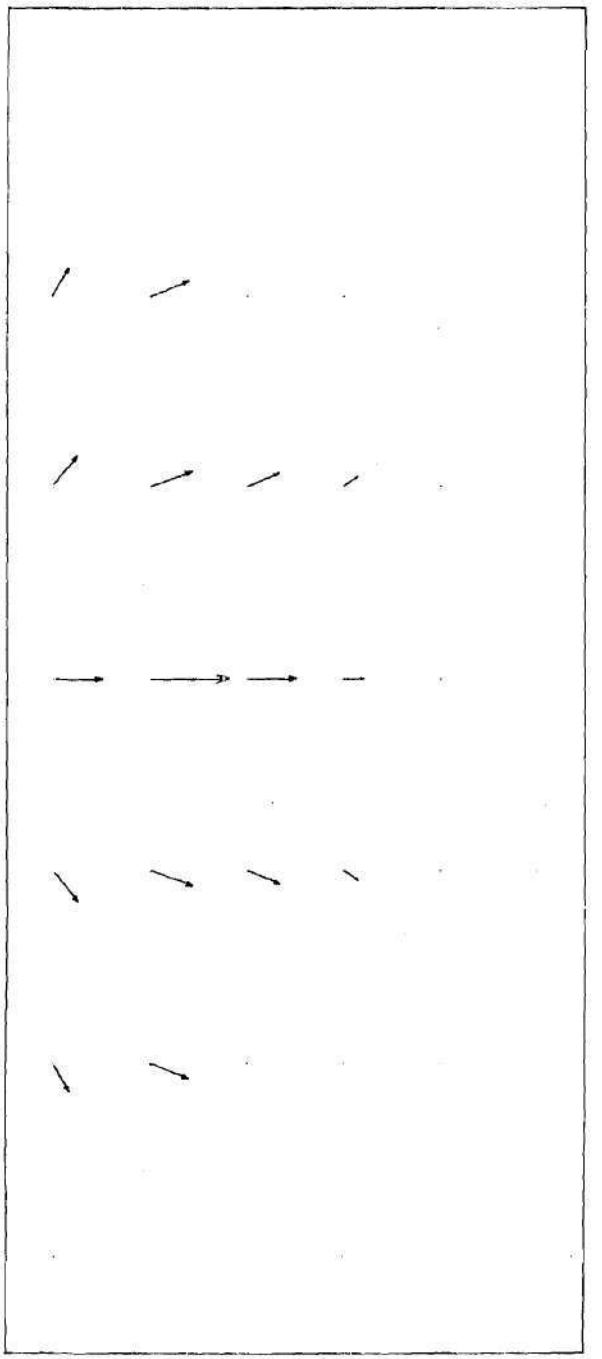

Figure 18: Vapor Fuel Velocity [T = 2.05200 sec]

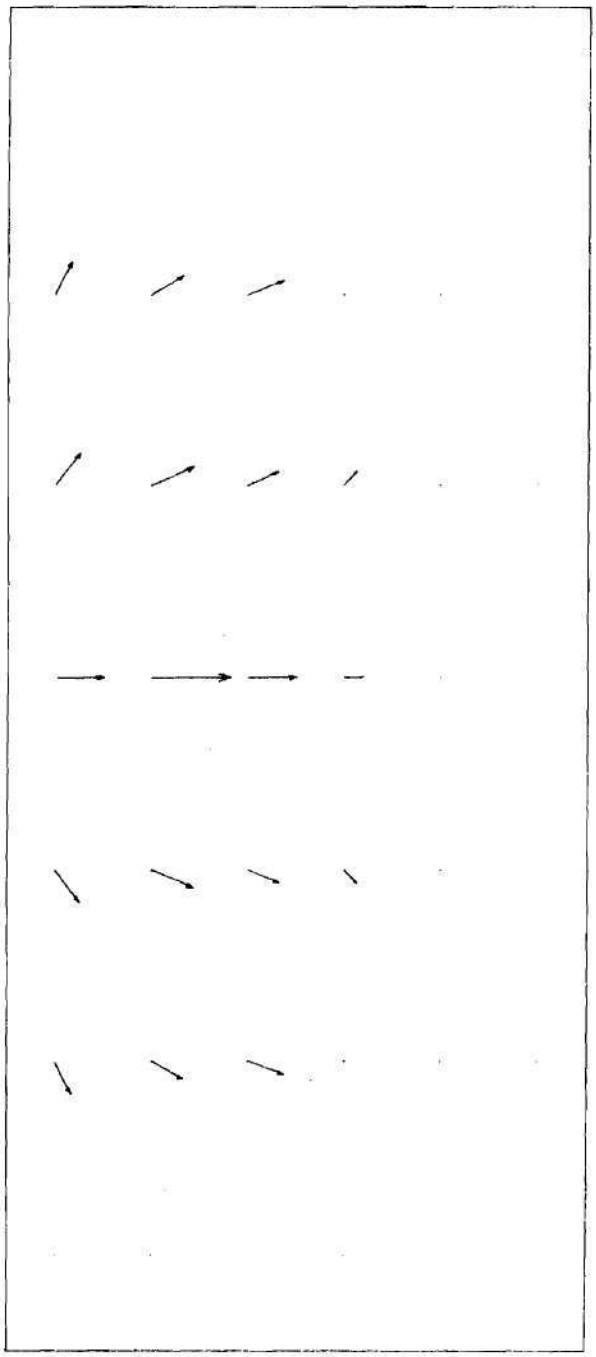

Figure 19: Vapor Fuel Velocity [T = 2.05202 sec]

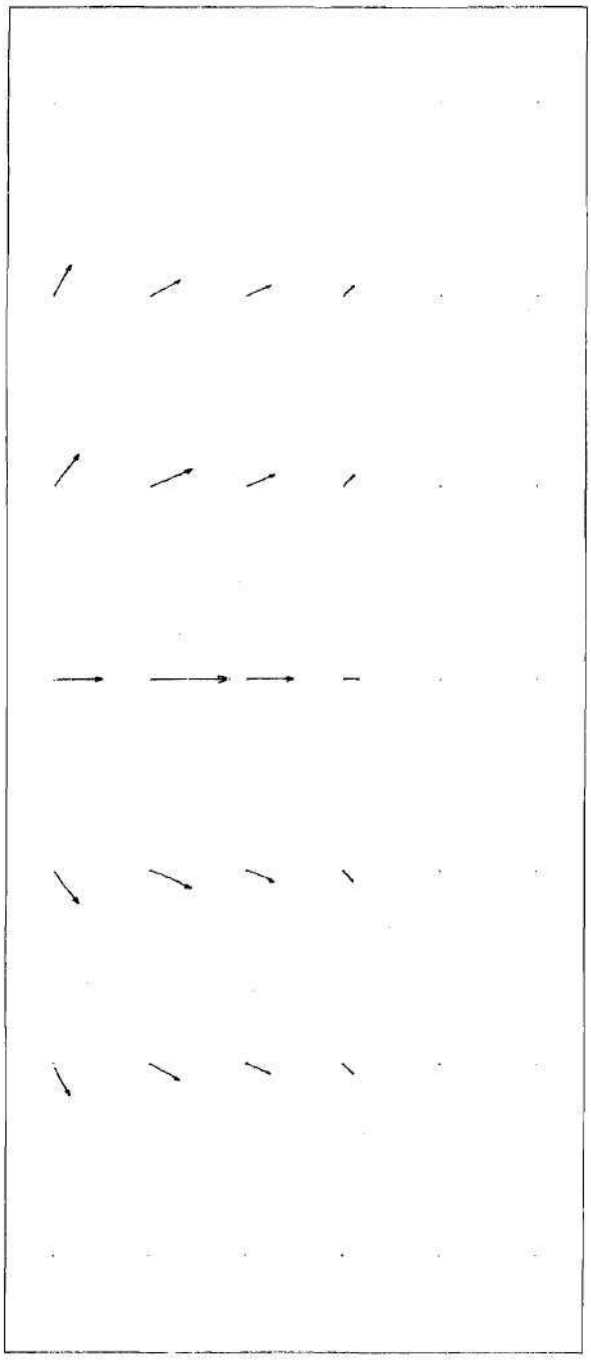

Figure 20: Vapor Fuel Velocity [T = 2.05204 sec]

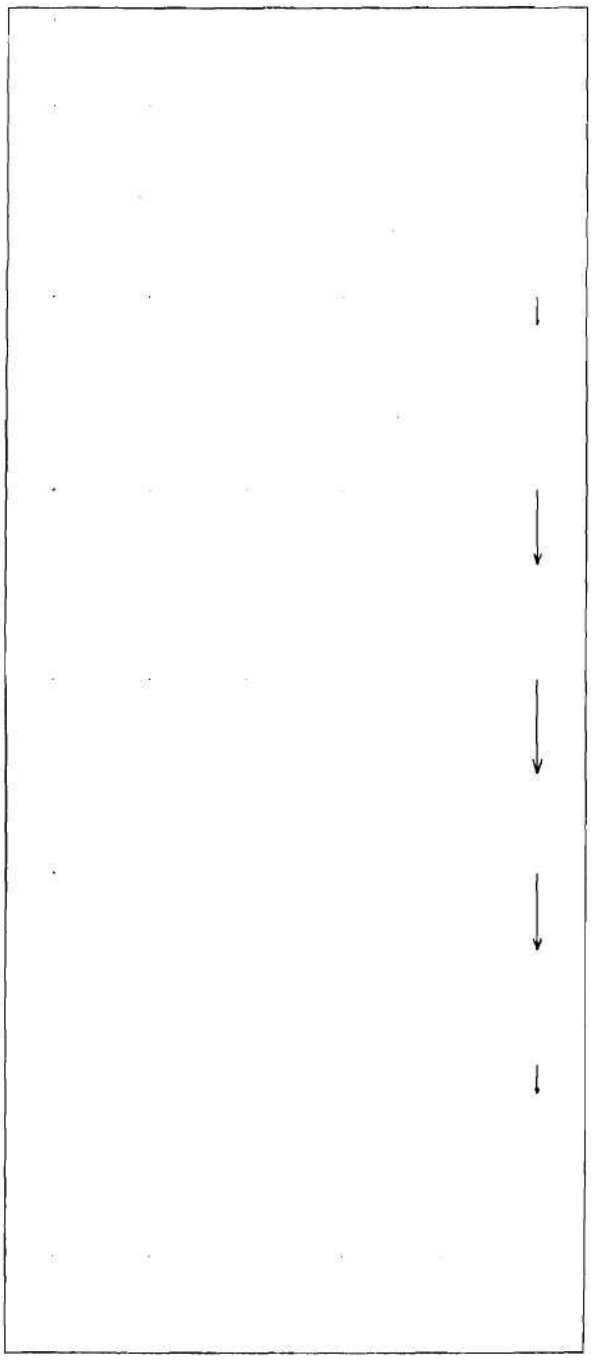

Figure 21: Fission Gas Velocity [T = 2.04889 sec]

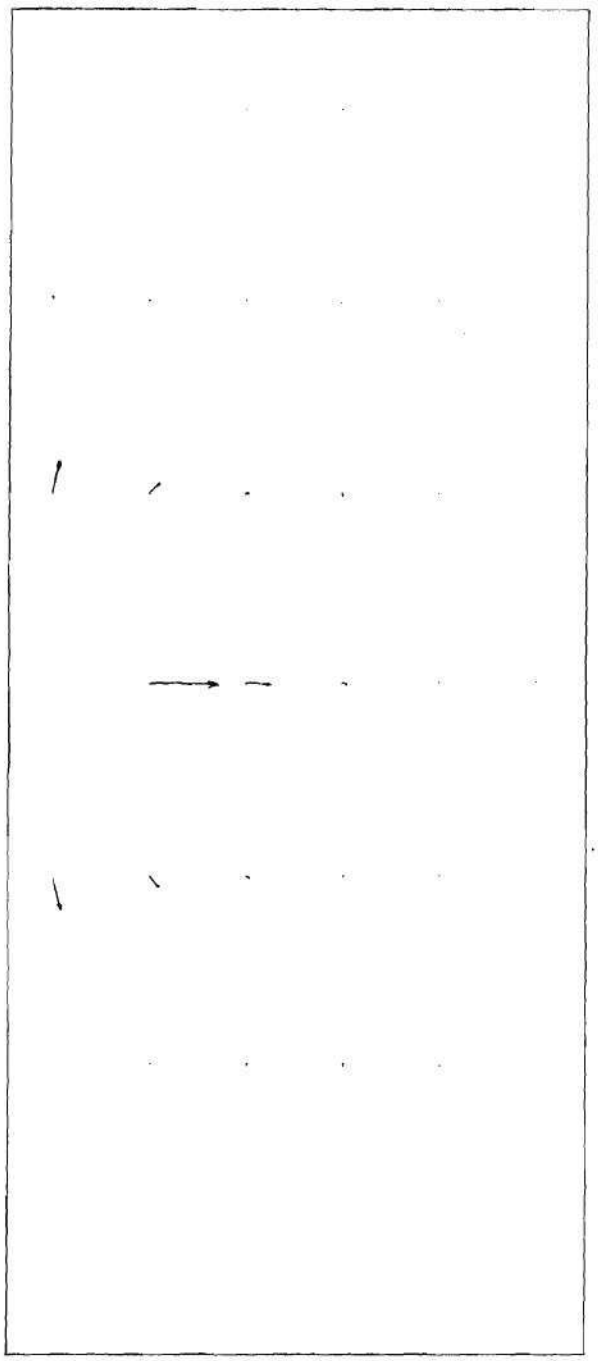

Figure 22: Fission Gas Velocity [T = 2.05197 sec]

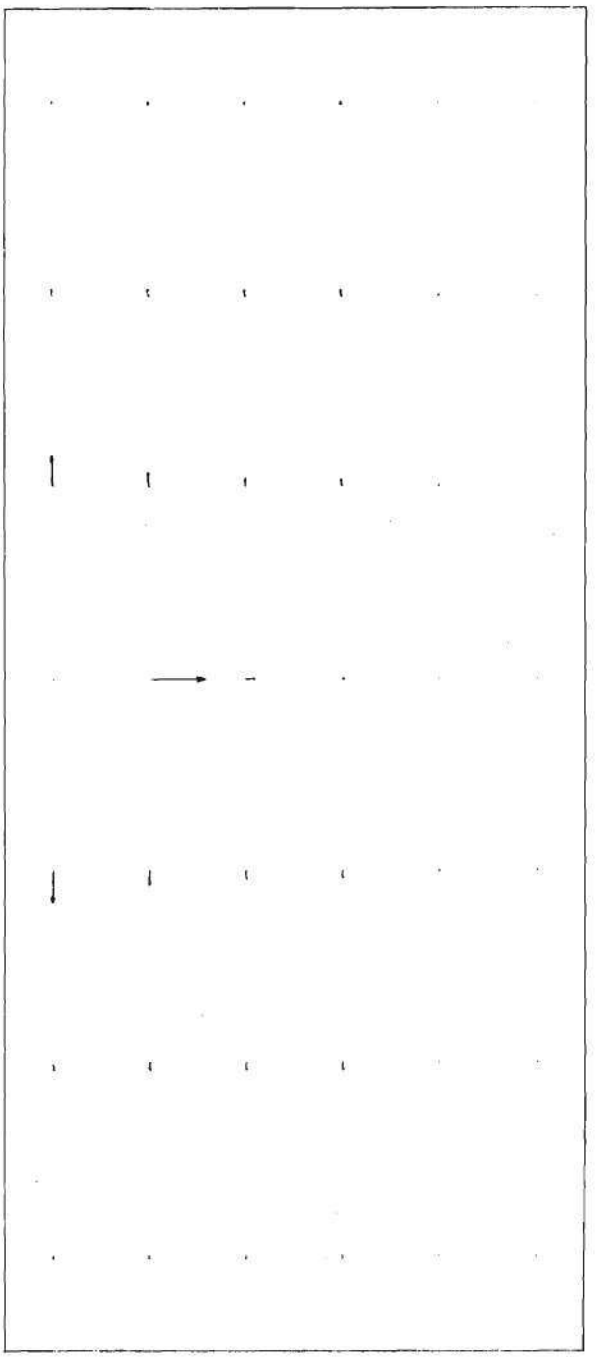

Figure 23: Fission Gas Velocity [T = 2.05198 sec]

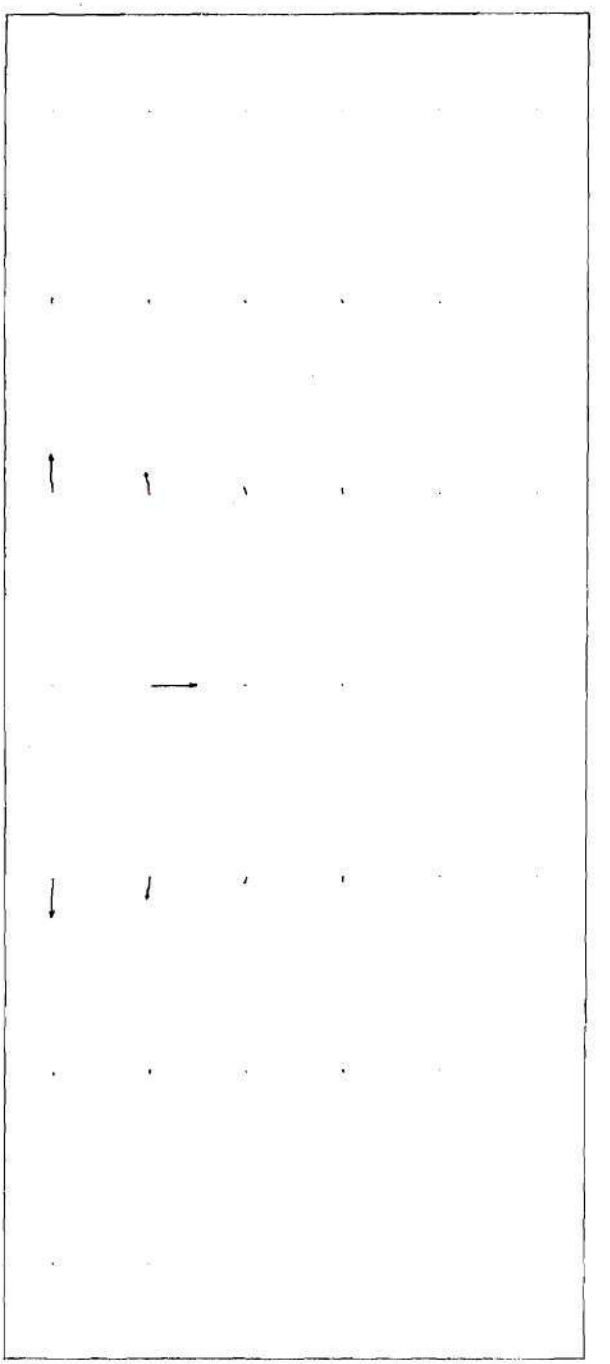

Figure 24: Fission Gas Velocity [T = 2.05200 sec]

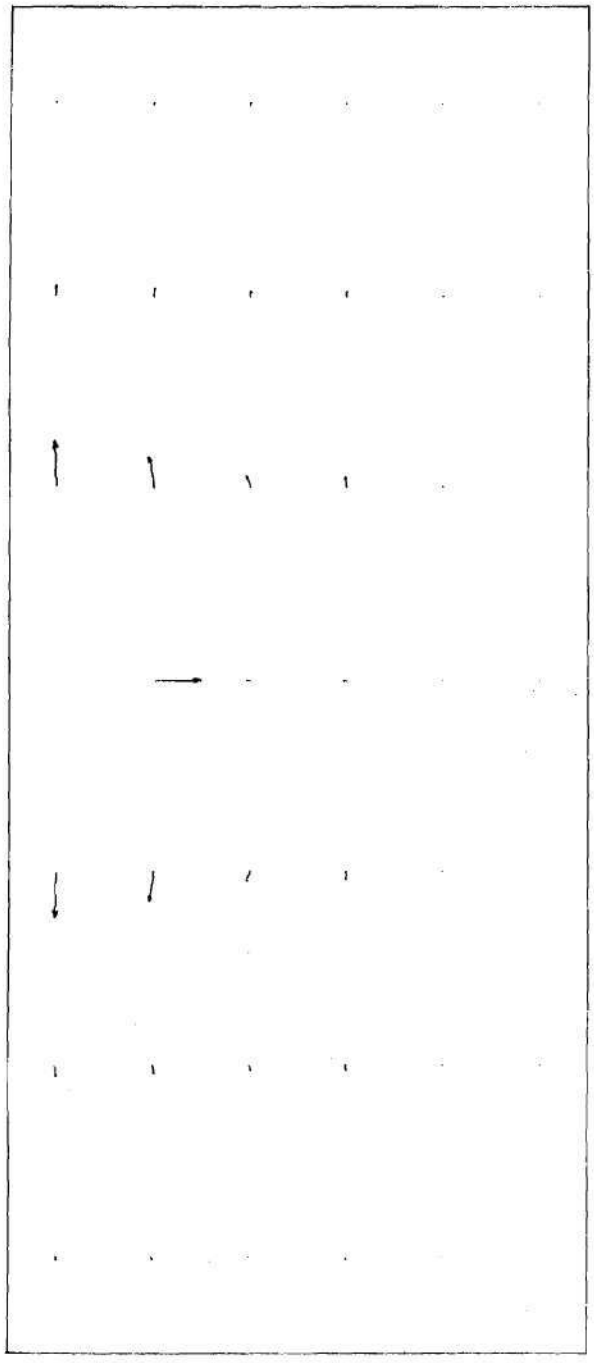

Figure 25: Fission Gas Velocity [T = 2.05202 sec]

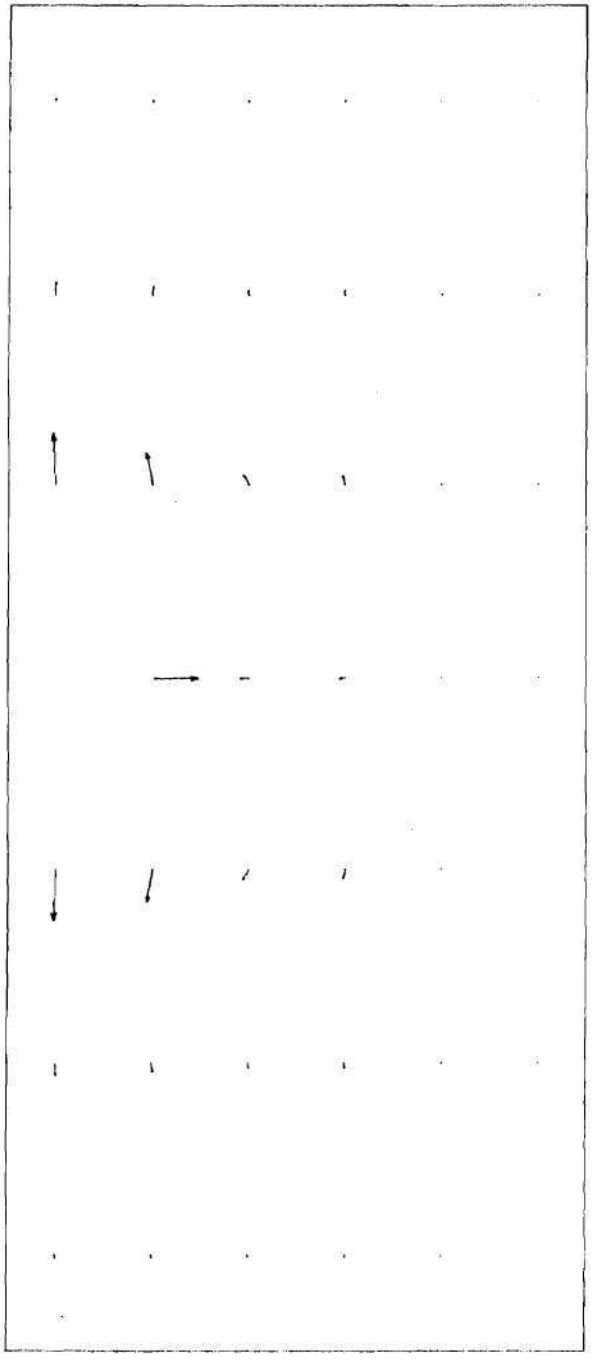

Figure 26: Fission Gas Velocity [T = 2.05204 sec]

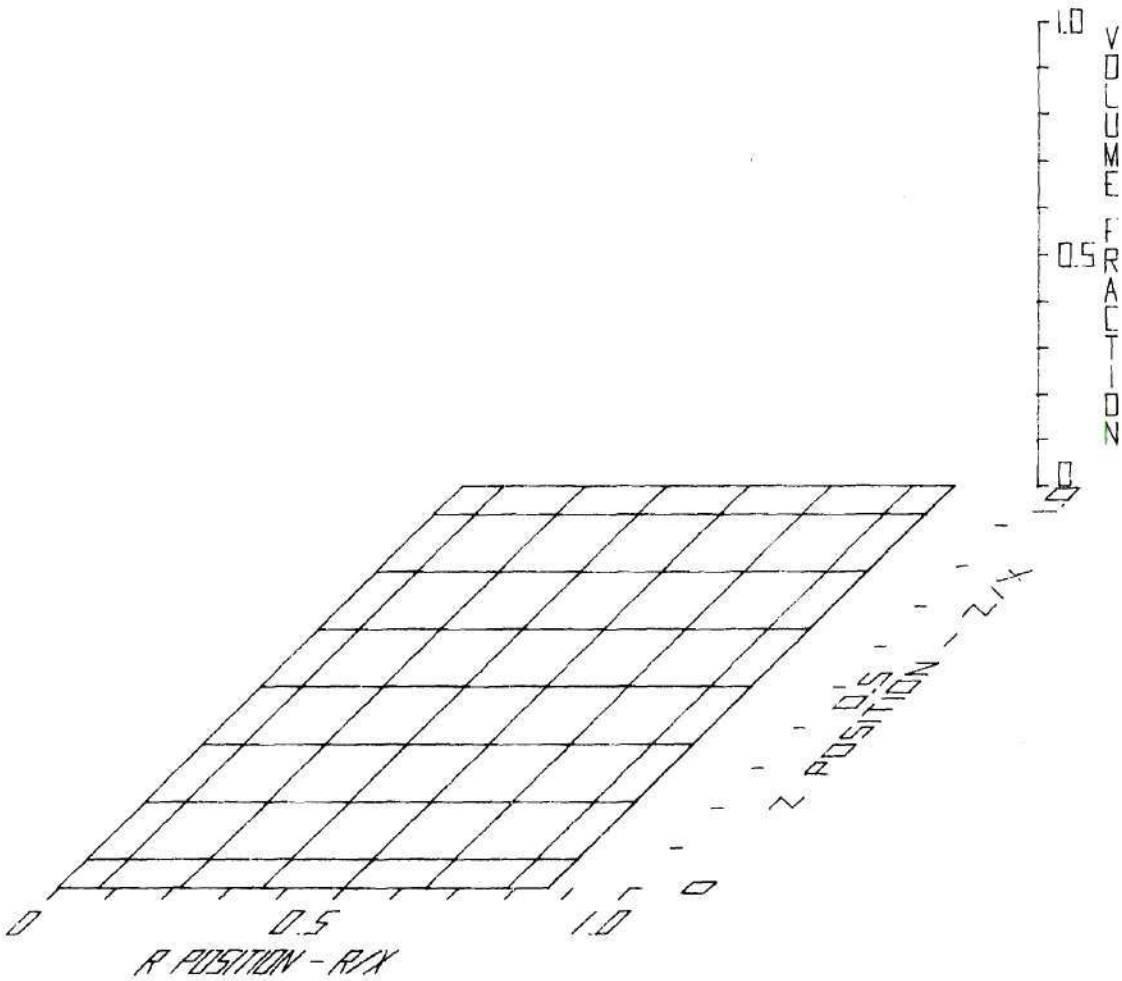

Figure 27: Liquid Fuel Volume Fraction [T = 0.00000 sec]

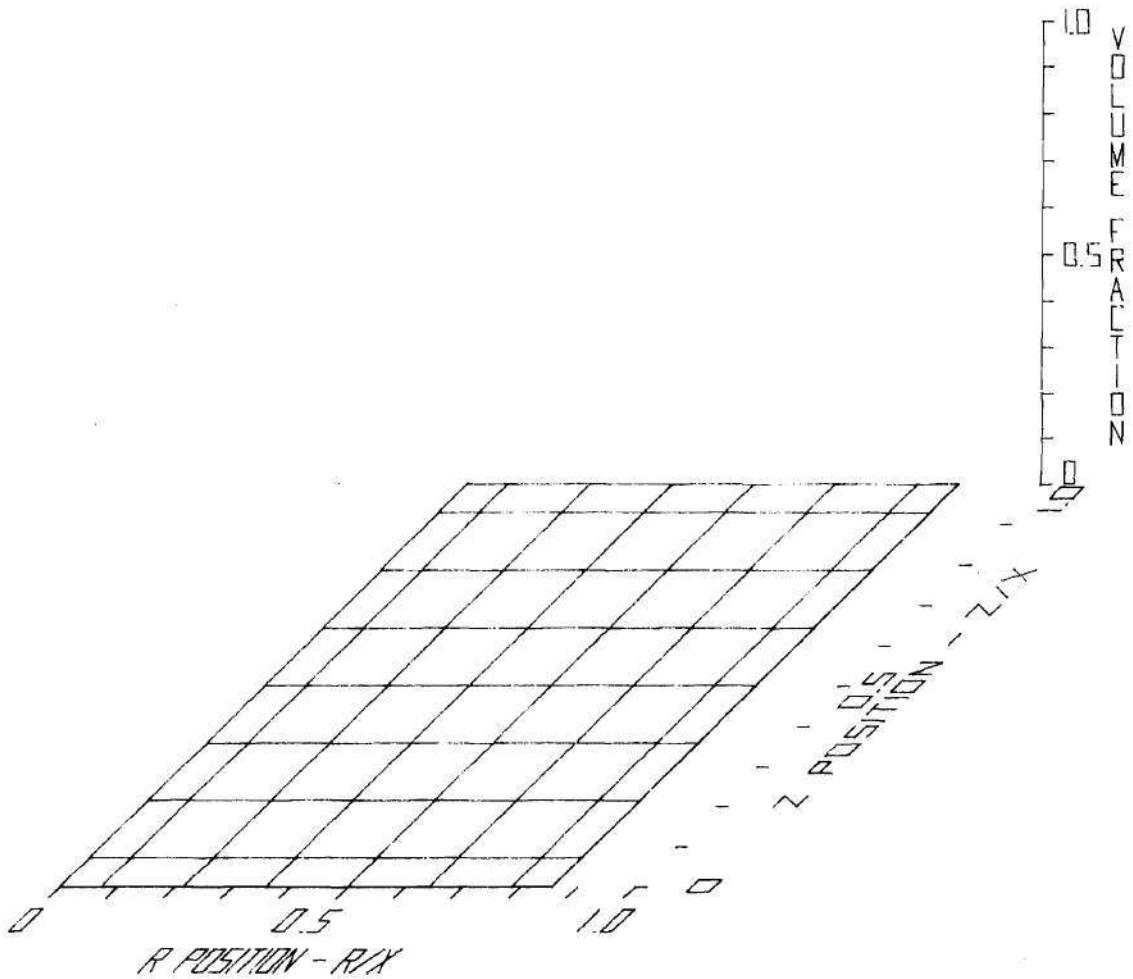

Figure 28: Liquid Fuel Volume Fraction [T = 2.04889 sec]

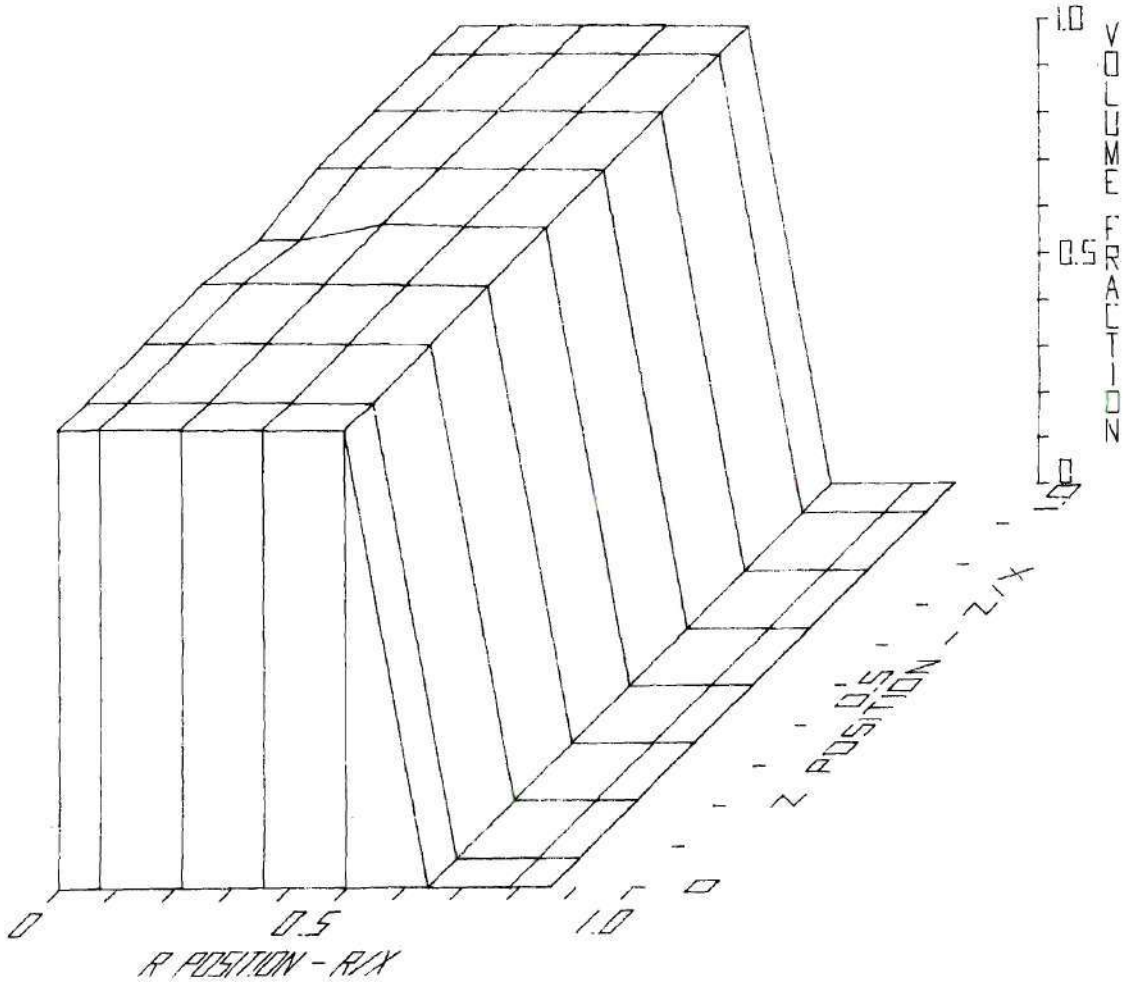

Figure 29: Liquid Fuel Volume Fraction [T = 2.05204 sec]

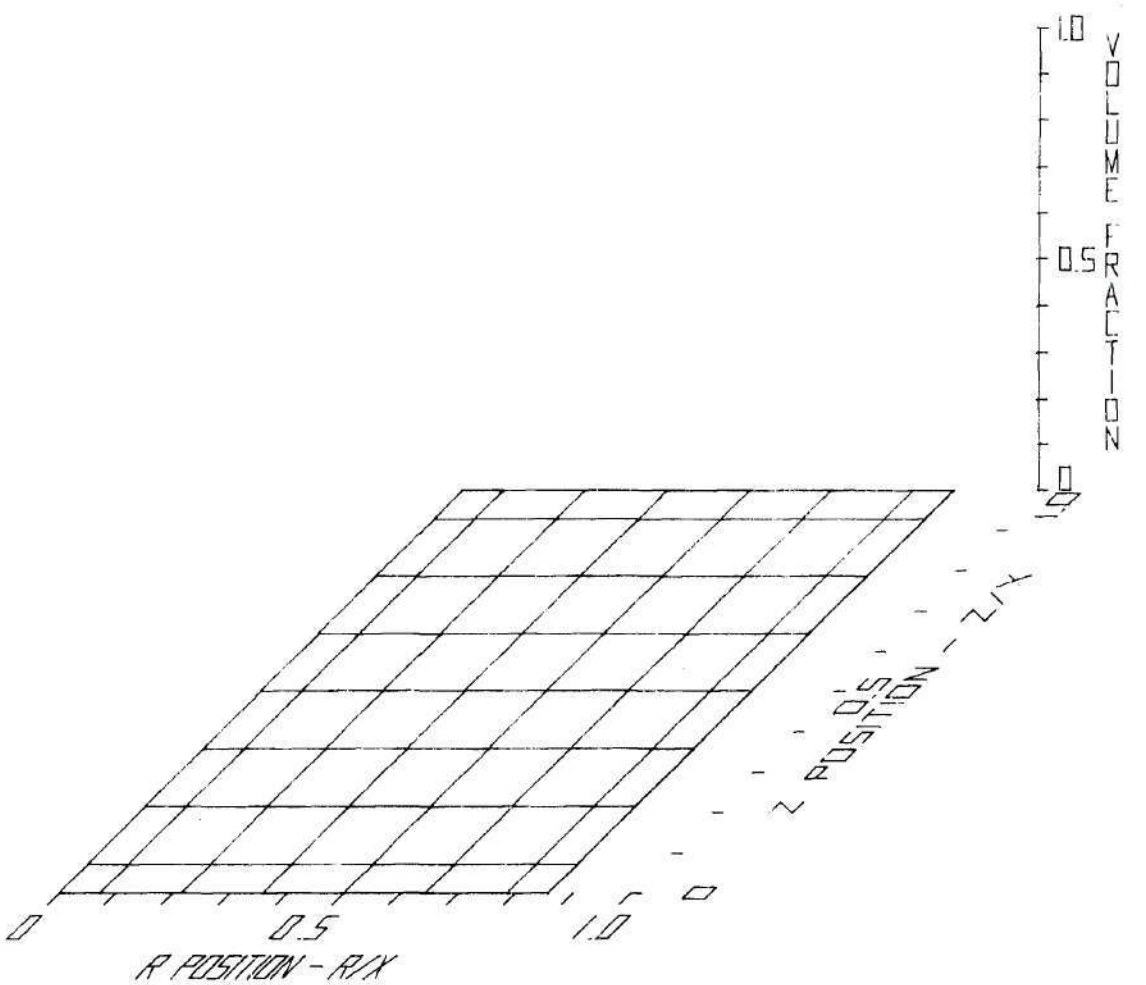

Figure 30: Liquid Steel Volume Fraction [T = 0.00000 sec]

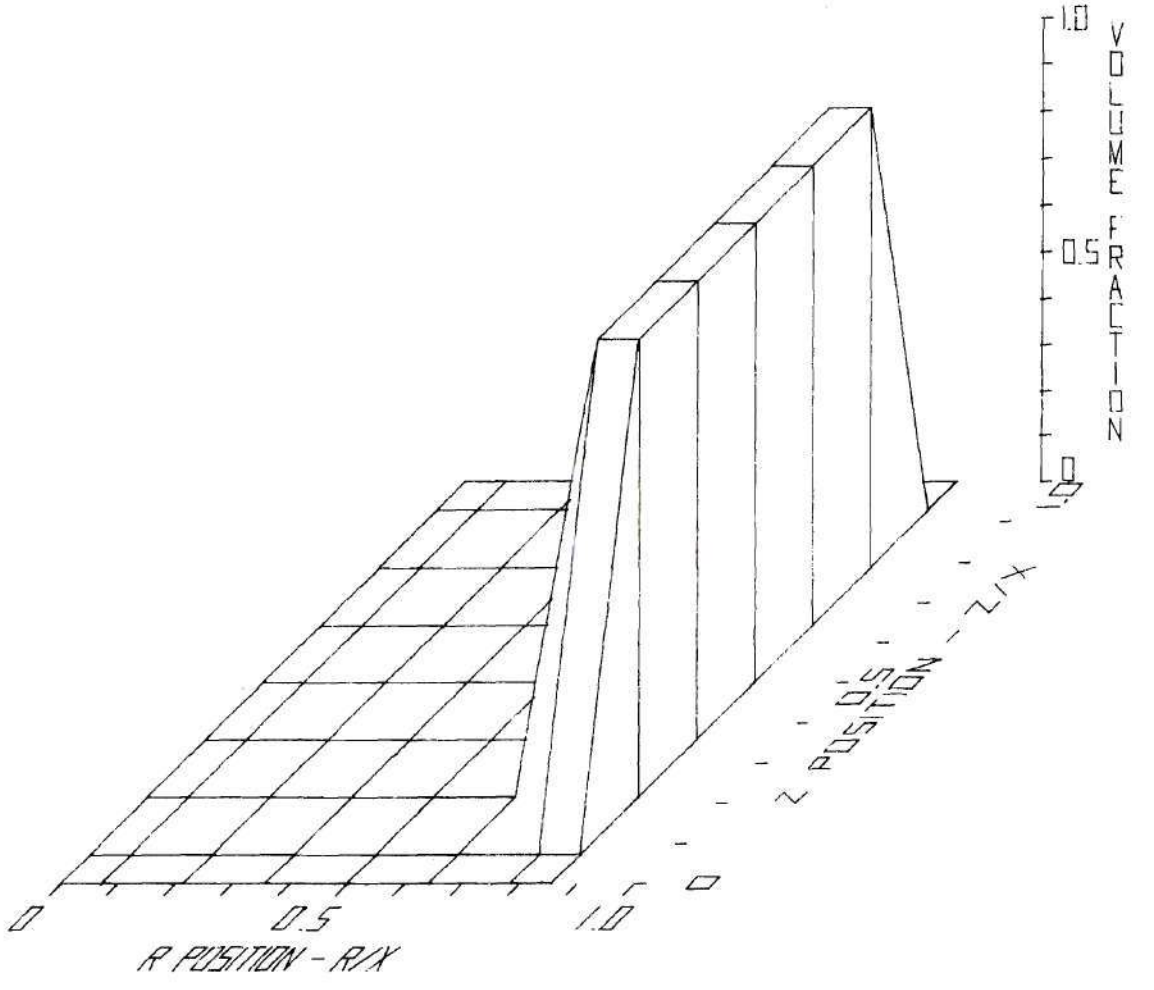

Figure 31: Liquid Steel Volume Fraction [T = 2.04889 sec]

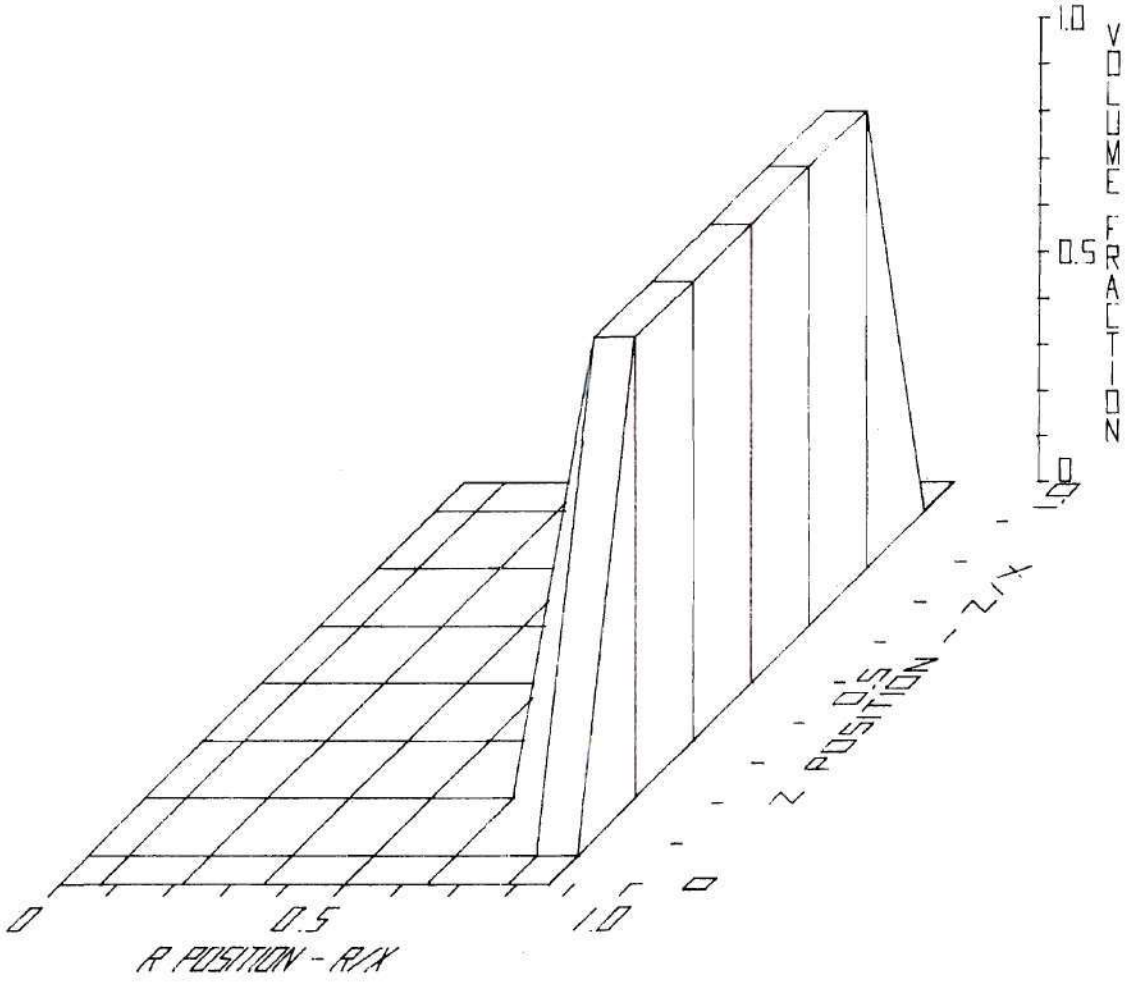

Figure 32: Liquid Steel Volume Fraction [T = 2.05204 sec]

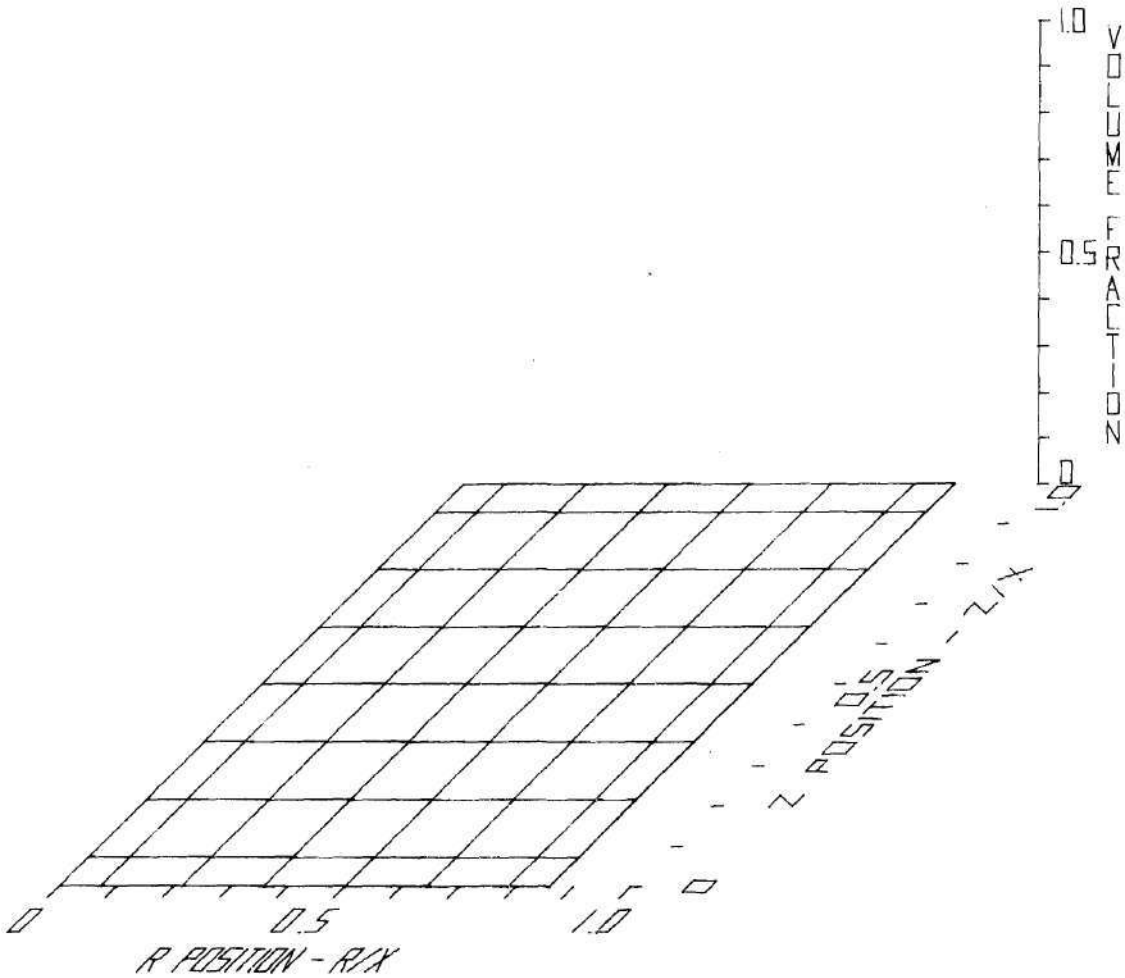

Figure 33: Vapor Fuel Volume Fraction [T = 0.00000 sec]

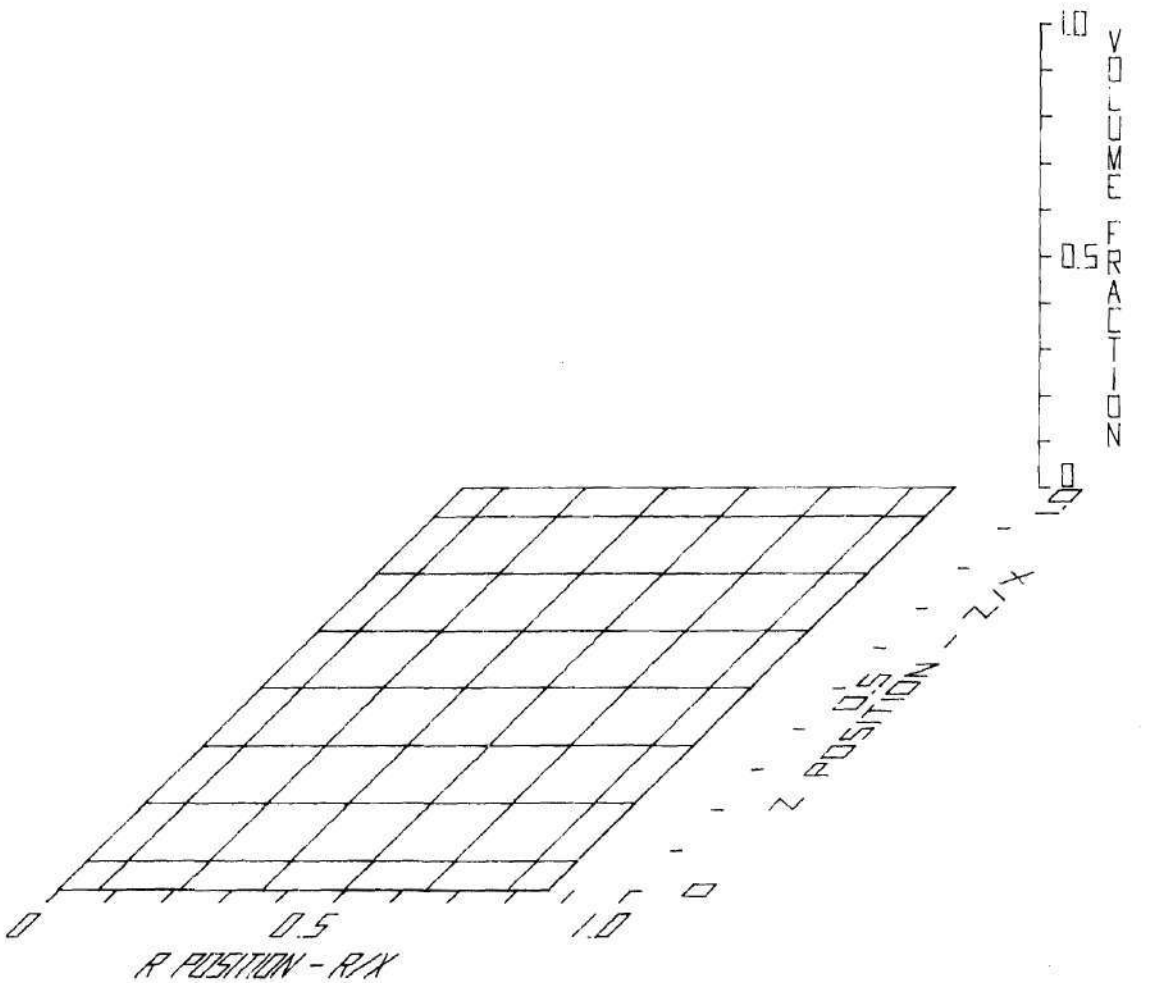

Figure 34: Vapor Fuel Volume Fraction [T = 2.04889]

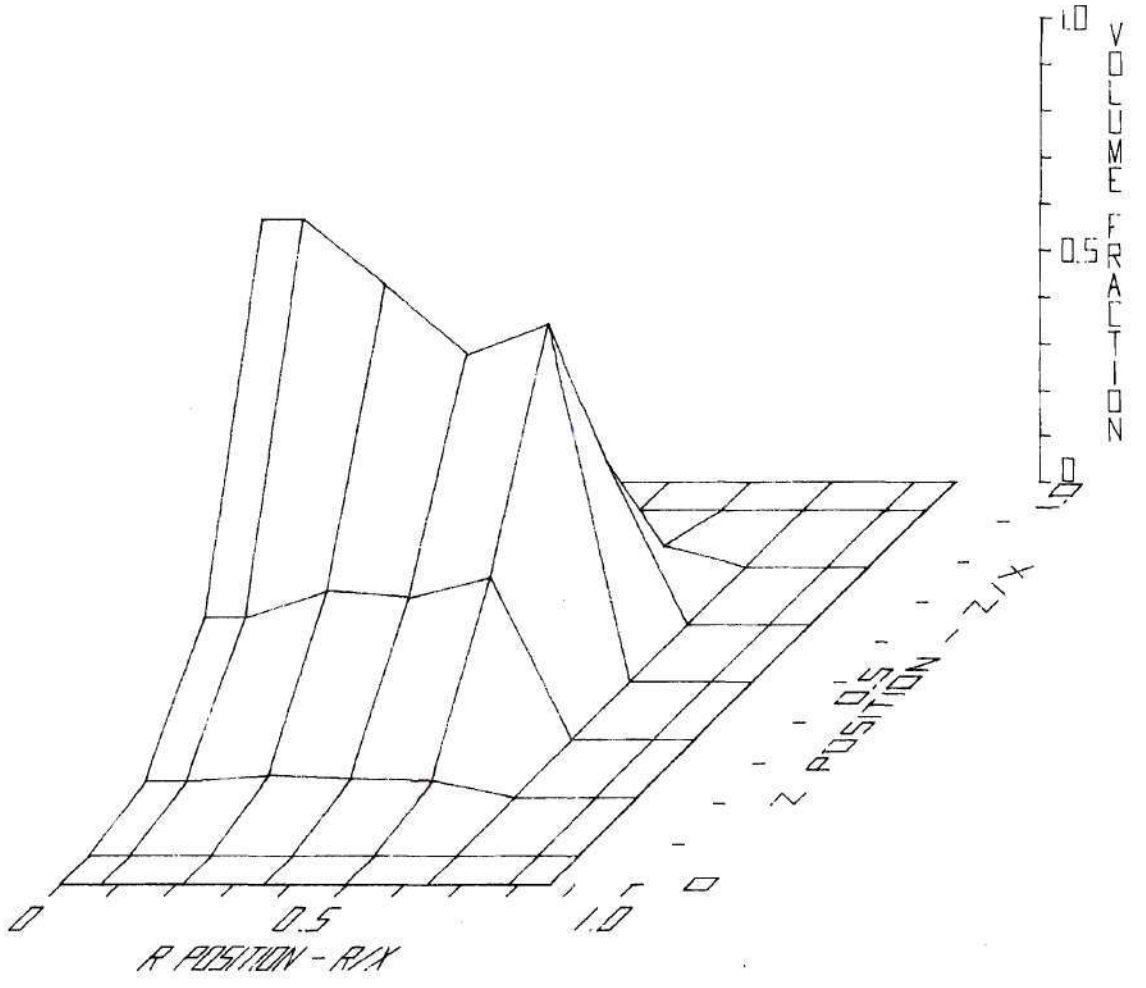

Figure 35: Vapor Fuel Volume Fraction [T = 2.05204 sec]

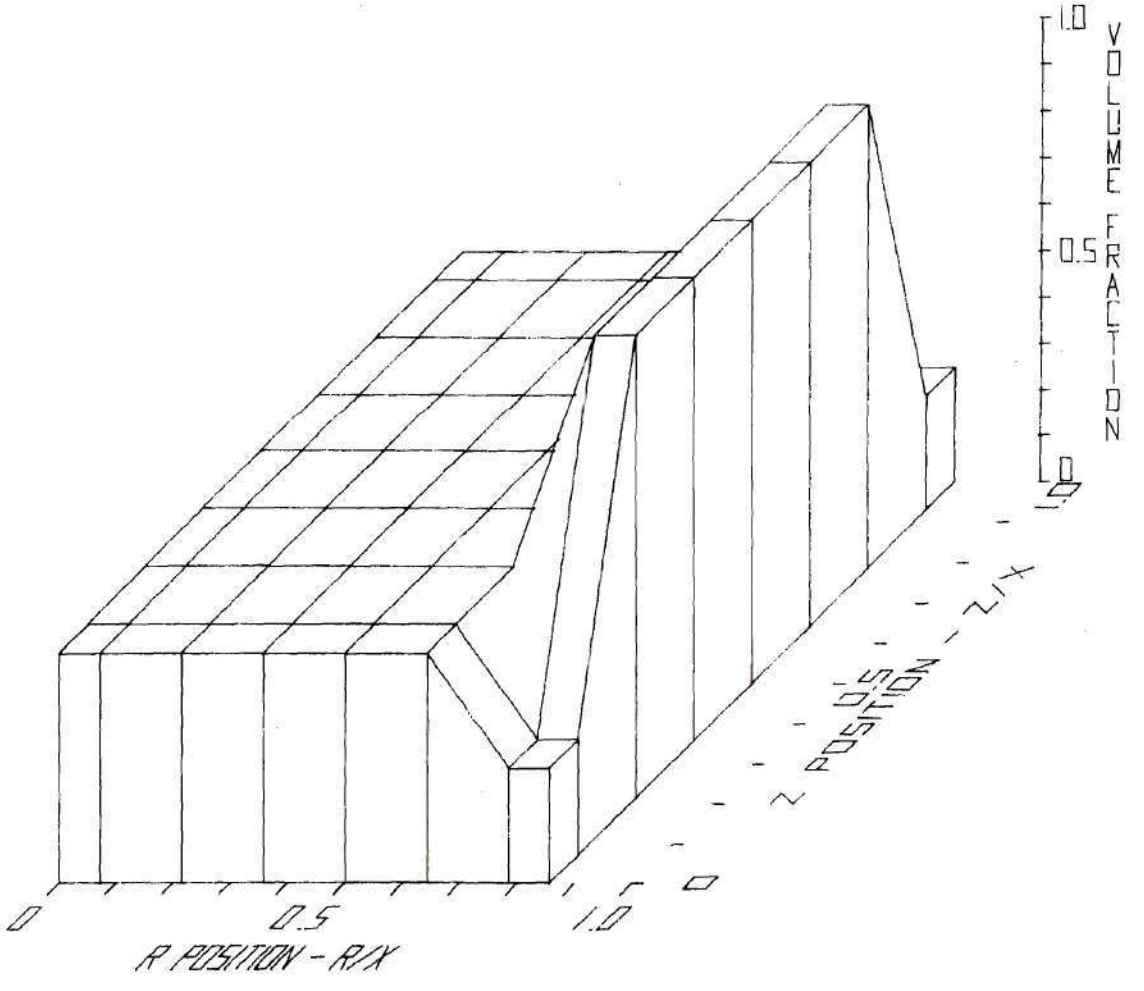

Figure 36: Fission Gas Volume Fraction [T = 0.00000 sec]

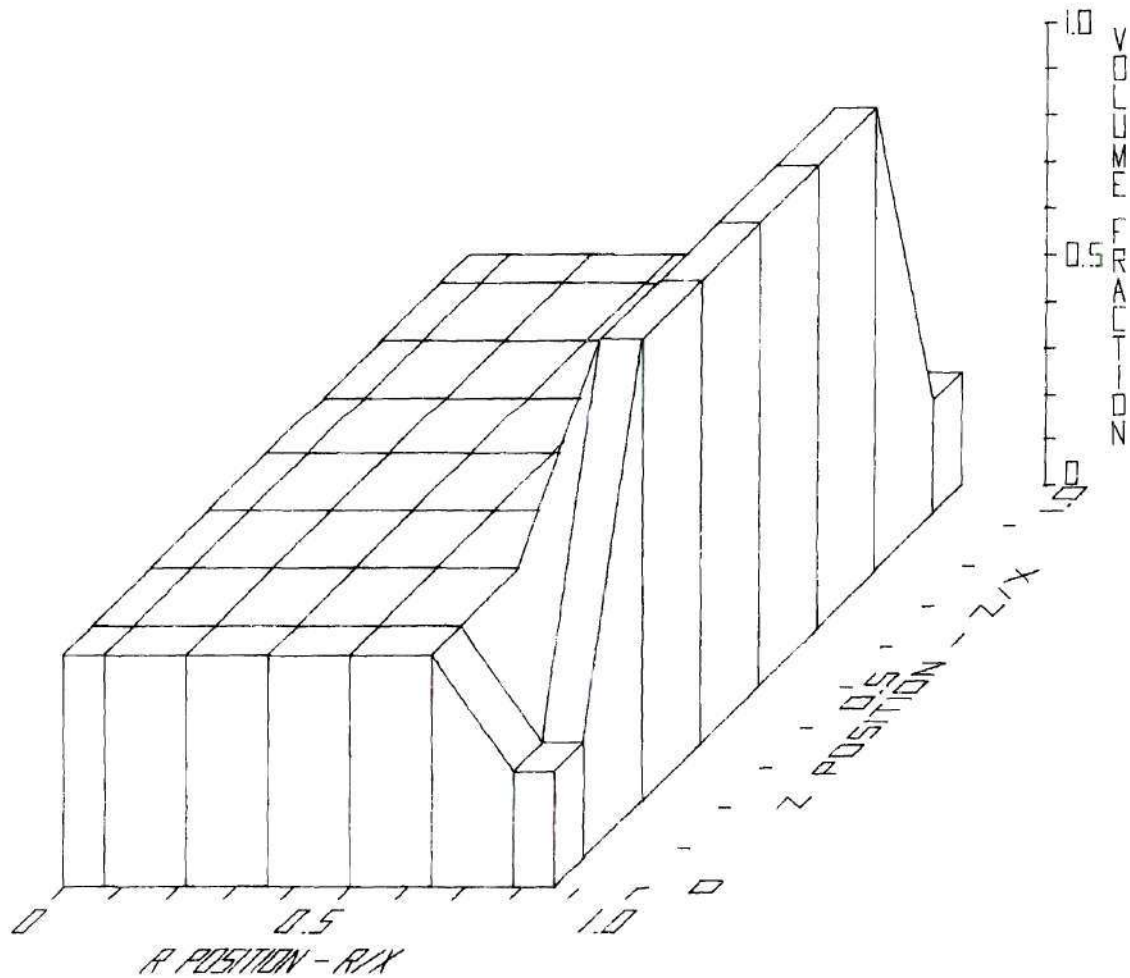

Figure 37: Fission Gas Volume Fraction [T = 2.04889 sec]

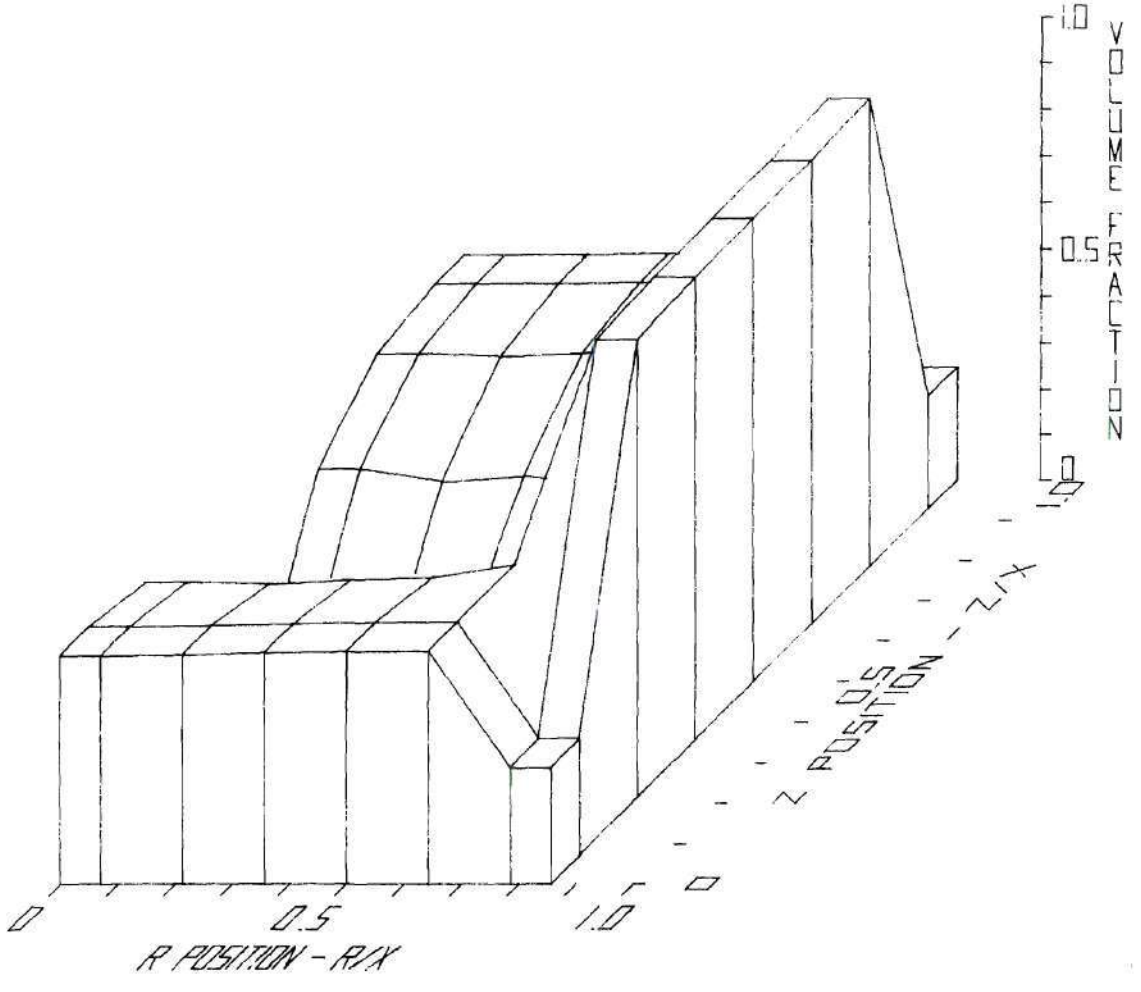

Figure 38: Fission Gas Volume Fraction [T = 2.05204 sec]

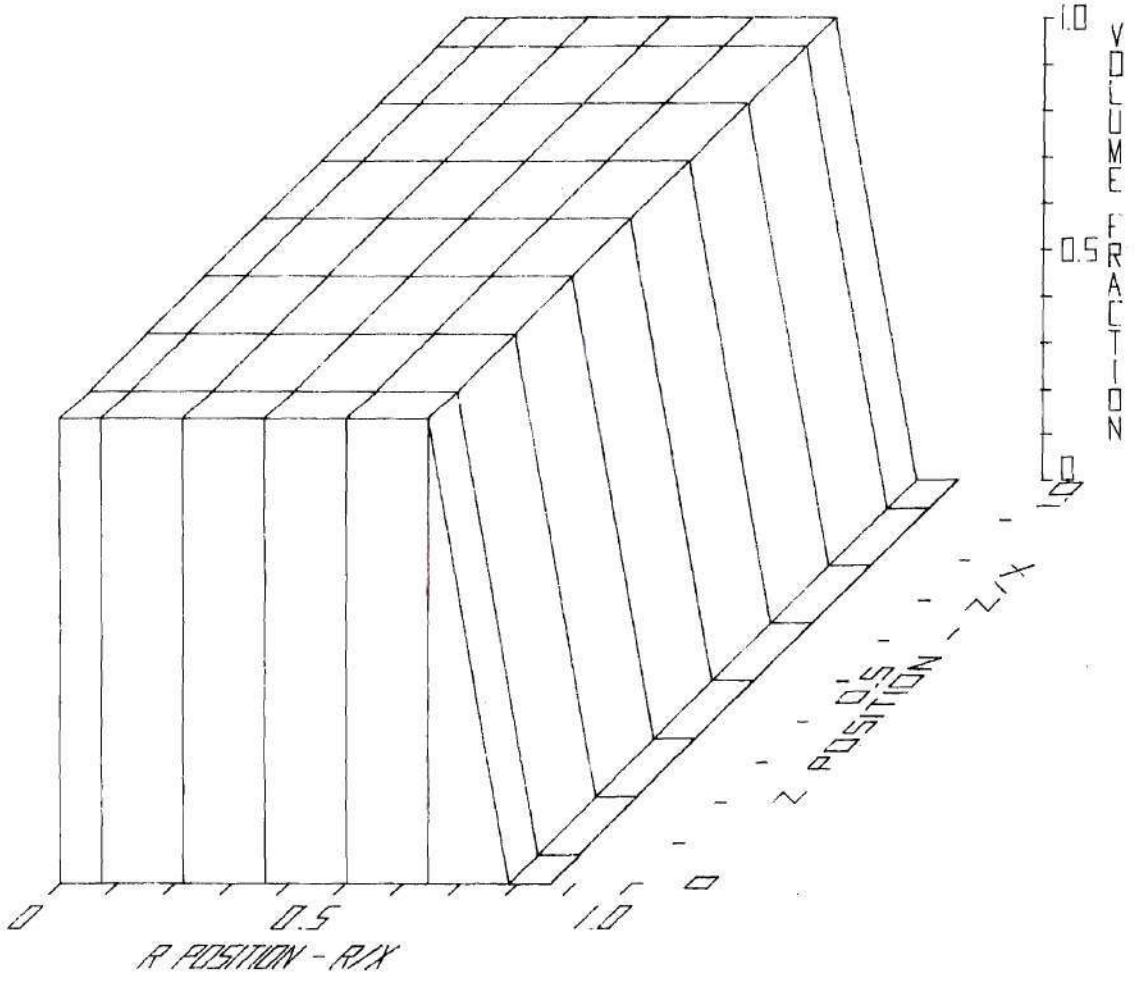

Figure 39: Solid Fuel Volume Fraction [T = 0.00000 sec]

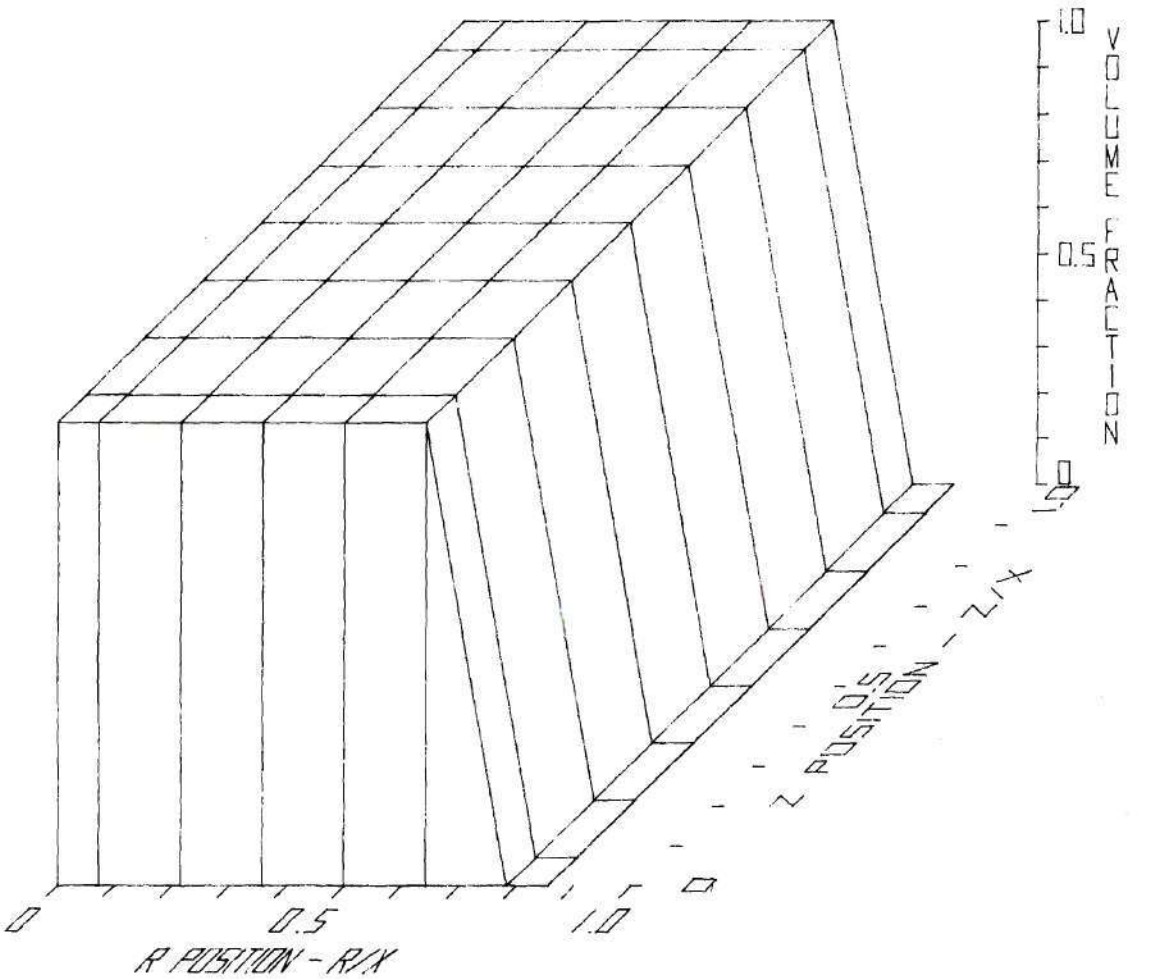

Figure 40: Solid Fuel Volume Fraction [T = 2.04889 sec]

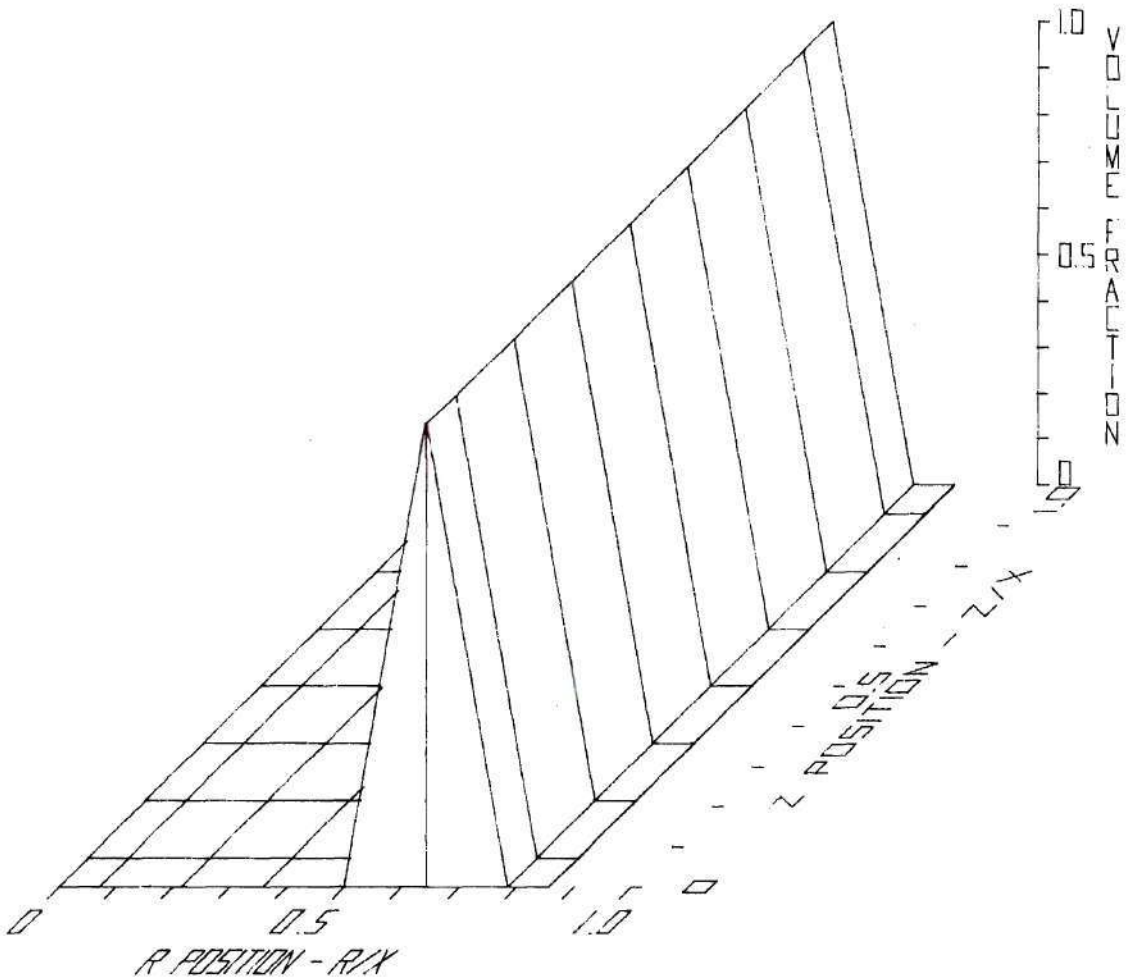

Figure 41: Solid Fuel Volume Fraction [T = 2.05204 sec]

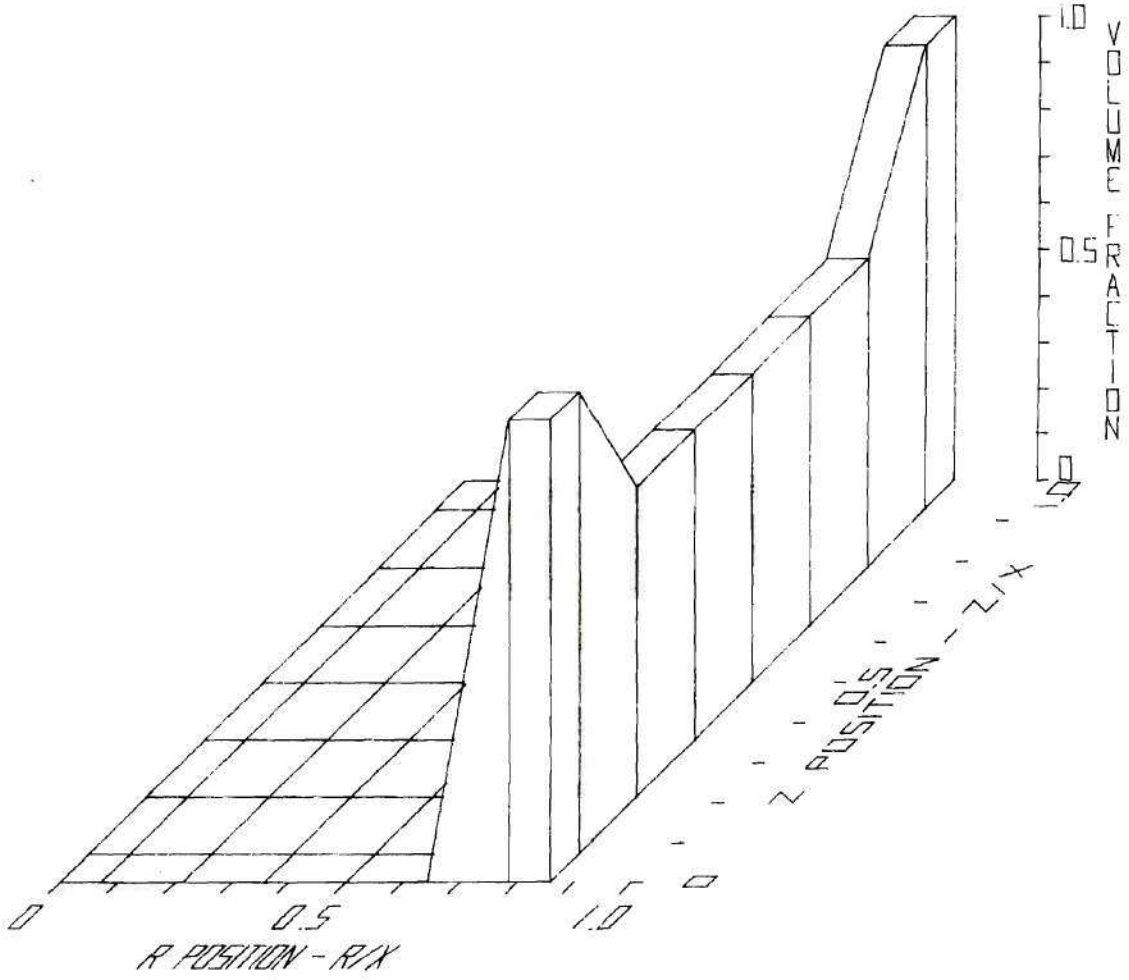

Figure 42: Solid Steel Volume Fraction [T = 0.00000 sec]

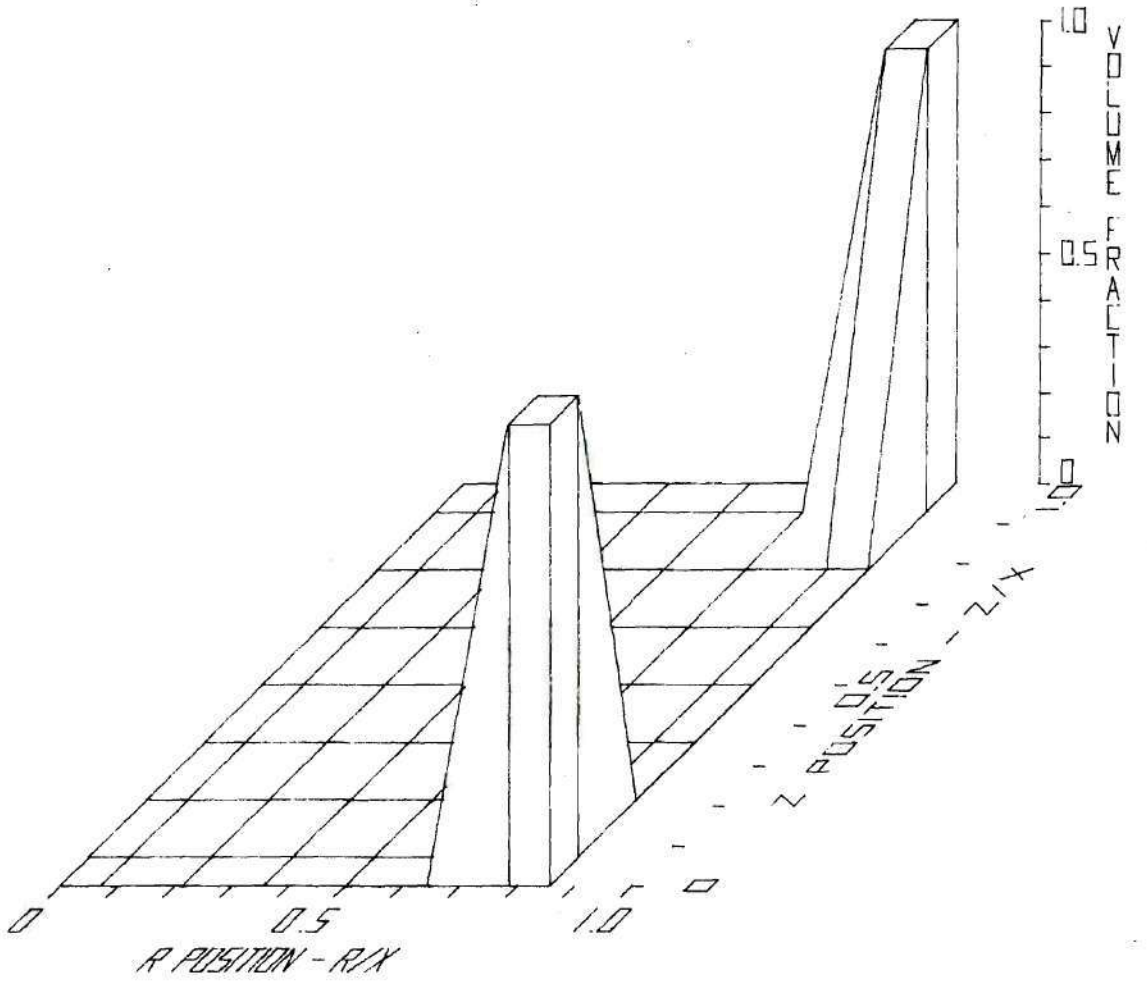

Figure 43: Solid Steel Volume Fraction [T = 2.04889 sec]

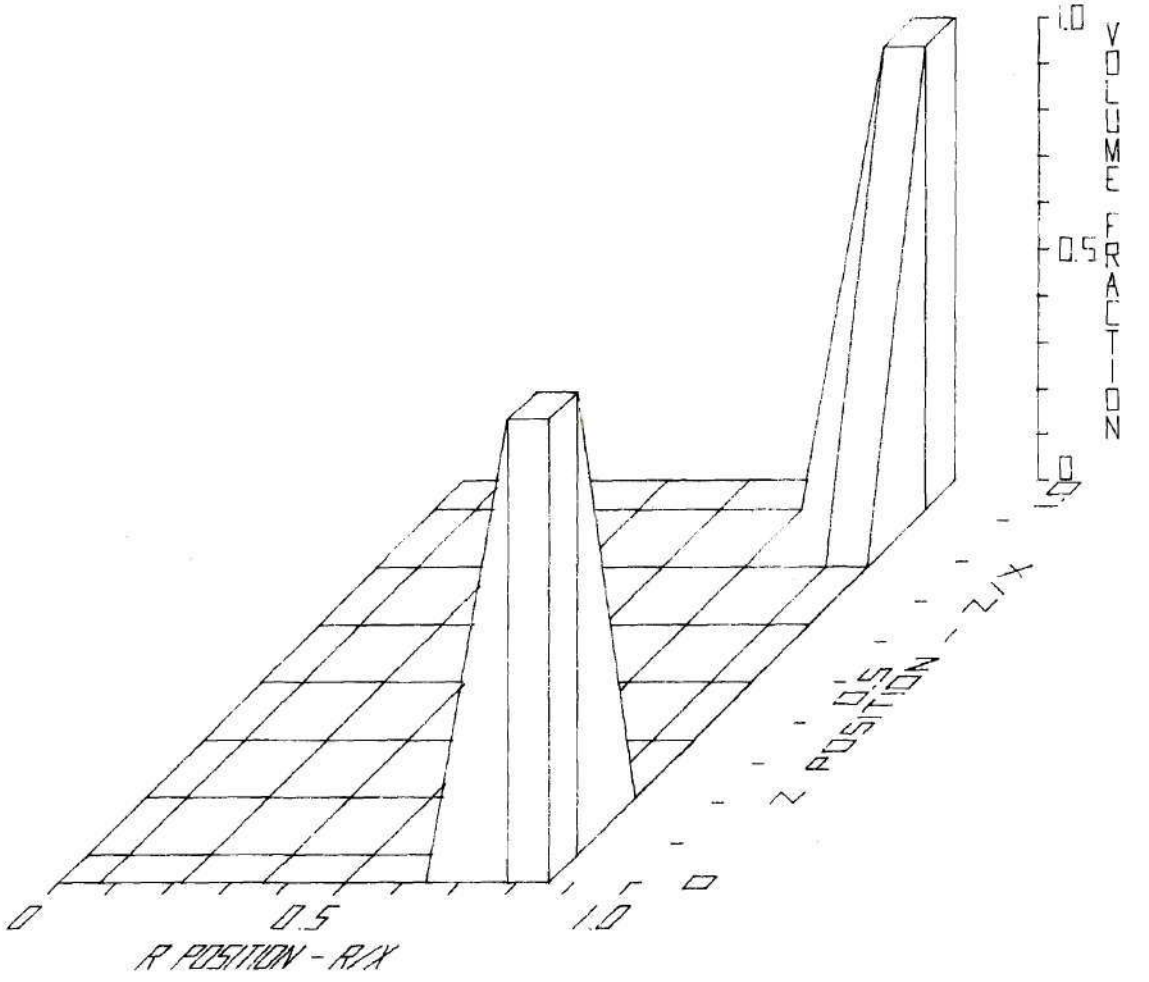

Figure 44: Solid Steel Volume Fraction [T = 2.05204 sec]

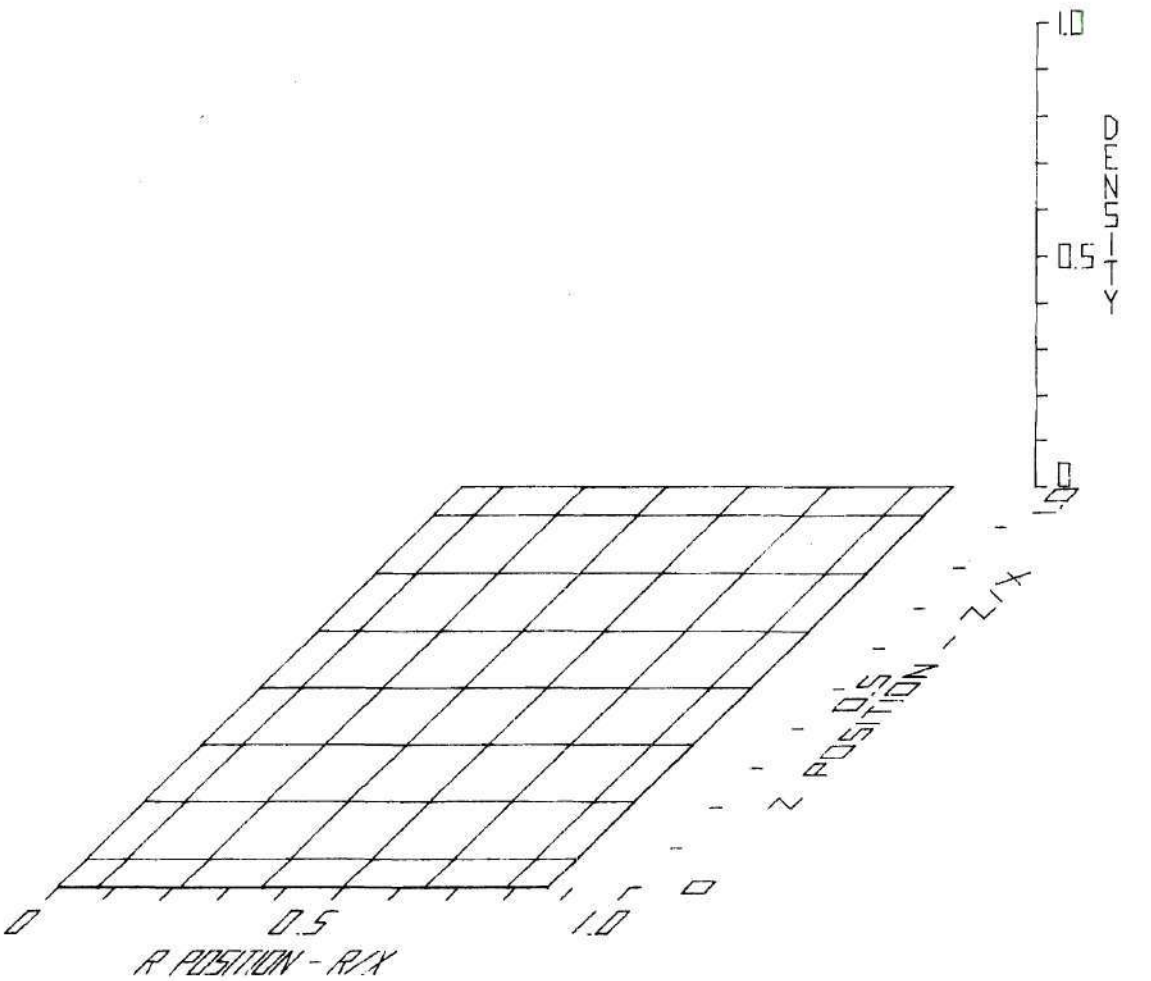

Figure 45: Liquid Fuel Density [T = 0.00000 sec]

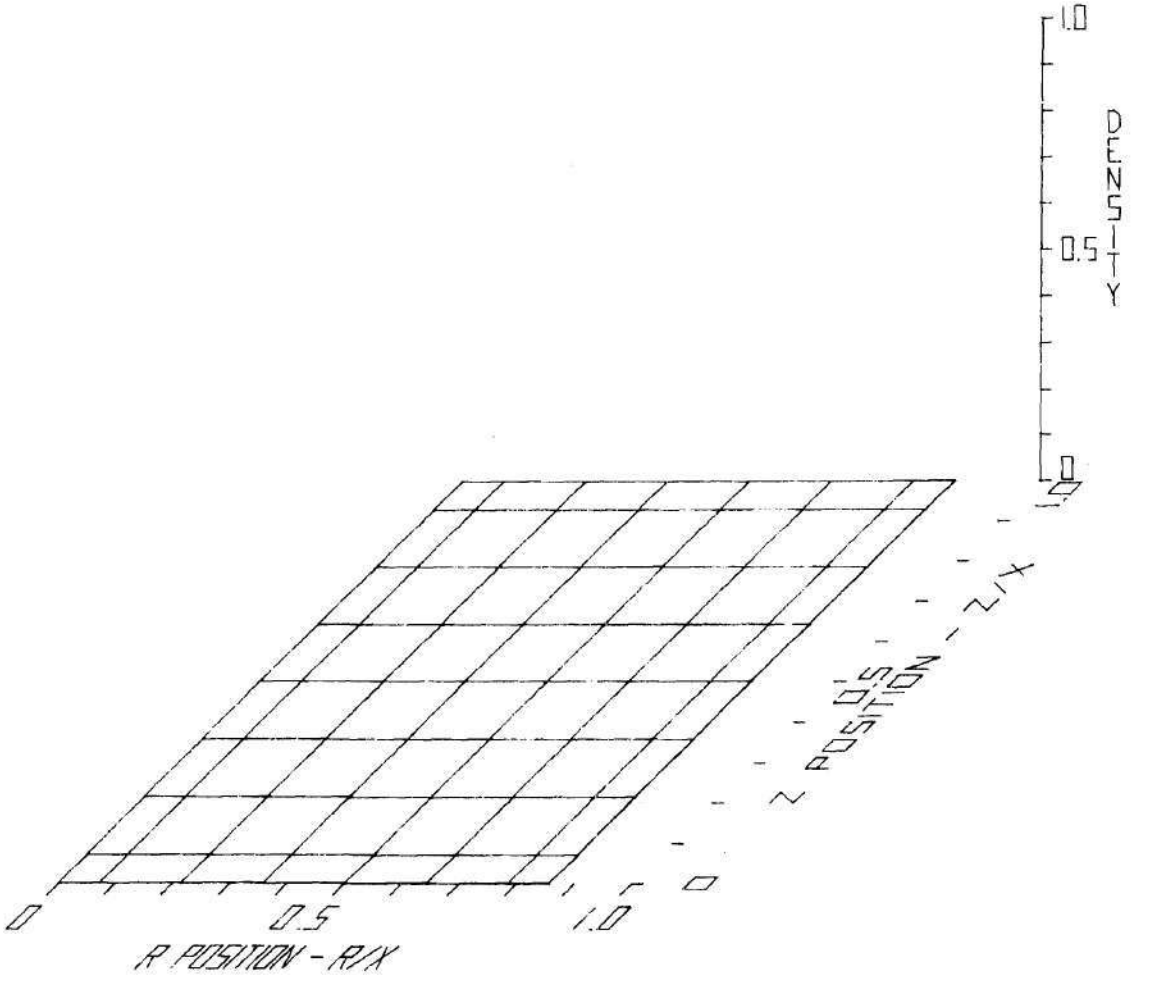

Figure 46: Liquid Fuel Density [T = 2.04889 sec]

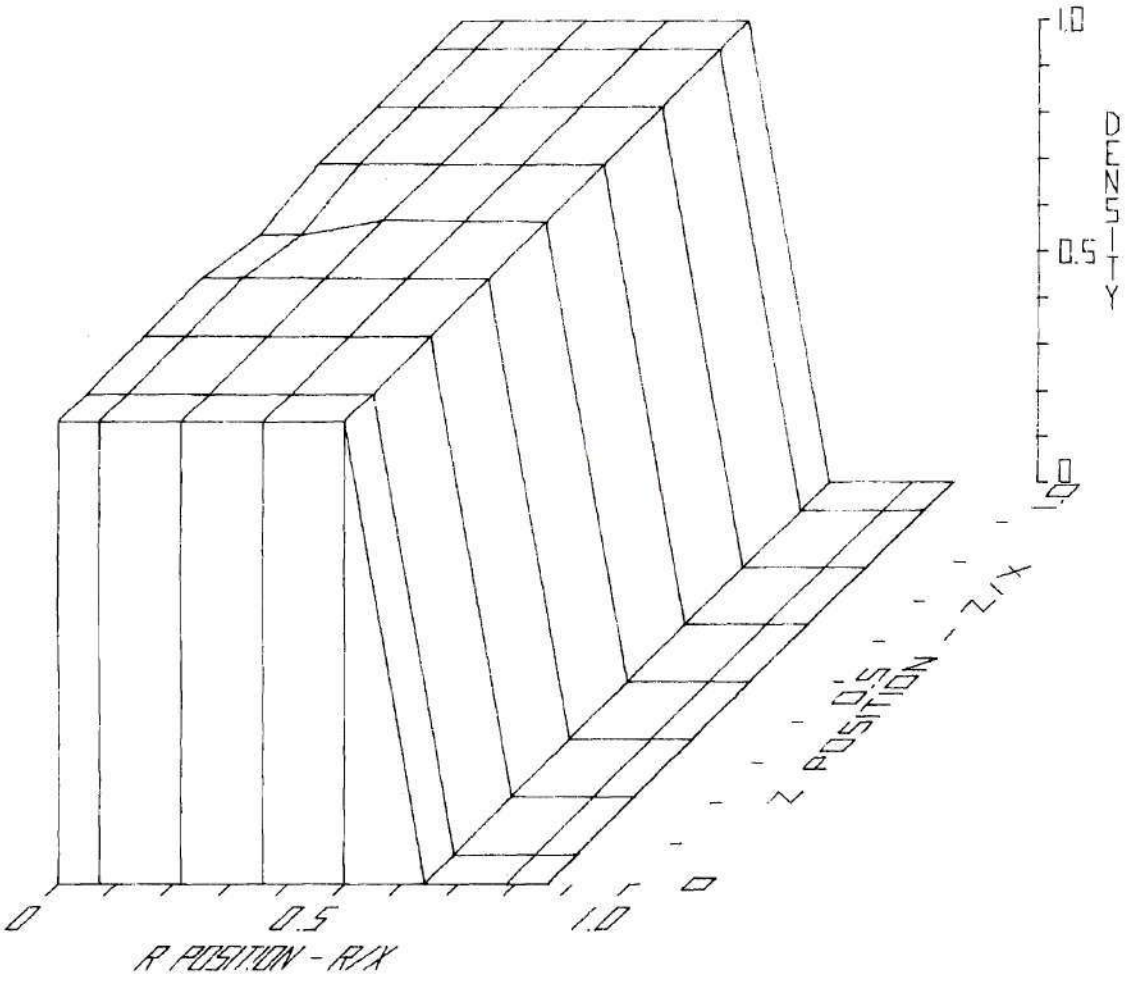

Figure 47: Liquid Fuel Density [T = 2.05204 sec]

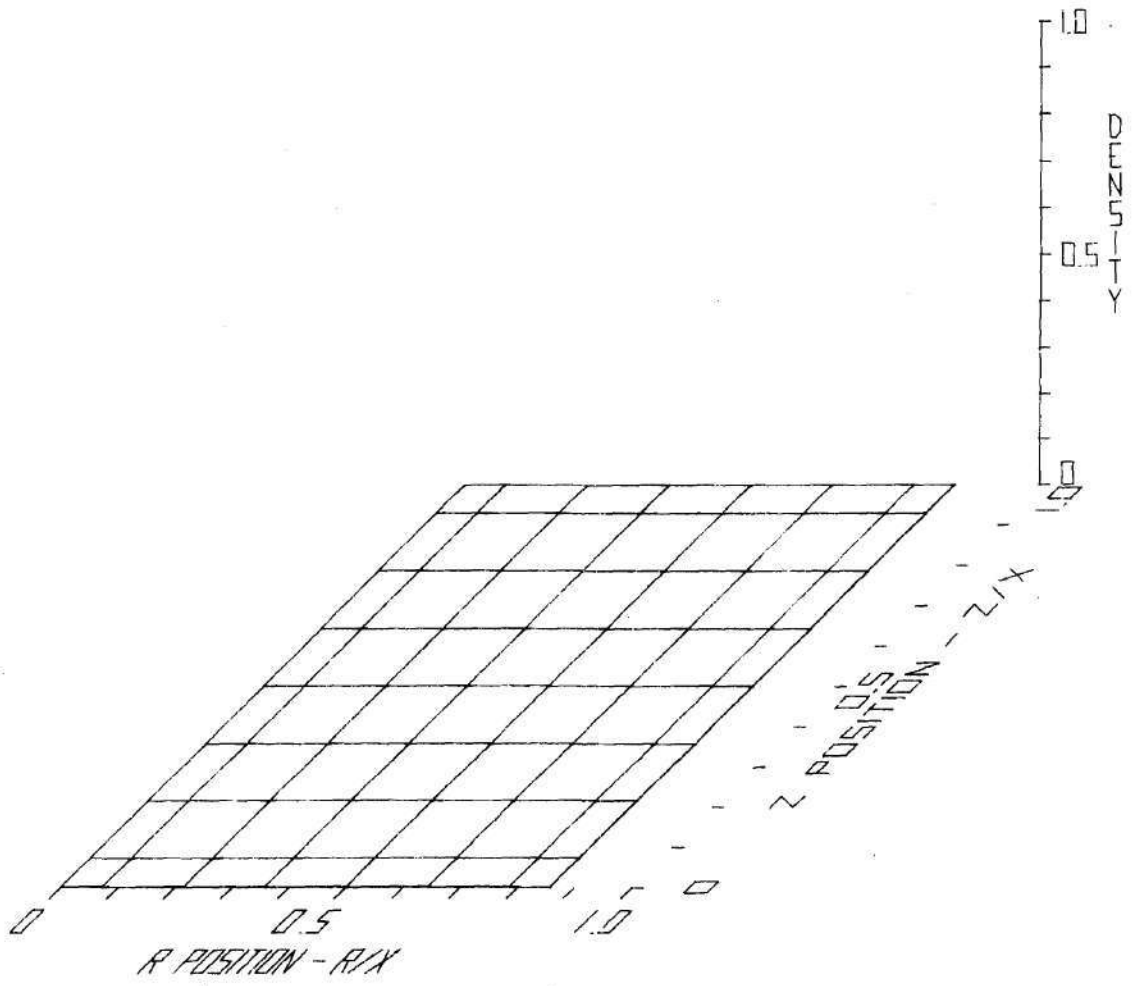

Figure 48: Liquid Steel Density [T = 0.00000 sec]

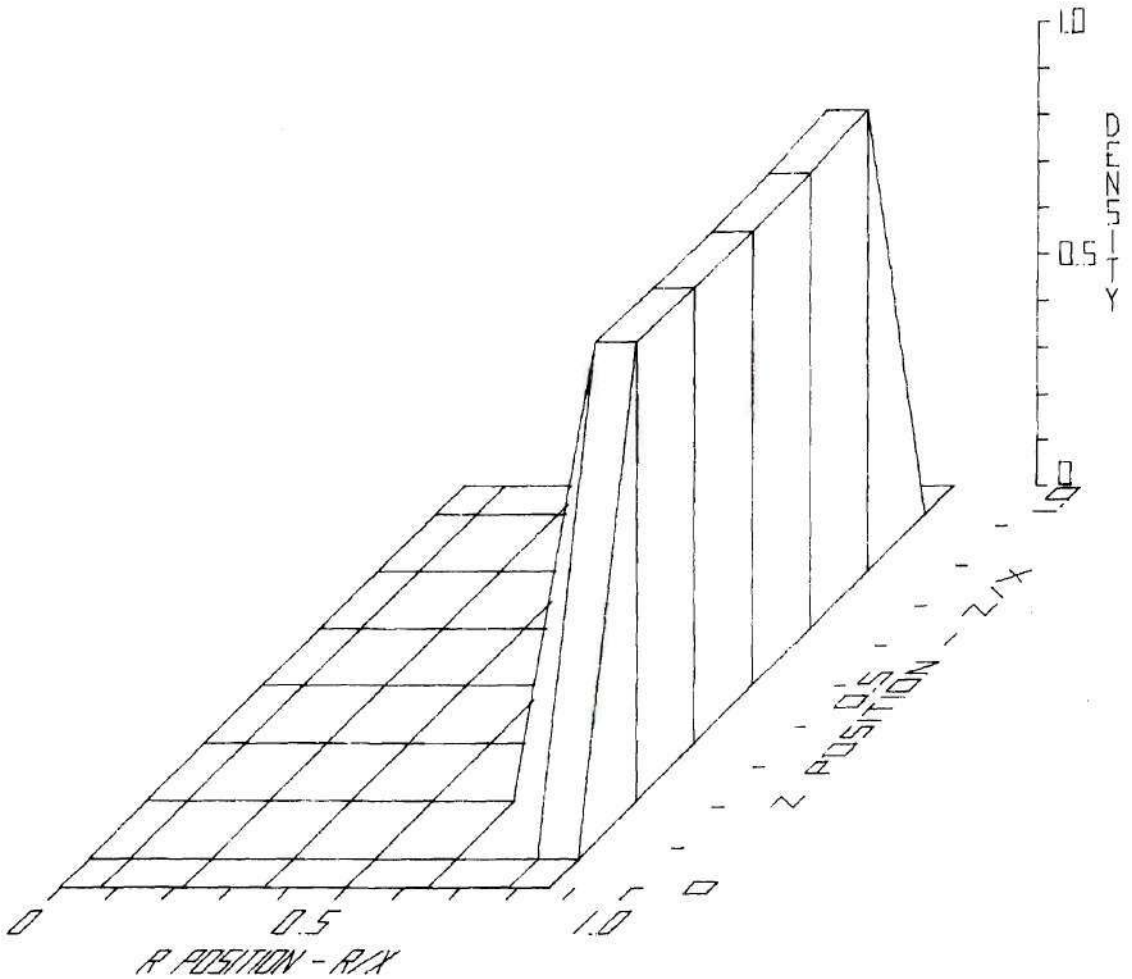

Figure 49: Liquid Steel Density [T = 2.04889 sec]

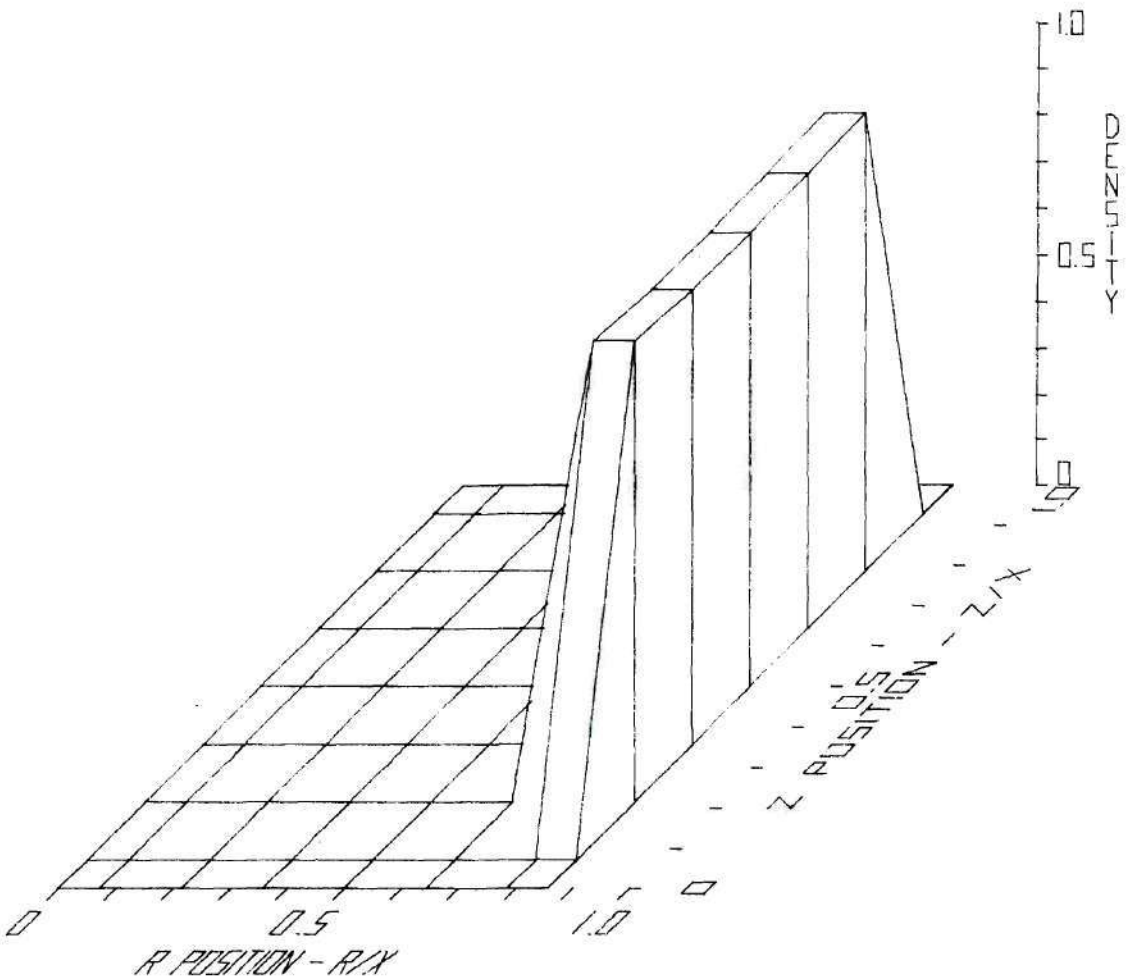

Figure 50: Liquid Steel Density [T = 2.05204 sec]

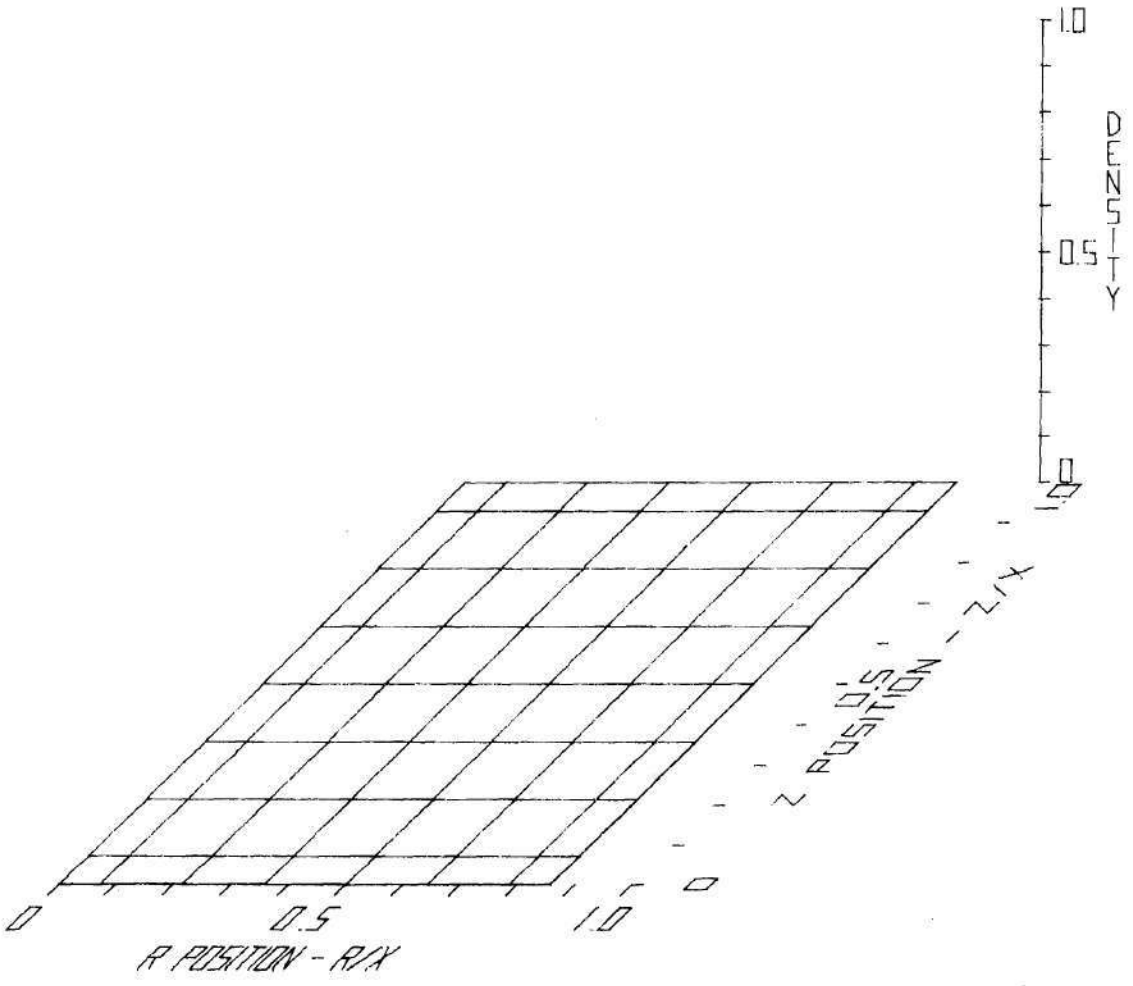

Figure 51: Vapor Fuel Density [T = 0.00000 sec]

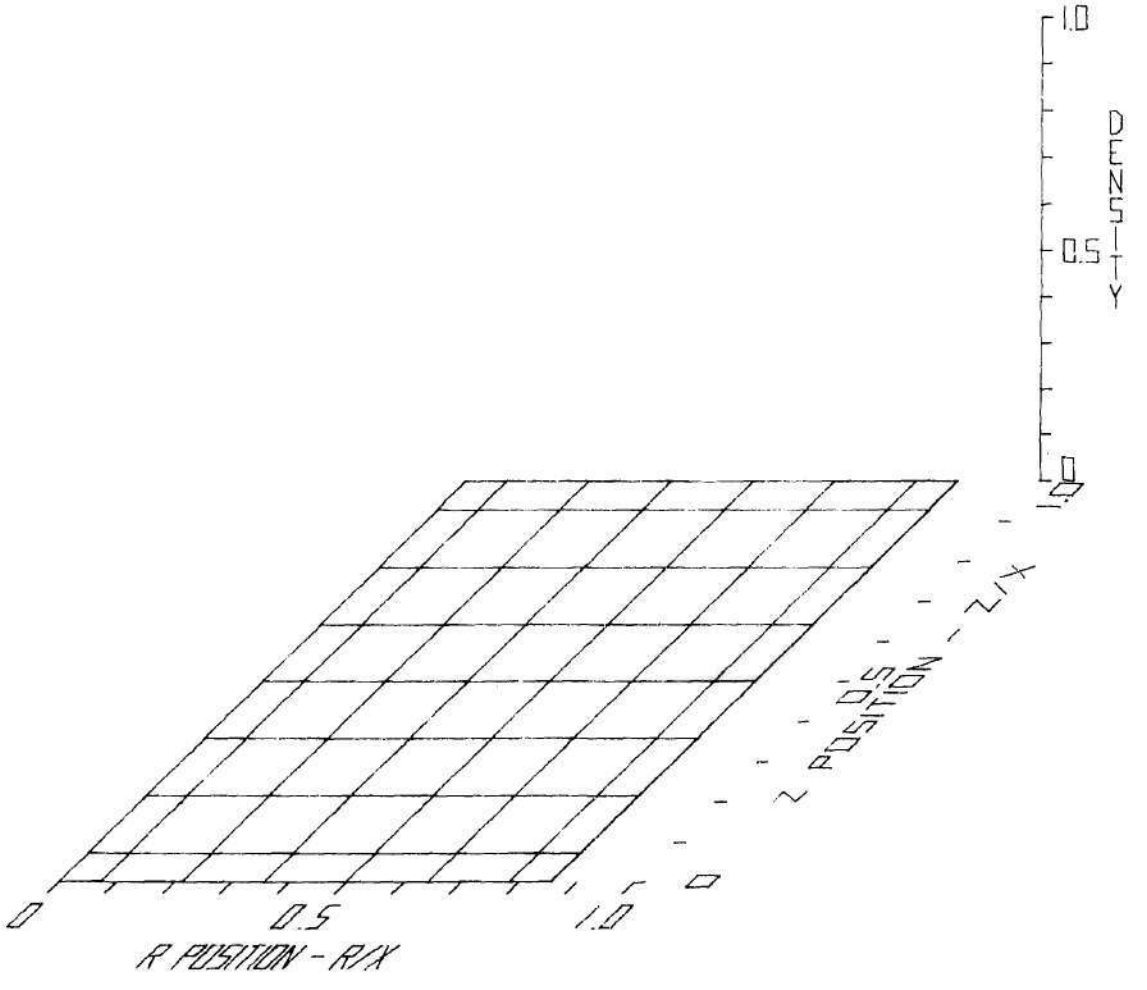

Figure 52: Vapor Fuel Density [T = 2.04889 sec]

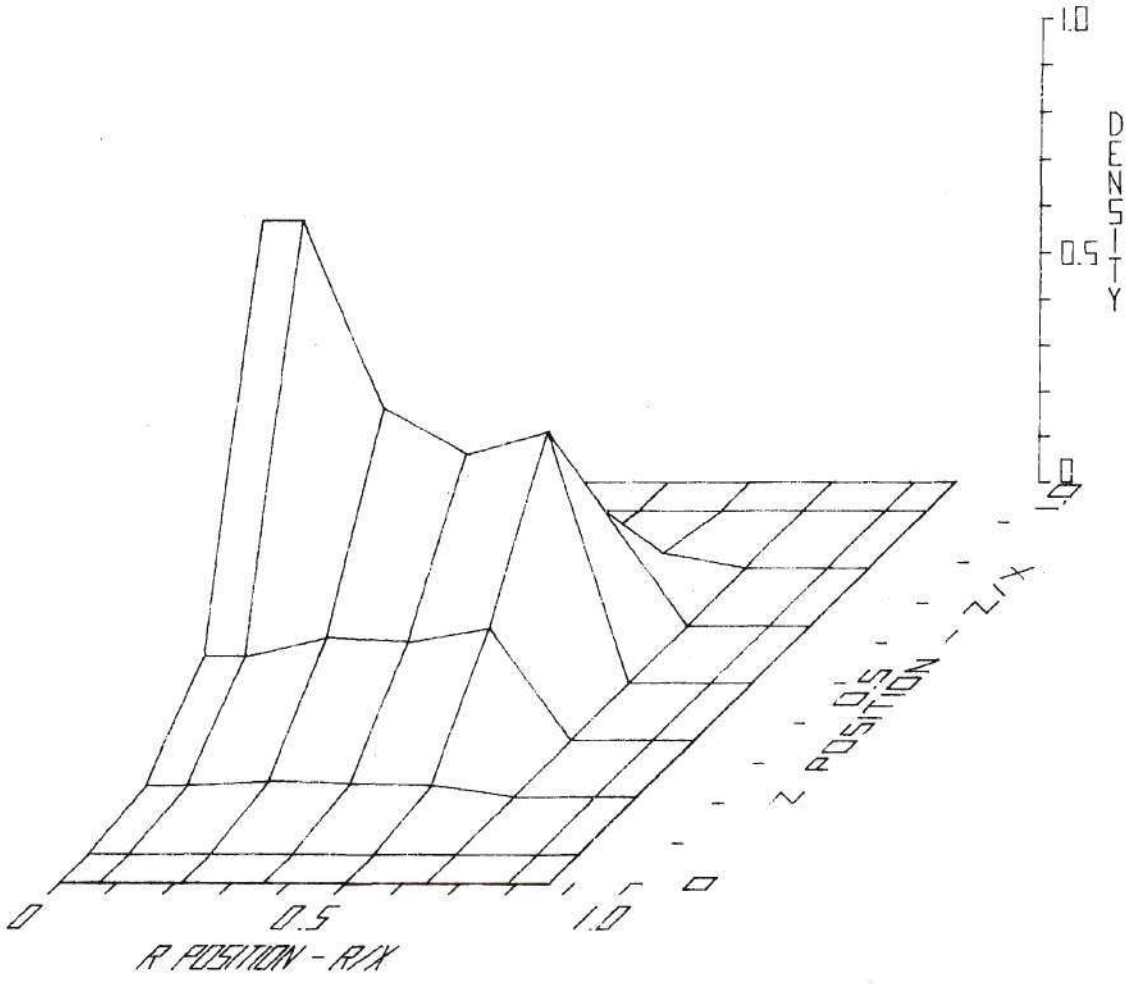

Figure 53: Vapor Fuel Density [T = 2.05204 sec]

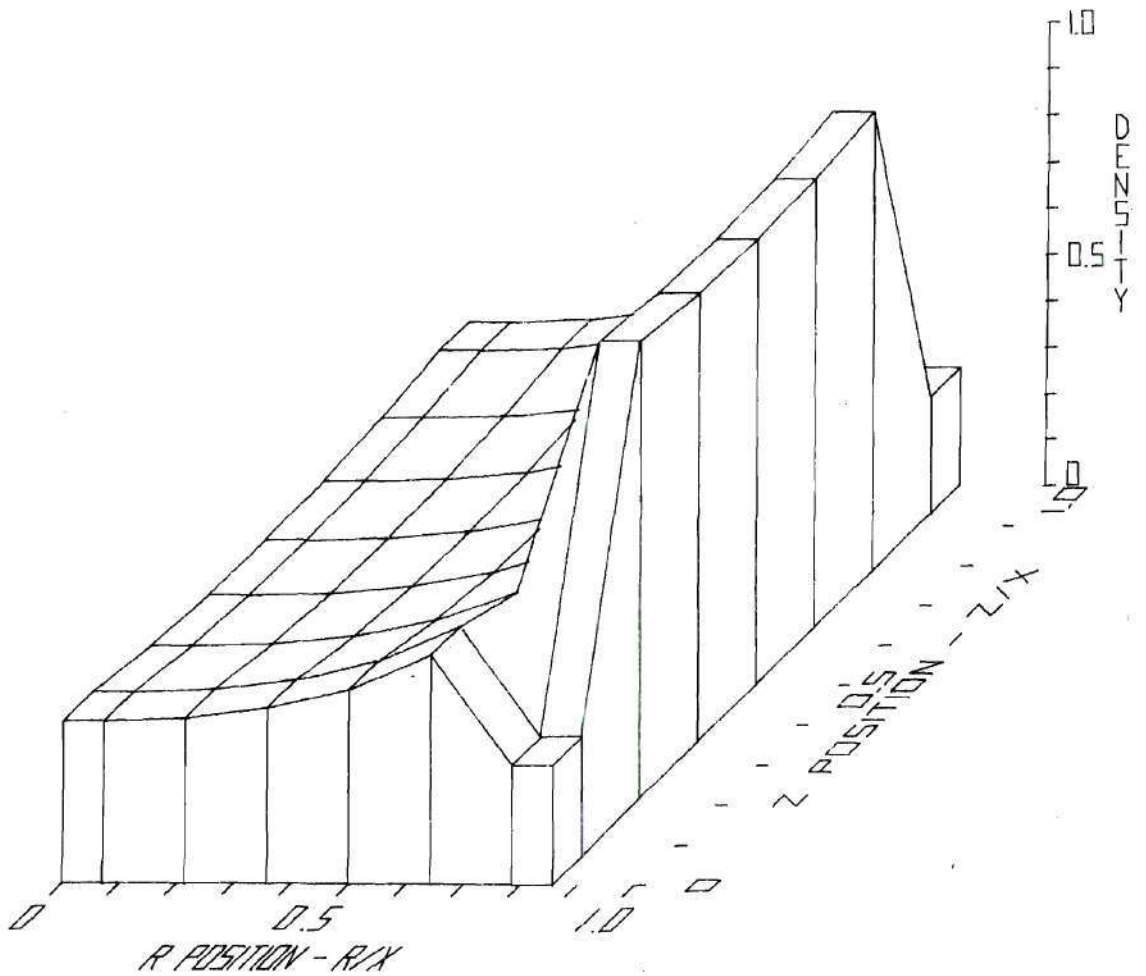

Figure 54: Fission Gas Density [T = 0.00000 sec]

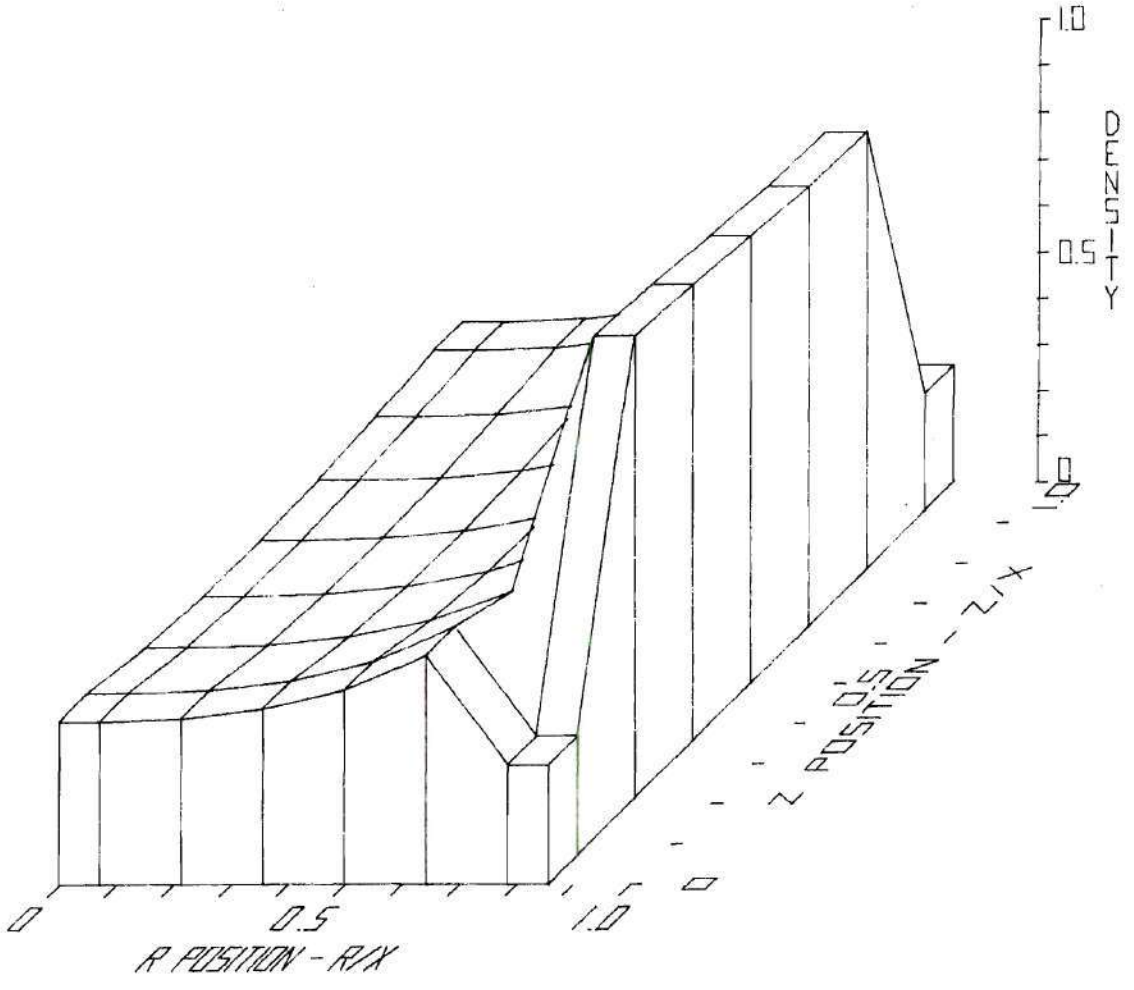

Figure 55: Fission Gas Density [T = 2.04889 sec]

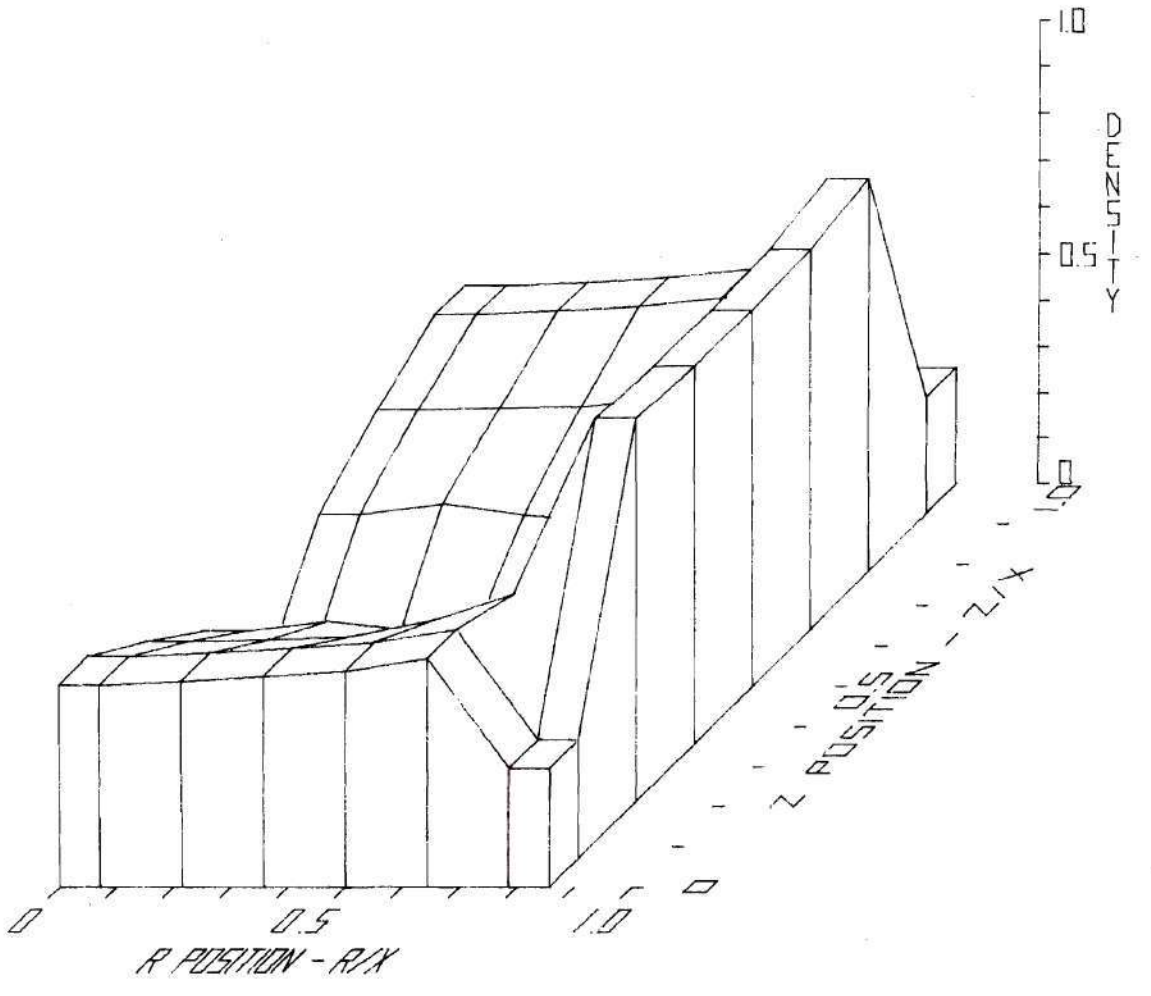

Figure 56: Fission Gas Density [T = 2.05204 sec]

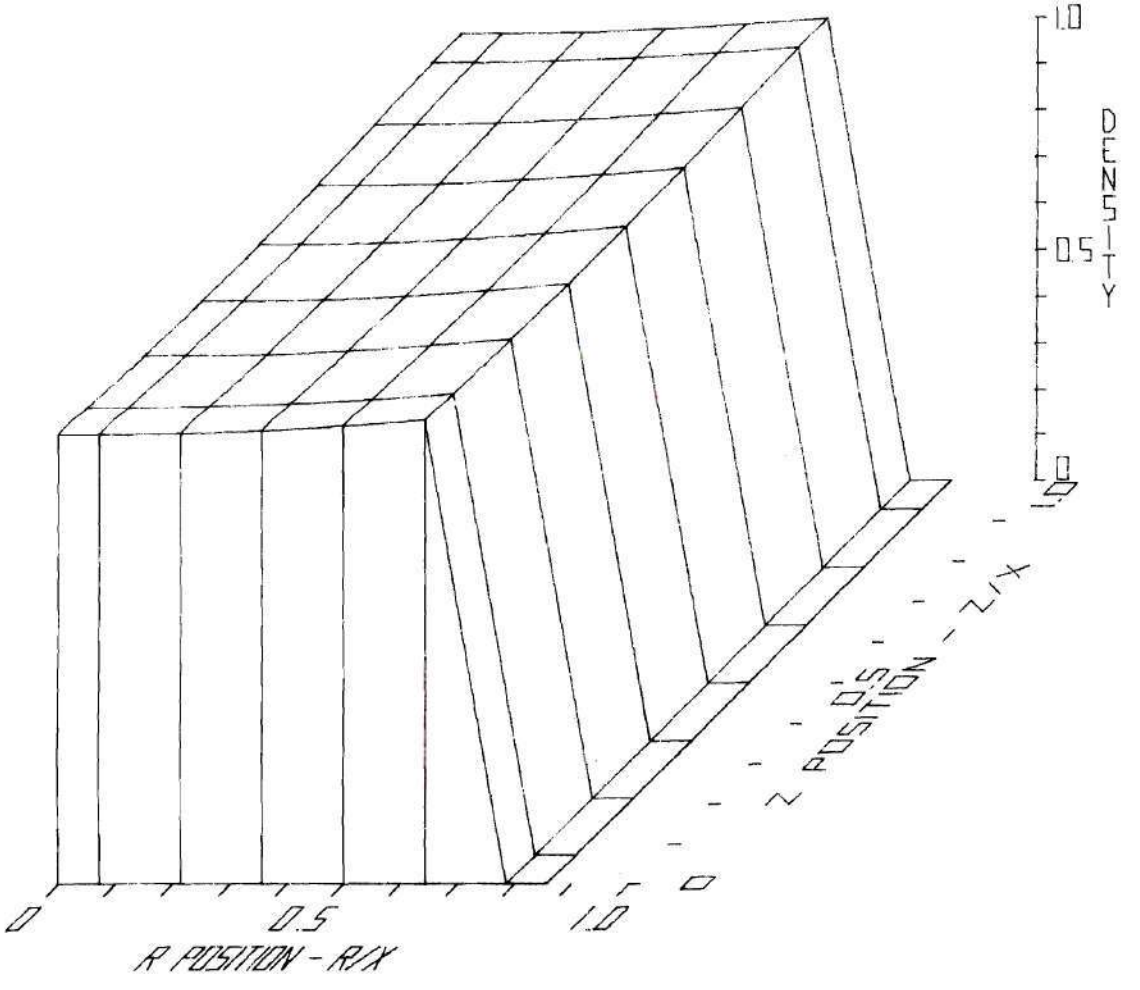

Figure 57: Solid Fuel Density [T = 0.00000 sec]

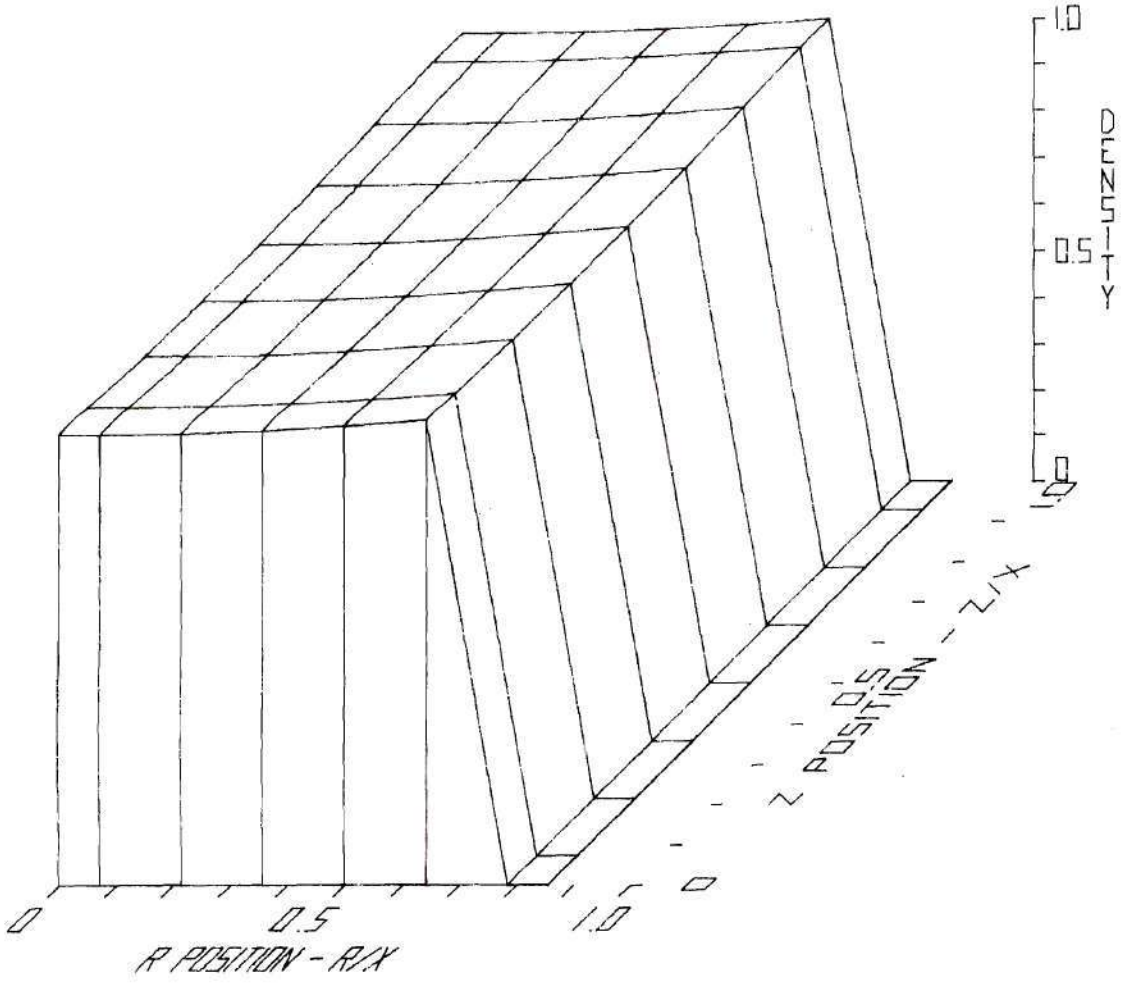

Figure 58: Solid Fuel Density [T = 2.04889 sec]

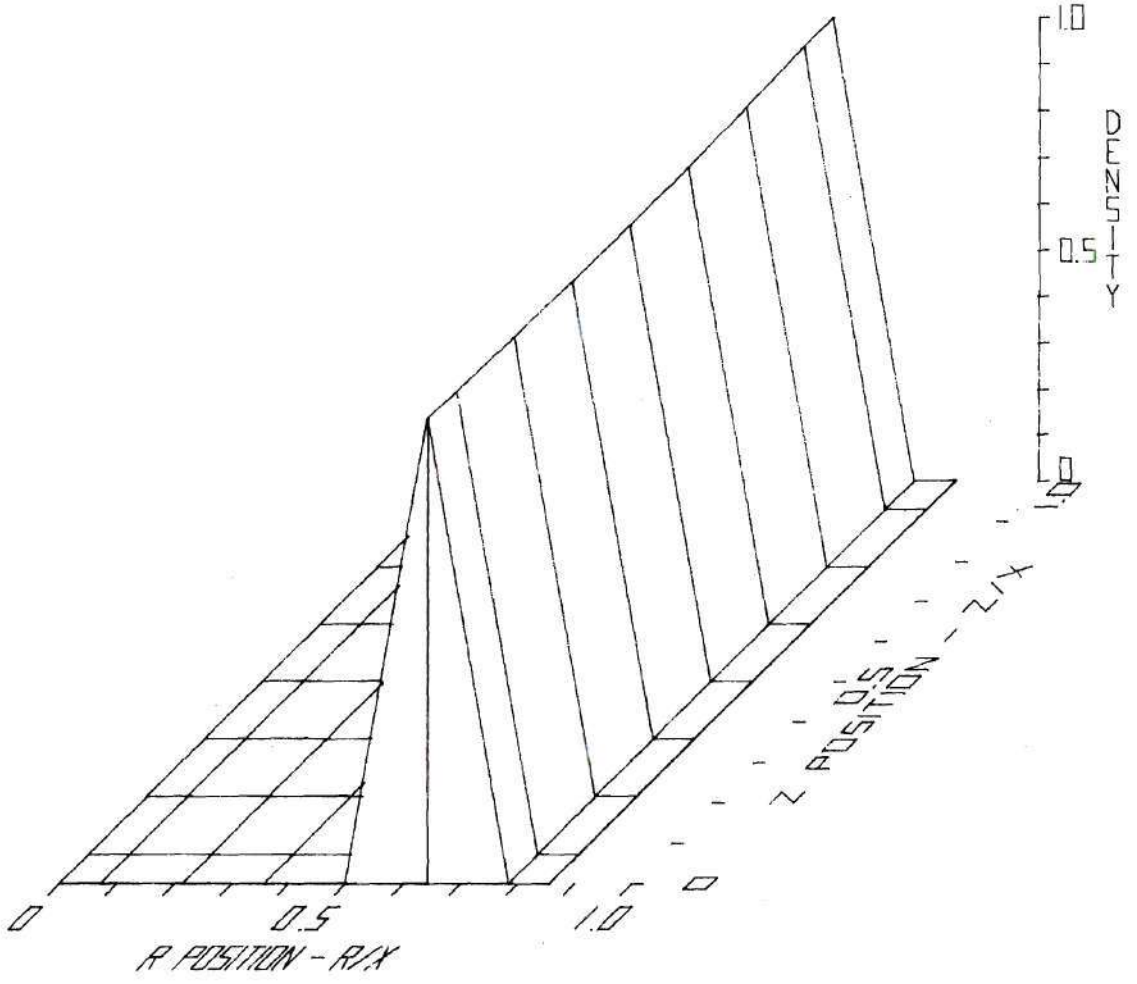

Figure 59: Solid Fuel Density [T = 2.05204 sec]

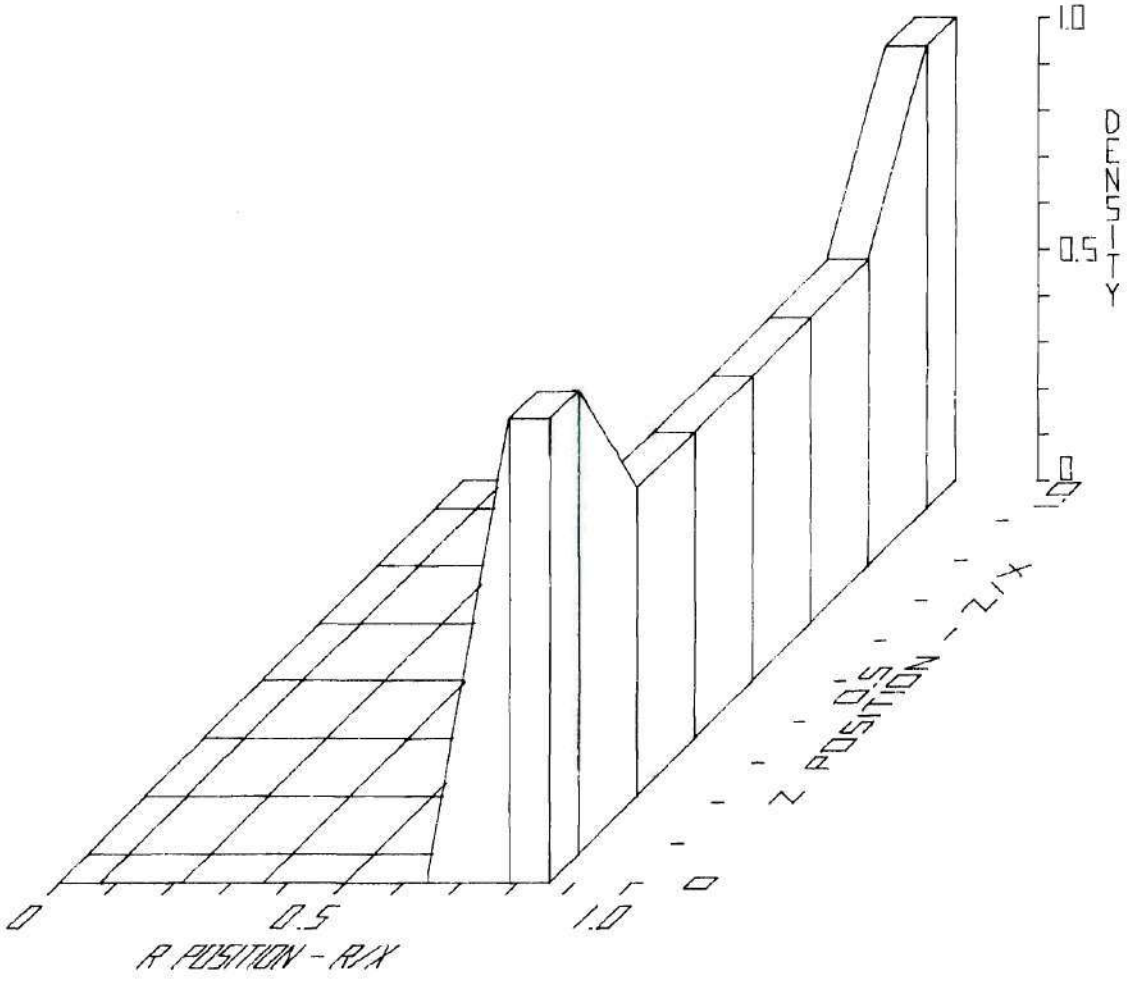

Figure 60: Solid Steel Density [T = 0.00000 sec]

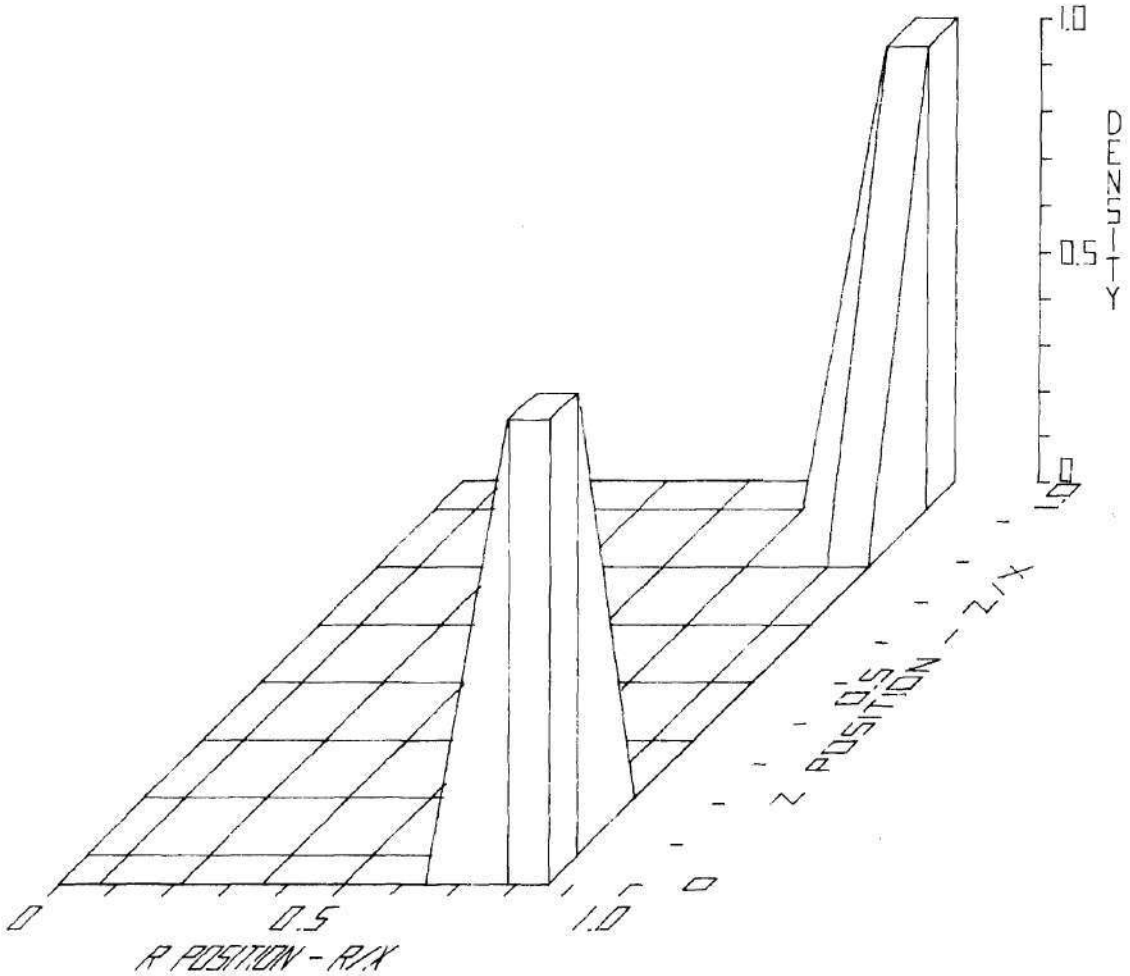

Figure 61: Solid Steel Density [T = 2.04889 sec]

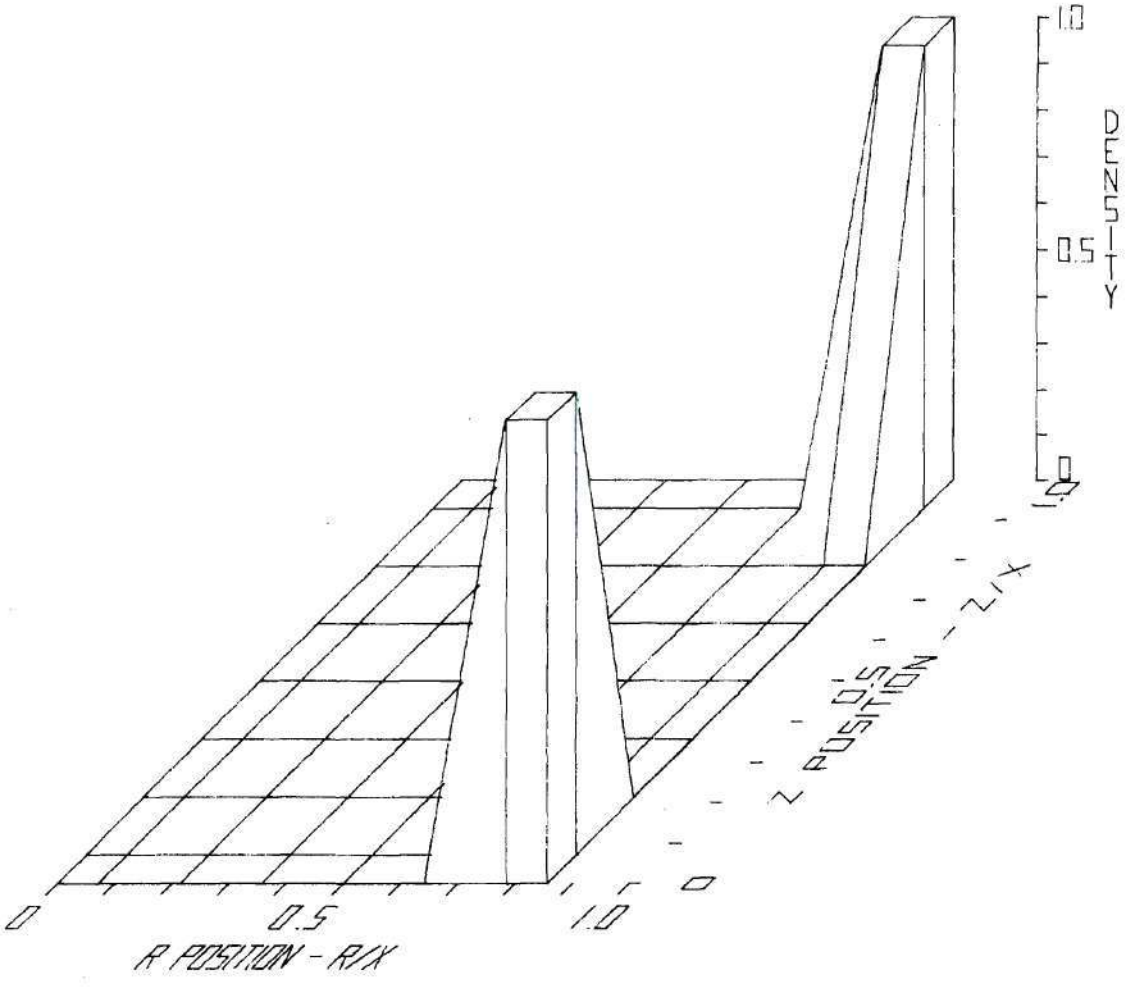

Figure 62: Solid Steel Density [T = 2.05204 sec]

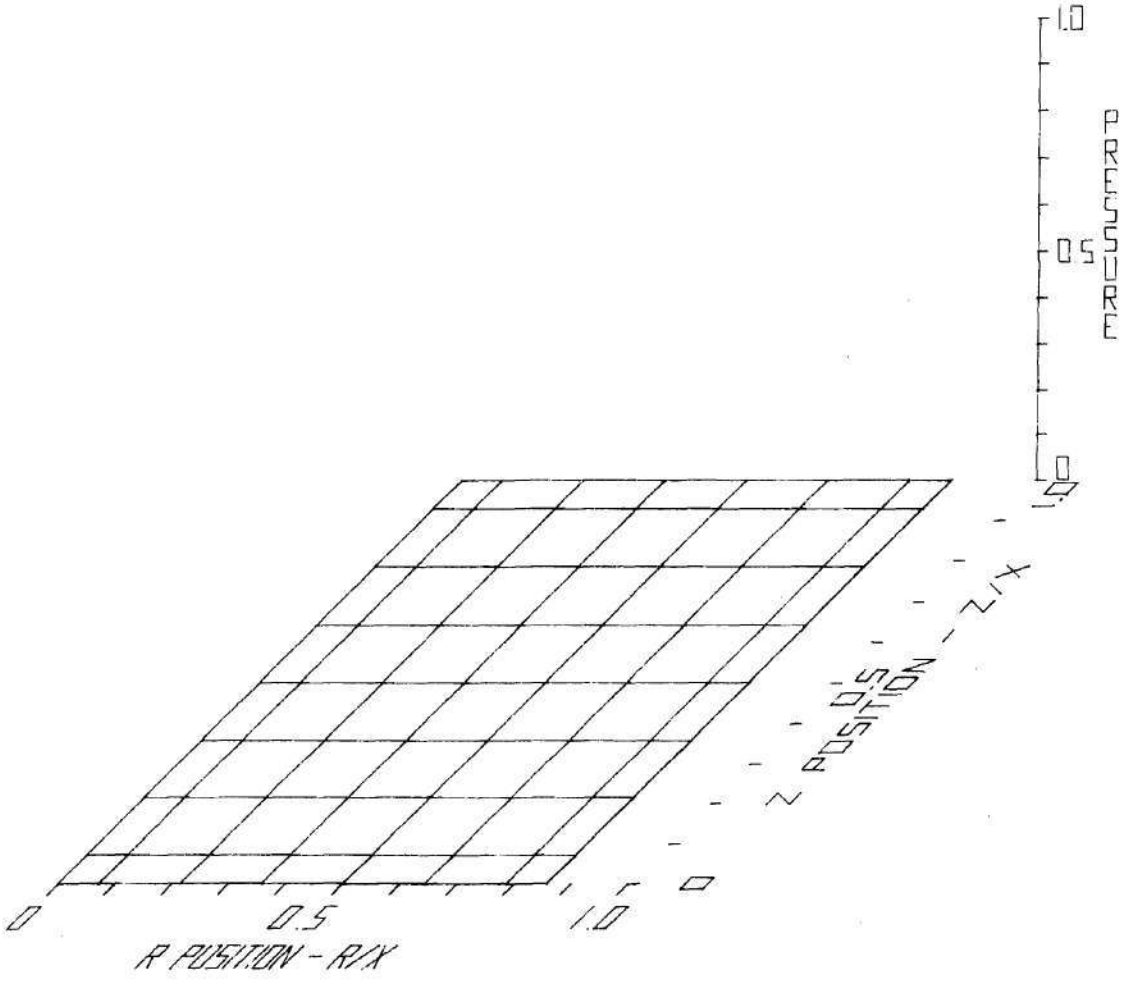

Figure 63: Liquid Fuel Pressure [T = 0.00000 sec]

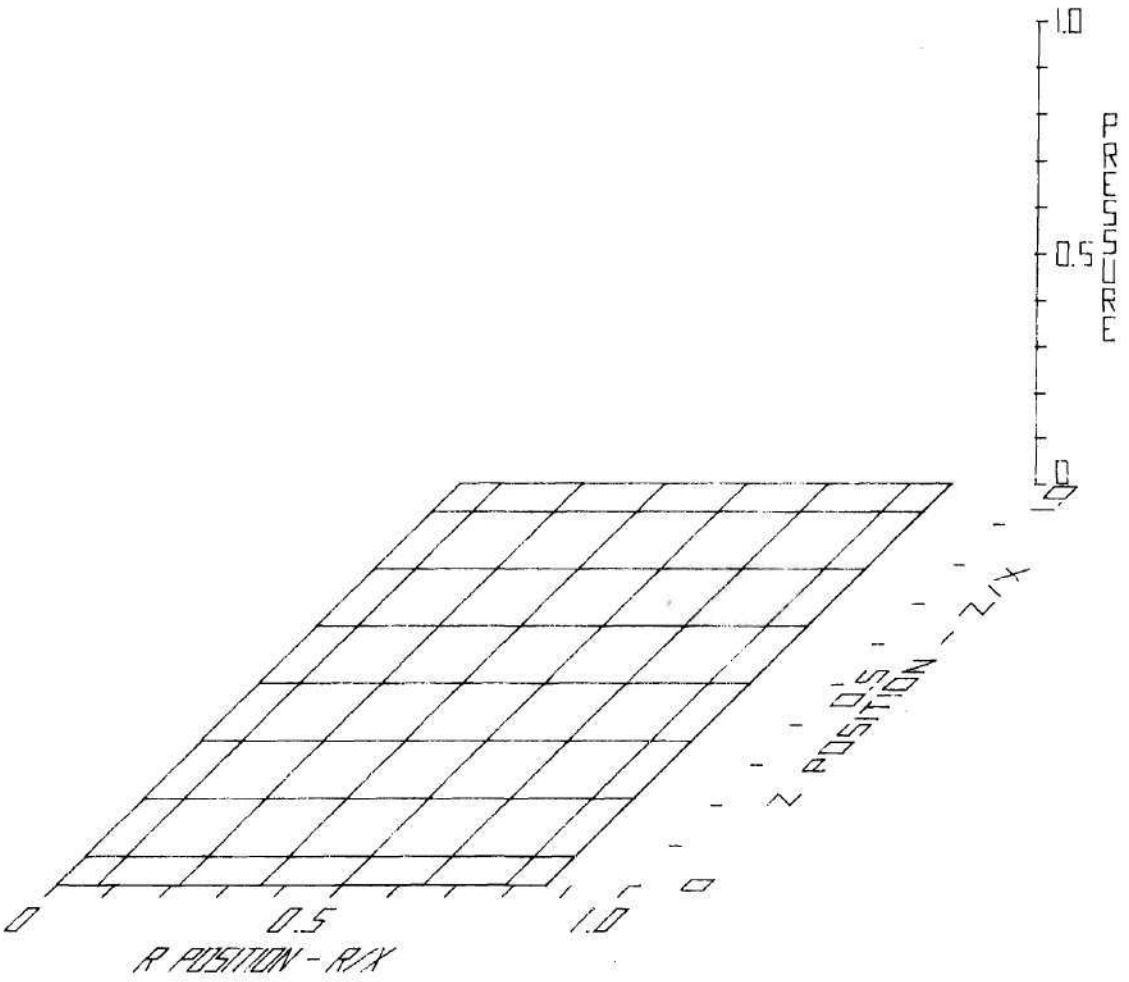

Figure 64: Liquid Fuel Pressure [T = 2.04889 sec]

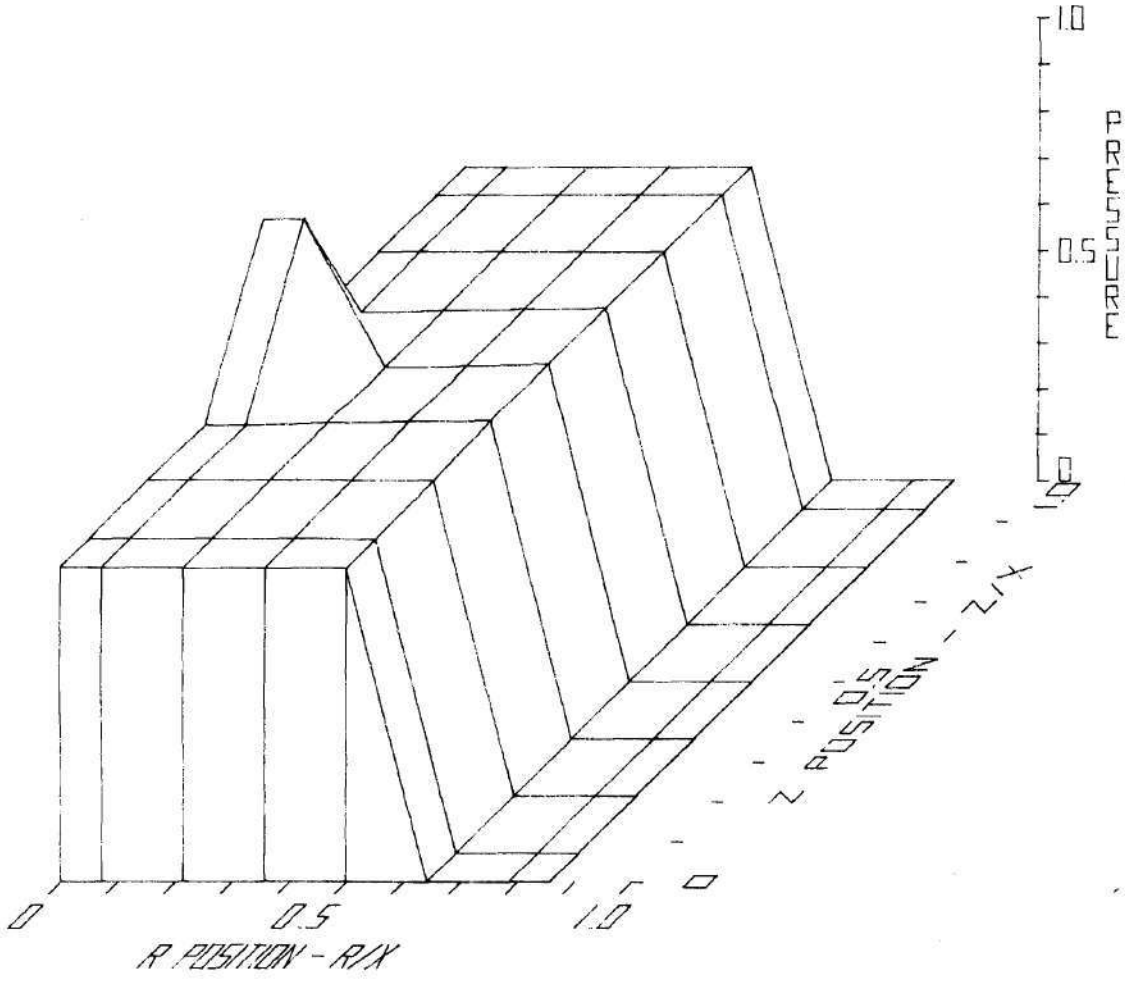

Figure 65: Liquid Fuel Pressure [T = 2.05204 sec]

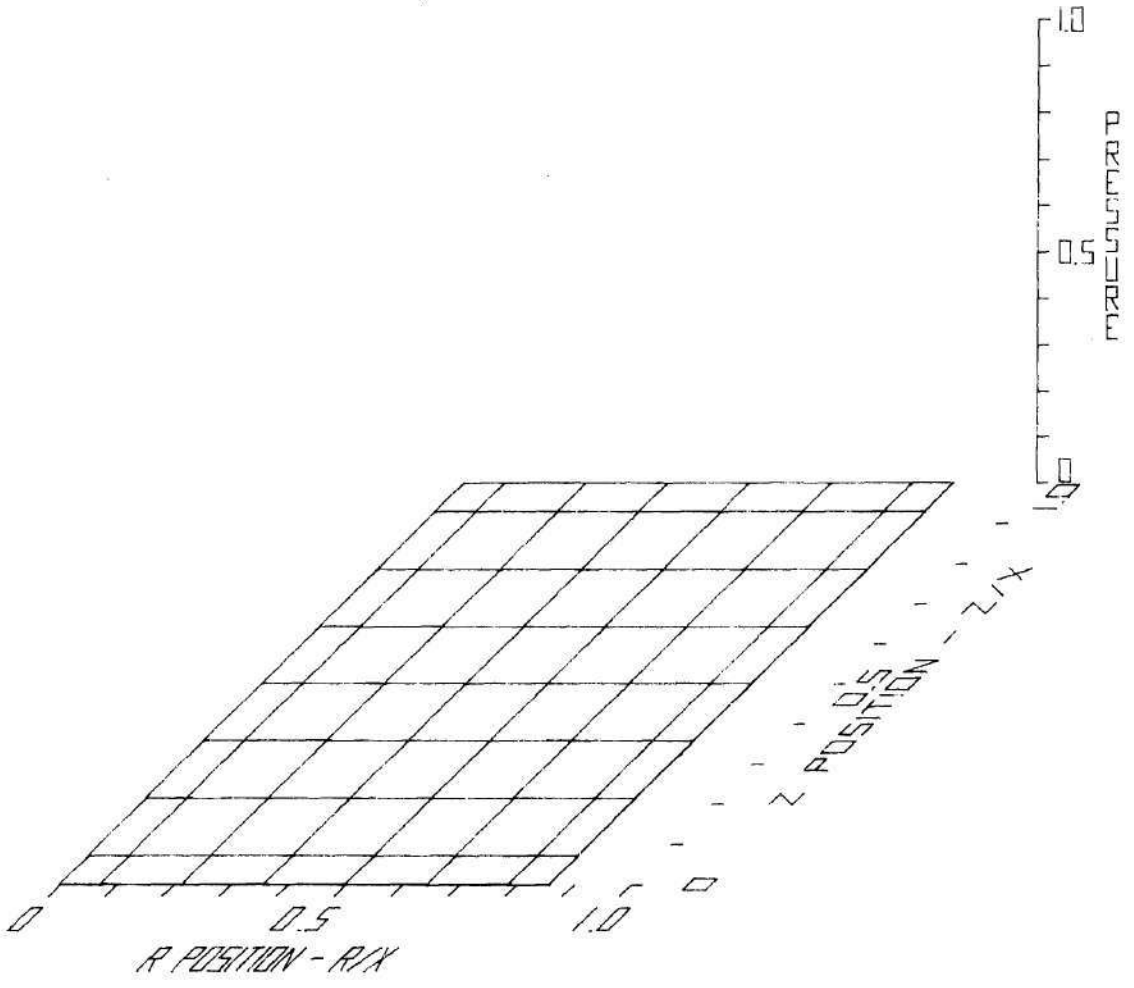

Figure 66: Liquid Steel Pressure [T = 0.00000 sec]

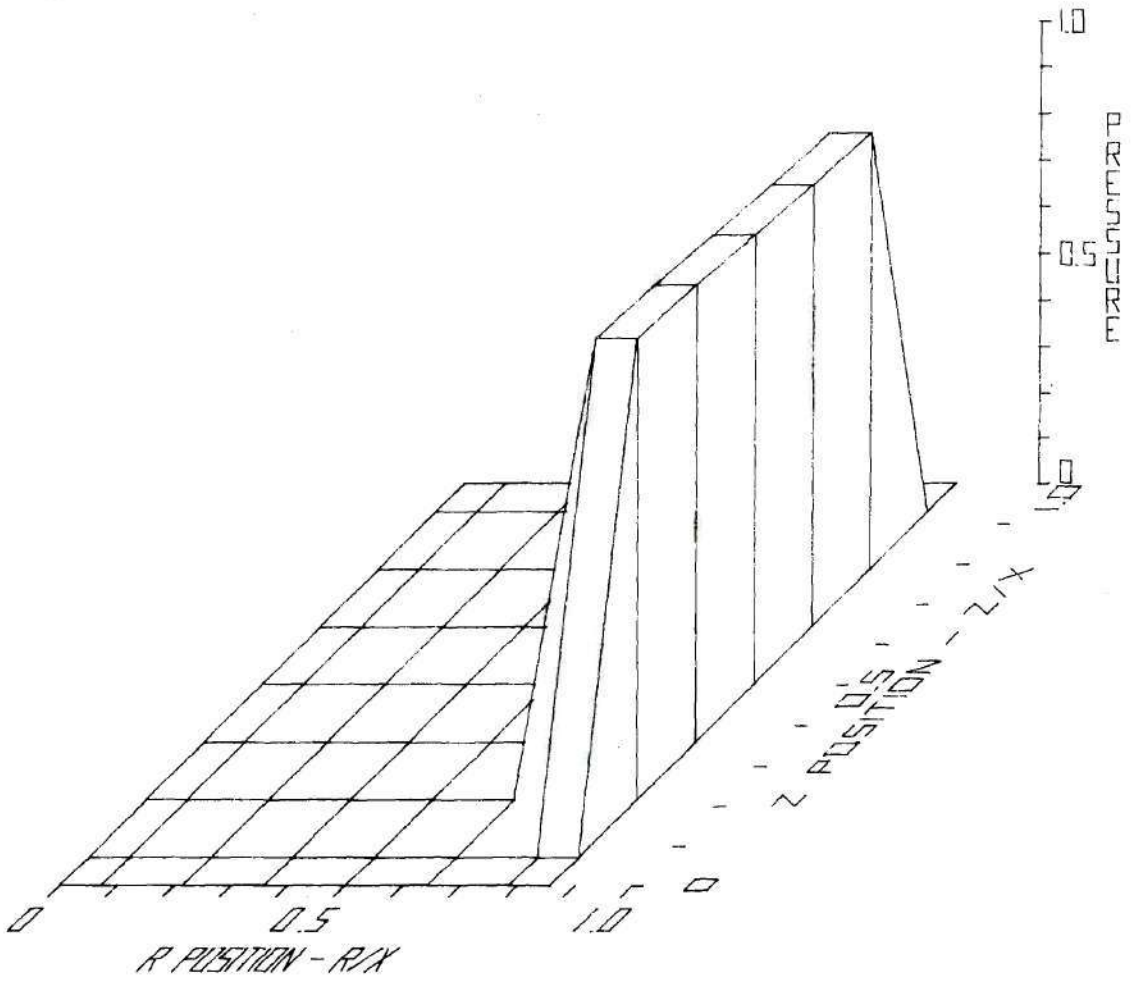

Figure 67: Liquid Steel Pressure [T = 2.04889 sec]

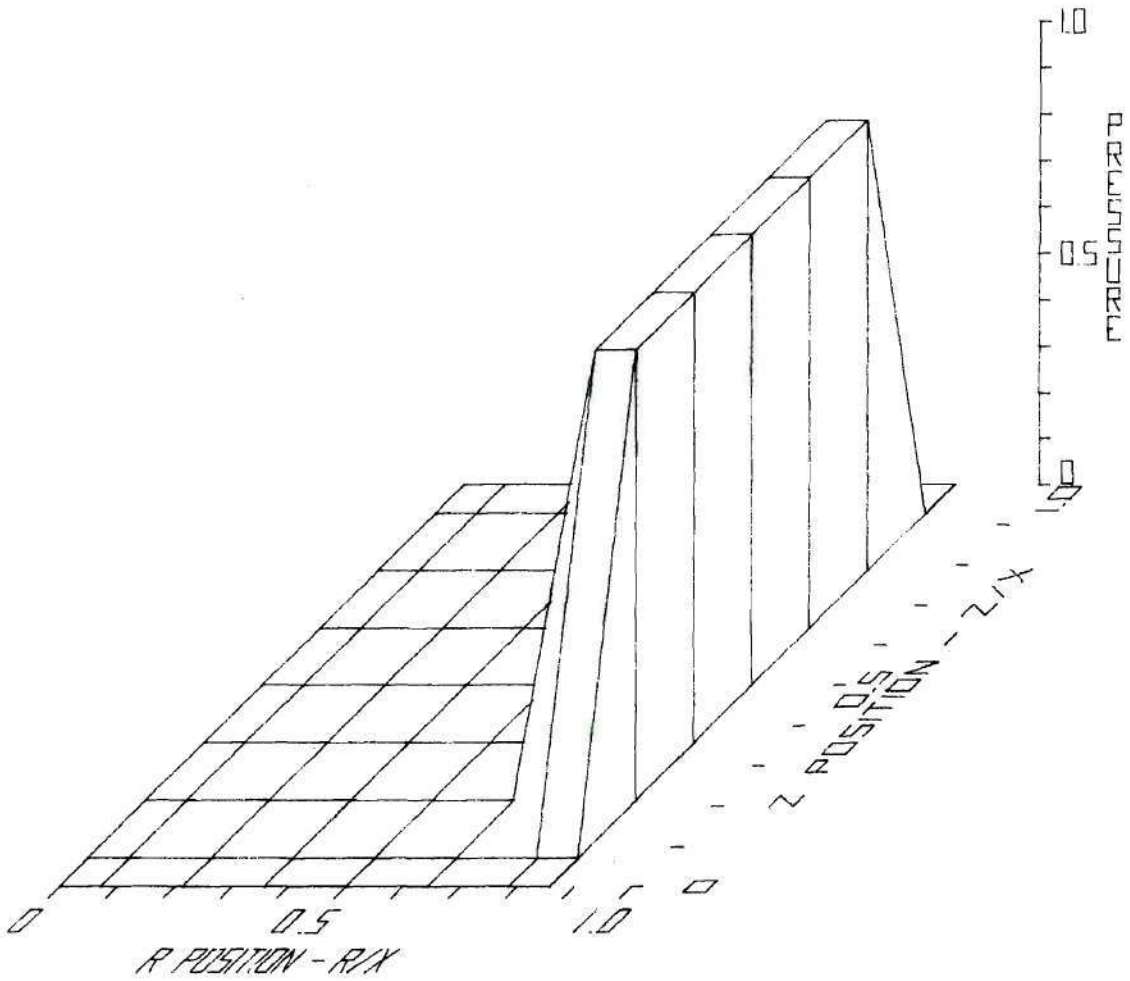

Figure 68: Liquid Steel Pressure [T = 2.05204 sec]

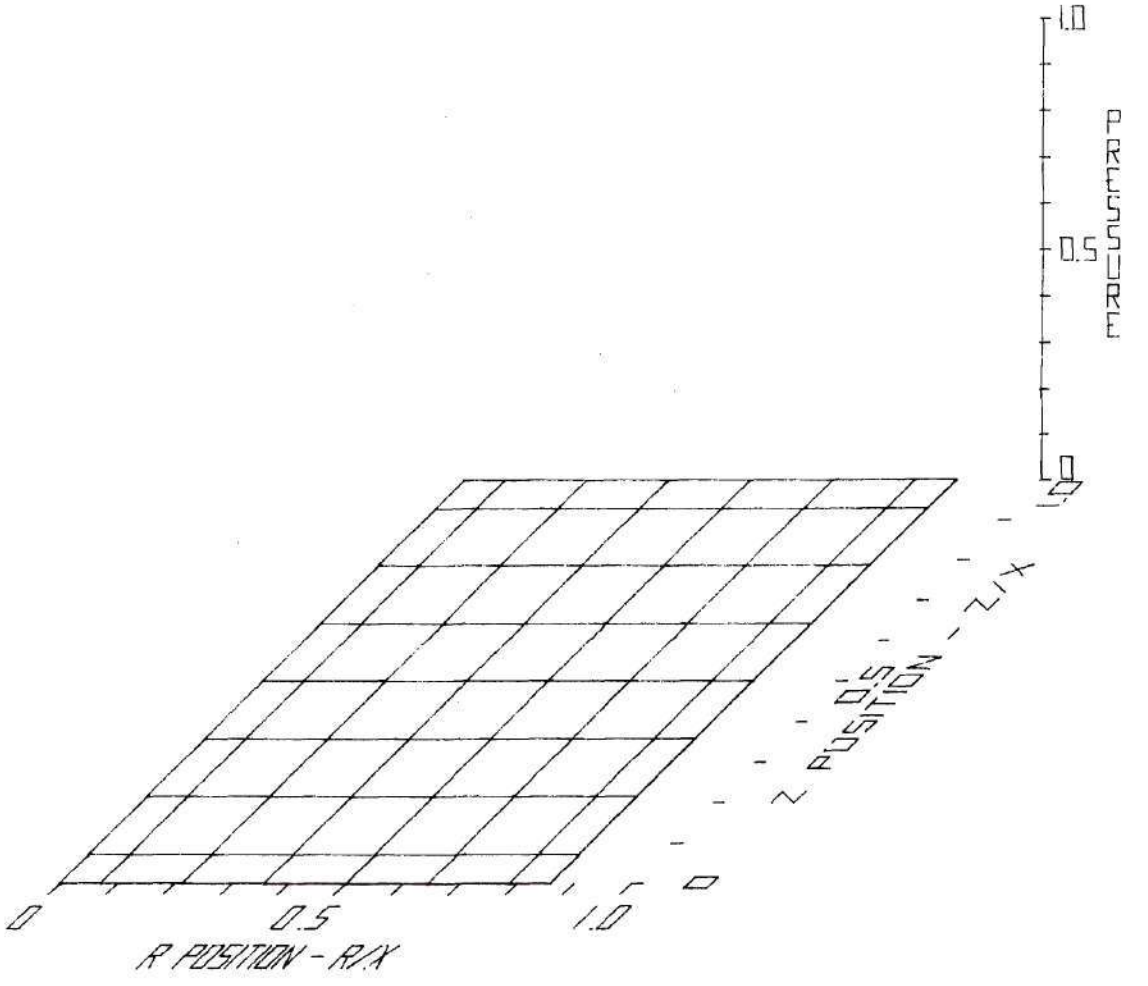

Figure 69: Vapor Fuel Pressure [T = 0.00000 sec]

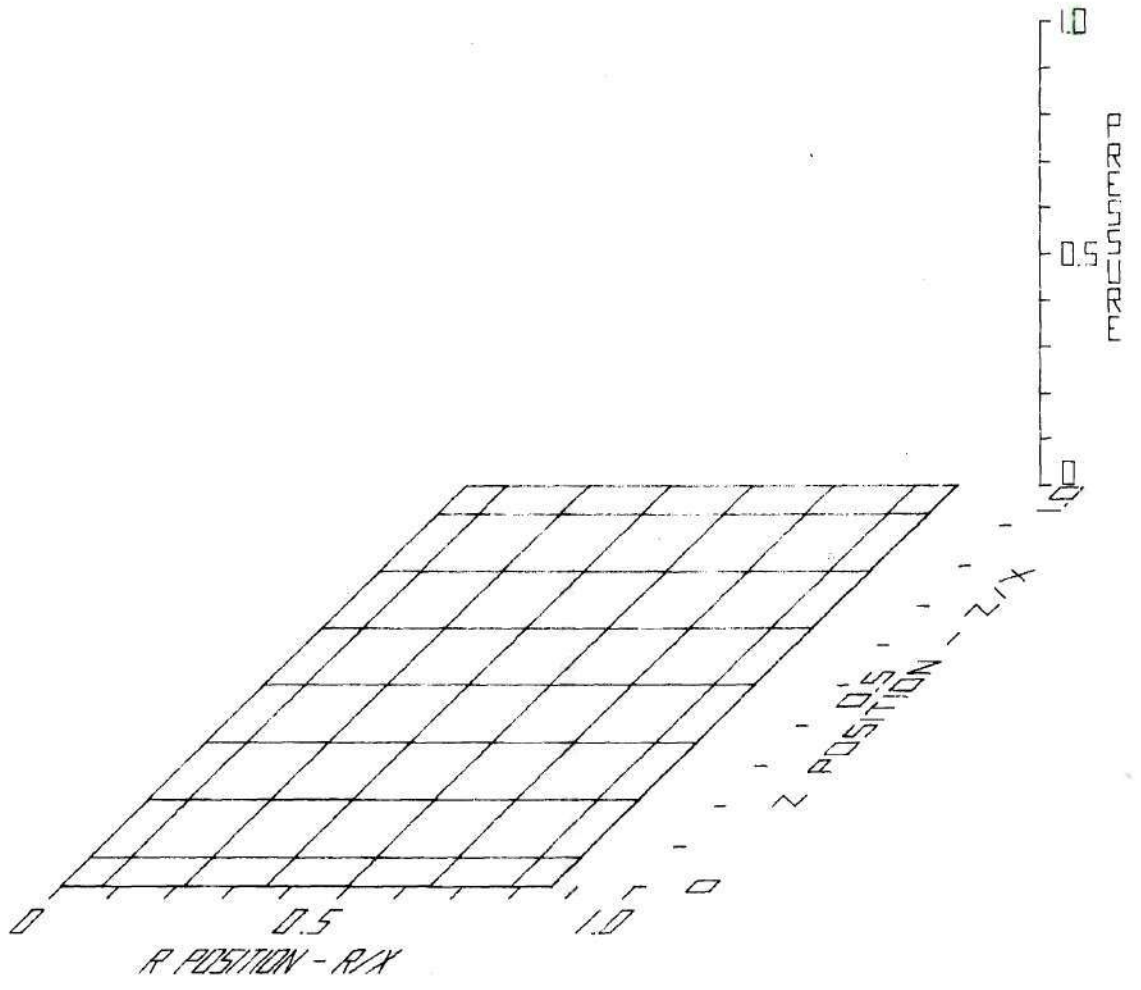

Figure 70: Vapor Fuel Pressure [T = 2.04889 sec]

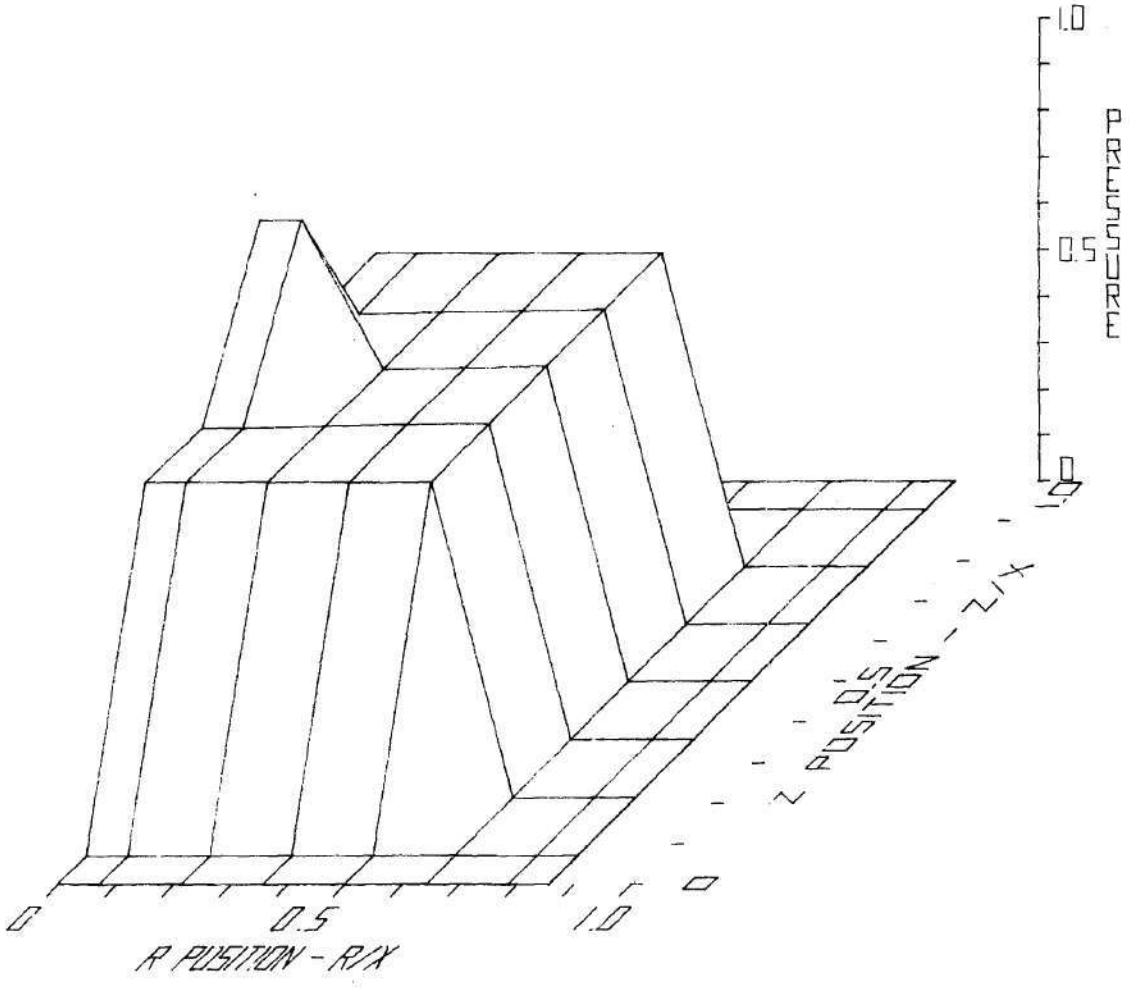

Figure 71: Vapor Fuel Pressure [T = 2.05204 sec]

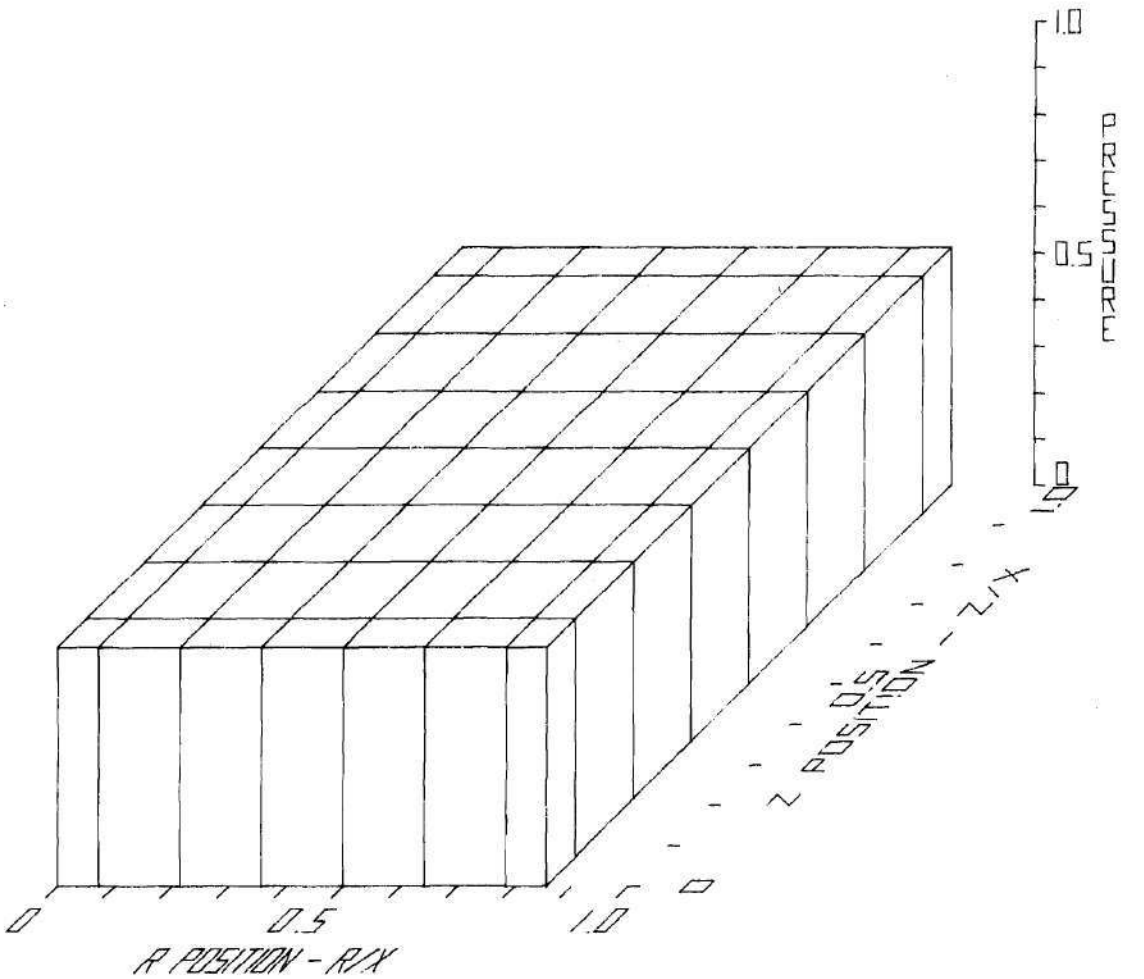

Figure 72: Fission Gas Pressure [T = 0.00000 sec]

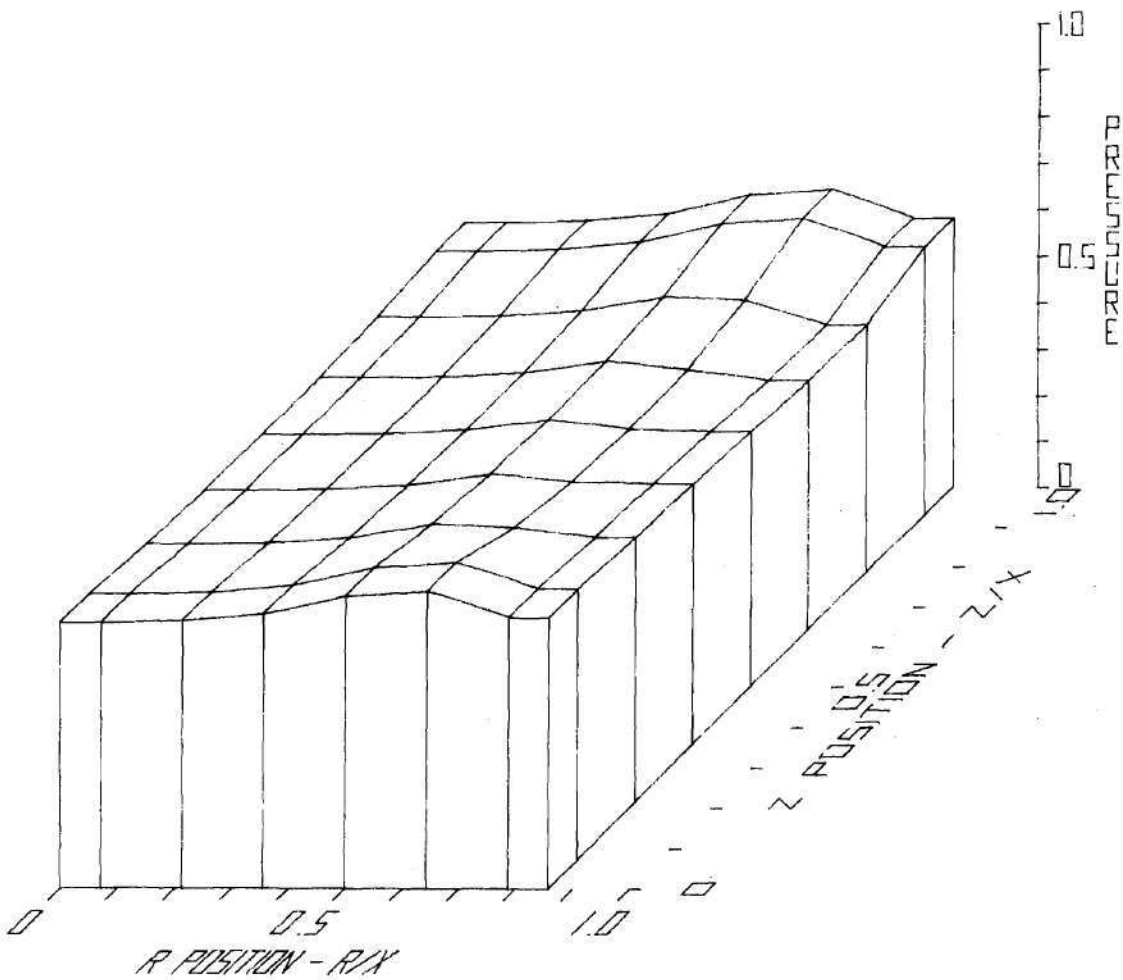

Figure 73: Fission Gas Pressure [T = 2.04889 sec]

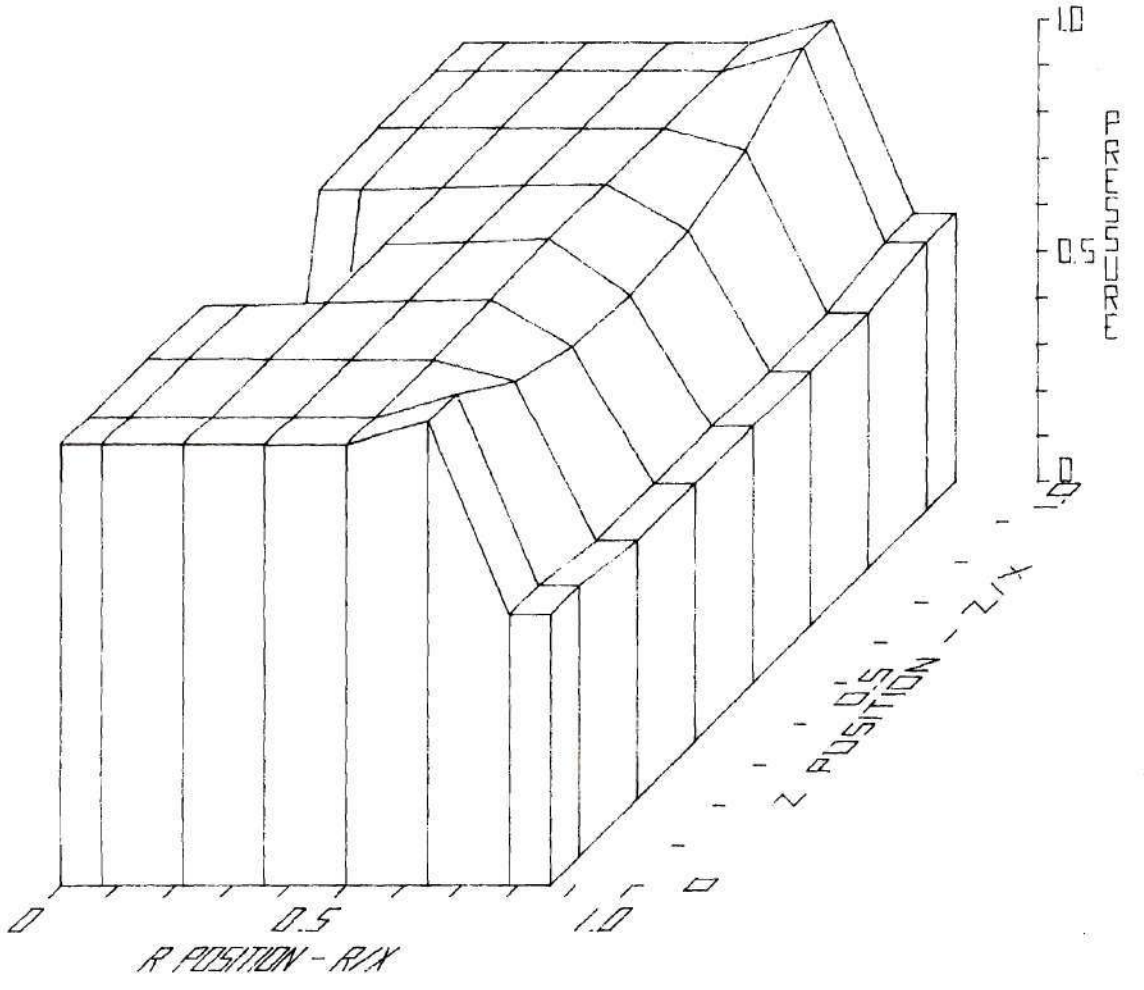

Figure 74: Fission Gas Pressure [T = 2.05204 sec]

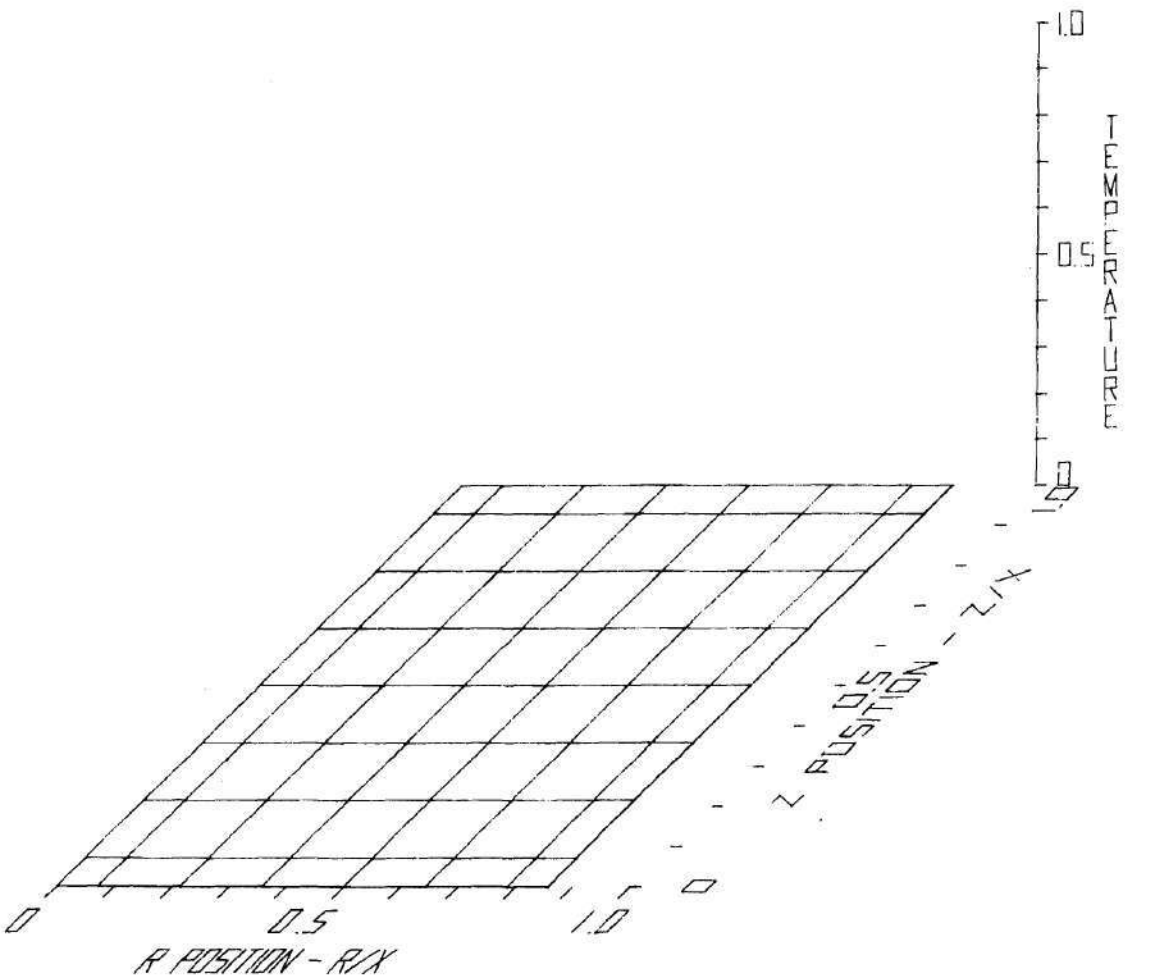

Figure 75: Liquid Fuel Temperature [T = 0.00000 sec]

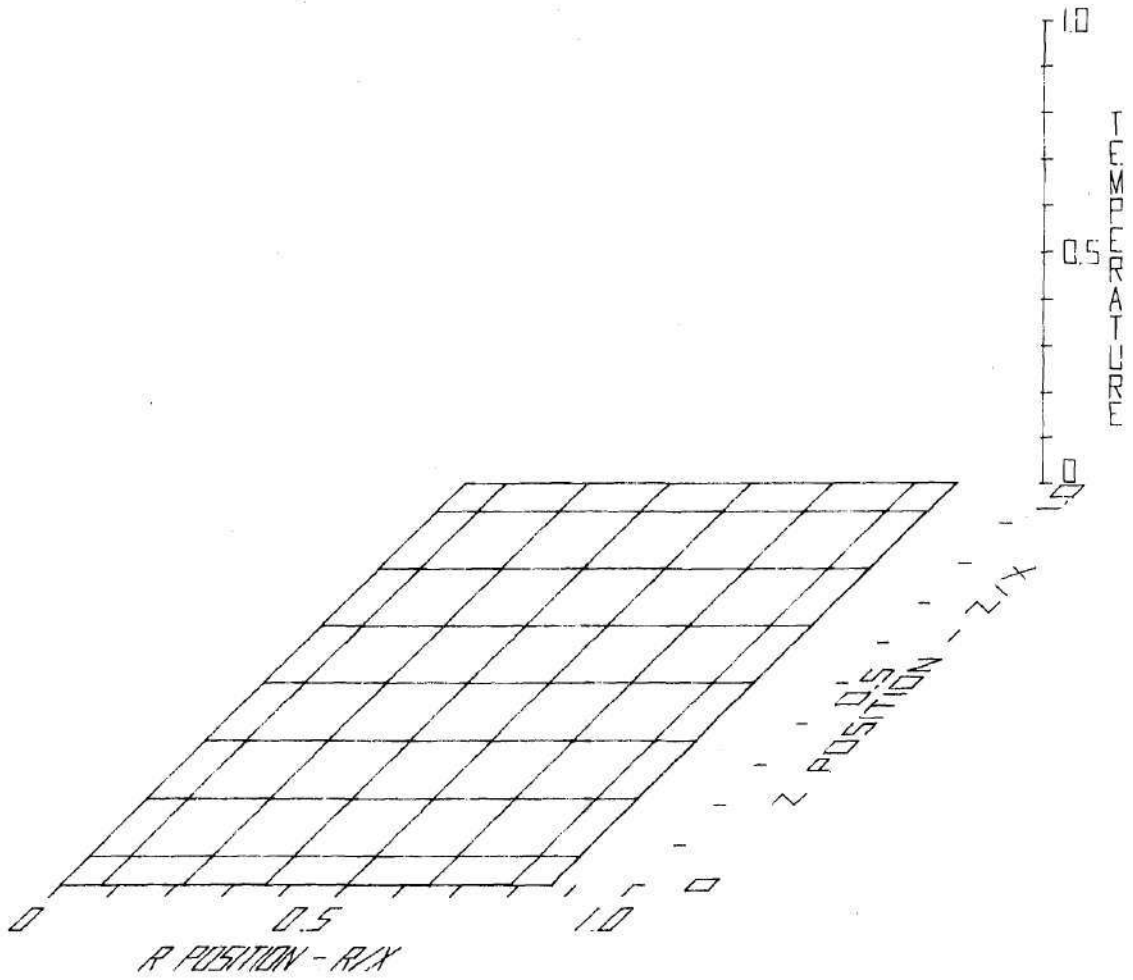

Figure 76: Liquid Fuel Temperature [T = 2.04889 sec]

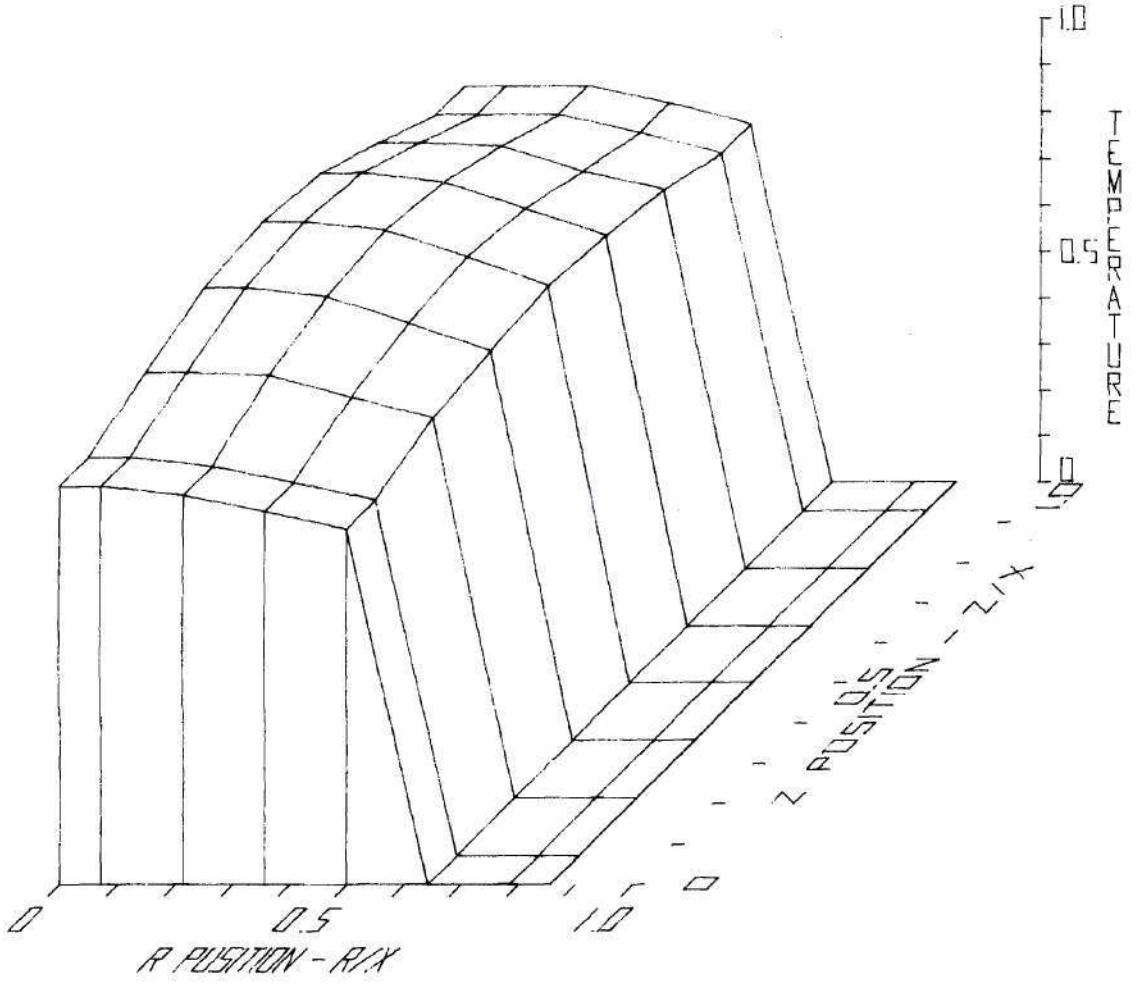

Figure 77: Liquid Fuel Temperature [T = 2.05204 sec]

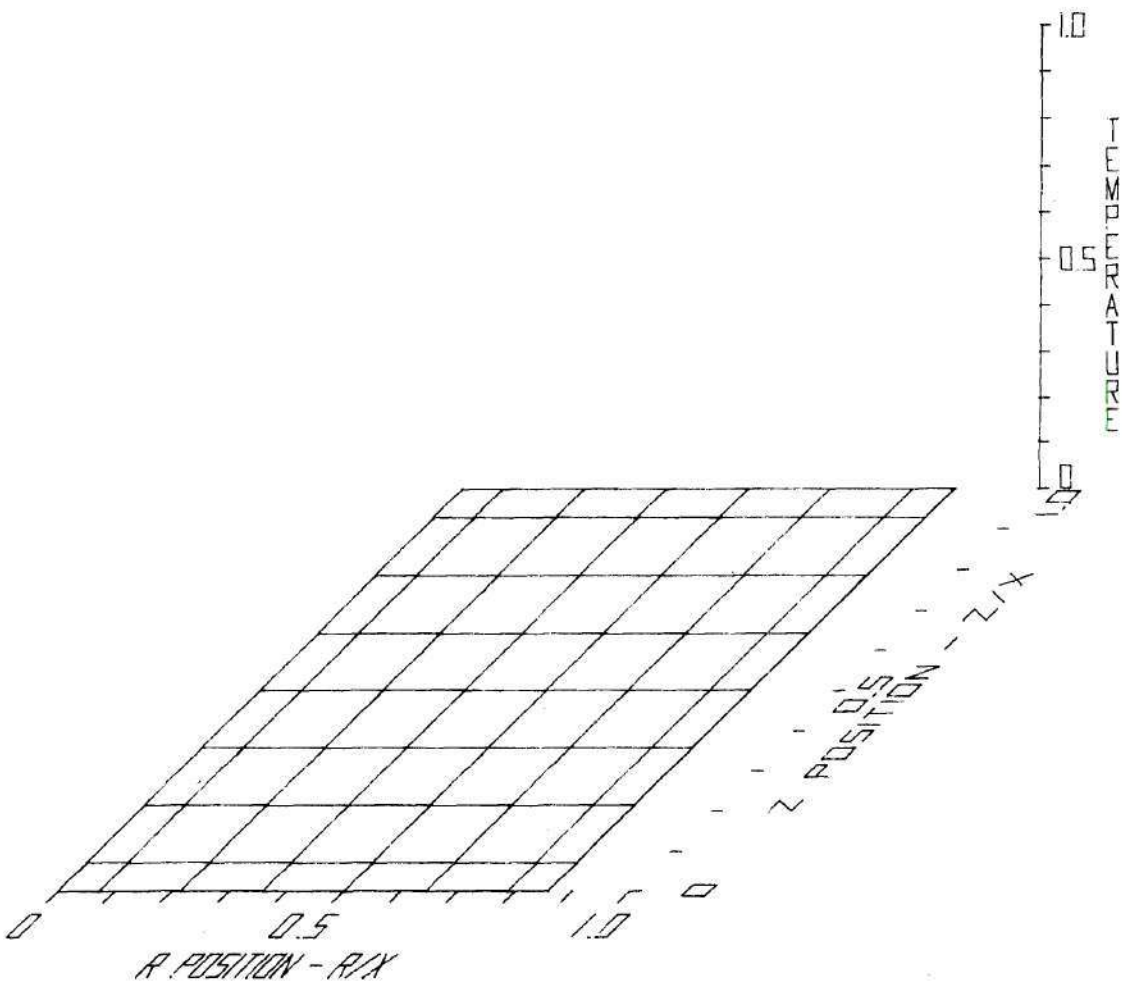

Figure 78: Liquid Steel Temperature [T = 0.00000 sec]

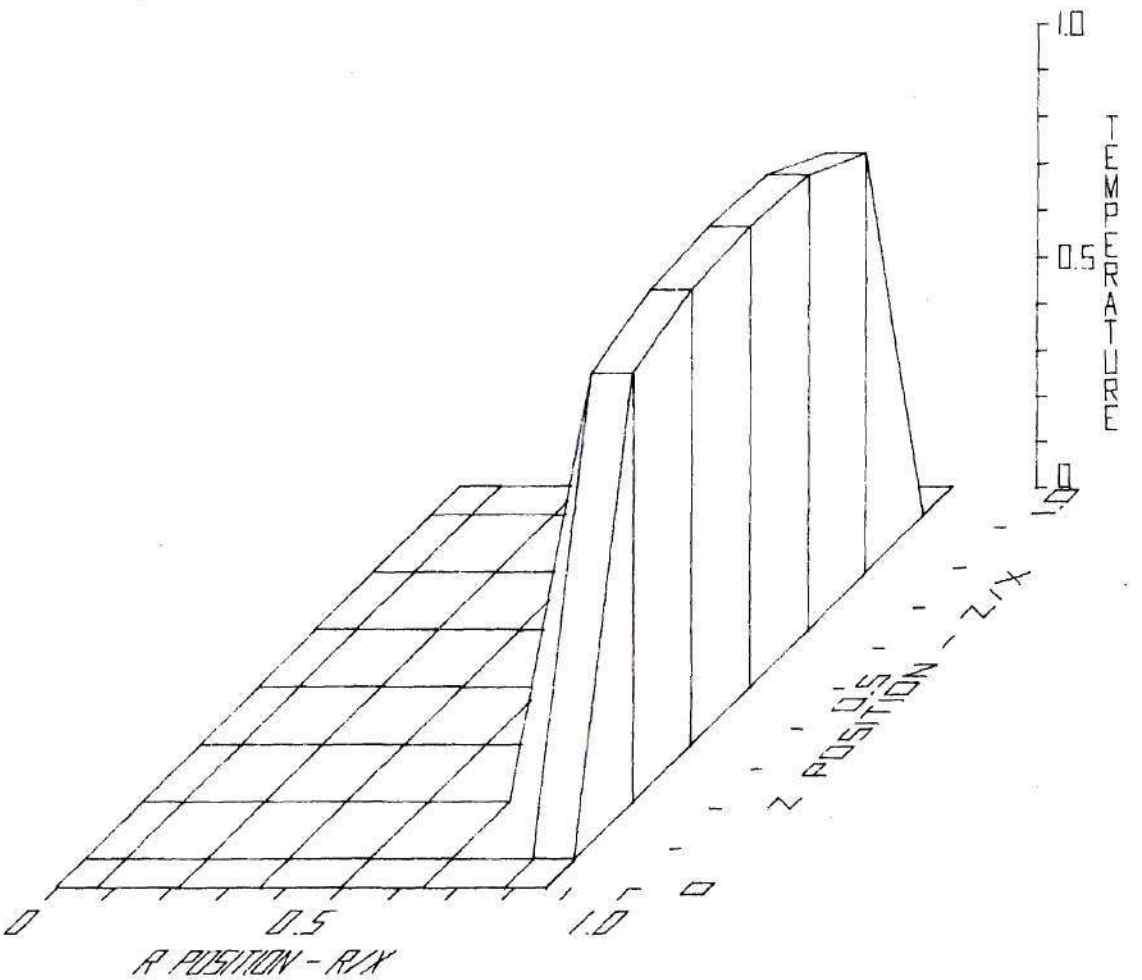

Figure 79: Liquid Steel Temperature [T = 2.04889 sec]

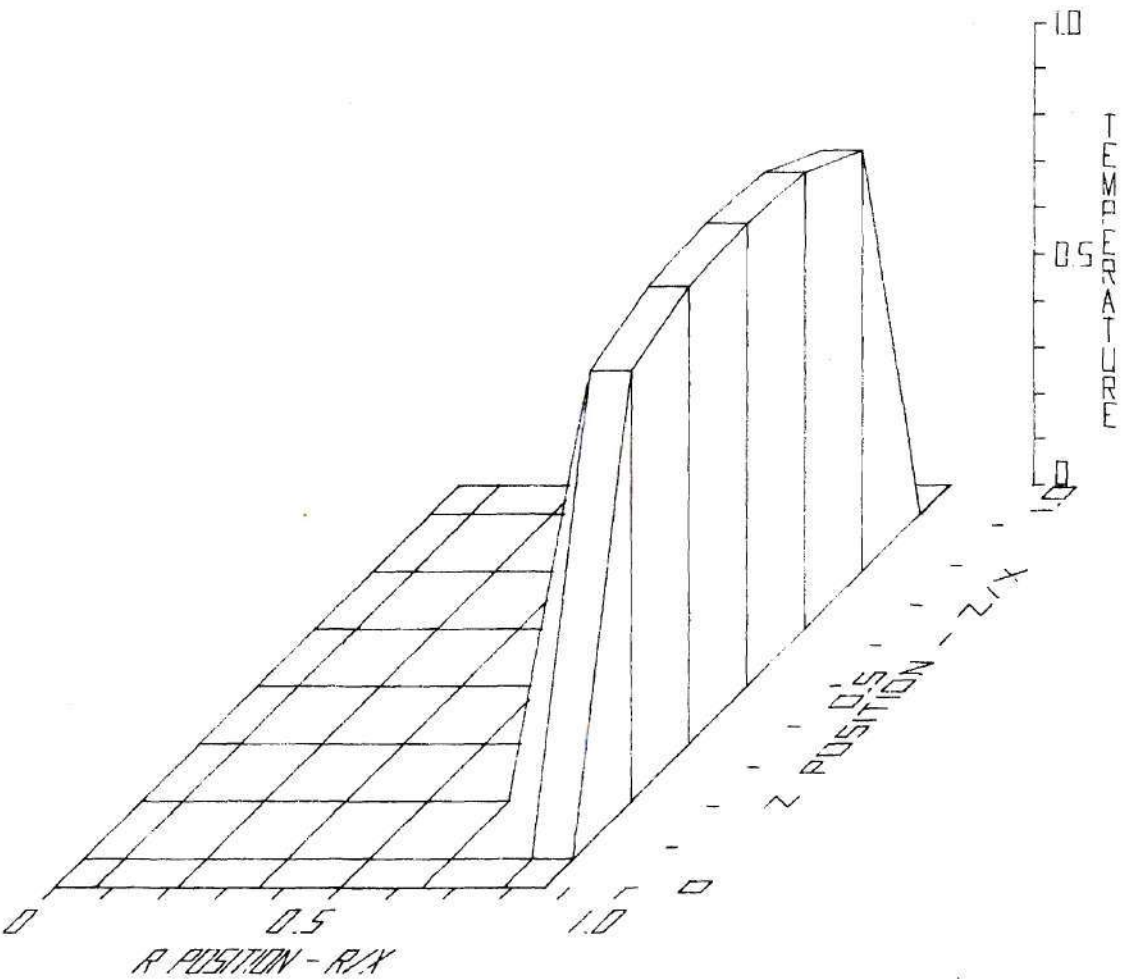

Figure 80: Liquid Steel Temperature [T = 2.05204 sec]

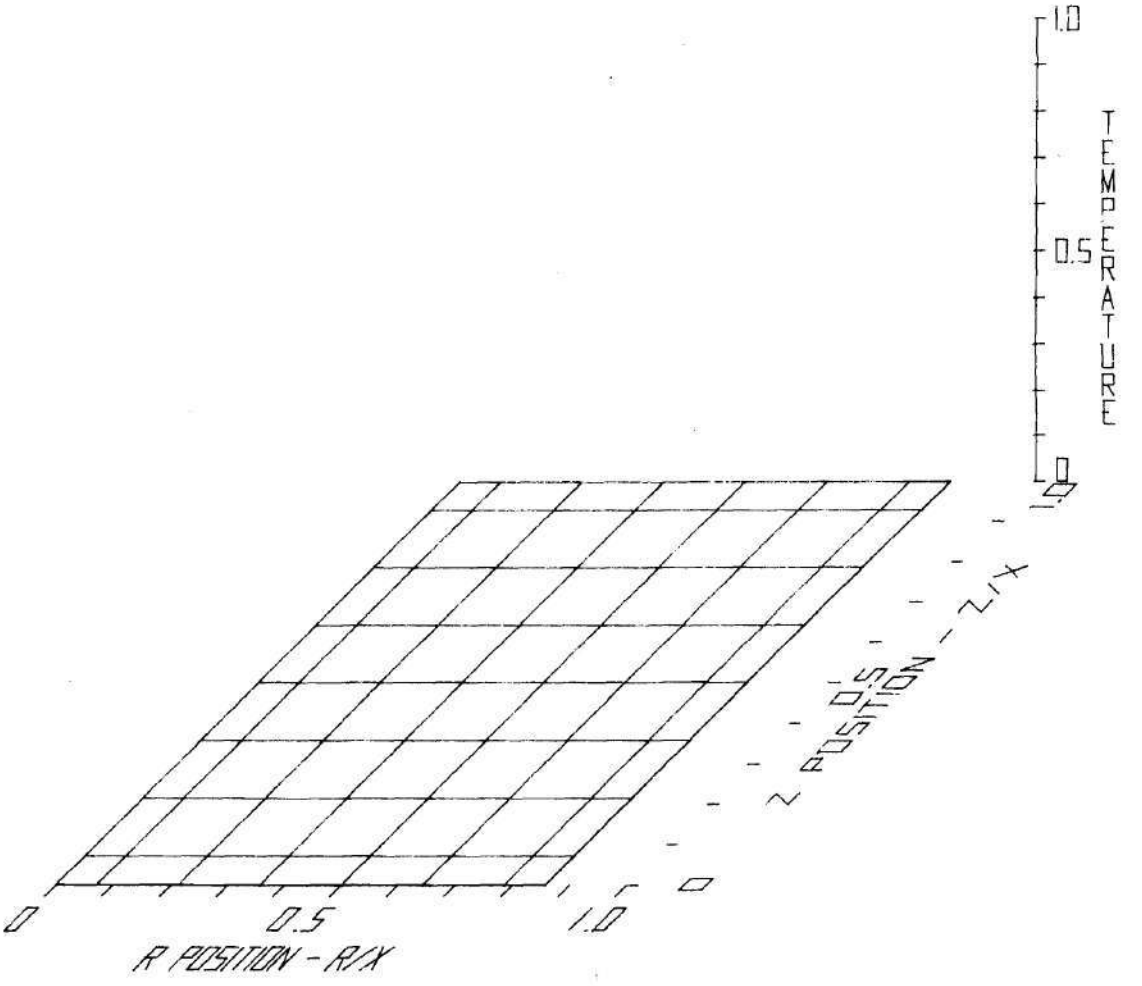

Figure 81: Vapor Fuel Pressure [T = 0.00000 sec]

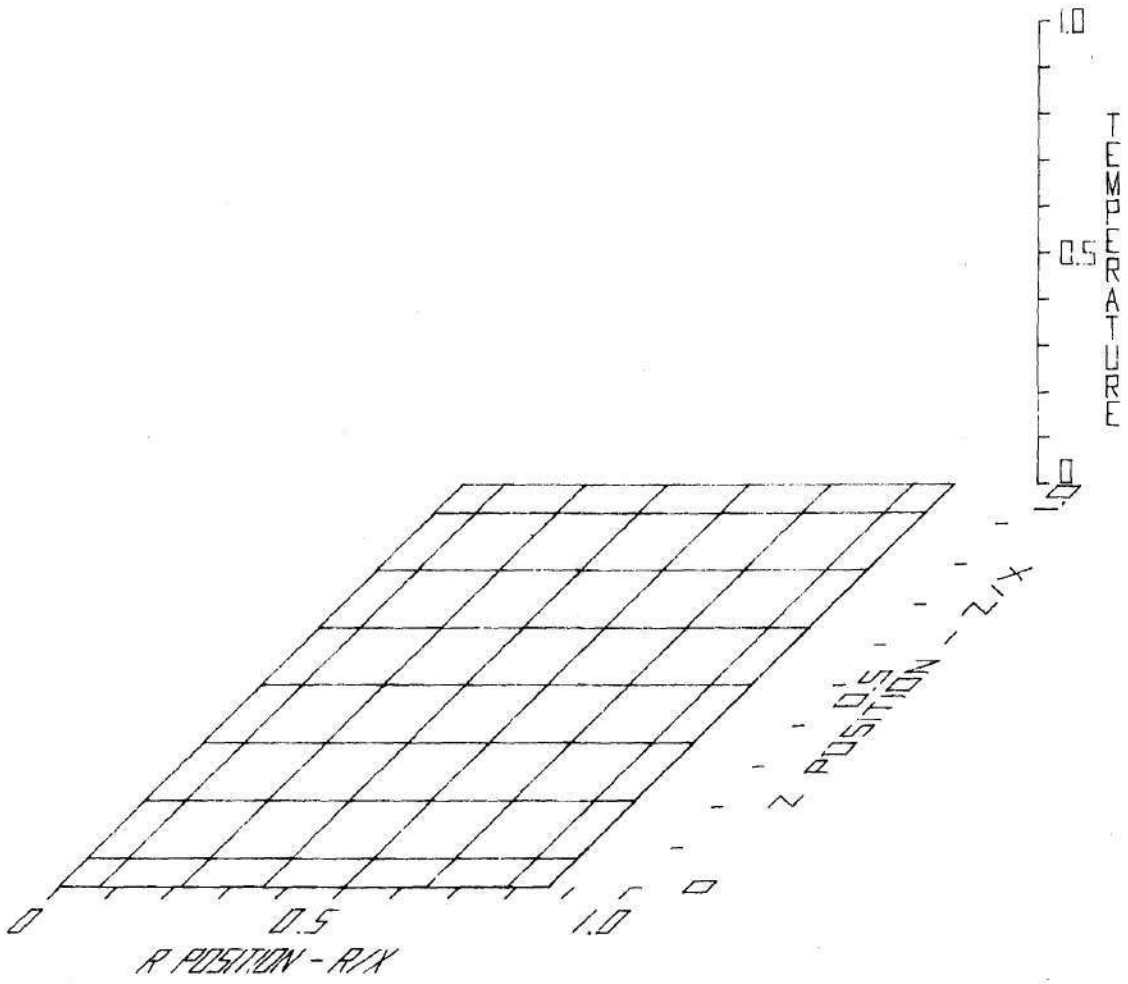

Figure 82: Vapor Fuel Temperature [T = 2.04889 sec]

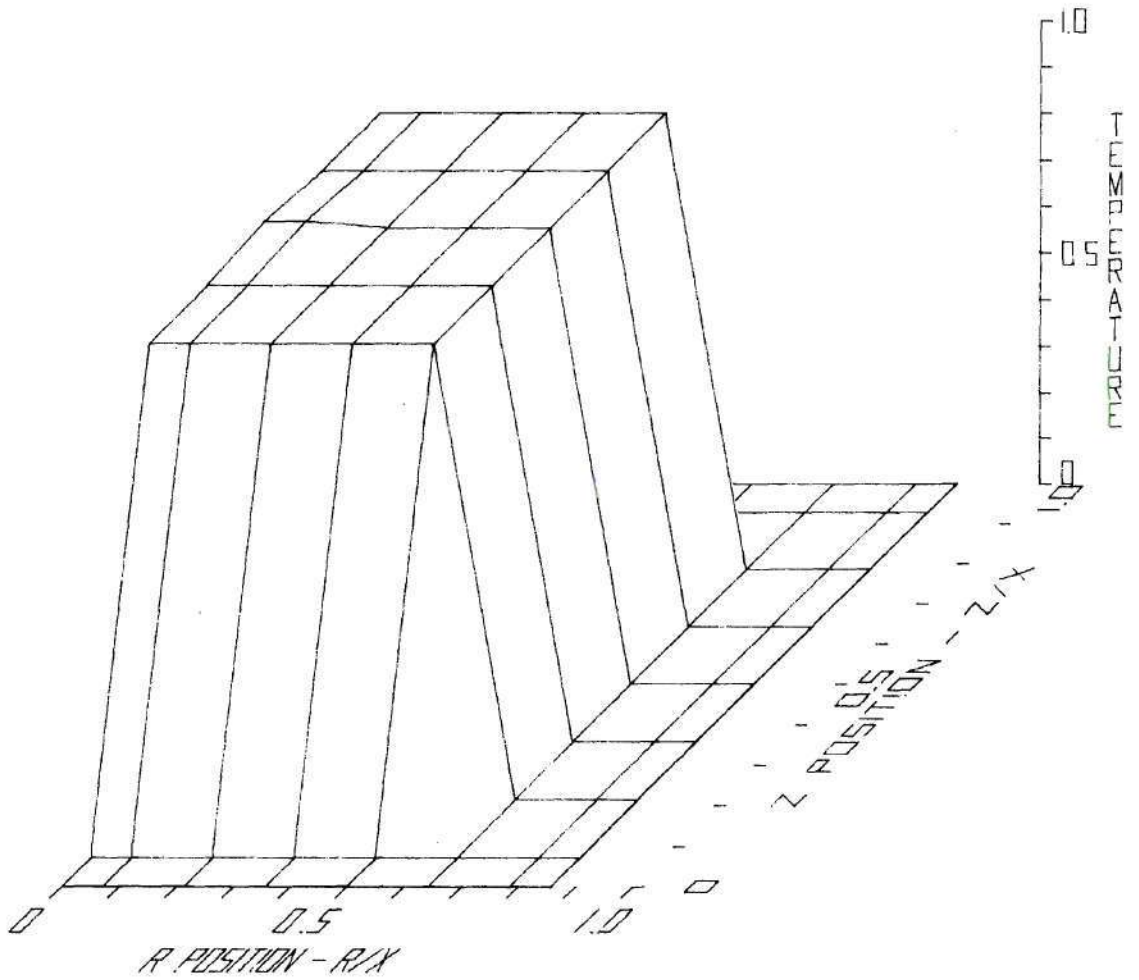

Figure 83: Vapor Fuel Temperature [T = 2.05204 sec]

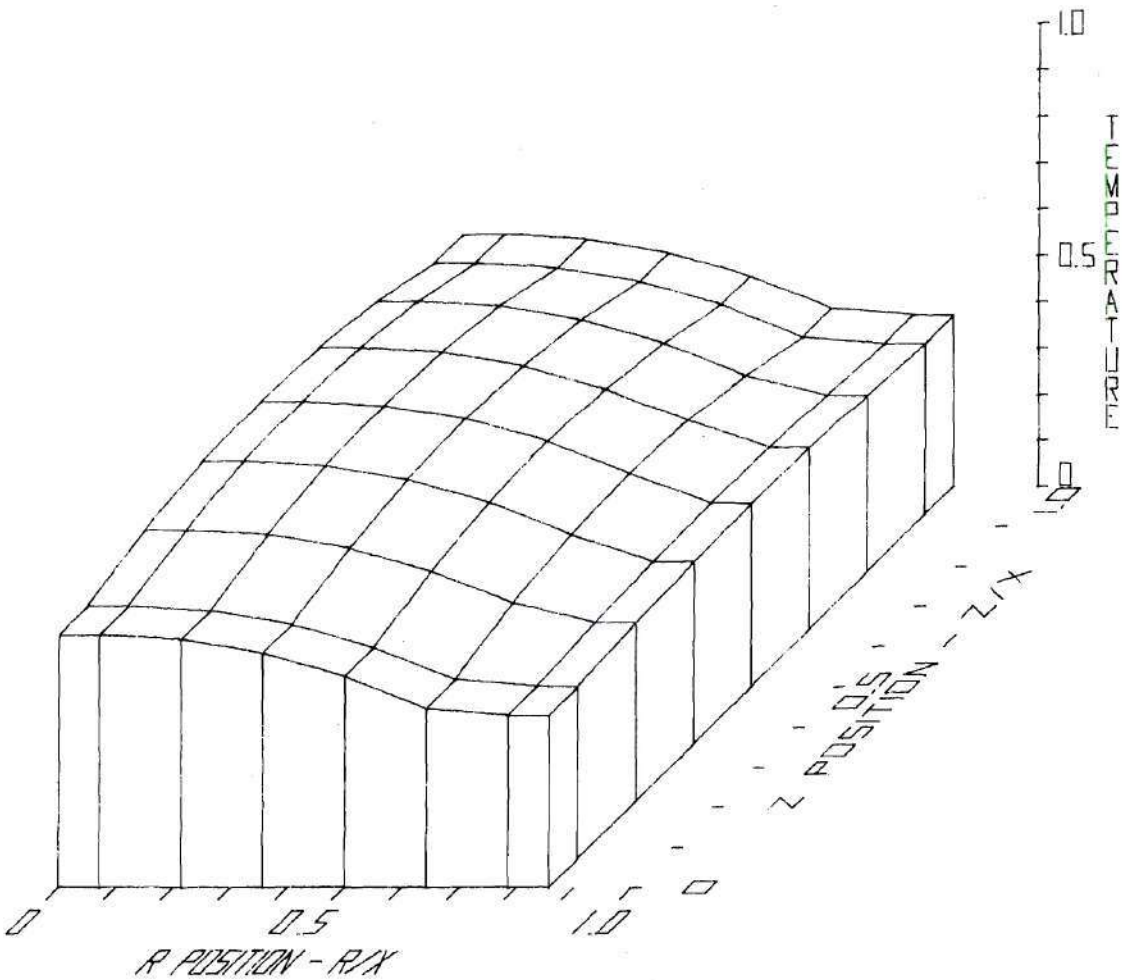

Figure 84: Fission Gas Temperature [T = 0.00000 sec]

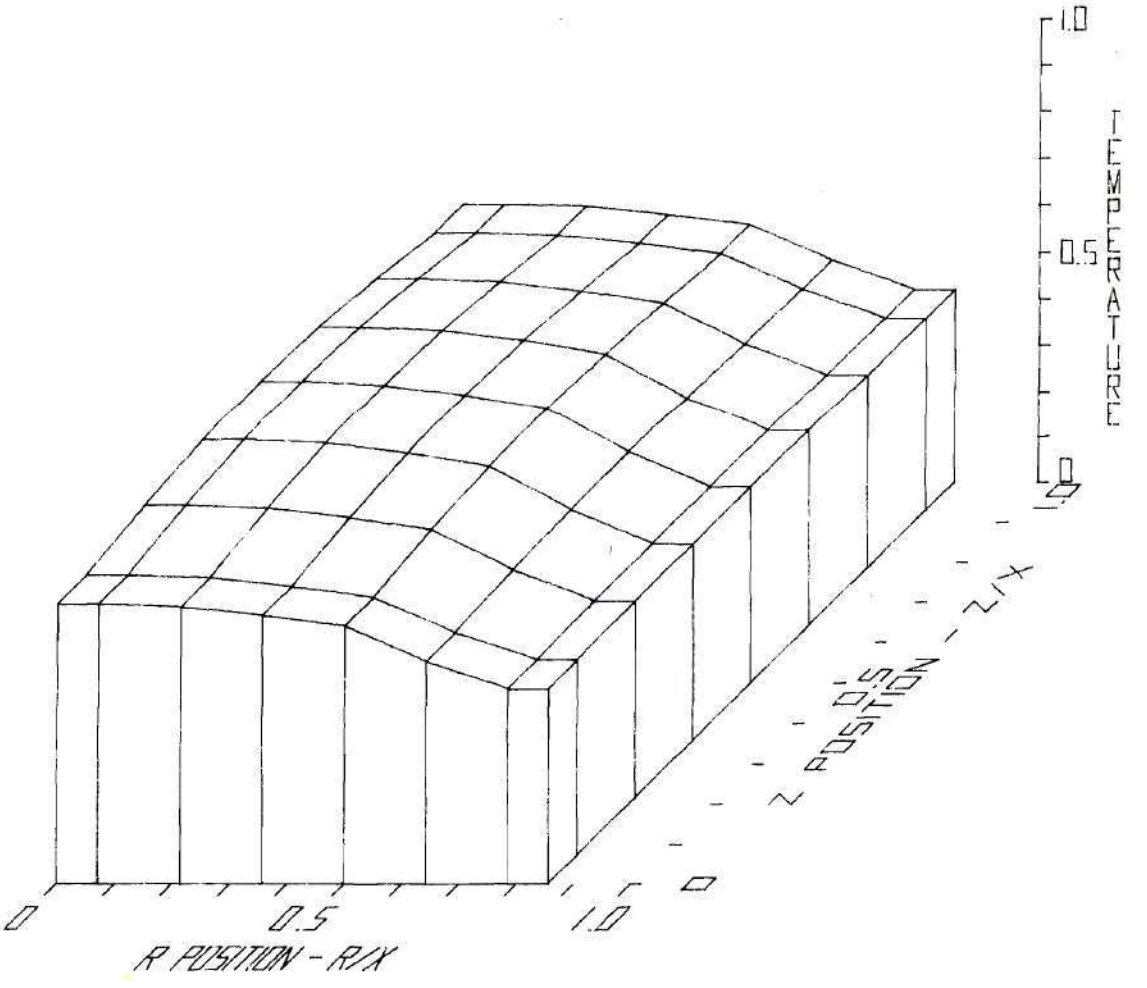

Figure 85: Fission Gas Temperature [T = 2.04889 sec]

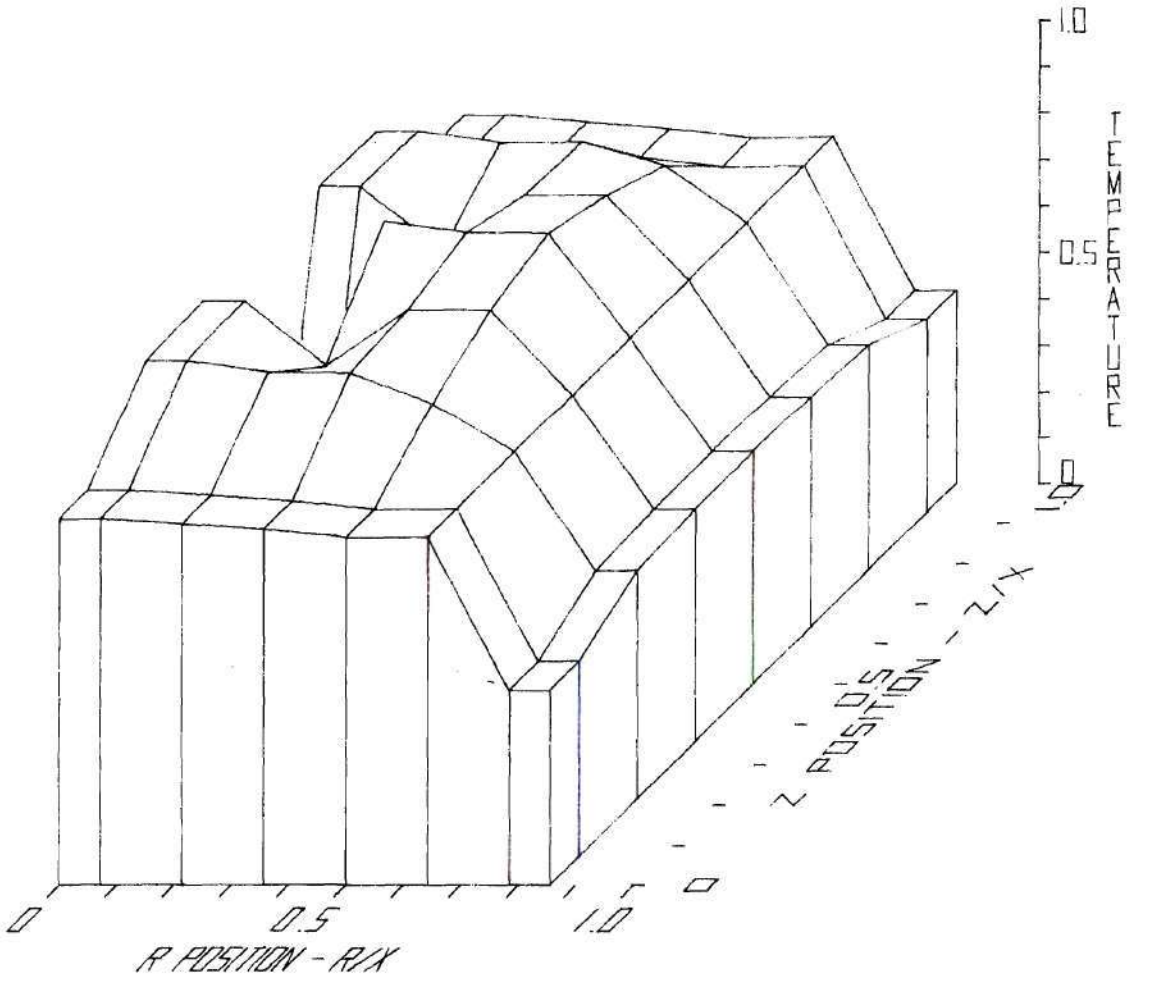

Figure 86: Fission Gas Temperature [T = 2.05204 sec]

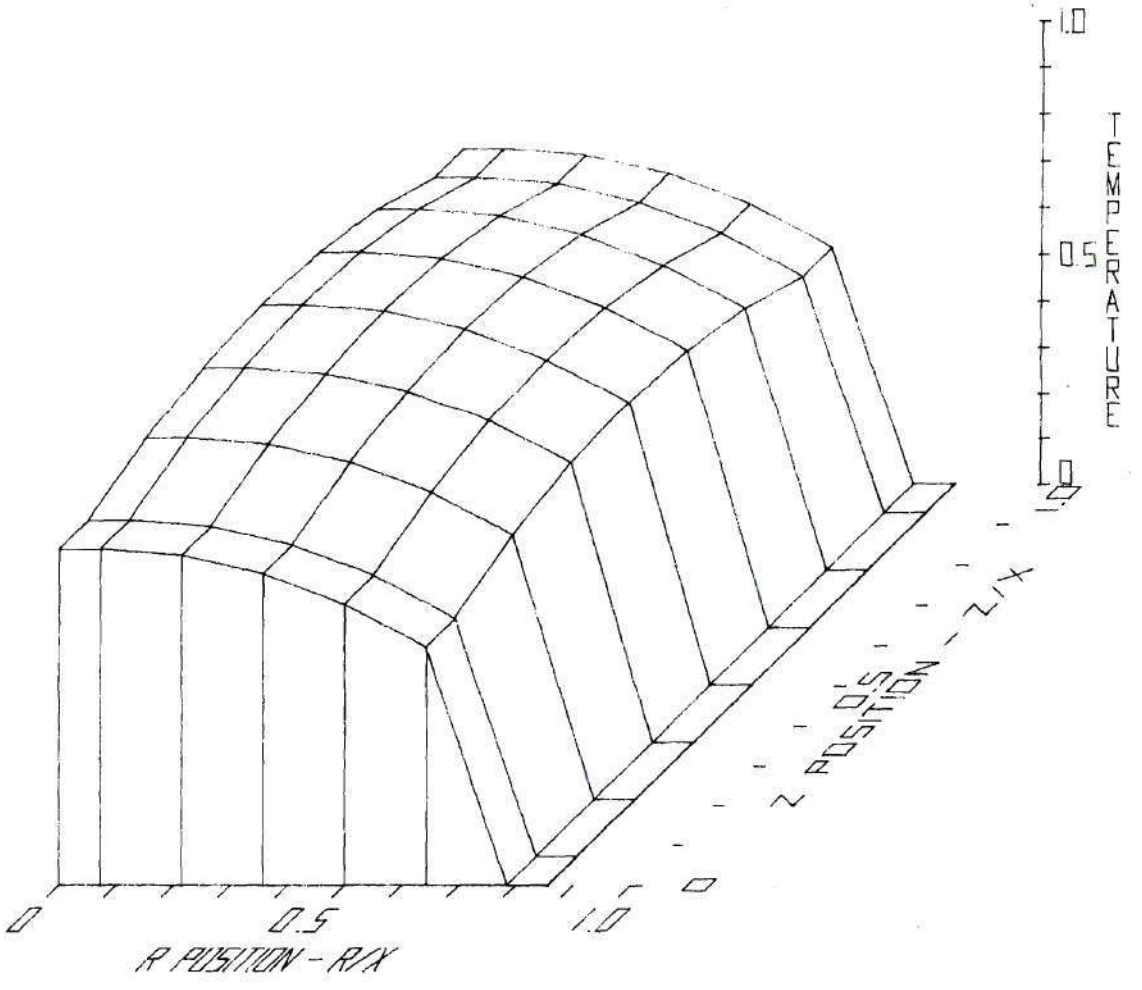

Figure 87: Solid Fuel Temperature [T = 0.00000 sec]

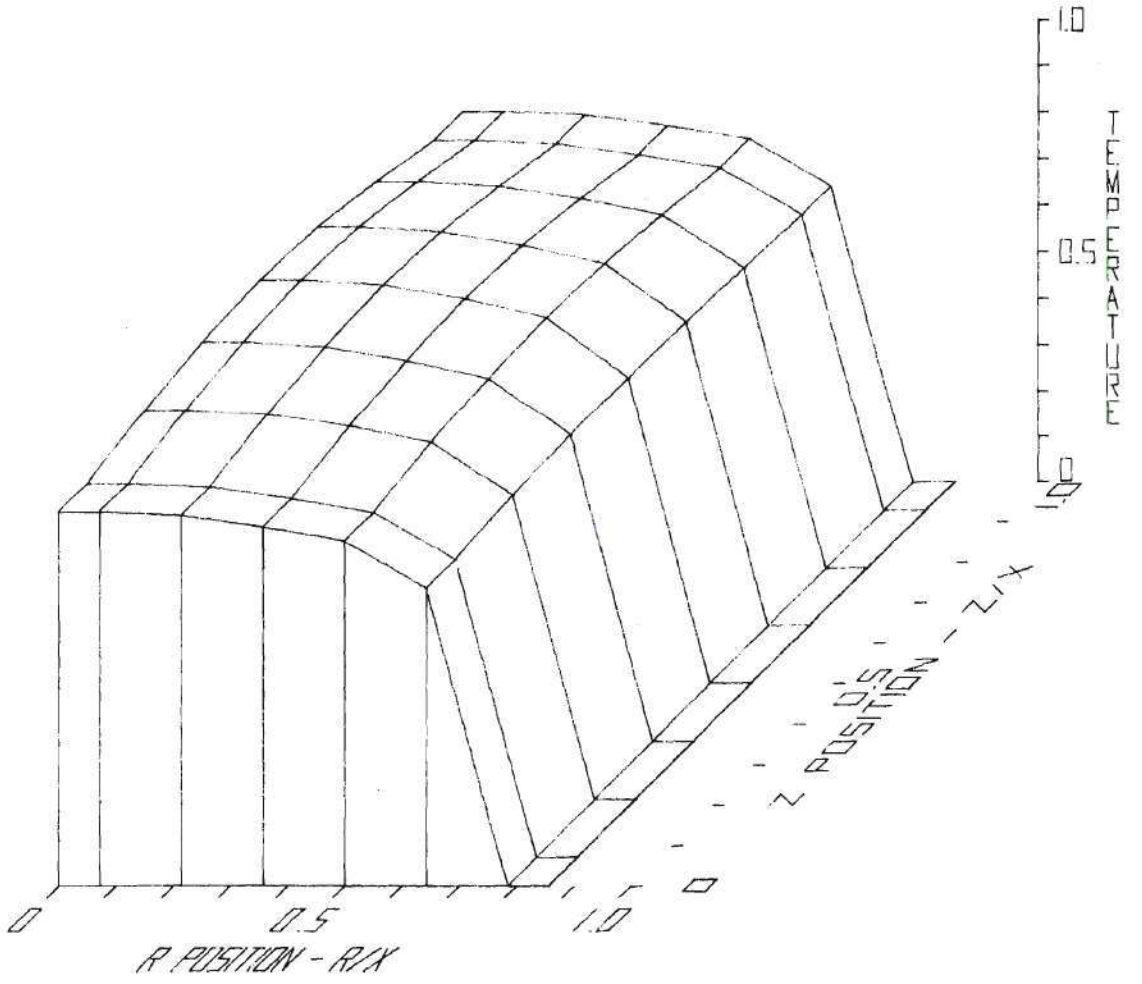

Figure 88: Solid Fuel Temperature [T = 2.04889 sec]

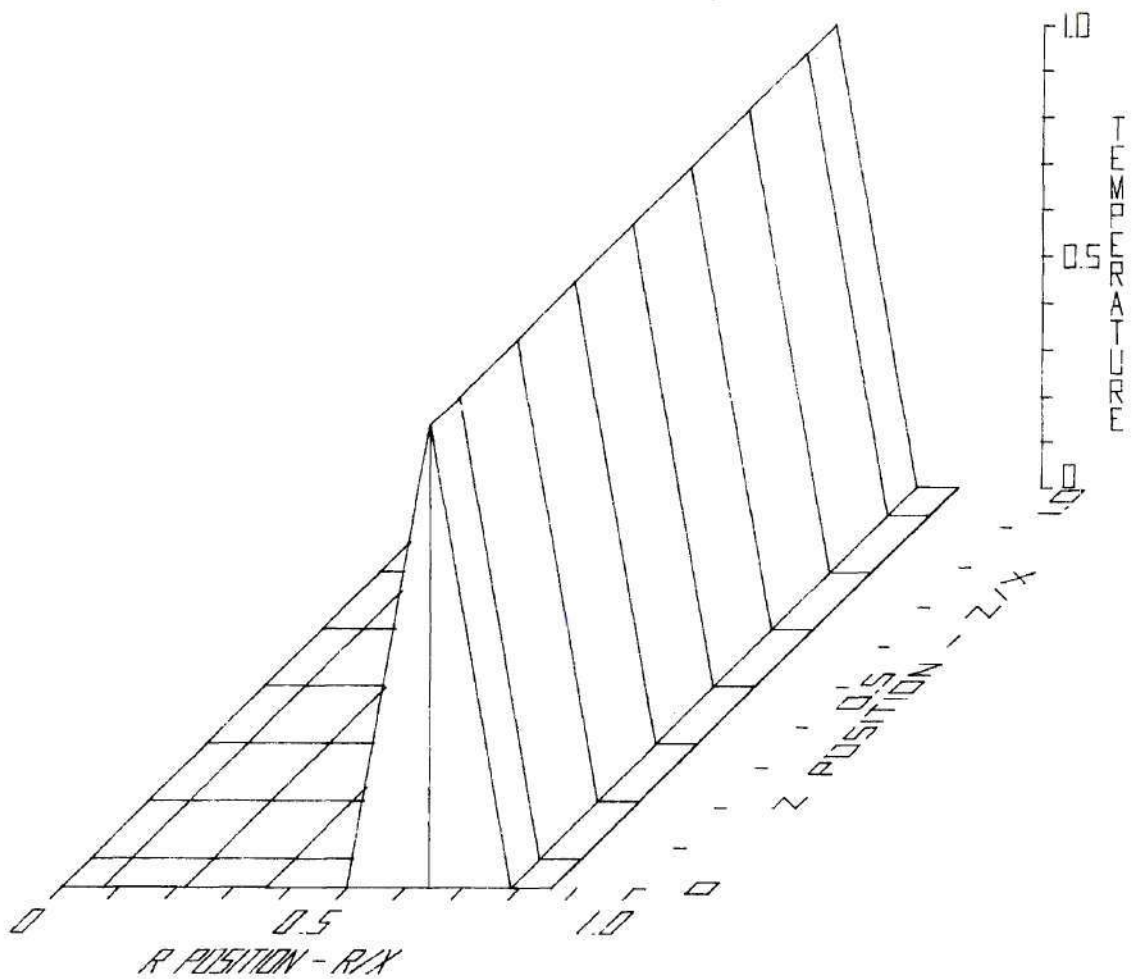

Figure 89: Solid Fuel Temperature [T = 2.05204 sec]

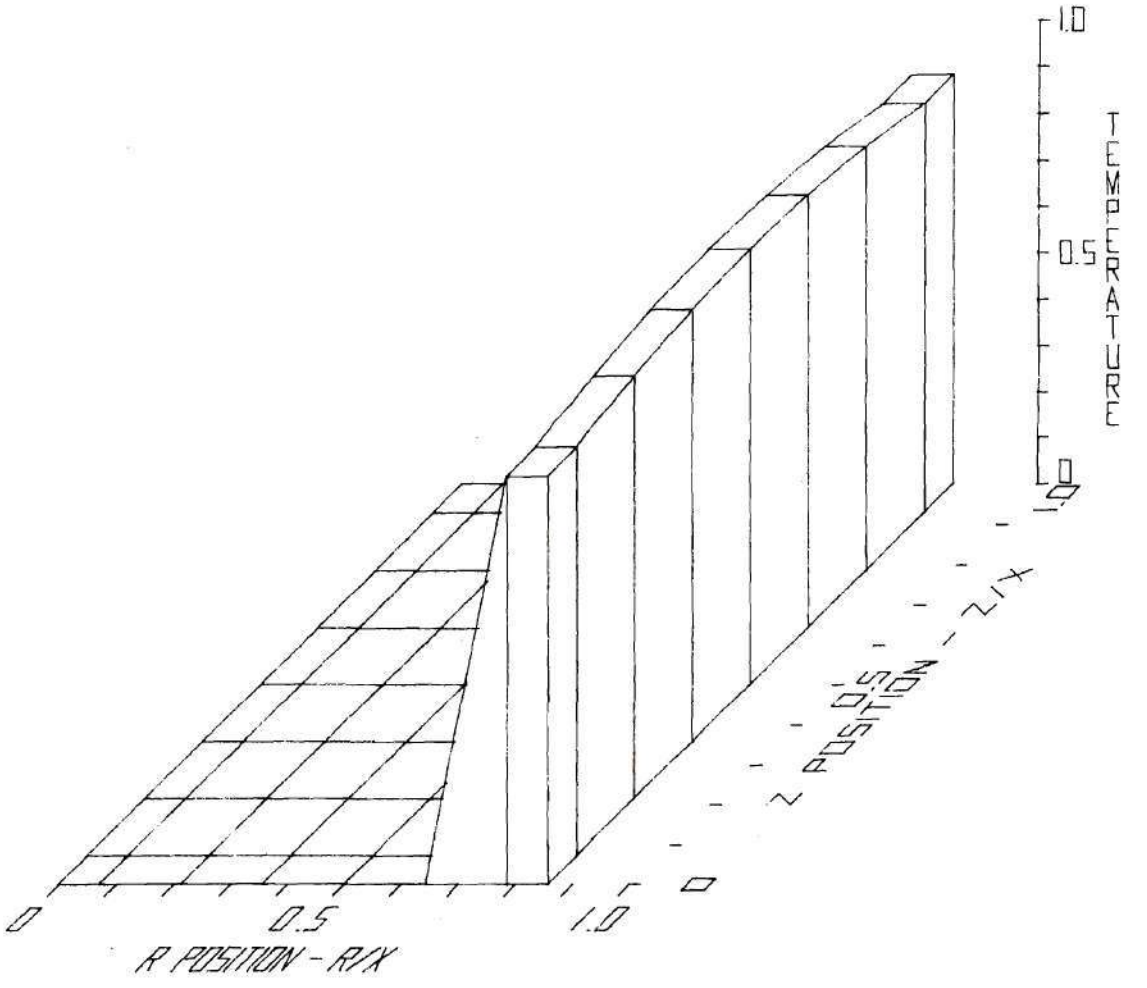

Figure 90: Solid Steel Temperature [T = 0.00000 sec]

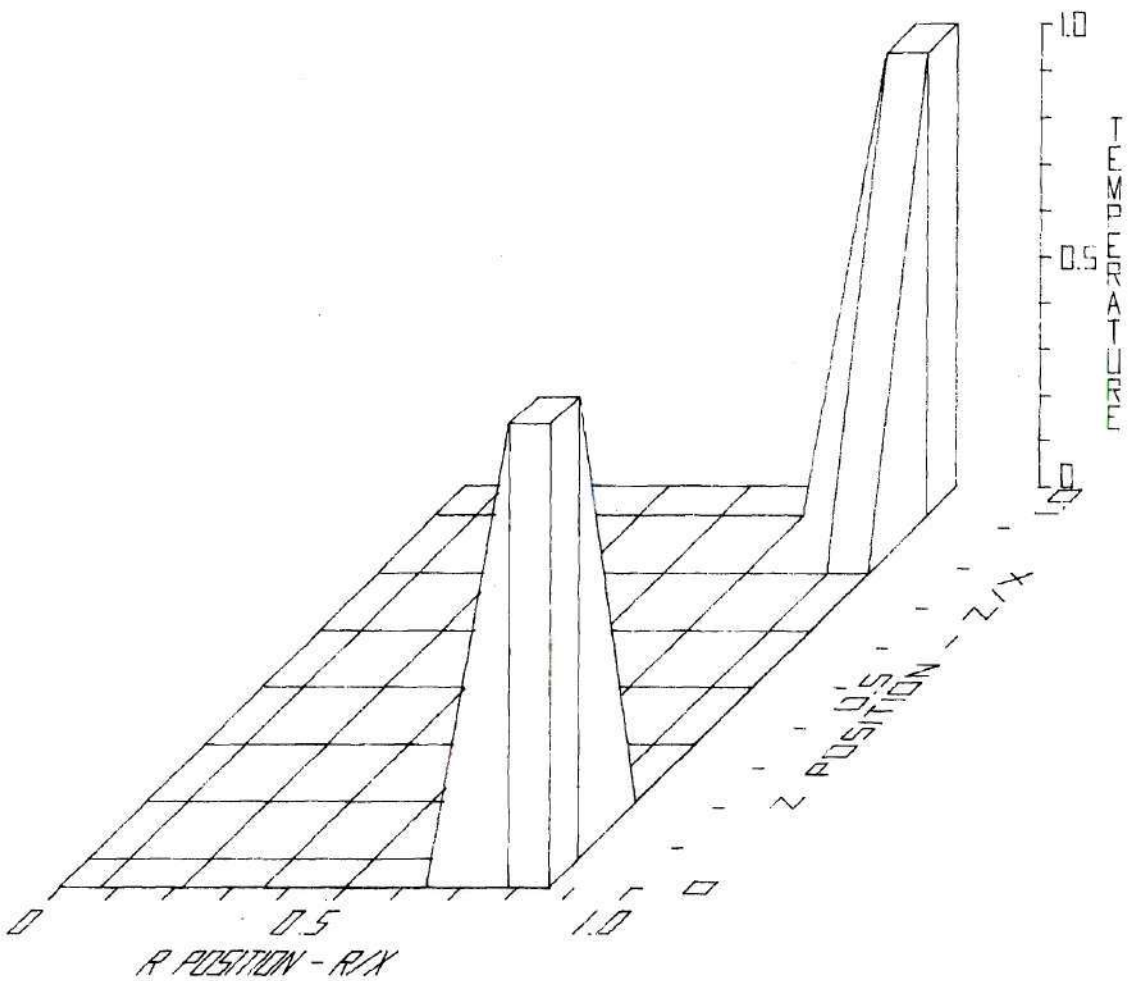

Figure 91: Solid Steel Temperature [T = 2.04889 sec]

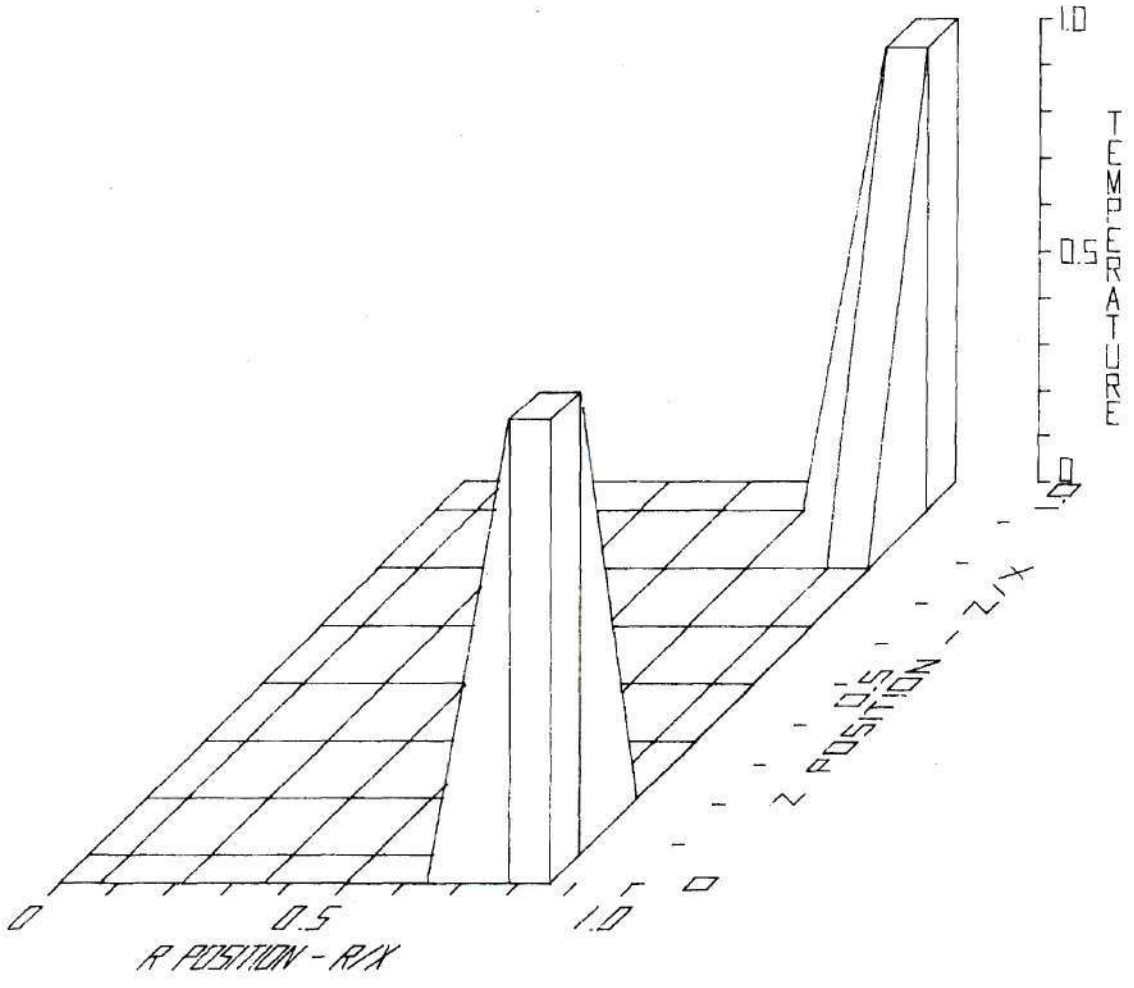

Figure 92: Solid Steel Temperature [T = 2.05204 sec]

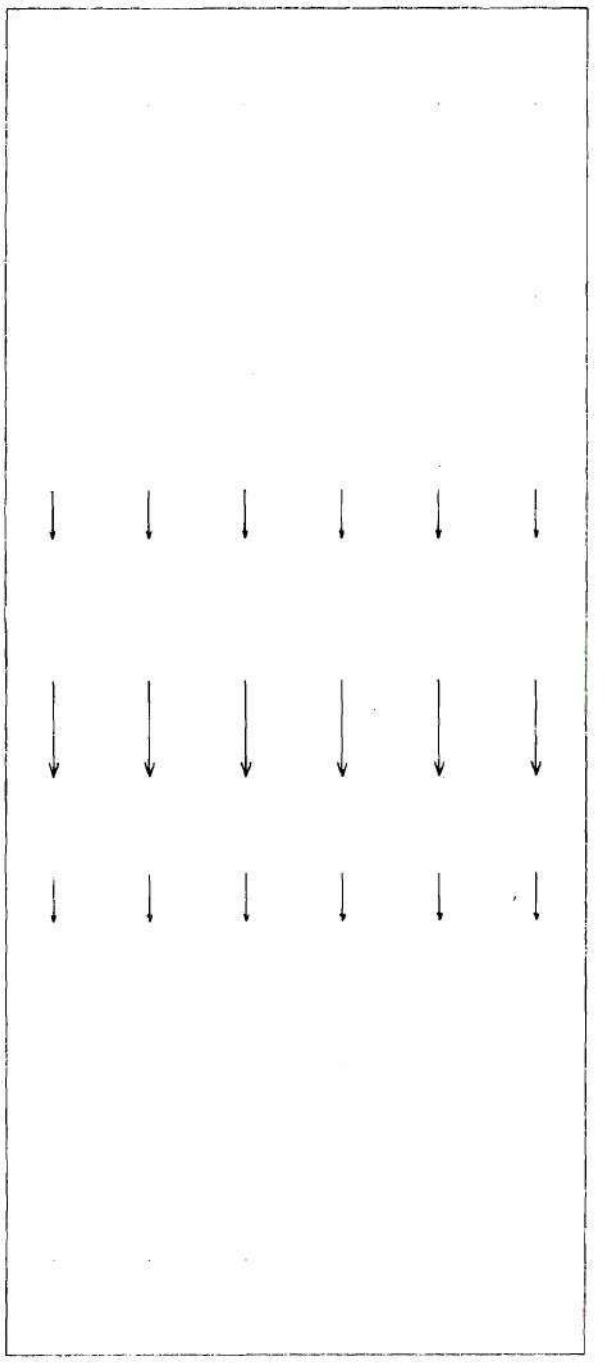

Figure 93: Liquid Fuel Velocity [T = 2.05164 sec]

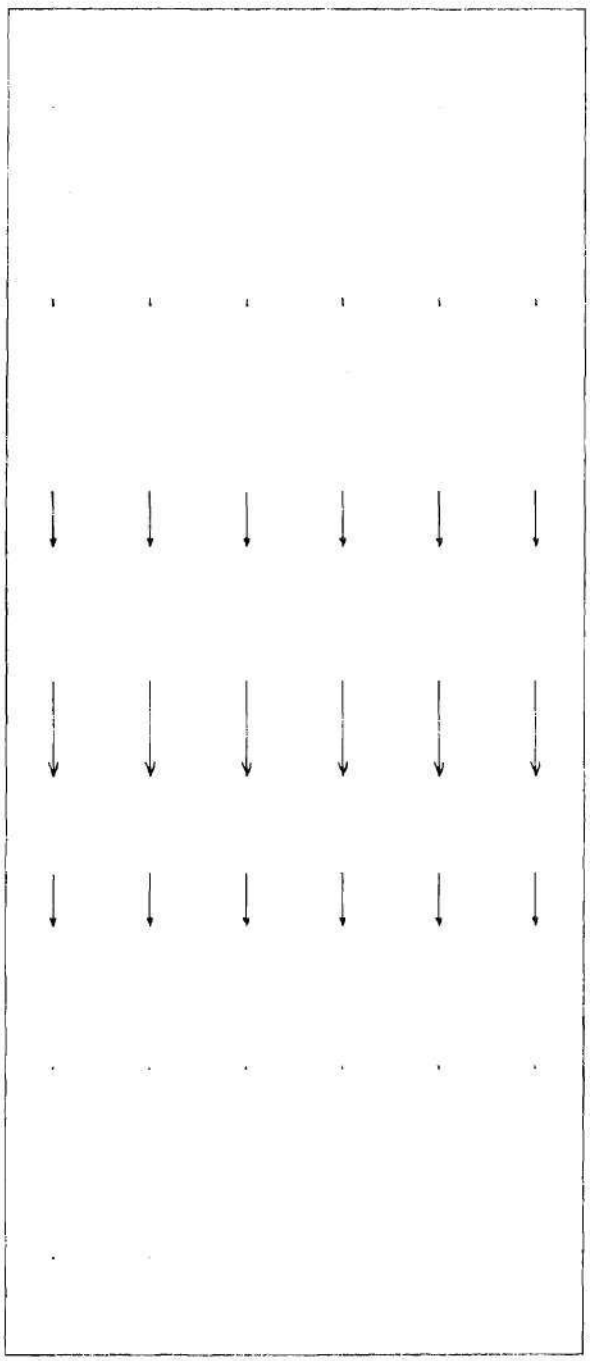

Figure 94: Liquid Fuel Velocity [T = 2.05172 sec]

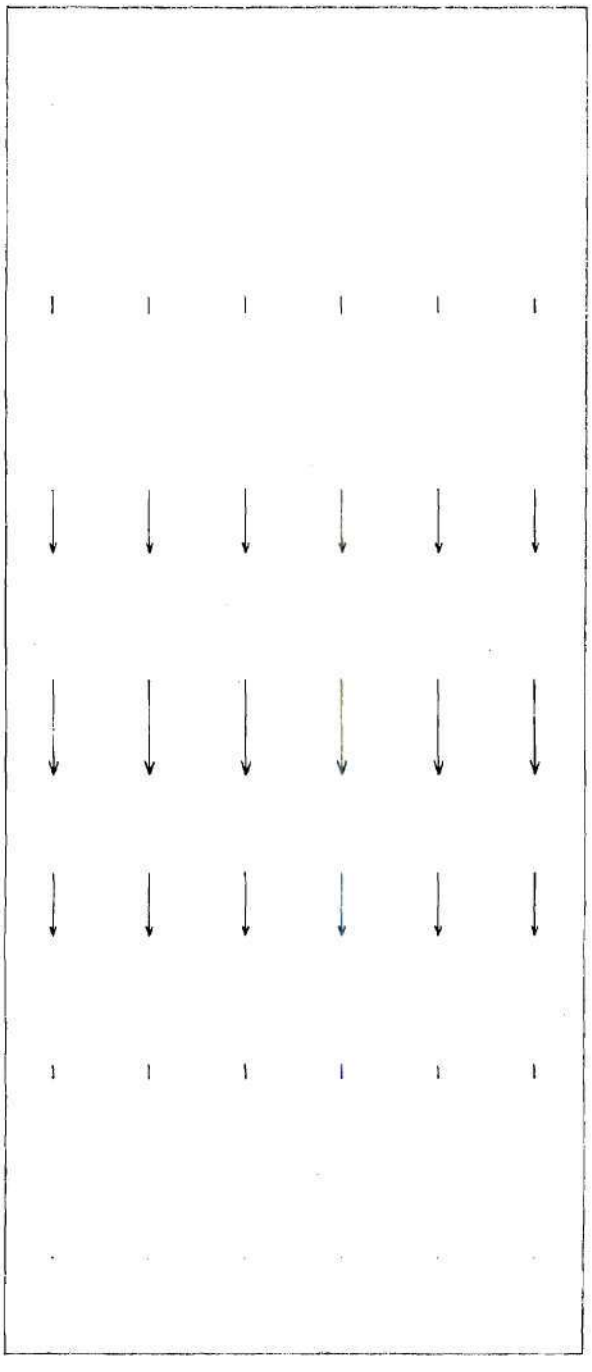

Figure 95: Liquid Fuel Velocity [T = 2.05185 sec]

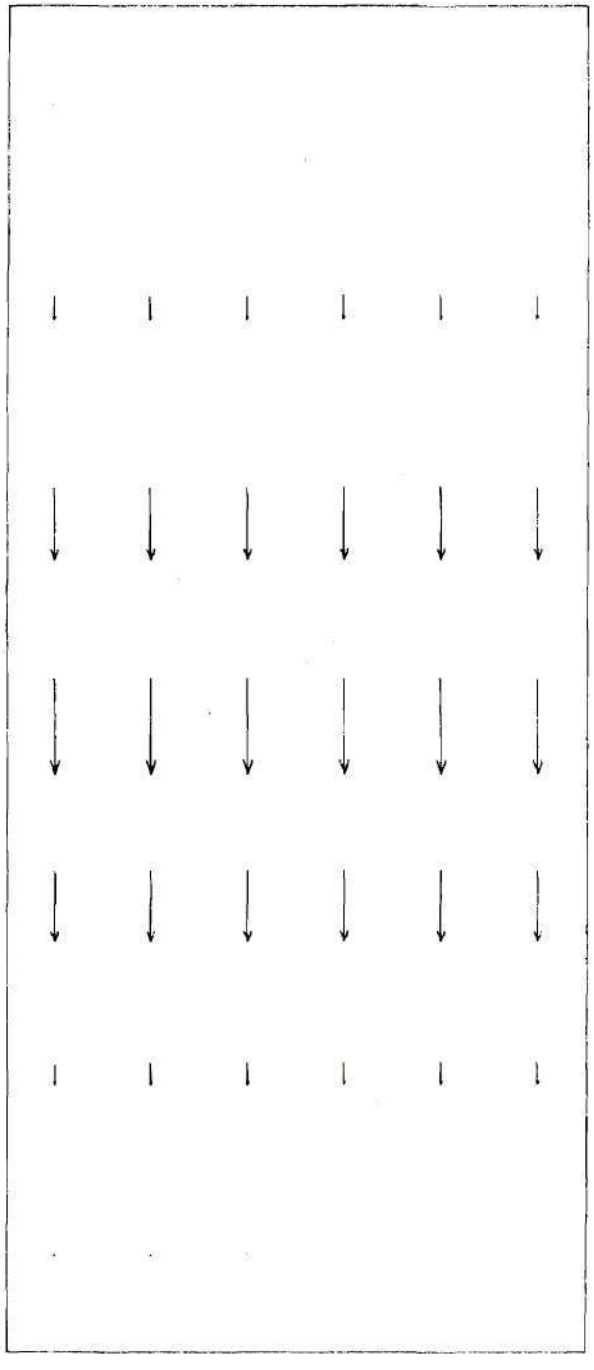

Figure 96: Liquid Fuel Velocity [T = 2.05204 sec]

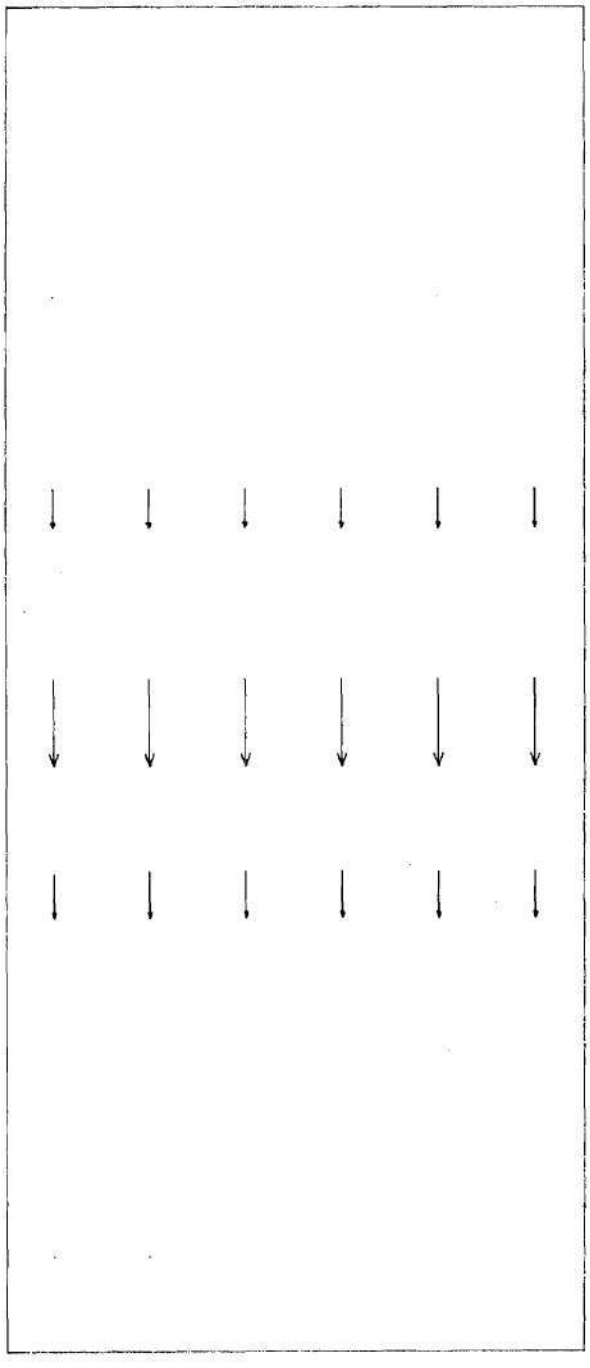

Figure 97· Fission Gas Velocity [T = 2.05164 sec]

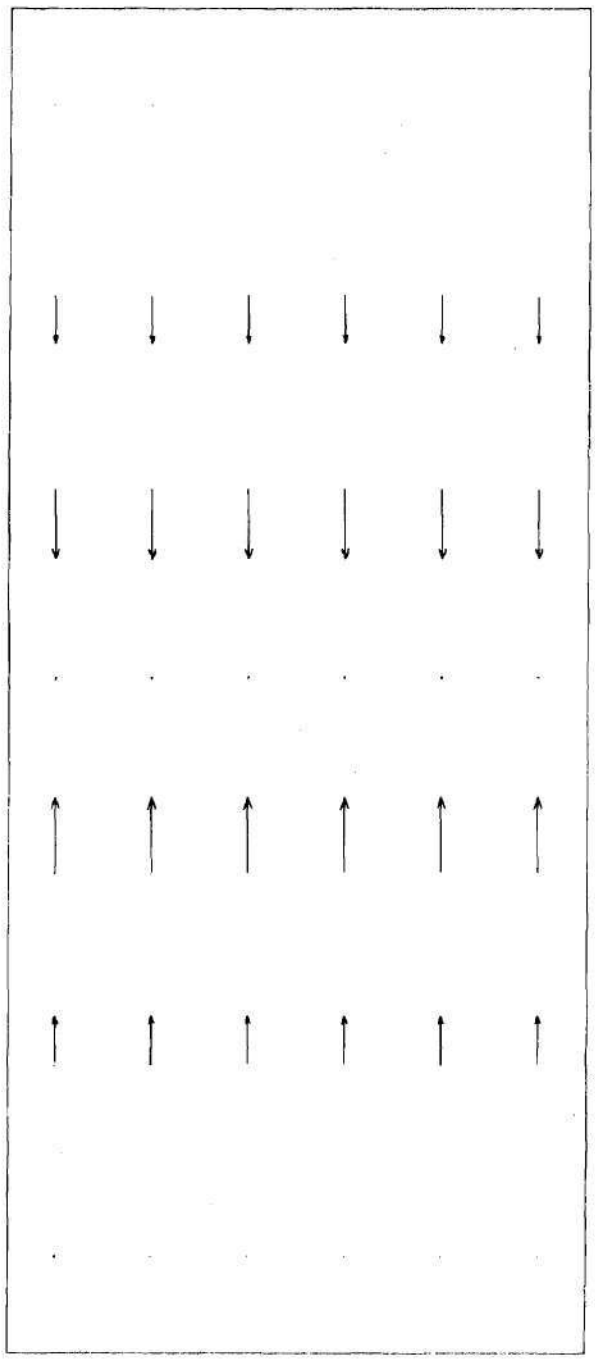

Figure 98: Fission Gas Velocity [T = 2.05172 sec]

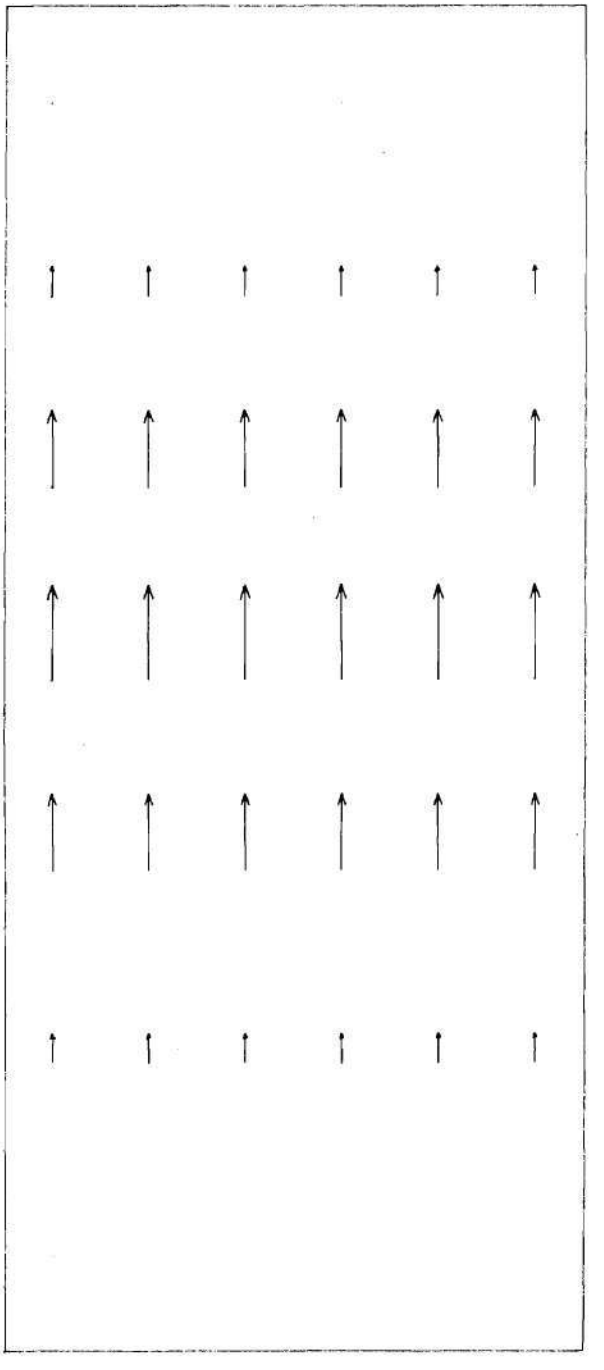

Figure 99: Fission Gas Velocity [T = 2.05185 sec]

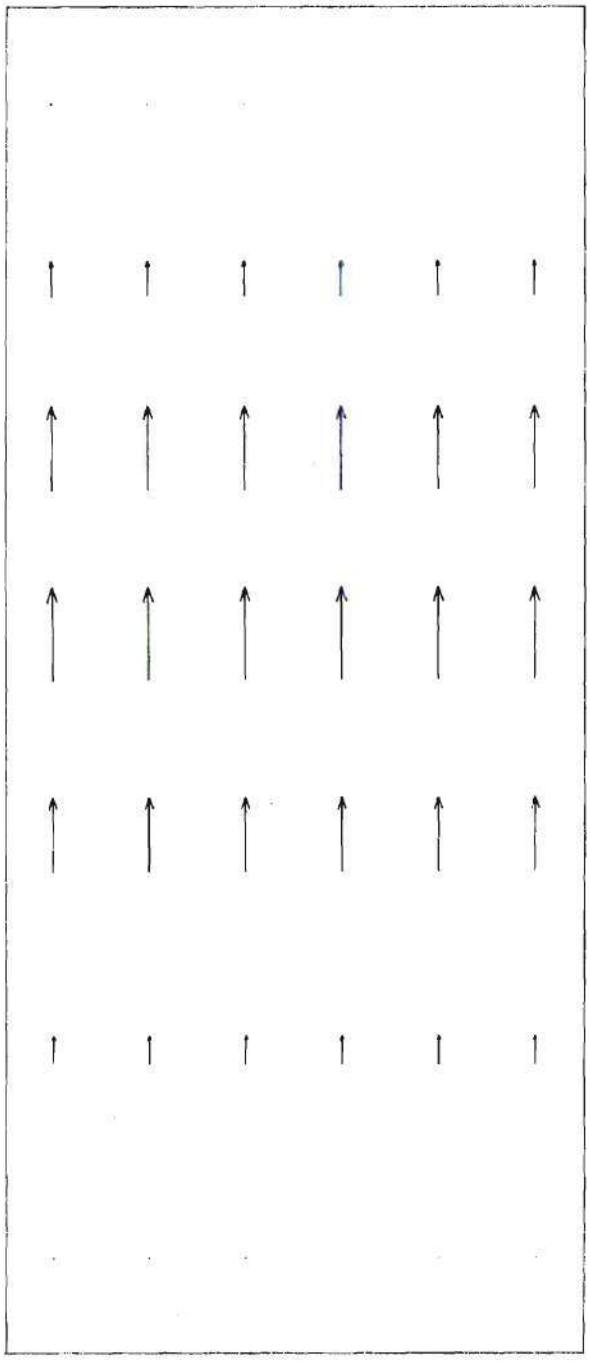

Figure 100: Fission Gas Velocity [T = 2.05204 sec]

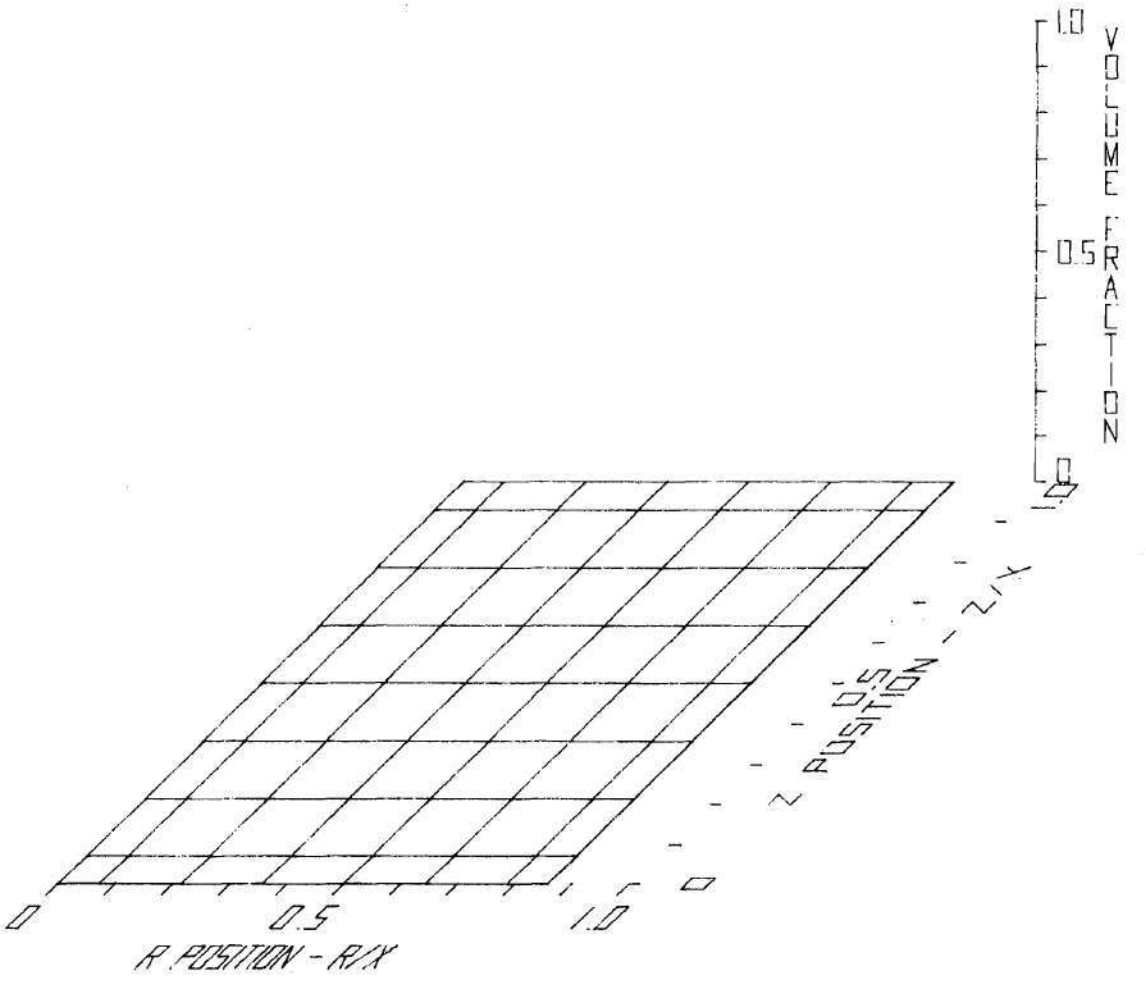

Figure 101: Liquid Fuel Volume Fraction [T = 0.00000 sec]

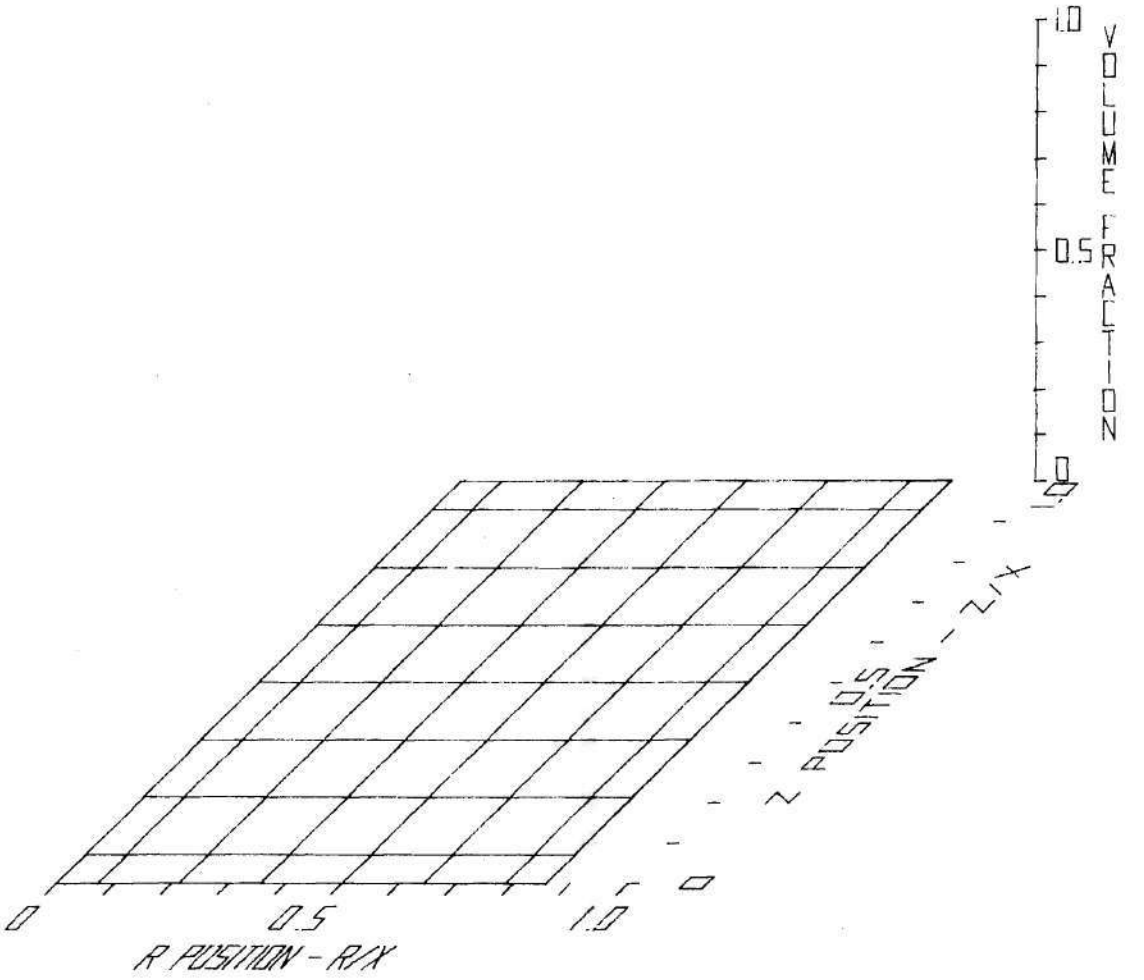

Figure 102: Liquid Fuel Volume Fraction [T = 2.04889 sec]

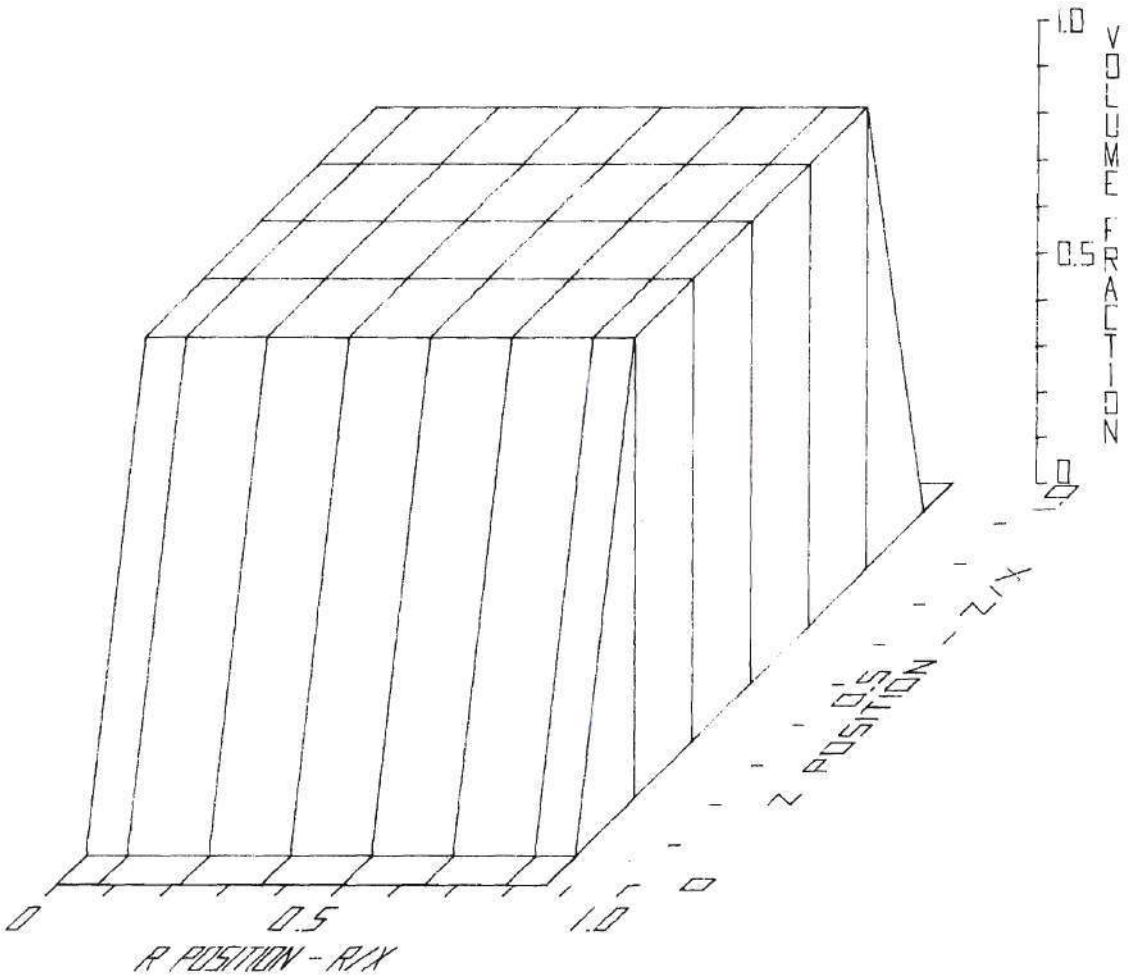

Figure 103: Liquid Fuel Volume Fraction [T = 2.05204 sec]

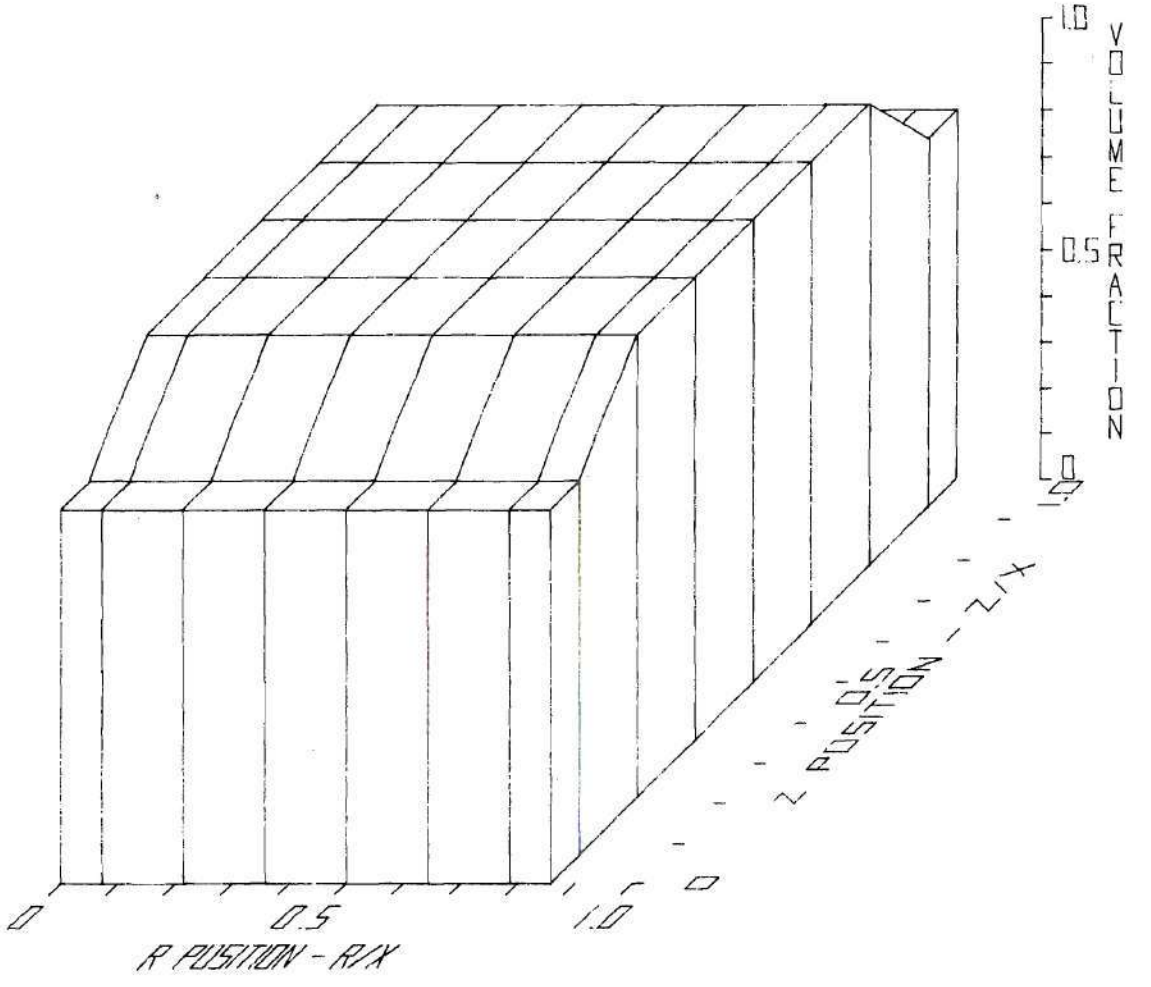

Figure 104: Fission Gas Volume Fraction [T = 0.00000 sec]

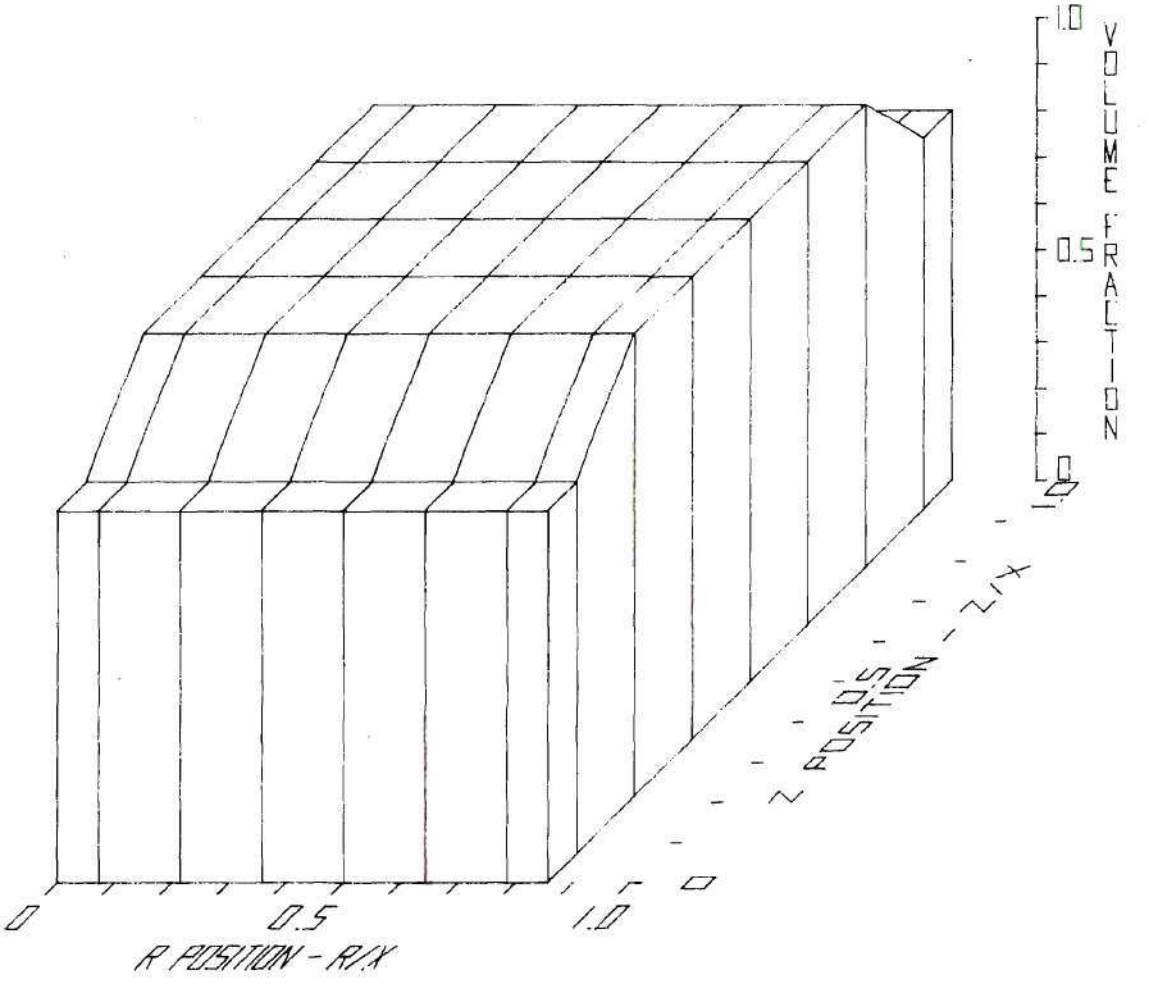

Figure 105: Fission Gas Volume Fraction [T = 2.04889 sec]

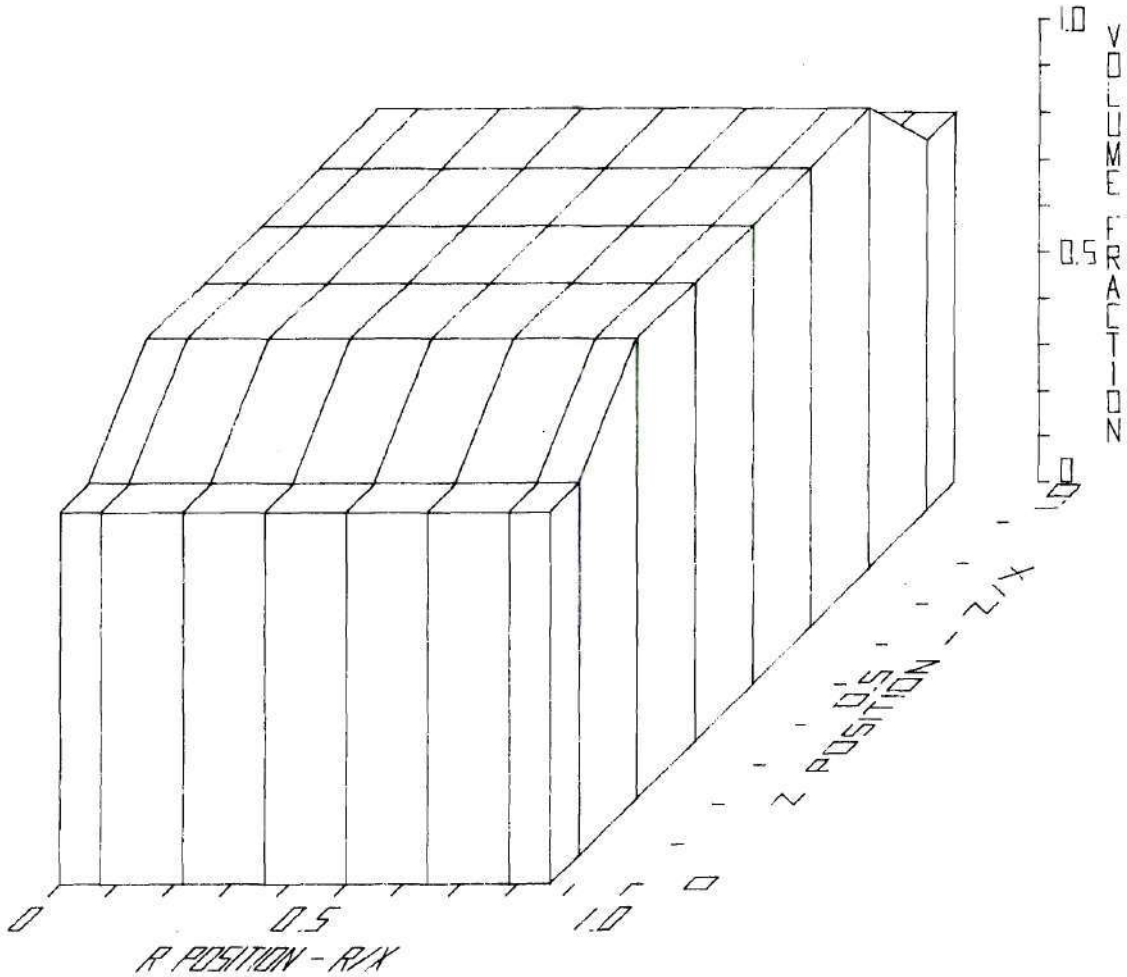

Figure 106: Fission Gas Volume Fraction [T = 2.05204 sec]

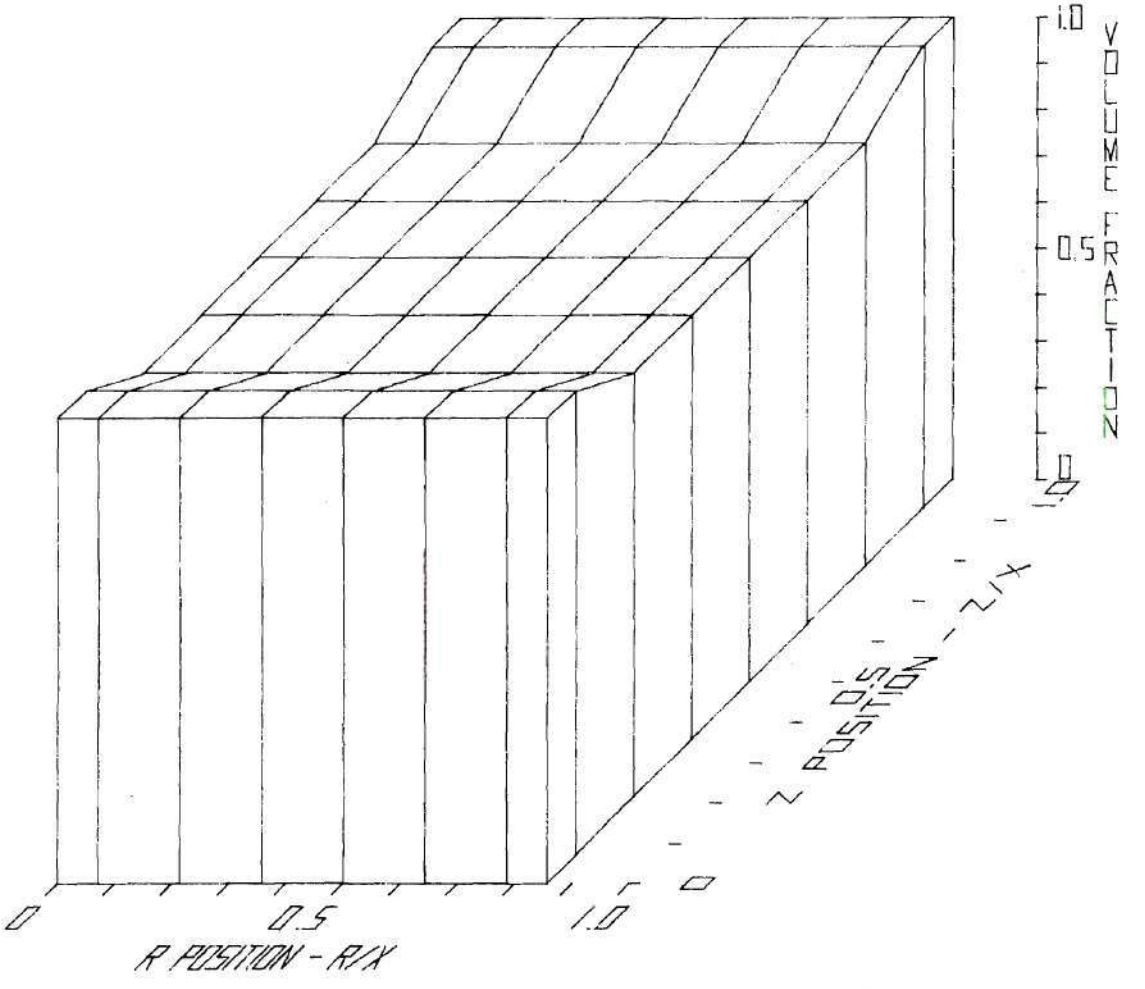

Figure 107: Solid Fuel Volume Fraction [T = 0.00000 sec]

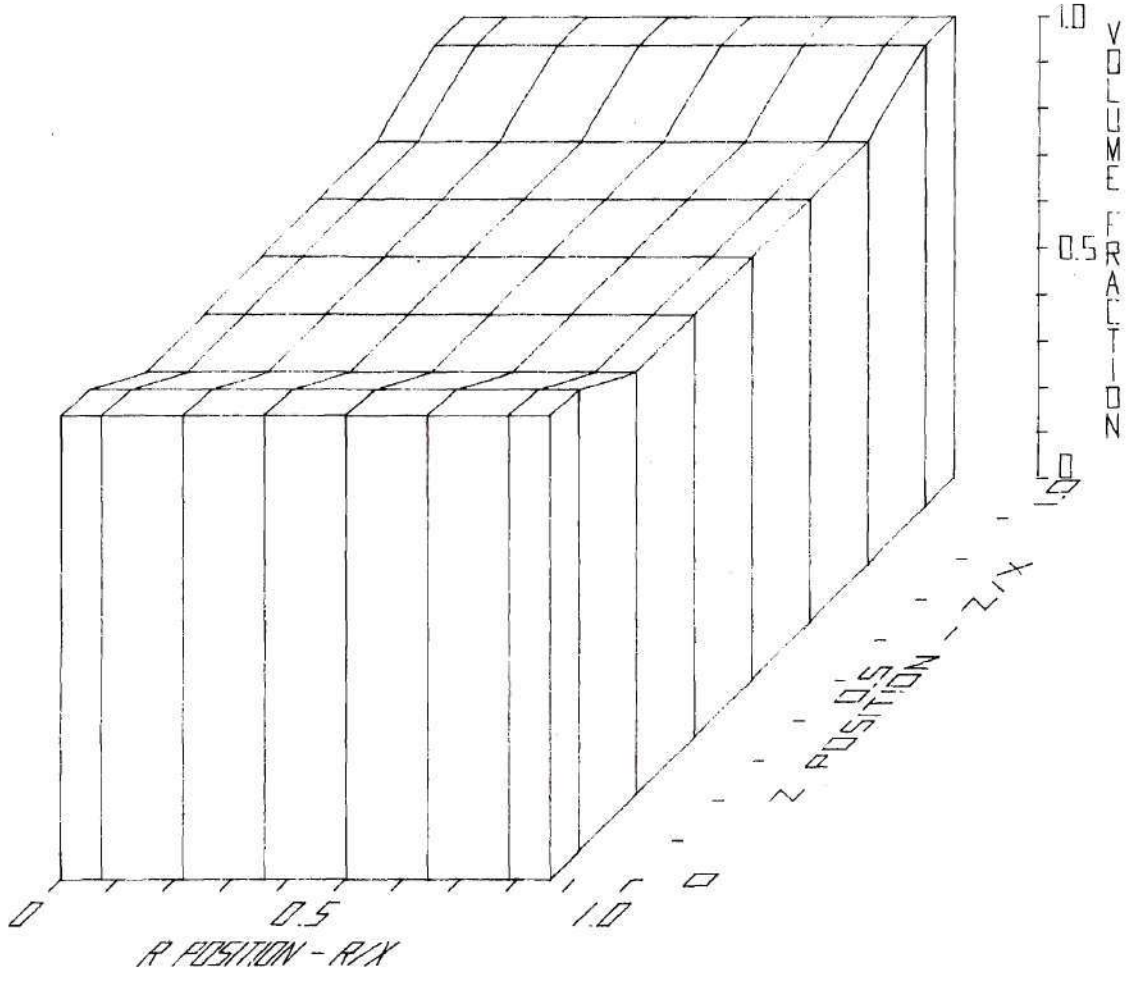

Figure 108: Solid Fuel Volume Fraction [T = 2.04889 sec]

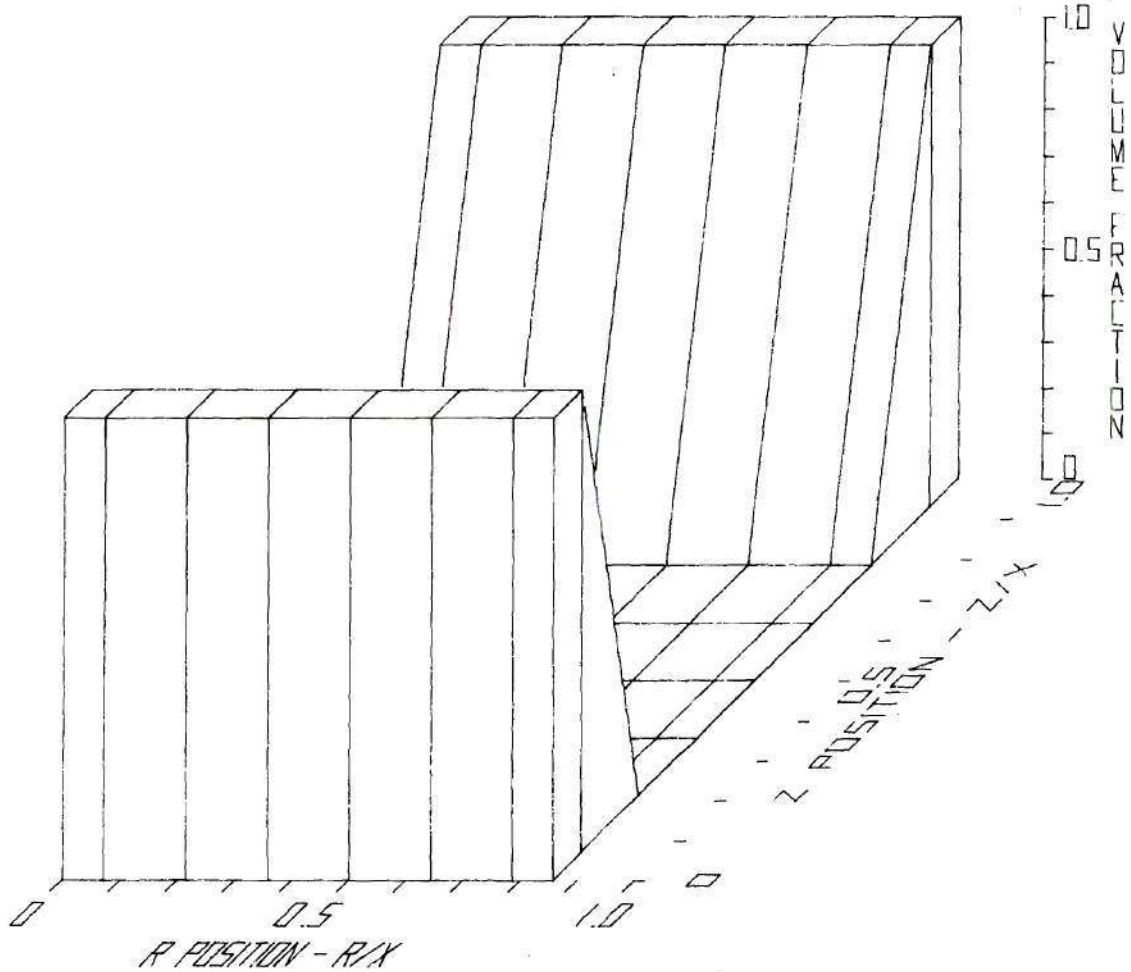

Figure 109: Solid Fuel Volume Fraction [T = 2.05204 sec]

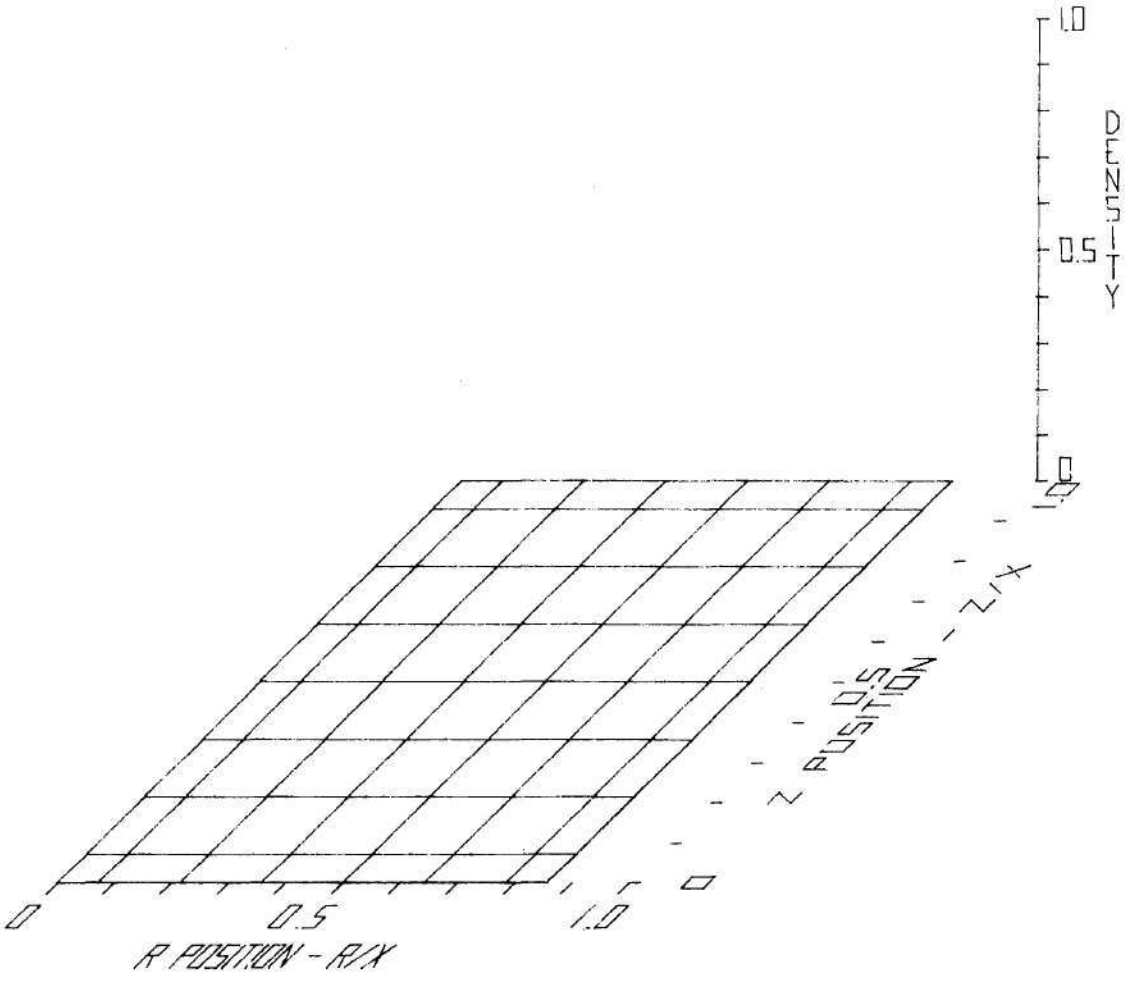

Figure 110: Liquid Fuel Density [T = 0.00000 sec]

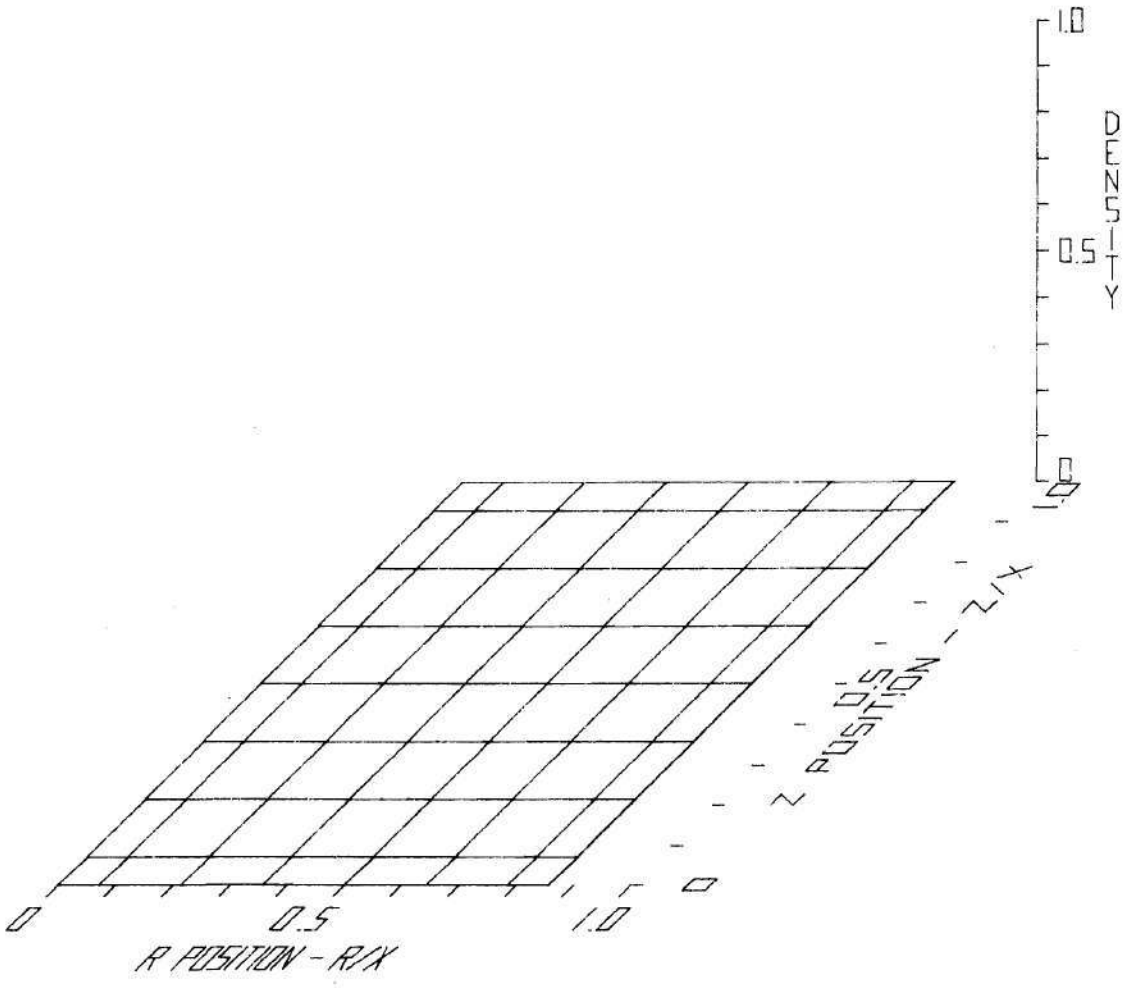

Figure 111: Liquid Fuel Density [T = 2.04889 sec]

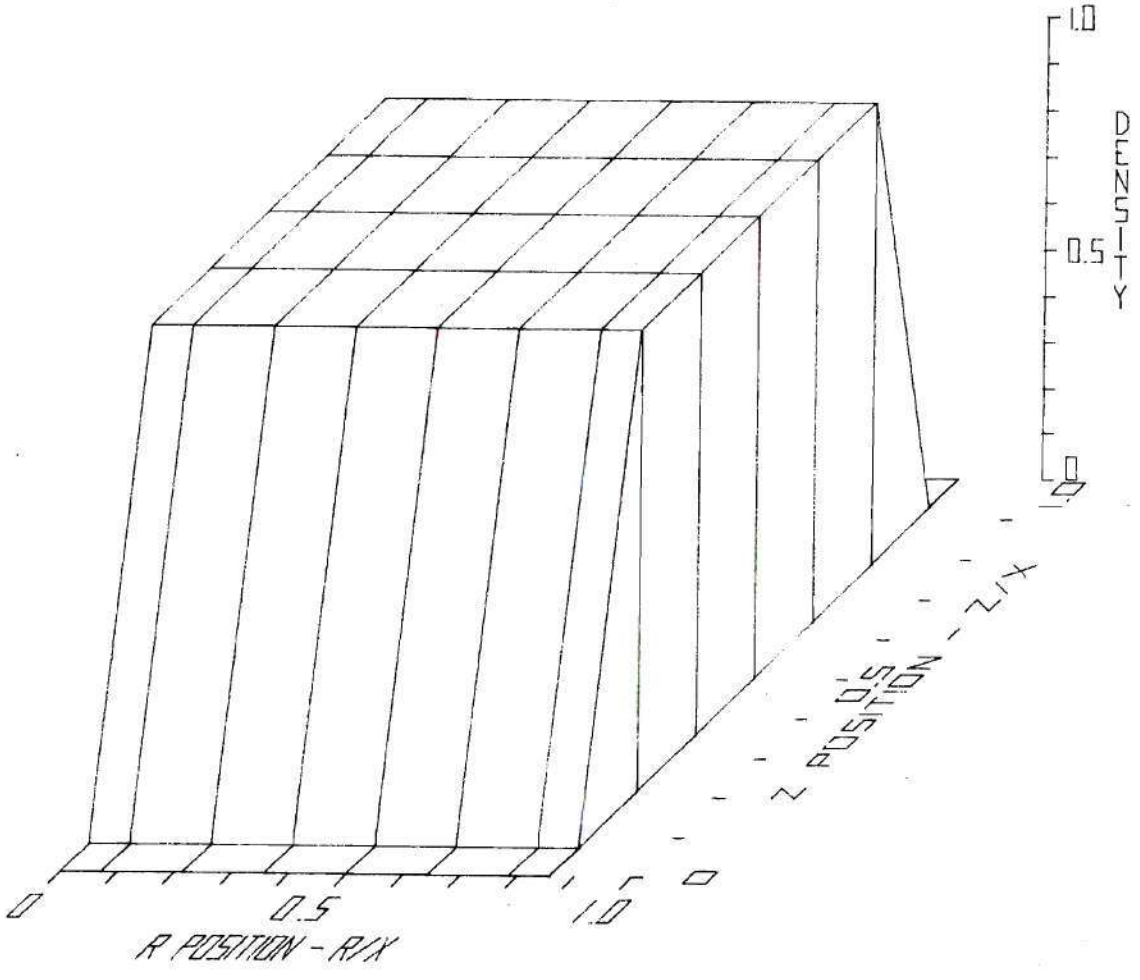

Figure 112: Liquid Fuel Density [T = 2.05204 sec]

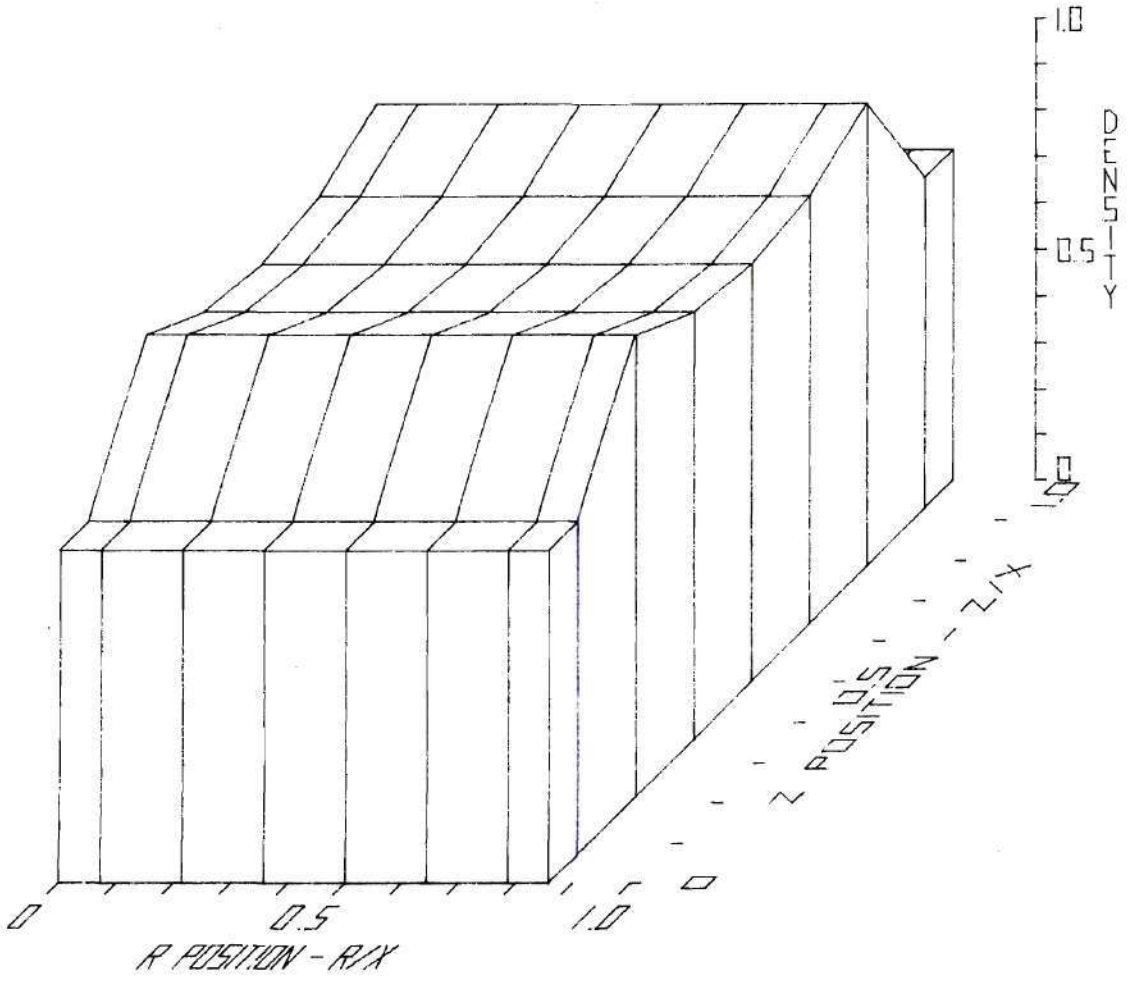

Figure 113: Fission Gas Density [T = 0.00000 sec]

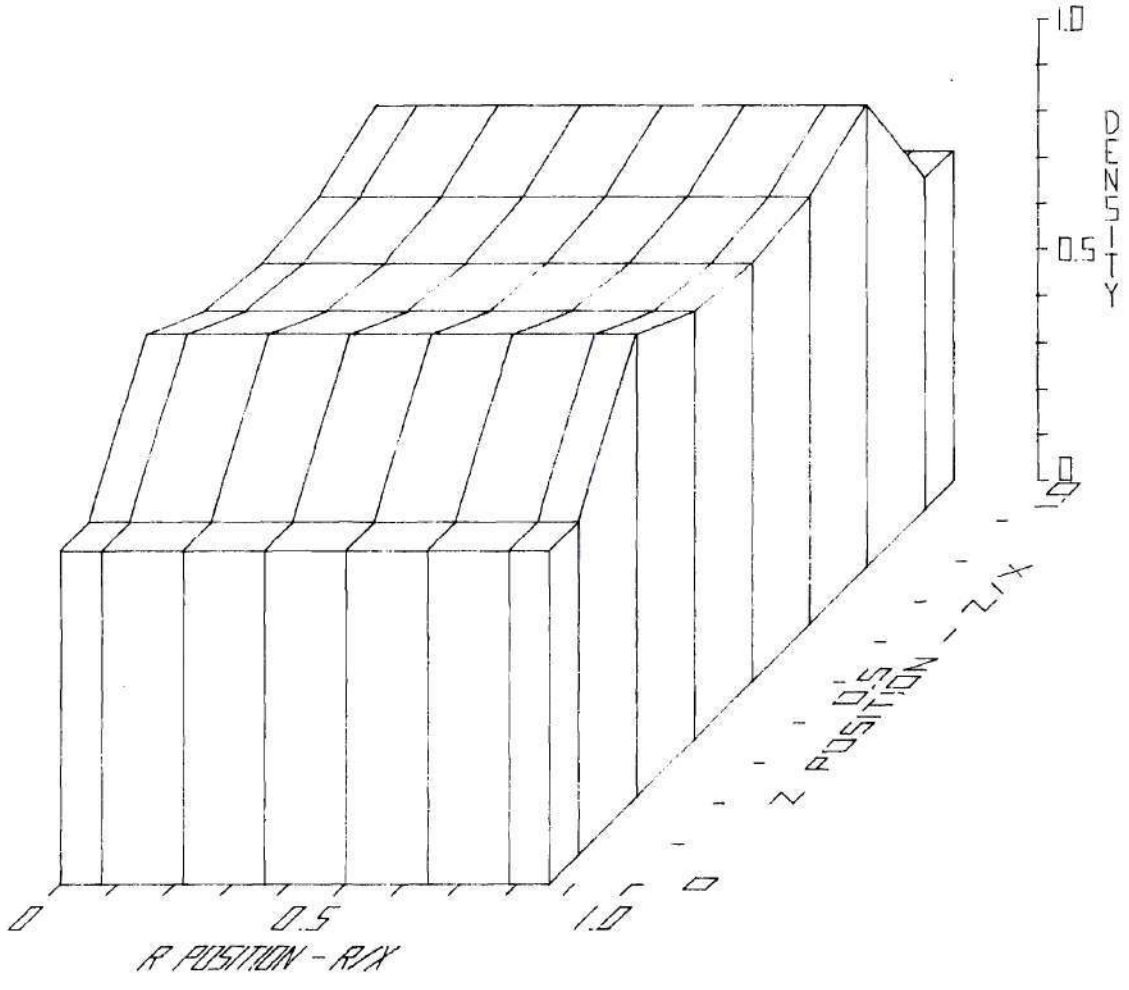

Figure 114: Fission Gas Density [T = 2.04889 sec]

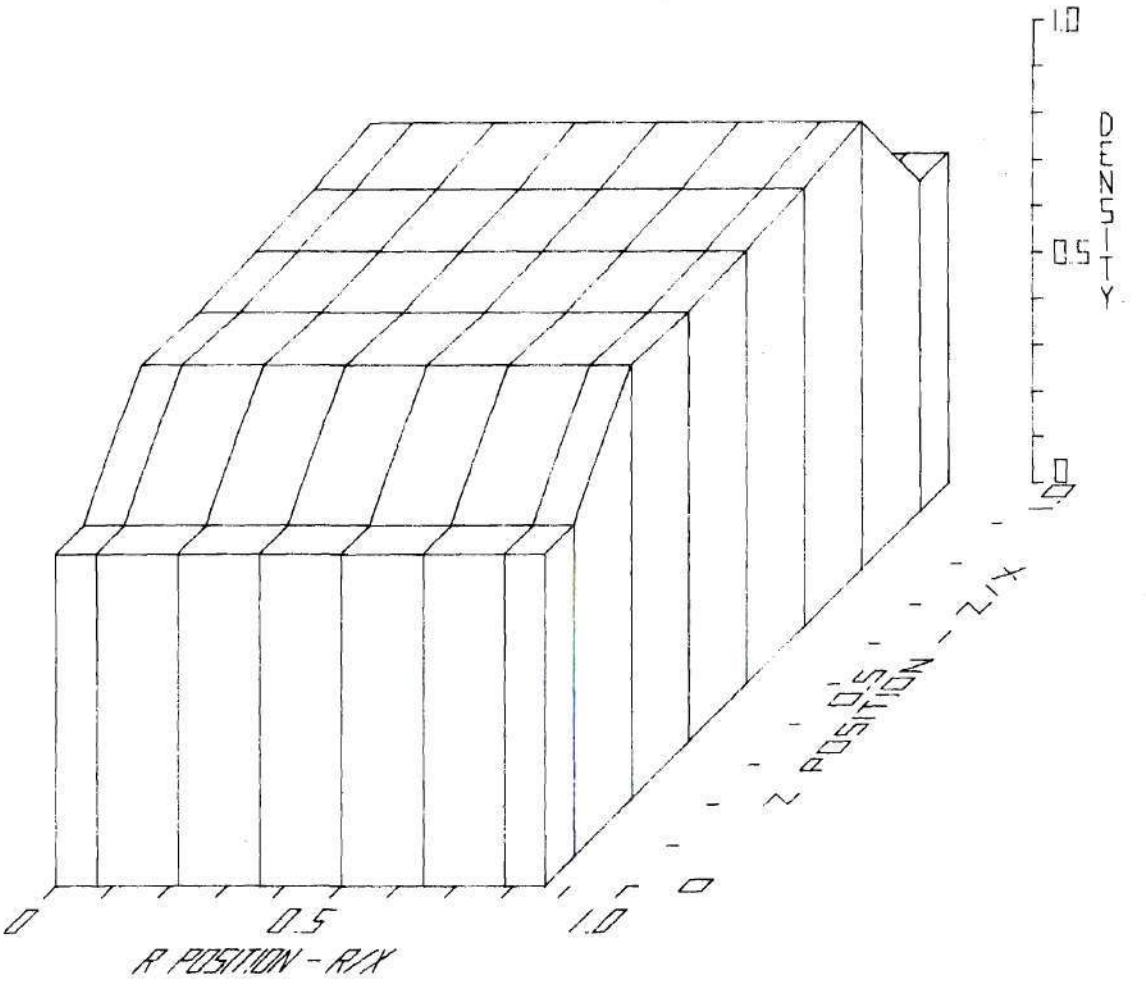

Figure 115: Fission Gas Density [T = 2.05204 sec]

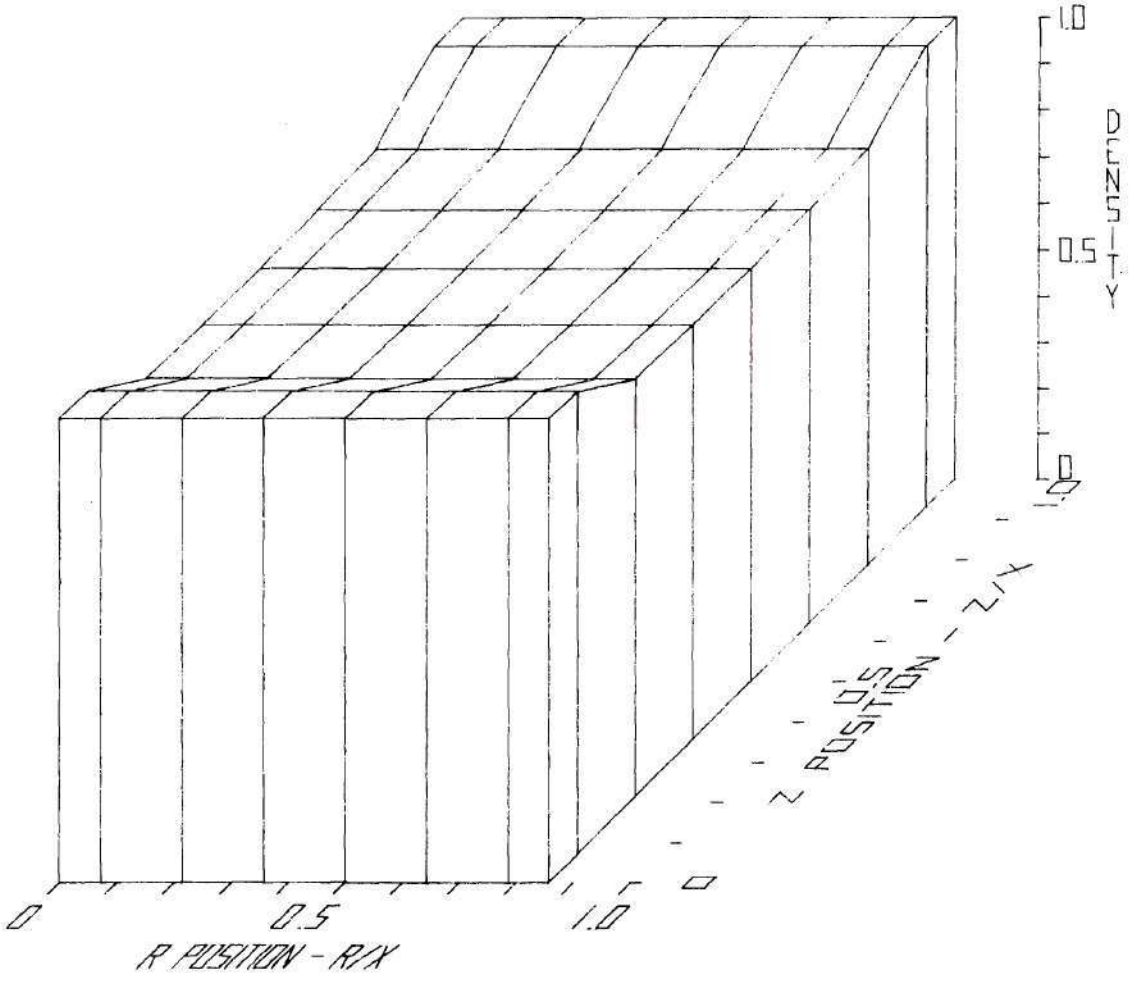

Figure 116: Solid Fuel Density [T = 0.00000 sec]

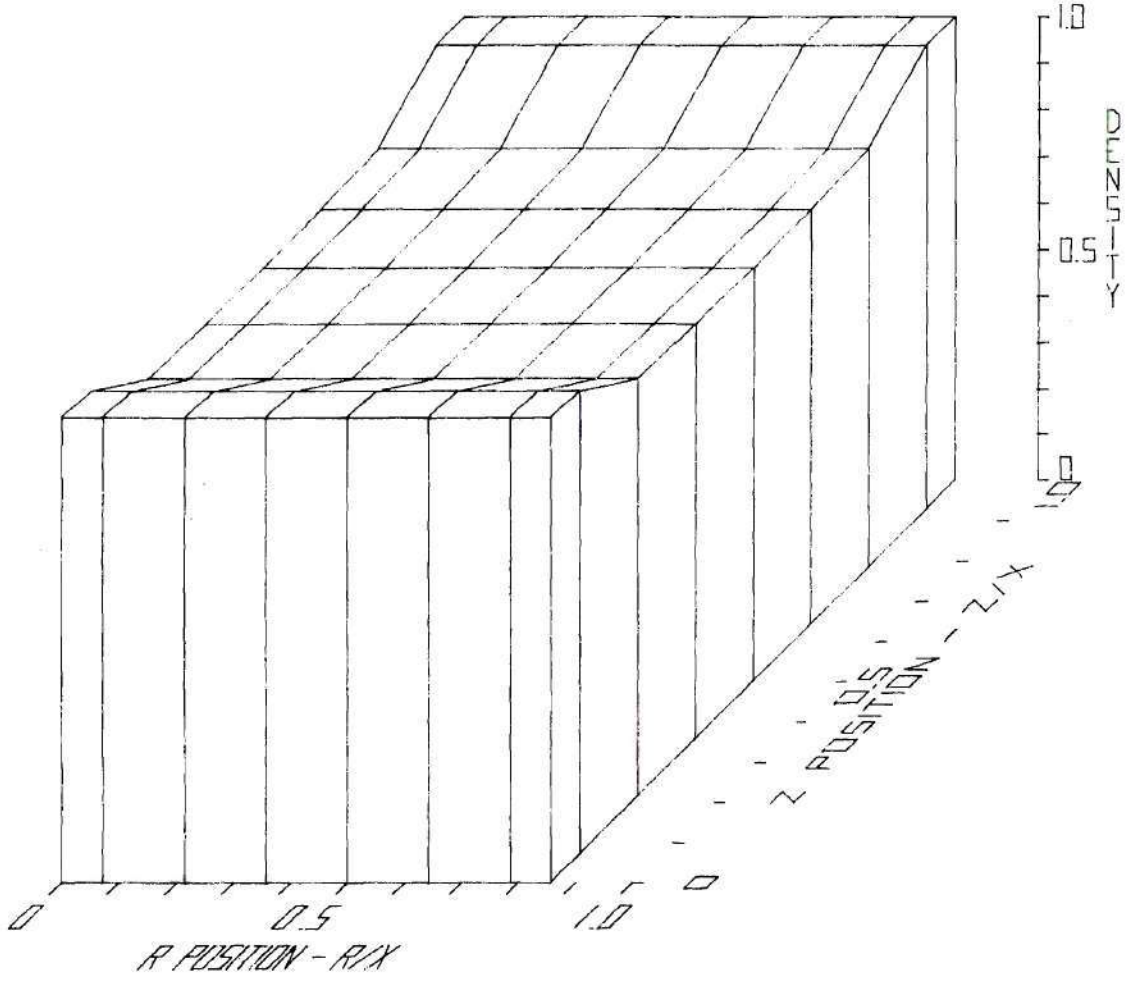

Figure 117: Solid Fuel Density [T = 2.04889 sec]

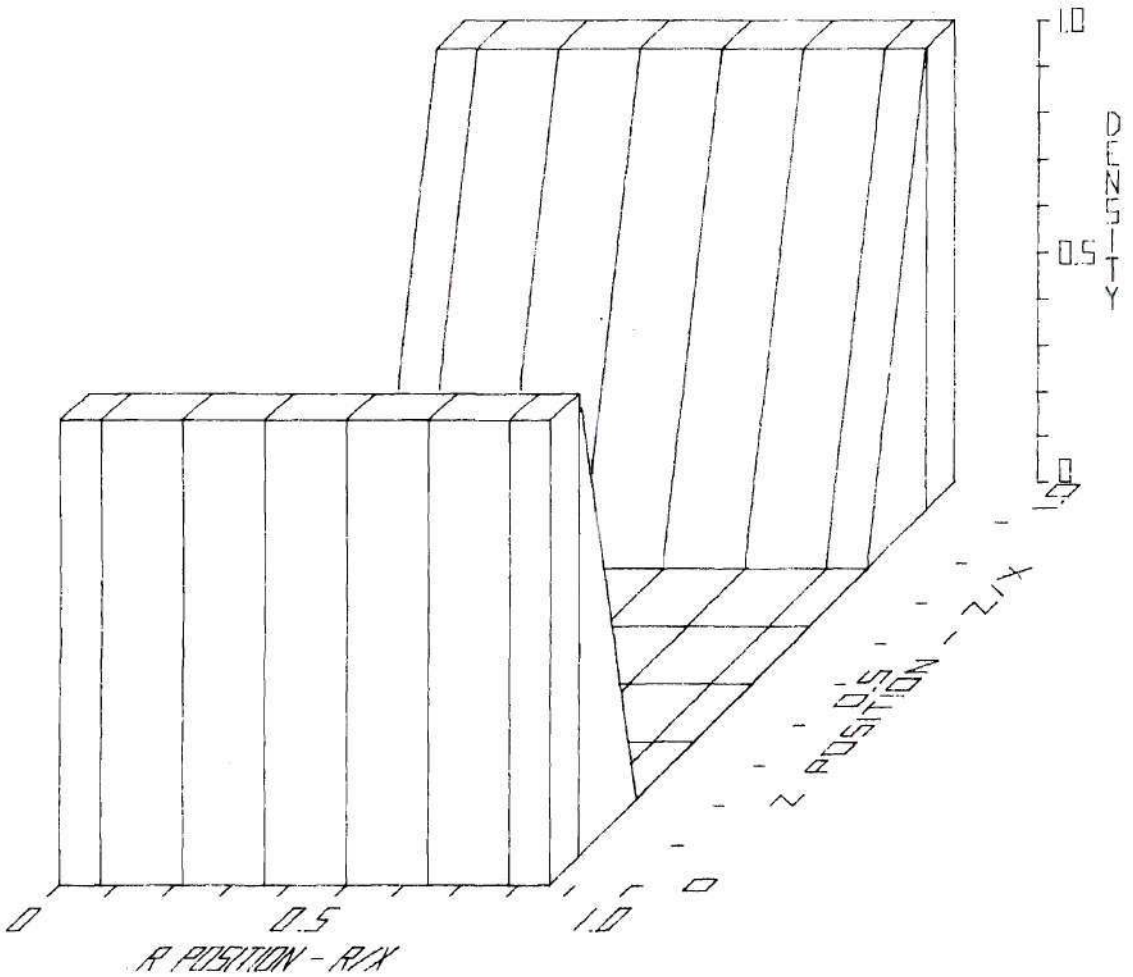

Figure 118: Solid Fuel Density [T = 2.05204 sec]

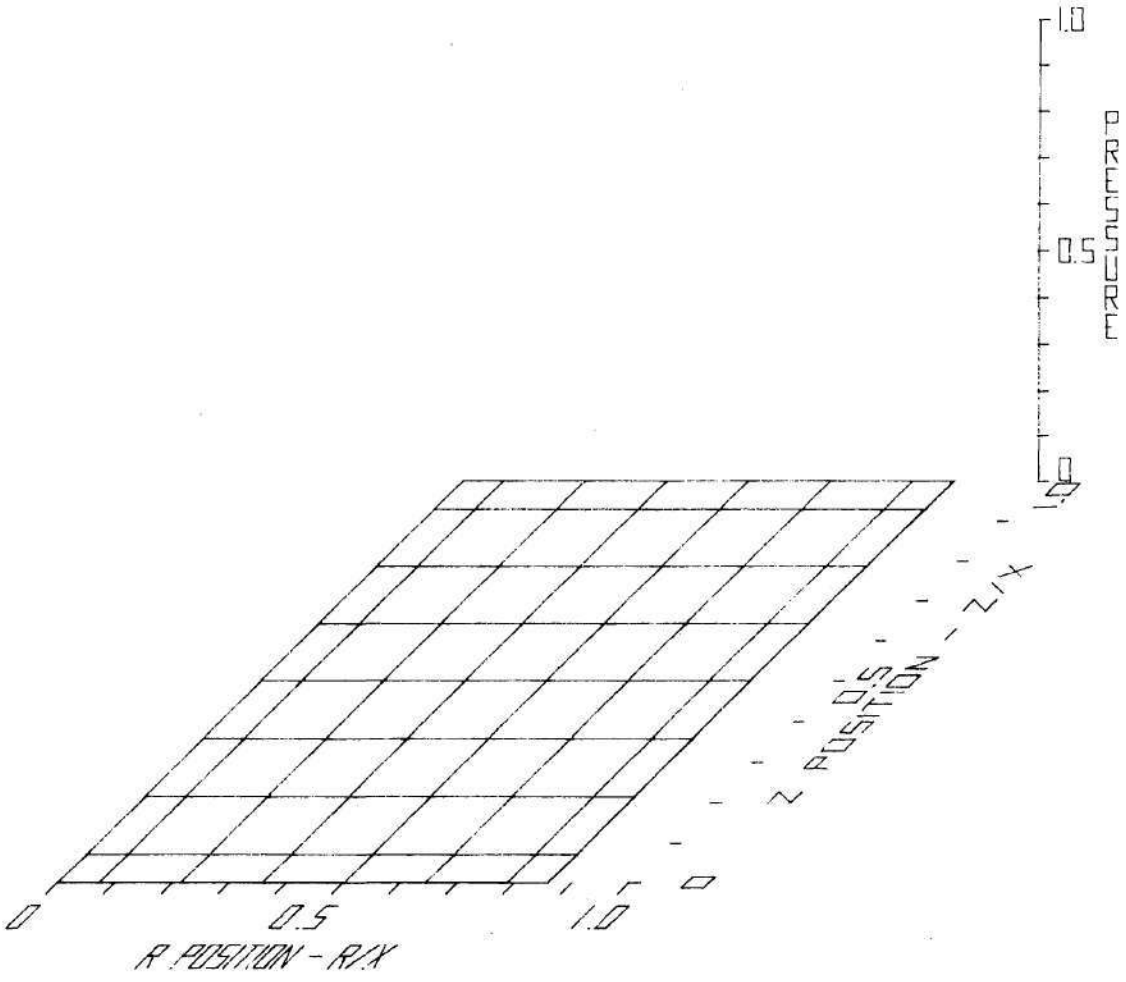

Figure 119: Liquid Fuel Pressure [T = 0.00000 sec]

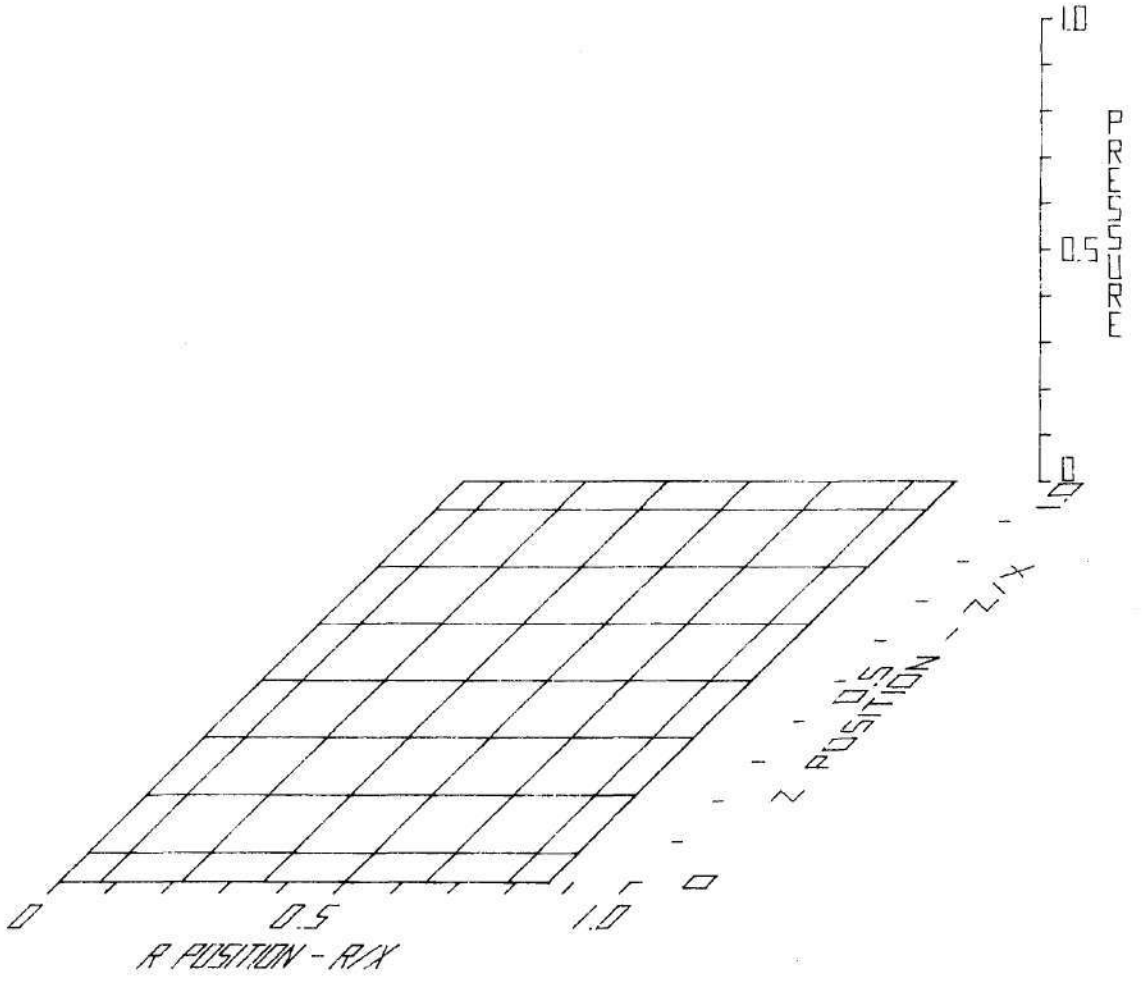

Figure 120: Liquid Fuel Pressure [T = 2.04889 sec]

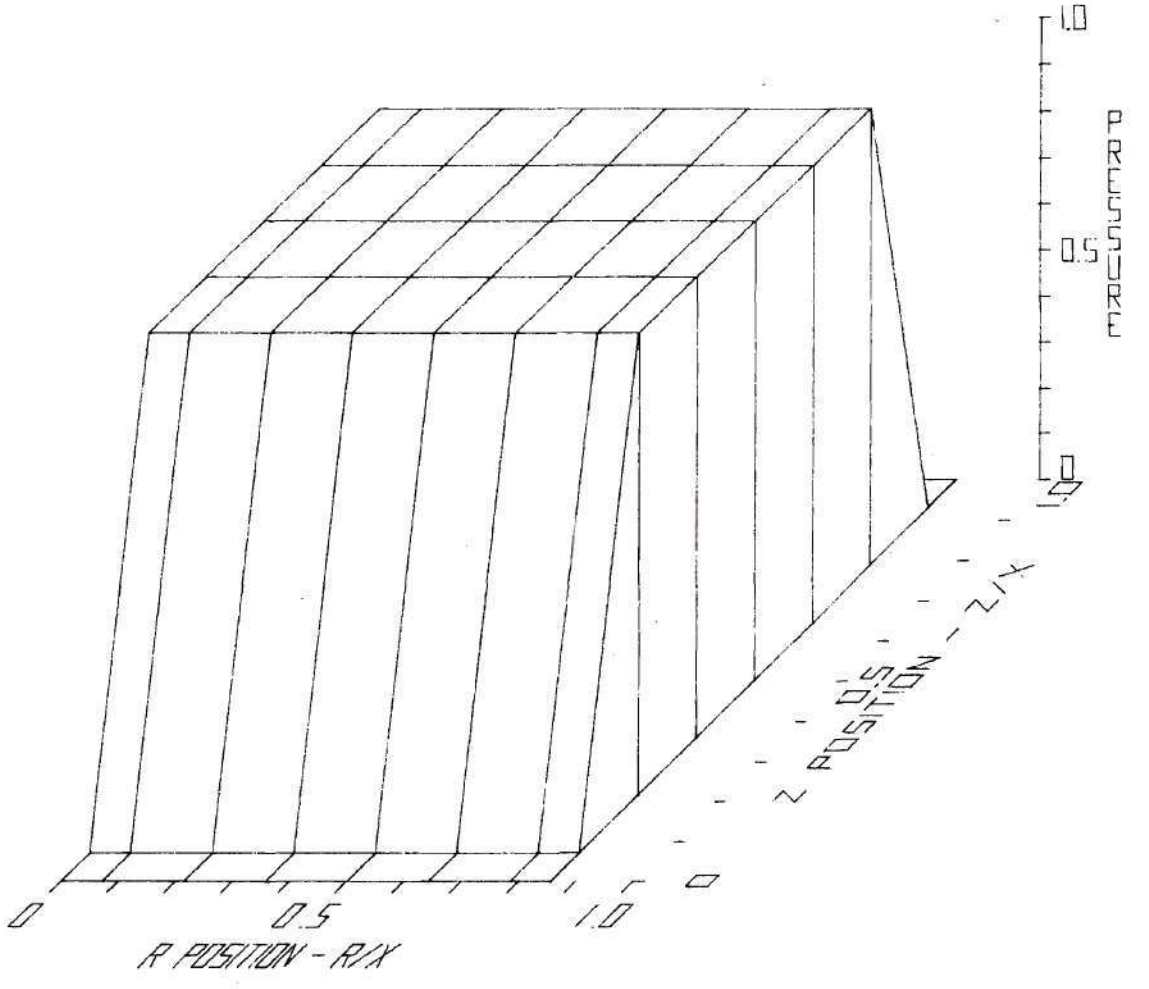

Figure 121: Liquid Fuel Pressure [T = 2.05204 sec]

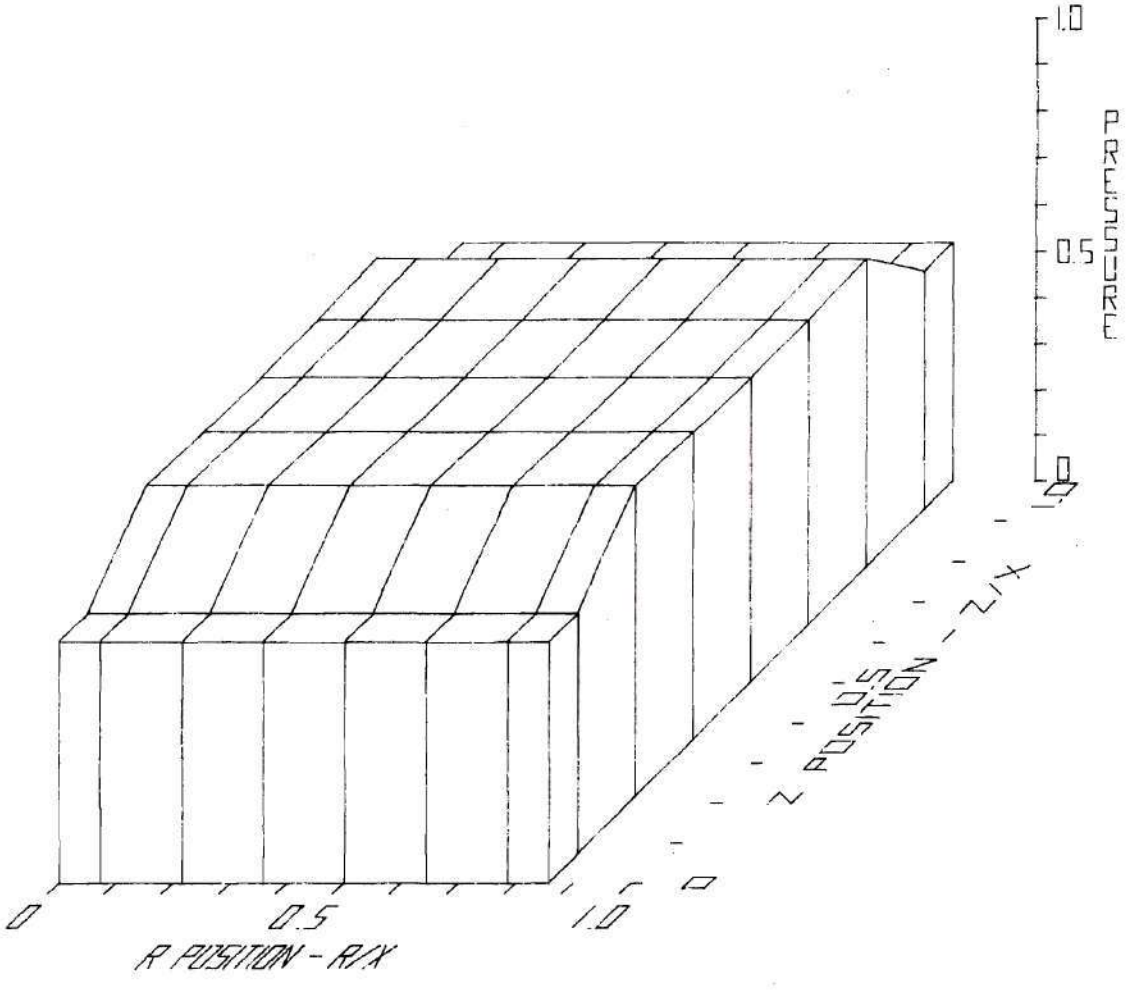

Figure 122: Fission Gas Pressure [T = 0.00000 sec]

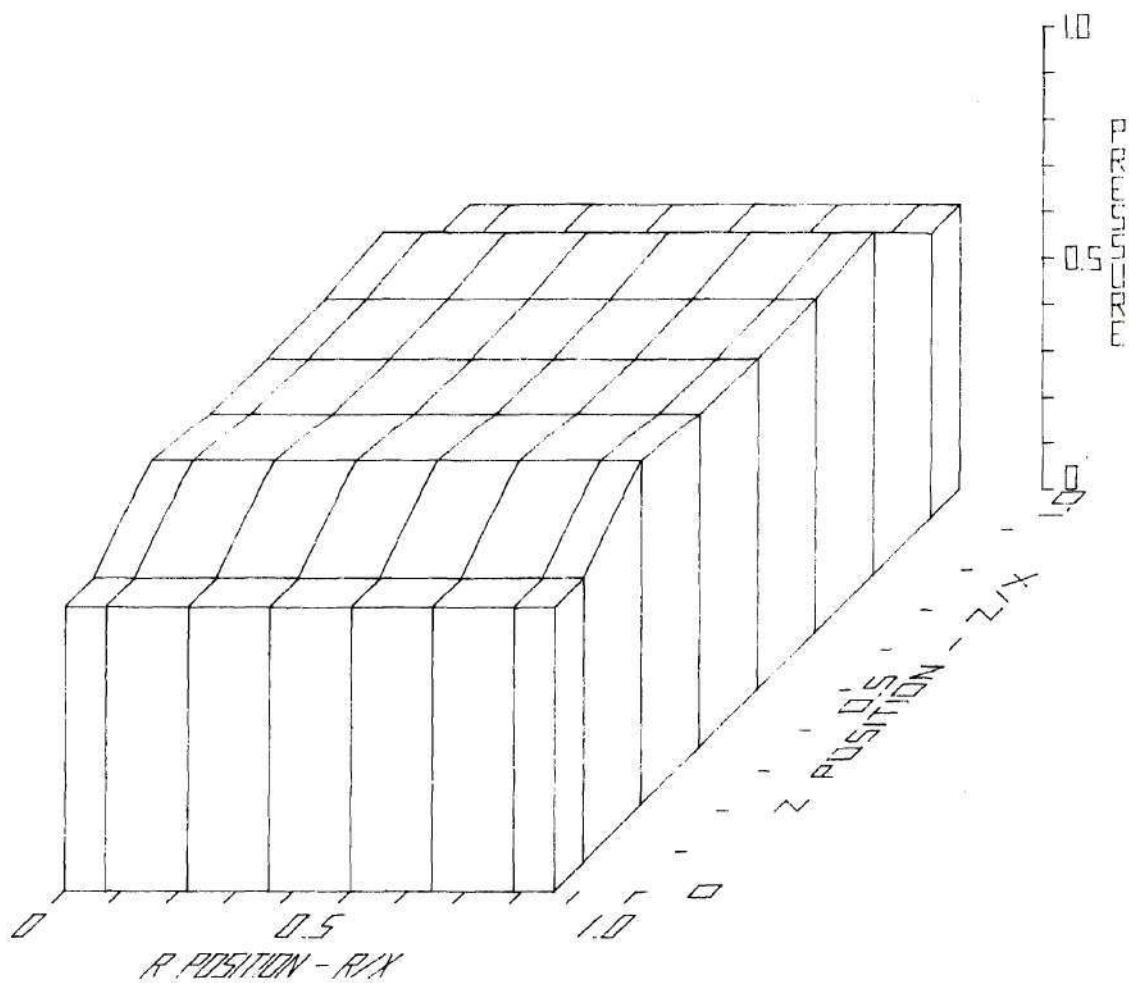

Figure 123: Fission Gas Pressure [T = 2.04889 sec]

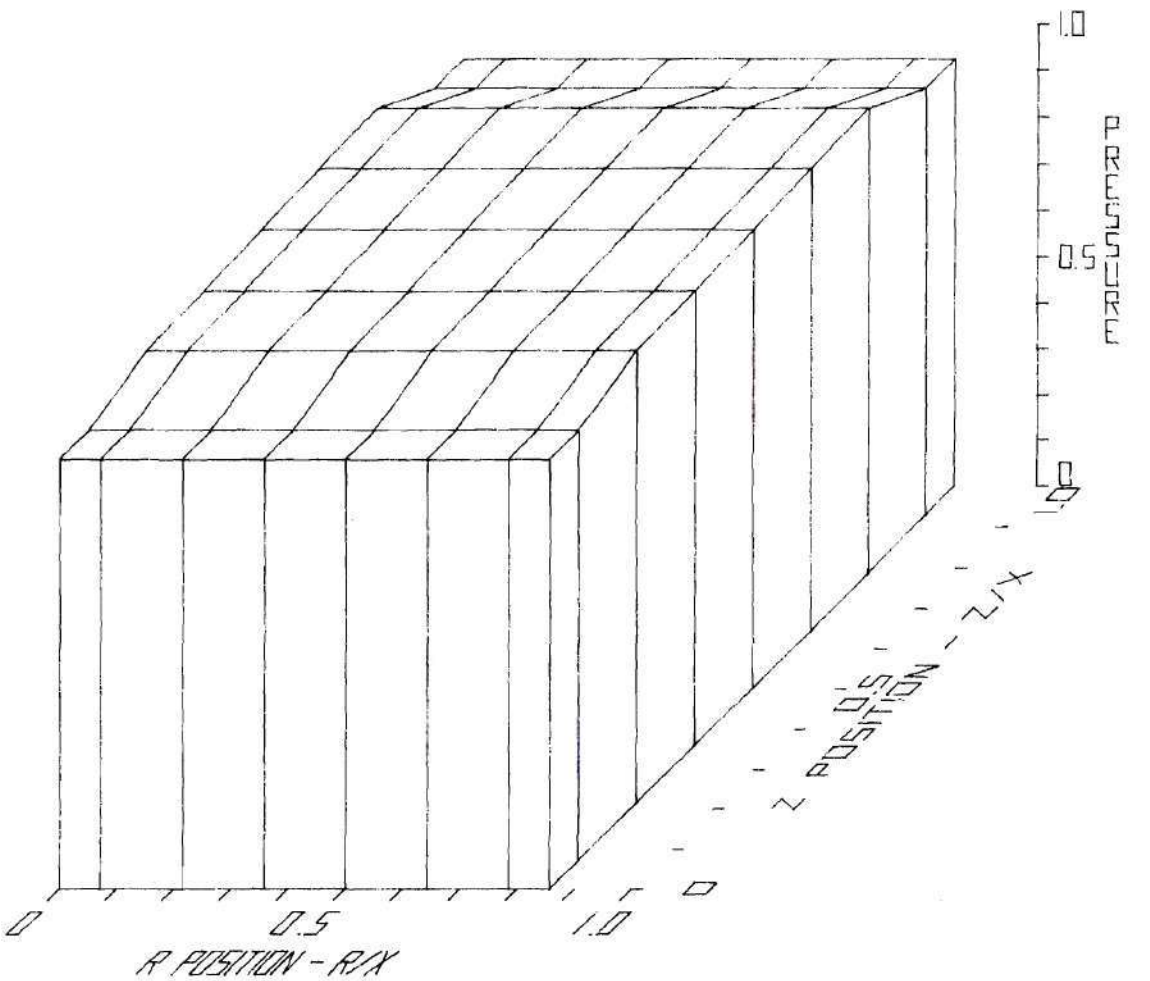

Figure 124: Fission Gas Pressure [T = 2.05204 sec]

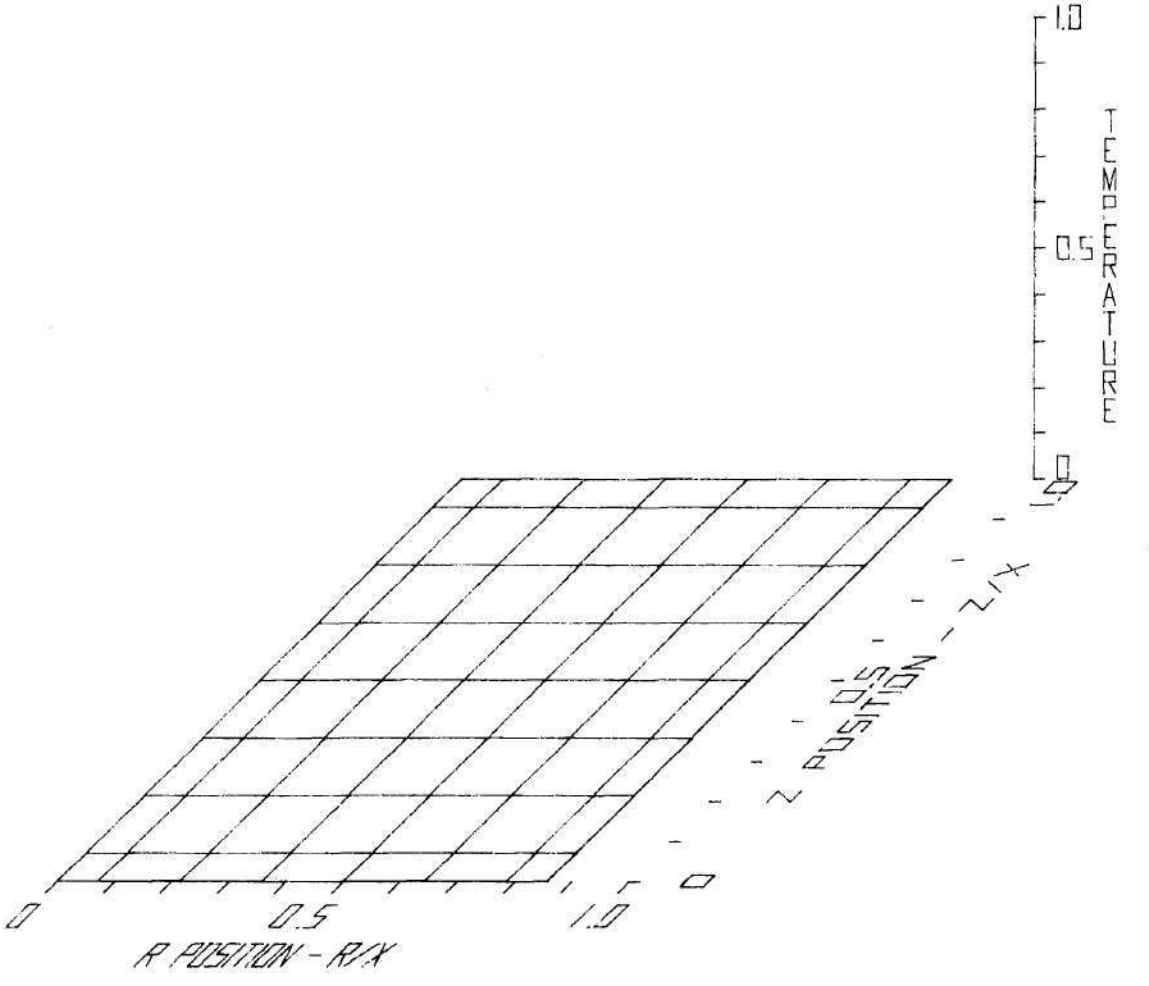

Figure 125: Liquid Fuel Temperature [T = 0.00000 sec]

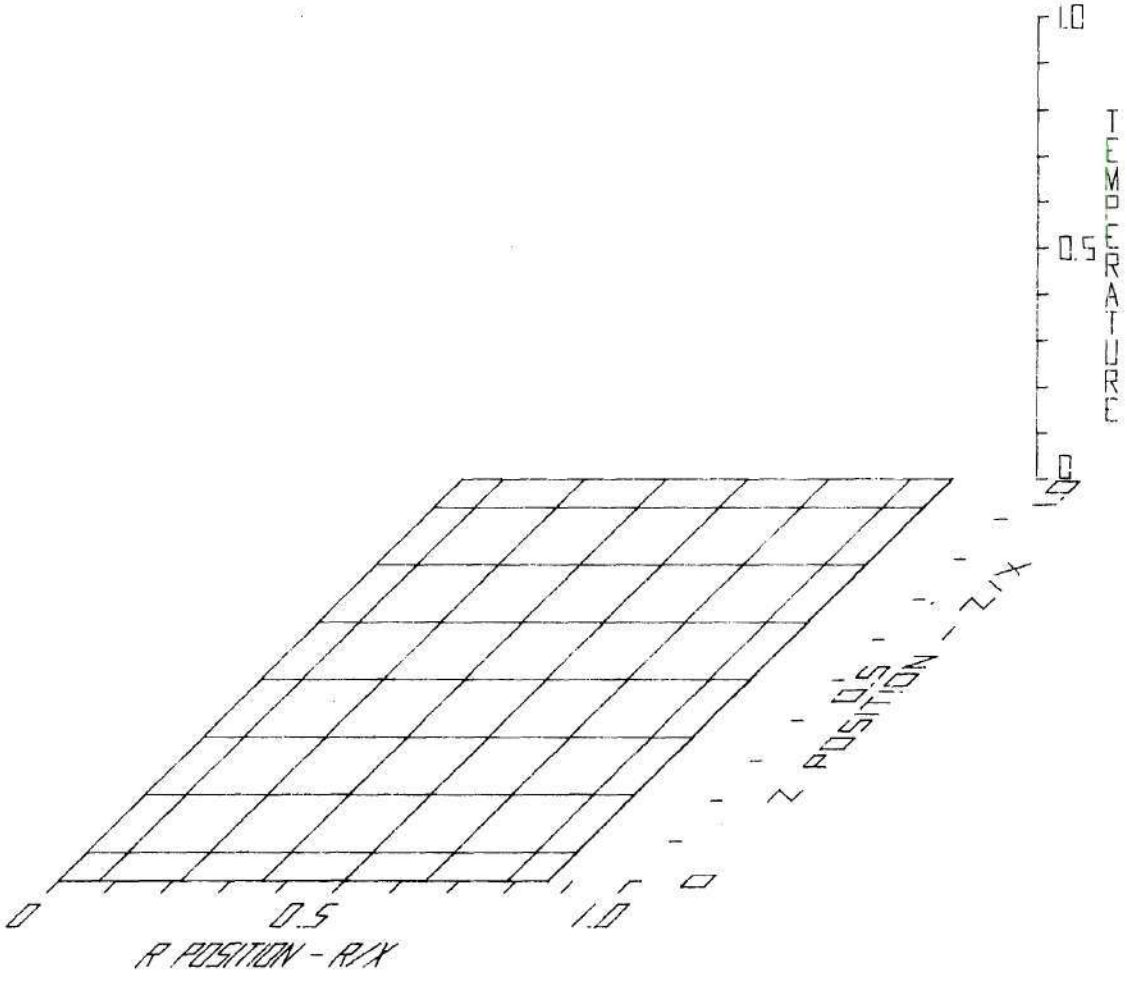

Figure 126: Liquid Fuel Temperature [T = 2.04889 sec]

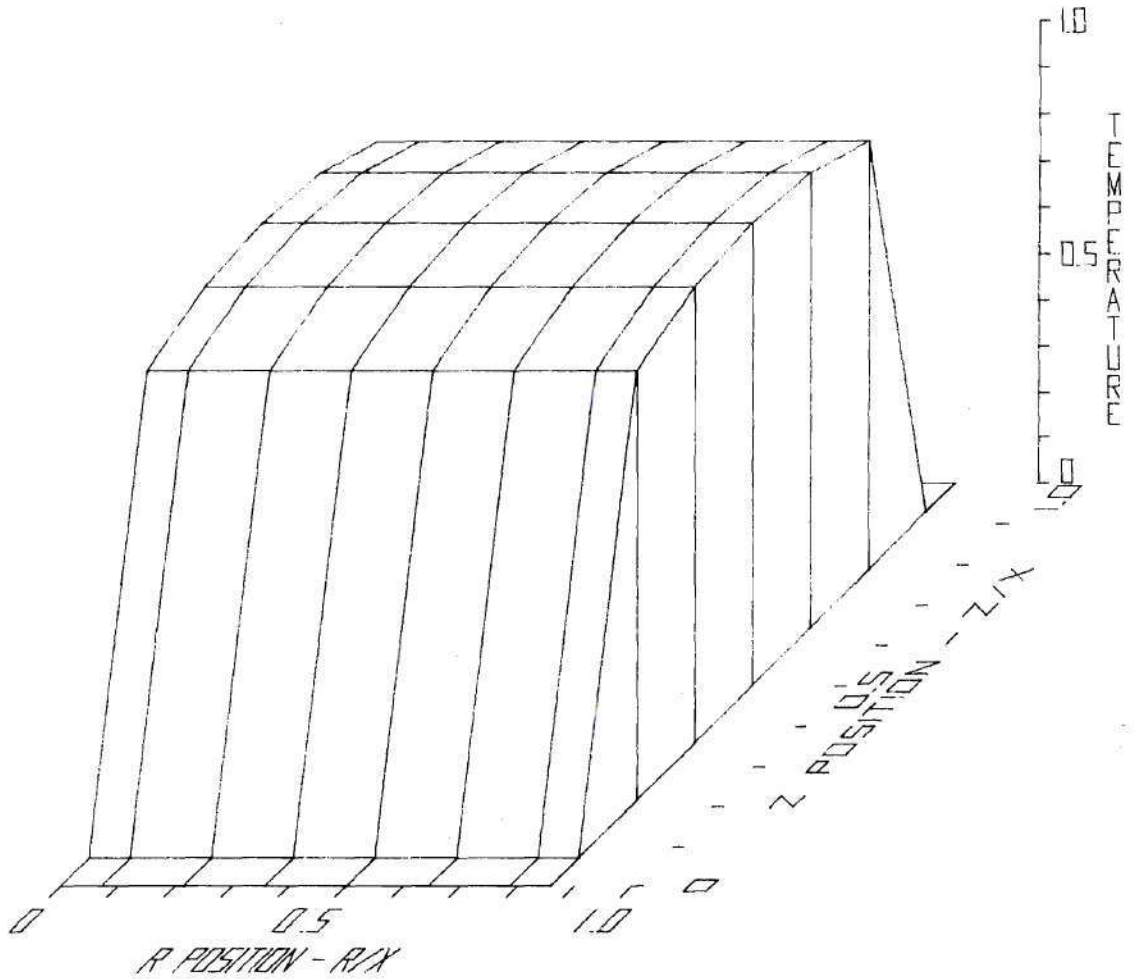

Figure 127: Liquid Fuel Temperature [T = 2.05204 sec]

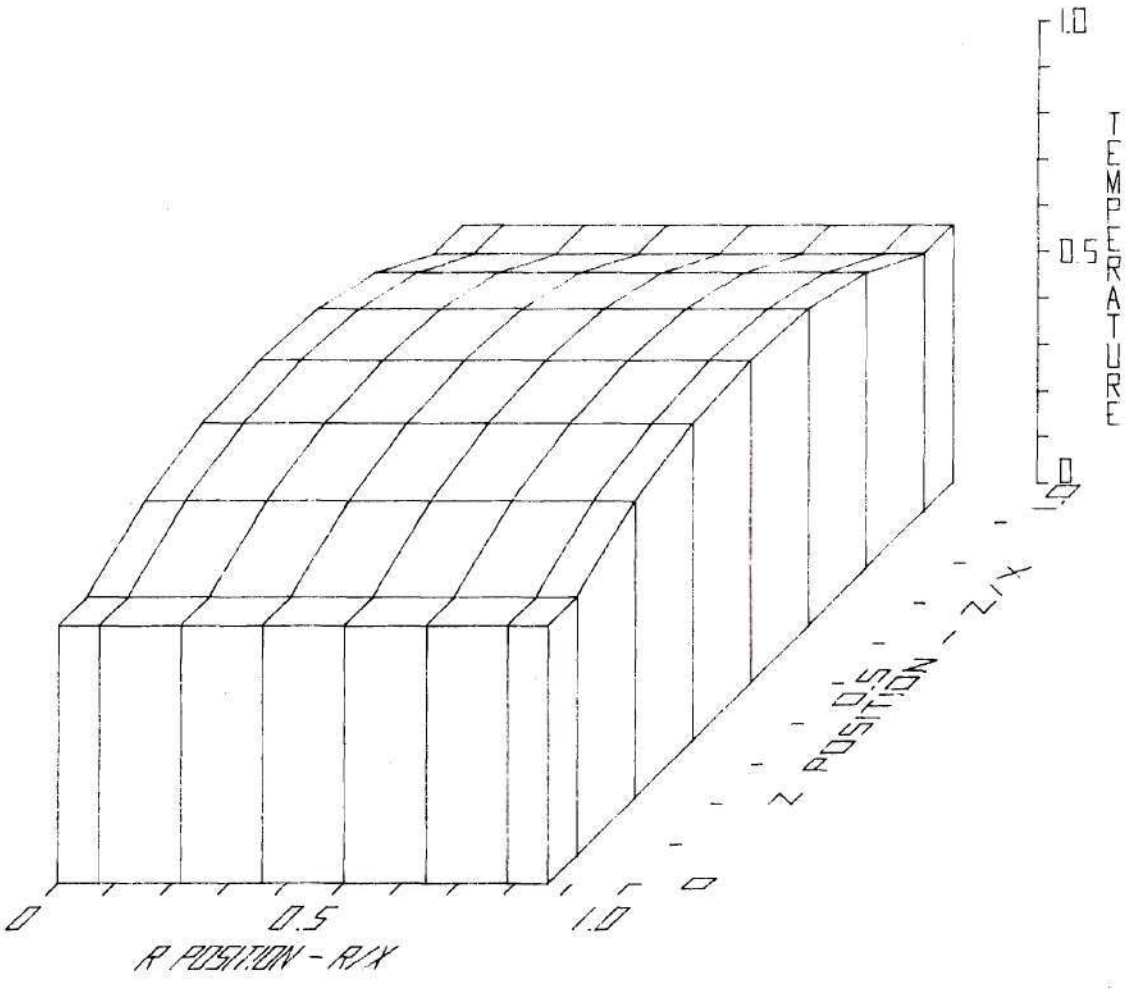

Figure 128: Fission Gas Temperature [T = 0.00000 sec]

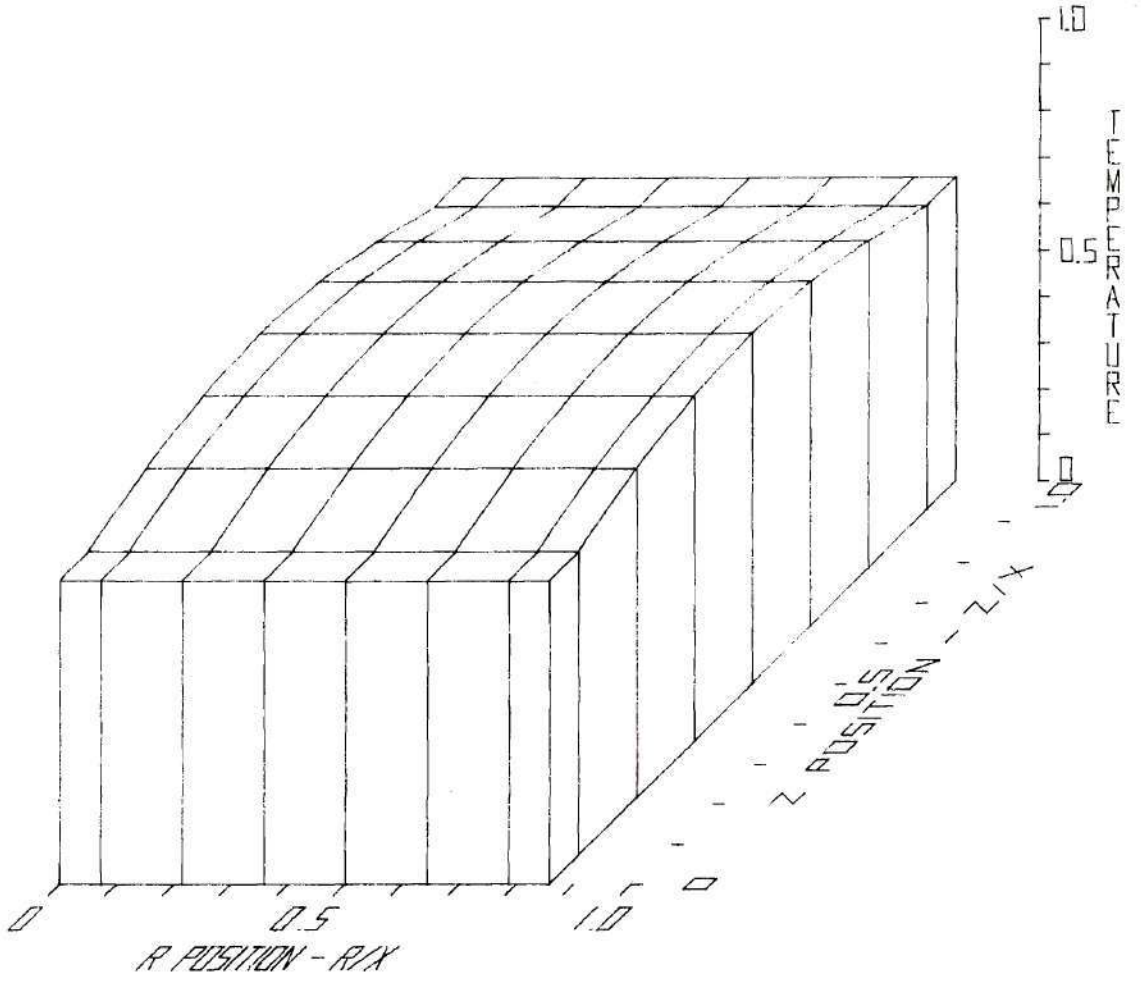

Figure 129: Fission Gas Temperature [T = 2.04889 sec]

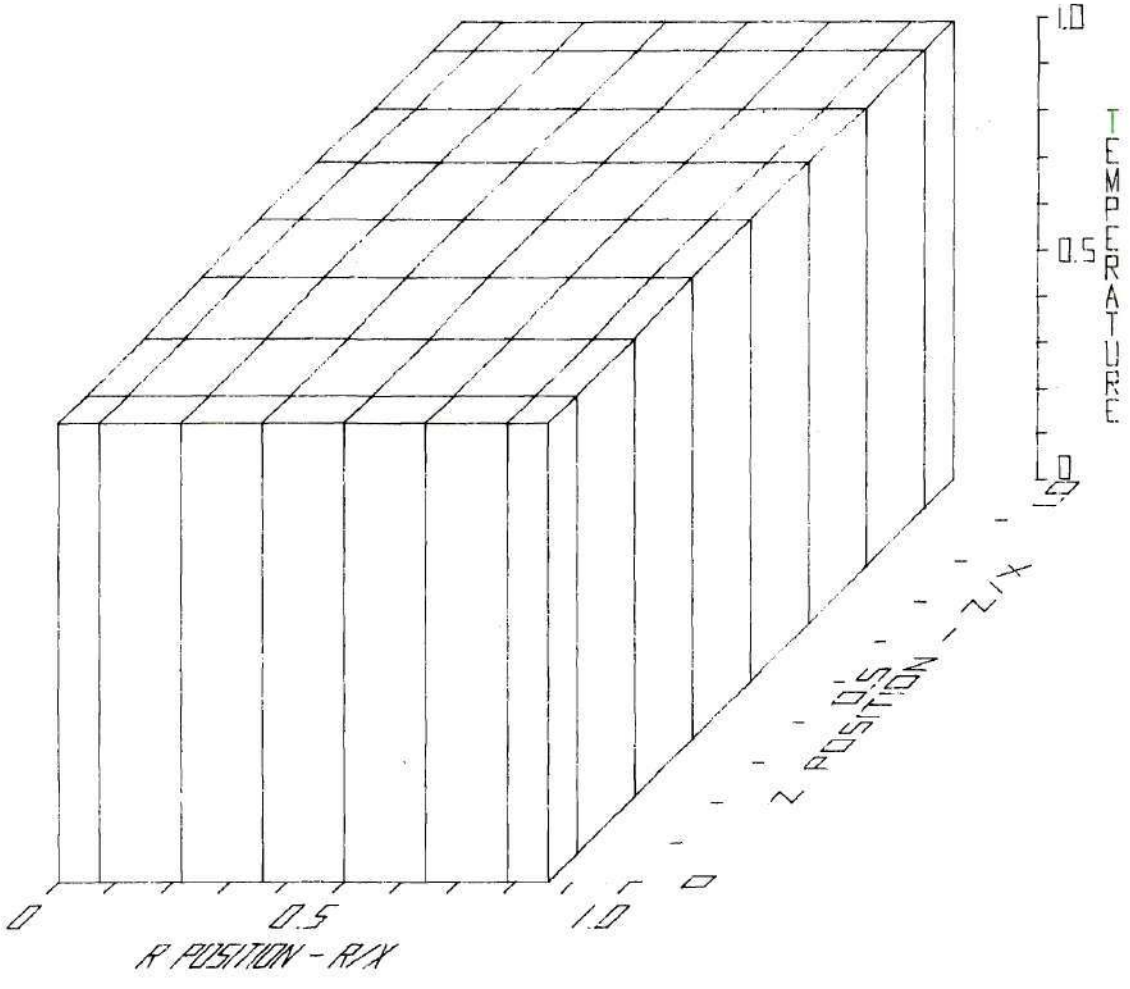

Figure 130: Fission Gas Temperature [T = 2.05204 sec]

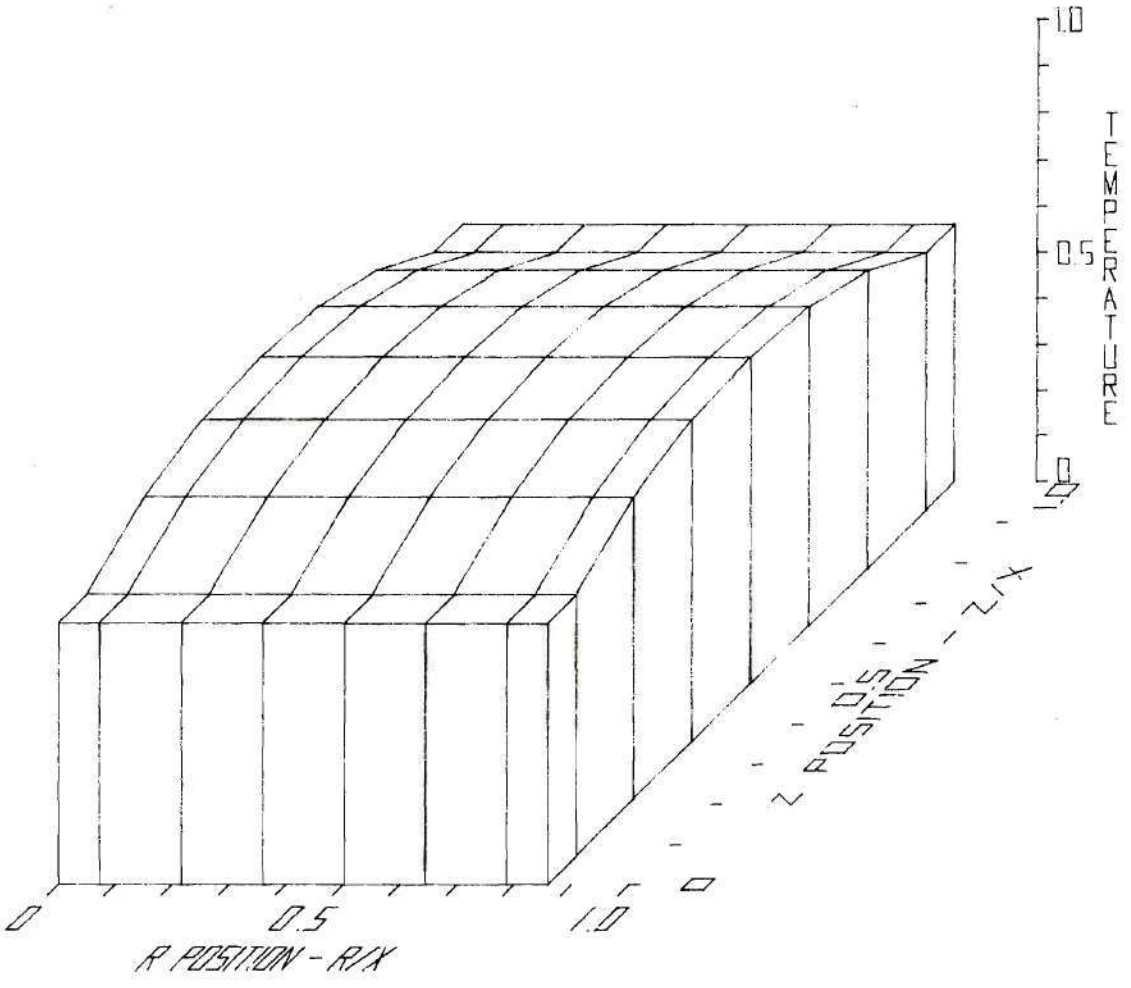

Figure 131: Solid Fuel Temperature [T = 0.00000 sec]

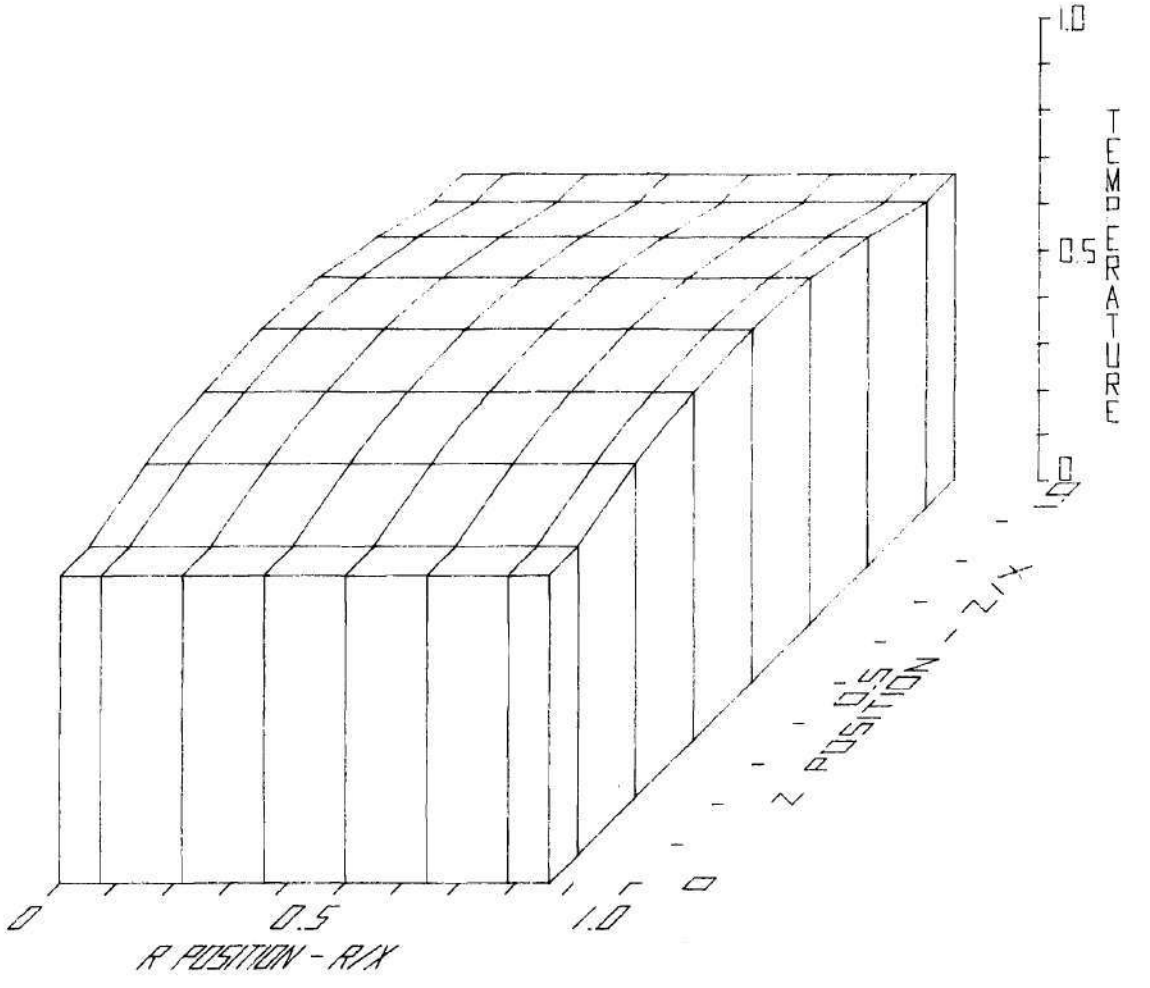

Figure 132: Solid Fuel Temperature [T = 2.04889 sec]

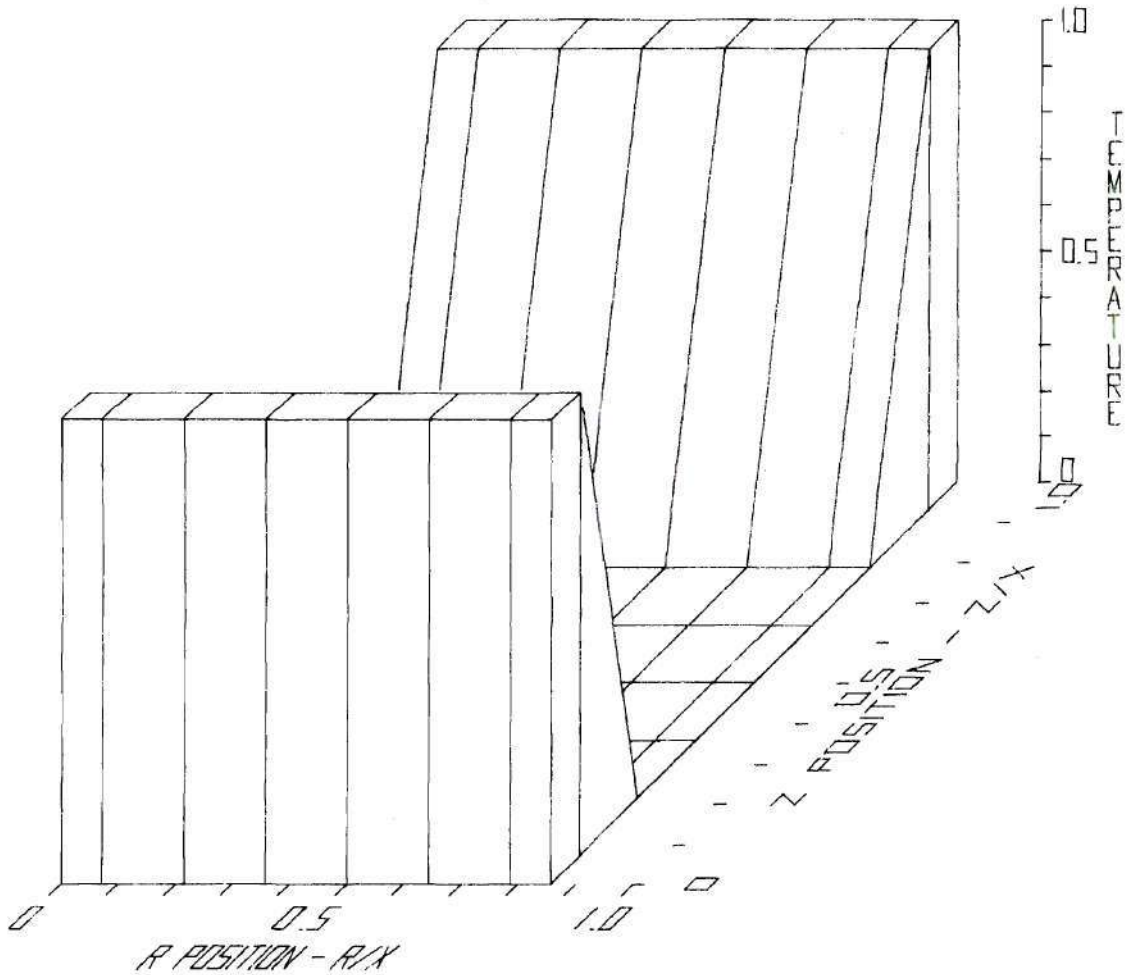

Figure 133: Solid Fuel Temperature [T = 2.05204 sec]

CHAPTER V

CONCLUSIONS AND RECOMMENDATIONS

5.1 Conclusions

Experience with PLOFA indicates that for a wide range of problems a one dimensional approach is inadequate, and the reality of radial non-uniformity becomes a necessity rather than a luxury. Only in simple cases like the slumping of fresh fuel under gravity, with negligible fission gas, no fuel vaporization, and the neglect of simultaneous clad motion, does a single dimension offer acceptable modeling.

In a reactor environment considerable error is introduced at the very onset by averaging data to get a uniform radial distribution. This, in itself, clouds the remainder of the accident analysis. Further, vapors and gases would have distinctly vertical motion only if present in very small quantities and strongly tied to falling liquid. If there is more fission gas present, or any vaporization, the high localized pressures cause significant radial motion.

Unrealistic heat transfer modeling occurs with one dimensional calculations by lumping the radial energy distribution into a constant value. Localized melting or vaporization [such as along the centerline], an extremely common occurrence in an accident situation, cannot be treated with a one dimensional analysis, wiping out accurate modeling of a major segment of safety studies associated with fuel motion.

In the example discussed in Chapter IV, the one dimensional calculations yielded results significantly different from the two dimensional case, and fuel vaporization did not occur. These types of fluid dynamic differences may be expected for a wide range of accident problems. It is the conclusion of this research that in the area of breeder safety analysis, the extra time and money spent in introducing a radial dimension is vitally necessary for adding credibility to the accident modeling.

5.2 Suggested Future Work

PLOFA improves upon previous research not only by the addition of a new dimension, but also by its multi-field approach it permits greater freedom in the treatment of individual materials and avoids the lumping of multiple materials into a single fluid with average properties. Its inclusion in an overall safety analysis code, such as SAS, with linkage between the fluid dynamics and neutronics calculations, would permit improved accident modeling and add its share to LMFBR safety research.

The code has been designed for the easy incorporation of enlargements and modifications, and several areas of accident modeling offer opportunities for this. These include: the addition of liquid and vapor sodium; multi-channel analysis; use of PLOFA to perform whole core analysis in the accident disassembly phase; inclusion of angular non-uniformity. With appropriate changes in material properties, the code can also be applied to other areas of nuclear thermal hydraulic analysis.

Substantial numerical experimentation and refinement can be made in the exchange functions linking the various materials. In addition, the entire numerical scheme can be experimented with to achieve greater

efficiency, particularly in the area of increasing the time steps for vapor field calculations. Methods which could be tried include: a fully implicit treatment[26]; different approaches to pressure changes in the iterative process; modifications of the alternating direction implicit methods[27], where calculations alternate between the two principal directions; modifications of the hopscotch method[28], wherein a centered time differencing is used and calculations alternate for each cell from a one step to a two step method.

APPENDIX A

PRESSURE EQUILIBRATION

The pressure of the n^{th} compressible field is related to its microscopic density and internal energy by an equation of state as

$$p_n = p_n (\rho'_n, I_n),$$

where

$$\rho'_n = \frac{\rho_n}{\alpha_n} .$$

The pressures of the compressible fields need to be equilibrated, keeping ρ_n and I_n constant. This is equivalent to finding a pressure p and solving for a set of α_n which gives the zeros of the functions

$$P_n = p - p_n (\rho'_n, I_n), \qquad (1)$$

subject to the constraint that the sum of the volume fractions of the compressible fields adds up to the total volume fraction, α_o, available to the vapors at the start of the pressure equilibration, i.e.

$$\sum_n \alpha_n = \alpha_o,$$

where the summation is only over all compressible fields.

In Equation (1), p is a function of the set α_n, while p_n is a function of a particular α_n for constant ρ_n and I_n. Thus, the α_n satisfying the zeros of the P_n functions are readily obtained by a Newton iteration of the form

$$\left[\alpha_n\right]^{h+1} = \left[\alpha_n\right]^{h} - \frac{\left[P_n\right]^{h}}{\left[\frac{\partial P_n}{\partial \alpha_N}\right]^{h}}, \qquad (2)$$

where the superscript h indicates the iteration number.

But

$$\frac{\partial P_n}{\partial \alpha_n} = \frac{\partial p}{\partial \alpha_n} - \frac{\partial p_n}{\partial \alpha_n}$$

$$= \frac{\partial p}{\partial \alpha_n} - \frac{\partial p_n}{\partial \rho'_n}\frac{\partial \rho'_n}{\partial \alpha_n}$$

$$= \frac{\partial p}{\partial \alpha_n} + \frac{\rho_n}{\alpha_n^2}\frac{\partial p_n}{\partial \rho'_n}$$

$$= \frac{\partial p}{\partial \alpha_n} + Y_n,$$

where $\frac{\partial p_n}{\partial \rho'_n}$ can be calculated from the equation of state.

Thus Equation (2) becomes

$$\left[\alpha_n\right]^{h+1} = \left[\alpha_n\right]^{h} - \frac{\left[p\right]^{h} - \left[p_n\right]^{h}}{\left[\frac{\partial p}{\partial \alpha_n}\right]^{h} + \left[Y_n\right]^{h}}$$

If there is no change in p between two successive iterations, the corresponding volume fractions satisfy the relation

$$\left[\alpha_n\right]^{h+1} = \left[\alpha_n\right]^h - \frac{\left[p\right]^h - \left[p_n\right]^h}{\left[Y_n\right]^h} \qquad (3)$$

Summing this expression over all the compressible fields yields

$$\sum_n \left[\alpha_n\right]^{h+1} = \sum_n \left[\alpha_n\right]^h - \left[p\right]^h \sum_n \frac{1}{\left[Y_n\right]^h} + \sum_n \left[\frac{p_n}{Y_n}\right]^h \qquad (4)$$

But, $\sum_n \left[\alpha_n\right]^{h+1} = \alpha_o$.

Hence, subtracting equation (5) from (4) gives

$$\left[p\right]^h = \frac{\sum_n \left[\alpha_n\right]^h + \sum_n \left[\frac{p_n}{Y_n}\right]^h}{\sum \frac{1}{\left[Y_n\right]^h}}$$

But this relation was derived for the case of no pressure change between two iterations. Hence

$$\left[p\right]^{h+1} = \frac{\sum_n \left[\alpha_n\right]^h + \sum_n \left[\frac{p_n}{Y_n}\right]^h}{\sum_n \frac{1}{\left[Y_n\right]^h}}$$

Equations (6) and (3) can then be used to achieve pressure equilibration as follows:

(i) Choose a set of α_n

(ii) Calculate the corresponding pressure from Equation (6)

(iii) Plug this pressure back into Equation (3) to get a new set of α_n, use this α_n set to get a new p from Equation (6).

(iv) Repeat step (iii) till Equation (1) yields a set of P_n sufficiently close to zero.

The convergence of this iteration scheme achieves a pressure equilibration among the compressible fields and yields a set of corresponding volume fractions.

APPENDIX B

DERIVATION OF $\frac{\partial \tilde{B}^j}{\partial \tilde{p}_i^j}$

Consider the density transport equation in the form

$$\tilde{B}_i^j = \frac{1}{\delta t}\left[\tilde{\rho}_i^j - \rho_i^j\right] + \frac{1}{r_i\,\delta r}\left[\langle\tilde{\rho}\tilde{u}r\rangle^j_{i+\frac{1}{2}} - \langle\tilde{\rho}\tilde{u}r\rangle^j_{i-\frac{1}{2}}\right]$$

$$+ \frac{1}{\delta z}\left[\langle\tilde{\rho}\tilde{v}\rangle_i^{j+\frac{1}{2}} - \langle\tilde{\rho}\tilde{v}\rangle_i^{j-\frac{1}{2}}\right] - S_i^j \quad . \tag{1}$$

An expression is needed for the change of B with respect to the pressure $\left[\partial\tilde{B}_i^j/\partial\tilde{p}_i^j\right]$. However, since this is merely used in an iterative process to increment the pressure, the exact form of the expression is not important, providing the convergence rate is not significantly retarded. Therefore, the derivative of the density exchange function need not be included since this involves formulae for various types of phase interchanges. Also, one can approximate the convective fluxes with a strictly centered differencing form. Thus,

$$\langle\tilde{\rho}\tilde{u}r\rangle^j_{i+\frac{1}{2}} = \tilde{u}^j_{i+\frac{1}{2}}\, r_{i+\frac{1}{2}}\left[\tilde{\rho}_i^j + \tilde{\rho}_{i+1}^j\right]/2 = r_{i+\frac{1}{2}}\,(\tilde{\rho}\tilde{u})^j_{i+\frac{1}{2}} \quad ,$$

and $\langle\tilde{\rho}\tilde{v}\rangle_i^{j+\frac{1}{2}} = \tilde{v}_i^{j+\frac{1}{2}}\left[\tilde{\rho}_i^j + \tilde{\rho}_i^{j+1}\right]/2 = (\tilde{\rho}\tilde{v})_i^{j+\frac{1}{2}}$.

The pressure derivative of Equation (1) can now be approximated at the point i, j by

$$\frac{\partial \tilde{B}_i^j}{\partial \tilde{p}_i^j} = \frac{\partial}{\partial \tilde{p}_i^j}\left\{\frac{1}{\delta t}\left[\tilde{\rho}_i^j - \rho_i^j\right]\right\} + \frac{1}{r_i\,\delta r}\frac{\partial}{\delta \tilde{p}_i^j}\left[r_{i+\frac{1}{2}}\,(\tilde{\rho}\tilde{u})^j_{i+\frac{1}{2}} - r_{i-\frac{1}{2}}\,(\tilde{\rho}\tilde{u})^j_{i-\frac{1}{2}}\right]$$

$$+ \frac{1}{\delta z}\frac{\partial}{\partial \tilde{p}_i^j}\left[(\tilde{\rho}\tilde{v})_i^{j+\frac{1}{2}} - (\tilde{\rho}\tilde{v})_i^{j-\frac{1}{2}}\right] \quad . \tag{2}$$

Evaluate the derivative of each term individually.

(i) time term

$$\frac{\partial}{\partial p_i^j}\left\{\frac{1}{\delta t}\left[\tilde{\rho}_i^j - \rho_i^j\right]\right\} \approx \frac{\tilde{\alpha}_i^j}{\delta t}\frac{\partial \tilde{\rho}_i^{\prime,j}}{\partial \tilde{p}_i^j}$$

where $\dfrac{\partial \tilde{\rho}_i^{\prime,j}}{\partial \tilde{p}_i^j}$ is got from the equation of state.

(ii) radial convective term

Sutstitute for ρu from the momentum equation. Then,

$$\frac{\partial}{\partial p_i^j}\left[r_{i+\frac{1}{2}}\,(\tilde{\rho}\tilde{u})^j_{i+\frac{1}{2}} - r_{i-\frac{1}{2}}\,(\tilde{\rho}\tilde{u})^j_{i-\frac{1}{2}}\right]$$

$$= r_{i+\frac{1}{2}}\frac{\partial}{\partial \tilde{p}_i^j}\left\{\left(X_r\right)^j_{i+\frac{1}{2}} + D^j_{i+\frac{1}{2}}\,\delta t\left[\tilde{\tilde{u}}^j_{i+\frac{1}{2}} - \tilde{u}^j_{i+\frac{1}{2}}\right]\right.$$

$$+ \tilde{\alpha}^{j}_{i+\frac{1}{2}} \delta t \left[\tilde{p}^{j}_{i} - \tilde{p}^{j}_{i+1}\right]/\delta r \Bigg\}$$

$$- r_{i-\frac{1}{2}} \frac{\partial}{\partial \tilde{p}^{j}_{i}} \Bigg\{ \left(X_r\right)^{j}_{i-\frac{1}{2}} + D^{j}_{i-\frac{1}{2}} \delta t \left[\tilde{\tilde{u}}^{j}_{i-\frac{1}{2}} - \tilde{\tilde{u}}^{j}_{i-\frac{1}{2}} \right]$$

$$+ \tilde{\alpha}^{j}_{i-\frac{1}{2}} \delta t \left[\tilde{p}^{j}_{i-1} - \tilde{\tilde{p}}^{j}_{i}\right]/\delta r \Bigg\}$$

$$\approx \delta t \Bigg\{ - r_{i+\frac{1}{2}} D^{j}_{i+\frac{1}{2}} \frac{\partial \tilde{\tilde{u}}^{j}_{i+\frac{1}{2}}}{\partial \tilde{\tilde{p}}^{j}_{i}} + r_{i-\frac{1}{2}} D^{j}_{i-\frac{1}{2}} \frac{\partial \tilde{\tilde{u}}^{j}_{i-\frac{1}{2}}}{\partial \tilde{\tilde{p}}^{j}_{i}}$$

$$+ \left(r_{i+\frac{1}{2}} \tilde{\alpha}^{j}_{i+\frac{1}{2}} + r_{i-\frac{1}{2}} \tilde{\alpha}^{j}_{i-\frac{1}{2}}\right)/\delta r \Bigg\} \ ,$$

where the calculation has been simplified by not considering the X_r term and the velocity components of the other fields.

(iii) axial convective term

Proceeding in a fashion similar to that for the radial convective term,

$$\frac{\partial}{\partial \tilde{\tilde{p}}^{j}_{i}} \left[\left(\tilde{\rho}\tilde{\tilde{v}}\right)^{j+\frac{1}{2}}_{i} - \left(\tilde{\rho}\tilde{\tilde{v}}\right)^{j-\frac{1}{2}}_{i} \right]$$

$$\approx \delta t \Bigg\{ - D^{j+\frac{1}{2}}_{i} \left(\frac{\partial \tilde{\tilde{v}}^{j+\frac{1}{2}}_{i}}{\partial \tilde{\tilde{p}}^{j}_{i}} \right) + D^{j-\frac{1}{2}}_{i} \left(\frac{\partial \tilde{\tilde{v}}^{j-\frac{1}{2}}_{i}}{\partial \tilde{\tilde{p}}^{j}_{i}} \right)$$

$$+\left(\tilde{\alpha}_i^{j+\frac{1}{2}} + \tilde{\alpha}_i^{j-\frac{1}{2}}\right)/\delta z$$

$$+ g\ \tilde{\alpha}_i^{j+\frac{1}{2}} \frac{\partial \tilde{\rho}'^{\,j+\frac{1}{2}}}{\partial \tilde{p}_i^j} - \tilde{\alpha}_i^{j-\frac{1}{2}} \frac{\partial \tilde{\rho}'^{\,j-\frac{1}{2}}_i}{\partial \tilde{p}_i^j} \Bigg] \Bigg\} .$$

The insertion of these three terms in Equation (2) yields an expression for $\frac{\partial \tilde{B}_i^j}{\partial \tilde{p}_i^j}$ as

$$\frac{\partial \tilde{B}_i^j}{\partial \tilde{p}_i^j} = \frac{\tilde{\alpha}_i^j}{\delta t} \frac{\partial \tilde{\rho}'^{\,j}_i}{\partial \tilde{p}_i^j} + g \frac{\delta t}{\delta z} \left[\tilde{\alpha}_i^{j+\frac{1}{2}} \frac{\partial \tilde{\rho}'^{\,j+\frac{1}{2}}_i}{\partial \tilde{p}_i^j} - \tilde{\alpha}_i^{j-\frac{1}{2}} \frac{\partial \tilde{\rho}'^{\,j-\frac{1}{2}}_i}{\partial \tilde{p}_i^j} \right]$$

$$+ \frac{\delta t}{r_i \delta r} \left\{ - r_{i+\frac{1}{2}} D^j_{i+\frac{1}{2}} \left(\frac{\partial \tilde{u}^j_{i+\frac{1}{2}}}{\partial \tilde{p}_i^j} \right) + r_{i-\frac{1}{2}} D^j_{i-\frac{1}{2}} \left(\frac{\partial \tilde{u}^j_{i-\frac{1}{2}}}{\partial \tilde{p}_i^j} \right) \right.$$

$$+ \left(r_{i+\frac{1}{2}} \tilde{\alpha}^j_{i+\frac{1}{2}} + r_{i-\frac{1}{2}} \tilde{\alpha}^j_{i-\frac{1}{2}} \right)/\delta r$$

$$+ \frac{\delta t}{\delta z} \left\{ \left(\tilde{\alpha}_i^{j+\frac{1}{2}} + \tilde{\alpha}_i^{j-\frac{1}{2}} \right)/\delta z \right.$$

$$+ D_i^{j-\frac{1}{2}} \left(\frac{\partial \tilde{v}_i}{\partial \tilde{p}_i^j} \right)^{j-\frac{1}{2}} - D_i^{j+\frac{1}{2}} \left(\frac{\partial \tilde{v}_i}{\partial \tilde{p}_i^j} \right)^{j+\frac{1}{2}} \Bigg\} \quad , \tag{3}$$

where the density derivatives are obtained from the equation of state for each field.

Expressions are required for the various velocity derivatives. These are obtained by simple manipulation of the momentum equations. Consider, for example, the radial momentum equation

$$(\tilde{\rho}\tilde{u})^j_{i+\frac{1}{2}} = (X_r)^j_{i+\frac{1}{2}} + D^j_{i+\frac{1}{2}} \delta t \left[\tilde{\tilde{u}}^j_{i+\frac{1}{2}} - \tilde{u}^j_{i+\frac{1}{2}} \right]$$

$$- \tilde{\alpha}^j_{i+\frac{1}{2}} \delta t \left[\tilde{p}^j_{i+1} - \tilde{p}^j_i \right] / \delta r.$$

Differentiating with respect to pressure yields

$$\tilde{\alpha}^j_{i+\frac{1}{2}} \tilde{u}^j_{i+\frac{1}{2}} \frac{\partial \tilde{\rho}'^j_{i+\frac{1}{2}}}{\partial \tilde{p}^j_i} + \rho^j_{i+\frac{1}{2}} \frac{\partial \tilde{u}^j_{i+\frac{1}{2}}}{\partial p^j_i}$$

$$= - D^j_{i+\frac{1}{2}} \delta t \frac{\partial \tilde{u}^j_{i+\frac{1}{2}}}{\partial \tilde{p}^j_i}$$

$$+ \tilde{\alpha}^j_{i+\frac{1}{2}} \frac{\delta t}{\delta r} \quad ,$$

omitting the terms due to X_r and the velocity components of other fields.

This equation can be rearranged to give

$$\frac{\partial \tilde{u}^{j}_{i+\frac{1}{2}}}{\partial \tilde{p}^{j}_{i}} = \left\{ \tilde{\alpha}^{j}_{i+\frac{1}{2}} \left(\frac{\delta t}{\delta r}\right) - \tilde{\alpha}^{j}_{i+\frac{1}{2}} \tilde{u}^{j}_{i+\frac{1}{2}} \frac{\partial \tilde{\rho}'^{j}_{i+\frac{1}{2}}}{\partial \tilde{p}^{j}_{i}} \right\} \Bigg/ \left\{ \tilde{\rho}^{j}_{i+\frac{1}{2}} + D^{j}_{i+\frac{1}{2}} \delta t \right\} \quad . \quad (4)$$

Proceeding in a similar fashion, we get

$$\frac{\partial \tilde{u}^{j}_{i-\frac{1}{2}}}{\partial \tilde{p}^{j}_{i}} = \left\{ - \tilde{\alpha}^{j}_{i-\frac{1}{2}} \left(\frac{\delta t}{\delta r}\right) - \tilde{\alpha}^{j}_{i-\frac{1}{2}} \tilde{u}^{j}_{i-\frac{1}{2}} \frac{\partial \tilde{\rho}'^{j}_{i-\frac{1}{2}}}{\partial \tilde{p}^{j}_{i}} \right\} \Bigg/ \left\{ \tilde{\rho}^{j}_{i-\frac{1}{2}} + D^{j}_{i-\frac{1}{2}} \delta t \right\} \quad (5)$$

$$\frac{\partial \tilde{v}^{j+\frac{1}{2}}_{i}}{\partial \tilde{p}^{j}_{i}} = \frac{\tilde{\alpha}^{j+\frac{1}{2}}_{i} \left(\frac{\delta t}{\delta z}\right) - \tilde{\alpha}^{j+\frac{1}{2}}_{i} \tilde{v}^{j+\frac{1}{2}}_{i} \frac{\partial \tilde{\rho}'^{j+\frac{1}{2}}_{i}}{\partial \tilde{p}^{j}_{i}} + g\, \delta t\, \tilde{\alpha}^{j+\frac{1}{2}}_{i} \frac{\partial \tilde{\rho}'^{j+\frac{1}{2}}_{i}}{\partial \tilde{p}^{j}_{i}}}{\tilde{\rho}^{j+\frac{1}{2}}_{i} + D^{j+\frac{1}{2}}_{i} \delta t} \quad (6)$$

$$\frac{\partial \tilde{v}^{j+\frac{1}{2}}_{i}}{\partial \tilde{p}^{j}_{i}} = \frac{- \tilde{\alpha}^{j-\frac{1}{2}}_{i} \left(\frac{\delta t}{\delta z}\right) - \tilde{\alpha}^{j-\frac{1}{2}}_{i} \tilde{v}^{j-\frac{1}{2}}_{i} \frac{\partial \tilde{\rho}'^{j-\frac{1}{2}}_{i}}{\partial p^{j}_{i}} + g\, \delta t\, \tilde{\alpha}^{j-\frac{1}{2}}_{i} \frac{\partial \tilde{\rho}'^{j-\frac{1}{2}}_{i}}{\partial \tilde{p}^{j}_{i}}}{\tilde{\rho}^{j-\frac{1}{2}}_{i} + D^{j-\frac{1}{2}}_{i} \delta t} \quad (7)$$

It may be noted here that Equation (5) cannot be obtained from Equation (4) by a mere change of index; similarly with Equations (6) and (7).

Equations (3) through (7) provide the necessary expressions for evaluating $\frac{\partial \tilde{B}_i^j}{\partial \tilde{p}_i^j}$. The derivation involves quantities evaluated at their latest known values between time step n and n + 1. However, since this derivative is used only in the iteration process and can be simplified to any suitable form that does not significantly retard the convergence rate, it might be computationally advisable to evaluate the derivative only once at the beginning of each time step.

APPENDIX C

STABILITY ANALYSIS

The truncation error technique requires that the coefficients of dissusion-like terms be positive for stability. These terms are obtained as follows:

(1) Expand each term in the finite difference equation by taking the product of the Taylor Series (in both time and space) of its individual components,

(2) Substitute the expansions in the finite difference equation to get an interim modified equation containing the original differential equation and higher order truncation errors.

(3) Get rid of higher order time terms by repeated use of the interim modified equation.

(4) Derive a final modified equation by keeping only the terms of the original differential equation and diffusion-like truncation errors, omitting all other higher order truncation errors.

Details of the application of this procedure to the finite difference equations for density, momentum and energy transport are presented here.

A. Density Transport Equation

The differential equation for density transport is

$$\frac{\partial \rho}{\partial t} + \frac{1}{r}\frac{\partial}{\partial r}(\rho u r) + \frac{\partial}{\partial z}(\rho v) = S, \qquad (1)$$

where

ρ = macroscopic density

$= \alpha\rho'$

ρ' = microscopic density

α = volume fraction of a field

u = radial component of velocity

v = axial component of velocity

S = density source function.

This differential equation can be replaced by a finite difference approximation which is first order accurate in time, and second order in space. Thus, for cell i, j

$$\frac{1}{\delta t}\left[{}^{n+1}\rho_i^j - {}^{n}\rho_i^j\right] + \frac{1}{r_i \delta r}\left[{}^{n+1}\langle \rho u r\rangle_{i+e}^{j} - {}^{n+1}\langle \rho u r\rangle_{i-e}^{j}\right]$$

$$+ \frac{1}{\delta z}\left[{}^{n+1}\langle \rho v\rangle_{i}^{j+e} - {}^{n+1}\langle \rho v\rangle_{i}^{j-e}\right] = {}^{n}S_i^j, \qquad (2)$$

where

i = radial coordinate index

j = axial coordinate index

n = time step index

δt = time step

e = 1/2.

Each term in Equation (2) needs to be expanded in a Taylor Series about some fixed reference point, the most convenient in this case being the point i,j at time step n+1. Consider each term individually.

(1) time term

$$\frac{1}{\delta t}\left[{}^{n+1}\rho_i^j - {}^{n}\rho_i^j\right]$$

This involves the two Taylor Series:

$${}^{n+1}\rho_i^j = \rho$$

$${}^{n}\rho_i^j = \rho - \delta t\,\frac{\delta\rho}{\partial t} + \frac{(\delta t)^2}{2}\,\frac{\partial^2\rho}{\partial t^2} + O(\delta t^3).$$

Hence, the time term reduces to

$$\frac{1}{\delta t}\left[{}^{n+1}\rho_i^j - {}^{n}\rho_i^j\right] = \frac{\partial\rho}{\partial t} - \frac{\delta t}{2}\,\frac{\partial^2\rho}{\partial t^2}\,. \qquad (3)$$

(2) radial convective term

$$\frac{1}{r_i\delta r}\left[{}^{n+1}\langle\rho ur\rangle_{i+e}^{j} - {}^{n+1}\langle\rho ur\rangle_{i-e}^{j}\right]$$

where

$${}^{n+1}\langle\rho ur\rangle_{i+e}^{j} = {}^{n+1}u_{i+e}^{j}\; r_{i+e}\left[(1/2 + \xi_1)^{n+1}\rho_i^j + (1/2 - \xi_1)^{n+1}\rho_{i+1}^j\right]$$

$${}^{n+1}\langle\rho ur\rangle_{i-e}^{j} = {}^{n+1}u_{i-e}^{j}\; r_{i-e}\left[(1/2 + \xi_2)^{n+1}\rho_{i-1}^j + (1/2 - \xi_2)^{n+1}\rho_i^j\right]$$

$$\xi_1 = \beta_0\,\frac{\delta t}{\delta r}\;{}^{n+1}u_{i+e}^{j} + \theta_0\;\mathrm{sign}\left({}^{n+1}u_{i+e}^{j}\right)$$

$$\xi_2 = \left(\beta_0 \frac{\delta t}{\delta r}\right)^{n+1} u^j_{i-e} + \theta_0 \ \text{sign}\left(^{n+1}u^j_{i-e}\right).$$

Thus,

$$\frac{1}{r_i \delta r}\left[^{n+1}\langle \rho u r\rangle^j_{i+e} - {}^{n+1}\langle \rho u r\rangle^j_{i-e}\right]$$

$$= \frac{1}{r_i \delta r}\left\{\frac{1}{2}\ (A_1+A_2-A_3-A_4) + \xi_1\ (A_1-A_2) - \xi_2\ (A_3-A_4)\right\}, \qquad (4)$$

where

$$A_1 = \left(r_i + \frac{\delta r}{2}\right)^{n+1}(u^j_{i+e}\ \rho^j_i)$$

$$A_2 = \left(r_i + \frac{\delta r}{2}\right)^{n+1}(u^j_{i+e}\ \rho^j_{i+1})$$

$$A_3 = \left(r_i - \frac{\delta r}{2}\right)^{n+1}(u^j_{i-e}\ \rho^j_{i-1})$$

$$A_4 = \left(r_i - \frac{\delta r}{2}\right)^{n+1}(u^j_{i-e}\ \rho^j_i)\ .$$

Equation (4) involves the Taylor Series:

$$^{n+1}\rho^j_{i\pm1} = \rho \pm \delta r \frac{\partial \rho}{\partial r} + \frac{(\delta r)^2}{2}\frac{\partial^2 \rho}{\partial r^2} \pm \frac{(\delta r)^3}{6}\frac{\partial^3 \rho}{\partial r^3} + O(\delta r^4)$$

$$^{n+1}u^j_{i\pm e} = u \pm \frac{\delta r}{2}\frac{\partial u}{\partial r} + \frac{(\delta r)^2}{8}\frac{\partial^2 u}{r^2} \pm \frac{(\delta r)^3}{48}\frac{\partial^3 u}{\partial r^3} + O(\delta r^4)\ .$$

The expansion of Equation (4) then yields, after omitting derivative products higher than third order,

$$\frac{1}{r_i \delta r}\left[{}^{n+1}\langle \rho u r\rangle_{i+e}^{j} - {}^{n+1}\langle \rho u r\rangle_{i-e}^{j}\right] = \frac{1}{r}\frac{\partial}{\partial r}(\rho u r) - D_1 - E_1 - \frac{\delta r}{2}(\xi_1 + \xi_2)\frac{\partial u}{\partial r}\frac{\partial \rho}{\partial r} - (\xi_1 - \xi_2)\, u \frac{\partial \rho}{\partial r}, \qquad (5)$$

where

$$D_1 = \left[\frac{(\delta r)^2}{4}(\xi_1 - \xi_2 - 1)\frac{\partial u}{\partial r} + \frac{\delta r}{2}(\xi_1 + \xi_2)u\right]\frac{\partial^2 \rho}{\partial r^2} + \left[\frac{(\delta r)^2}{4}(\xi_1 - \xi_2 - 1)\frac{\partial u}{\partial r} + \frac{\delta r}{2}(\xi_1 + \xi_2)u\right]\frac{1}{r}\frac{\partial \rho}{\partial r},$$

$$E_1 = \frac{-(\delta r)^2}{24}\left\{\left[\rho\frac{\partial^3 u}{\partial r^3} + 3\frac{\partial \rho}{\partial r}\frac{\partial^2 u}{\partial r^2} + 4u\frac{\partial^3 \rho}{\partial r^3}\right] + \frac{1}{r}\left[3\rho\frac{\partial^2 u}{\partial r^2} + 6u\frac{\partial^2 \rho}{\partial r^2}\right]\right\}$$
$$+ \frac{(\delta r)^2}{24}\left\{(\xi_1 + \xi_2)\frac{1}{r}\left[\frac{3}{2}\delta r\frac{\partial \rho}{\partial r}\frac{\partial^2 u}{\partial r^2} + 3\frac{\partial u}{\partial r}\frac{\partial^2 \rho}{\partial r^2} + 2u\frac{\partial^3 \rho}{\partial r^3}\right]\right.$$
$$\left. + (\xi_1 - \xi_2)\left[3\frac{\partial^2 u}{\partial r^2}\frac{\partial \rho}{\partial r} + 4u\frac{\partial^3 \rho}{\partial r^3} + \frac{1}{r}\left(6u\frac{\partial^2 \rho}{\partial r^2} + 2u\frac{\partial^3 \rho}{\partial r^3}\right)\right]\right\}.$$

(3) <u>axial convective term</u>

$$\frac{1}{\delta z}\left[{}^{n+1}\langle \rho v\rangle_{i}^{j+e} - {}^{n+1}\langle \rho v\rangle_{i}^{j-e}\right]$$

where

$$ {}^{n+1}\langle \rho v \rangle_i^{j+e} = {}^{n+1}v_e^{j+e} \left[(1/2+\xi_3)\ {}^{n+1}\rho_i^{j} + (1/2-\xi_3)\ {}^{n+1}\rho_i^{j+1} \right] $$

$$ {}^{n+1}\langle \rho v \rangle_i^{j-e} = {}^{n+1}v_i^{j-e} \left[(1/2+\xi_4)\ {}^{n+1}\rho_i^{j-1} + (1/2-\xi_4)\ {}^{n+1}\rho_i^{j} \right] $$

$$ \xi_3 = \left(\beta_0 \frac{\delta t}{\delta z} \right) {}^{n+1}v_i^{j+e} + \theta_0\ \text{sign}({}^{n+1}v_i^{j+e}) $$

$$ \xi_4 = \left(\beta_0 \frac{\delta t}{\delta z} \right) {}^{n+1}v_i^{j-e} + \theta_0\ \text{sign}({}^{n+1}v_i^{j-e}) . $$

Thus,

$$ \frac{1}{\delta z} \left[{}^{n+1}\langle \rho v \rangle_i^{j+e} - {}^{n+1}\langle \rho v \rangle_i^{j-e} \right] $$

$$ = \frac{1}{\delta z} \left\{ \frac{1}{2} (A_5+A_6-A_7-A_8) + \xi_3 (A_5-A_6) - \xi_4 (A_7-A_8) \right\} , \qquad (6) $$

where

$$ A_5 = {}^{n+1}(v_i^{j+e}\ \rho_i^{j}) $$

$$ A_6 = {}^{n+1}(v_i^{j+e}\ \rho_i^{j+1}) $$

$$ A_7 = {}^{n+1}(v_i^{j-e}\ \rho_i^{j-1}) $$

$$ A_8 = {}^{n+1}(v_i^{j-e}\ \rho_i^{j}) . $$

Equation (6) involves the Taylor Series:

$$ {}^{n+1}\rho_i^{j\pm1} = \rho \pm \delta z \frac{\partial \rho}{\partial z} + \frac{(\delta z)^2}{2} \frac{\partial^2 \rho}{\partial z^2} \pm \frac{(\delta z)^3}{6} \frac{\partial^3 \rho}{\partial z^3} + O(\delta z^4) $$

$$ {}^{n+1}v_i^{j\pm1/2} = v \pm \frac{\delta z}{2} \frac{\partial v}{\partial z} + \frac{(\delta z)^2}{8} \frac{\partial^2 v}{\partial z^2} \pm \frac{(\delta z)^3}{48} \frac{\partial^3 v}{\partial z^3} + O(\delta z^4) \ . $$

The expansion of Equation (6) then yields, after omitting derivative products higher than third order,

$$ \frac{1}{\delta z} \left[{}^{n+1}\langle \rho v \rangle_i^{j+e} - {}^{n+1}\langle \rho v \rangle_i^{j-e} \right] $$

$$ = \frac{\partial}{\partial z}(\rho v) - D_2 - E_2 - \frac{\delta z}{2}(\xi_3+\xi_4) \frac{\partial v}{\partial z} \frac{\partial \rho}{\partial z} - (\xi_3-\xi_4)\, v \frac{\partial \rho}{\partial z} \ , \qquad (7) $$

where

$$ D_2 = \left[\frac{(\delta z)^2}{4} (\xi_3-\xi_4-1) \frac{\partial v}{\partial z} + \frac{\delta z}{2} (\xi_3+\xi_4)\, v \right] \frac{\partial^2 \rho}{\partial z^2} \ , $$

$$ E_2 = \frac{-(\delta z)^2}{24} \left[\rho \frac{\partial^3 v}{\partial z^3} + 3 \frac{\partial \rho}{\partial z} \frac{\partial^2 v}{\partial z^2} + 4v \frac{\partial^3 \rho}{\partial z^3} \right] + \frac{(\delta z)^2}{24} (\xi_3-\xi_4) \left[3 \frac{\partial^2 v}{\partial z^2} \frac{\partial \rho}{\partial z} + 4v \frac{\partial^3 \rho}{\partial z^3} \right] \ . $$

(4) source term

The source term can be expanded about the point i,j at time step n+1 as

$$ {}^{n}S_i^j = S - \delta t \frac{\partial S}{\partial t} + \frac{(\delta t)^2}{2} \frac{\partial^2 S}{\partial t^2} + O(\delta t^3) \ . \qquad (8) $$

Various expressions for the source term are listed in Chapter II. Basically, it is a function of pressure and temperature, and hence, of density. The time derivatives then become

$$\frac{\partial S}{\partial t} = \frac{\partial S}{\partial \rho} \frac{\partial \rho}{\partial t}$$

$$\frac{\partial}{\partial t}\left(\frac{\partial S}{\partial t}\right) = \frac{\partial S}{\partial \rho} \frac{\partial^2 \rho}{\partial t^2} + \frac{\partial \rho}{\partial t} \frac{\partial}{\partial t}\left(\frac{\partial S}{\partial \rho}\right) .$$

The insertion of these expressions in Equation (8) yields

$$^{n}S_i^j = S - \delta t \frac{\partial S}{\partial \rho} \frac{\partial \rho}{\partial t} + \frac{(\delta t)^2}{2}\left[\frac{\partial S}{\partial \rho} \frac{\partial^2 \rho}{\partial t^2} + \frac{\partial \rho}{\partial t} \frac{\partial}{\partial t}\left(\frac{\partial S}{\partial \rho}\right)\right] . \qquad (9)$$

Substitute Equations (3), (5), (7) and (9) back into Equation (2) to get the modified equation

$$\frac{\partial \rho}{\partial t} + \frac{1}{r} \frac{\partial}{\partial r} (\rho u r) + \frac{\partial}{\partial z} (\rho v) - S = \frac{\delta t}{2} \frac{\partial^2 \rho}{\partial t^2} - \delta t \frac{\partial S}{\partial \rho} \frac{\partial \rho}{\partial t} + \frac{(\delta t)^2}{2}\left[\frac{\partial S}{\partial \rho} \frac{\partial^2 \rho}{\partial t^2}\right.$$

$$\left. + \frac{\partial \rho}{\partial t} \frac{\partial}{\partial t}\left(\frac{\partial S}{\partial \rho}\right)\right] + D_1 + D_2 + E_1 + E_2 + (\xi_1 - \xi_2)\, u \frac{\partial \rho}{\partial r} + (\xi_3 - \xi_4)\, v \frac{\partial \rho}{\partial z}$$

$$+ \frac{\delta r}{2} (\xi_1 + \xi_2) \frac{\partial u}{\partial r} \frac{\partial \rho}{\partial r} + \frac{\delta z}{2} (\xi_3 + \xi_4) \frac{\partial v}{\partial z} \frac{\partial \rho}{\partial z} . \qquad (10)$$

The second order time derivatives in Equation (10) need to be evaluated. This can be done by operating on Equation (10) with $\frac{\delta t}{2} \frac{\partial}{\partial t}$ and adding the result to Equation (10) to get

$$\frac{\partial \rho}{\partial t} + \frac{1}{r} \frac{\partial}{\partial r} (\rho u r) + \frac{\partial}{\partial z} (\rho v) - S = D_1 + D_2 + E_1 + E_2 + T + (\xi_1 - \xi_2)\, u \frac{\partial \rho}{\partial r}$$

$$+ (\xi_3 - \xi_4)\, v \frac{\partial \rho}{\partial z} + \frac{\partial r}{2} (\xi_1 + \xi_2) \frac{\partial u}{\partial r} \frac{\partial \rho}{\partial r} + \frac{\delta z}{2} (\xi_3 + \xi_4) \frac{\partial v}{\partial z} \frac{\partial \rho}{\partial z} , \qquad (11)$$

where

$$T = \frac{\delta t}{2}\left\{-\frac{\partial S}{\partial \rho}\frac{\partial \rho}{\partial t} - \frac{1}{r}\frac{\partial}{\partial r}\left(r\,\frac{\partial \rho u}{\partial t}\right) - \frac{\partial}{\partial z}\left(\frac{\partial \rho v}{\partial t}\right) + (\xi_1-\xi_2)\,u\,\frac{\partial}{\partial r}\left(\frac{\partial \rho}{\partial t}\right)\right.$$

$$\left. + (\xi_3-\xi_4)\,v\,\frac{\partial}{\partial z}\left(\frac{\partial \rho}{\partial t}\right) + (\xi_1-\xi_2)\,\frac{\partial u}{\partial t}\frac{\partial \rho}{\partial r} + (\xi_3-\xi_4)\,\frac{\partial v}{\partial t}\frac{\partial \rho}{\partial z}\right. ,$$

retaining time derivatives or mixed time and space derivatives no higher than the second order.

The momentum time derivatives can be substituted from the momentum transport equations, while the density time derivatives are substituted from Equation (11). Carrying out the differentiations involved in the T expression, one finally gets

$$T = \frac{\delta t}{2}\left\{u^2 + \frac{\partial p}{\partial \rho'} + \left(\frac{\xi_1-\xi_2}{1+\delta t\,\frac{\partial S}{\partial \rho}}\right)\left[(\xi_1-\xi_2-1)\,u^2 + (\xi_1+\xi_2)\,\frac{\delta r}{2}\,u\,\frac{\partial u}{\partial r}\right]\right\}\frac{\partial^2 \rho}{\partial r^2}$$

$$+ \frac{\delta t}{2}\left\{u^2 - \left(\frac{\xi_1-\xi_2}{1+\delta t\,\frac{\partial S}{\partial \rho}}\right)u^2 + \frac{\partial p}{\partial \rho'}\right\}\frac{1}{r}\frac{\partial \rho}{\partial r}$$

$$+ \frac{\delta t}{2}\left\{v^2 + \frac{\partial p}{\partial \rho'} + \left(\frac{\xi_3-\xi_4}{1+\delta t\,\frac{\partial S}{\partial \rho}}\right)\left[(\xi_3-\xi_4-1)\,v^2 + (\xi_3+\xi_4)\,\frac{\delta z}{2}\,v\,\frac{\partial v}{\partial z}\right]\right\}\frac{\partial^2 \rho}{\partial z^2} ,$$

retaining only diffusion-like terms in ρ.

Substitute this expression for T into Equation (11), and retain only the original differential equation terms and diffusion-like terms in ρ. Then, the final modified equation for the density transport equation takes the form

$$\frac{\partial \rho}{\partial t} + \frac{1}{r}\frac{\partial}{\partial r}(\rho u r) + \frac{\partial}{\partial z}(\rho v) = S$$

$$+\left\{\frac{\delta t}{2}\left(u^2 + \frac{\partial p}{\partial \rho'}\right) + \frac{\delta t}{2}\left(\frac{\xi_1 - \xi_2}{1+\delta t \frac{\partial S}{\partial \rho}}\right)\left[(\xi_1 - \xi_2 - 1)\, u^2 + (\xi_1 + \xi_2)\frac{\delta r}{2} u \frac{\partial u}{\partial r}\right]\right.$$

$$\left. + (\xi_1 - \xi_2 - 1)\frac{(\delta r)^2}{4}\frac{\partial u}{\partial r} + \frac{\delta r}{2}(\xi_1 + \xi_2)\, u\right\}\frac{\partial^2 \rho}{\partial r^2}$$

$$+\left\{\frac{\delta t}{2}\left[u^2 - \left(\frac{\xi_1 - \xi_2}{1+\delta t \frac{\partial S}{\partial \rho}}\right)u^2 + \frac{\partial p}{\partial \rho'}\right] + (\xi_1 - \xi_2 - 1)\frac{(\delta r)^2}{4}\frac{\partial u}{\partial r} + \frac{\delta r}{2}(\xi_1 + \xi_2)\, u\right\}\frac{1}{r}\frac{\partial \rho}{\partial r}$$

$$+\left\{\frac{\delta t}{2}\left(v^2 + \frac{\partial p}{\partial \rho'}\right) + \frac{\delta t}{2}\left(\frac{\xi_3 - \xi_4}{1+\delta t \frac{\partial S}{\partial \rho}}\right)\left[(\xi_3 - \xi_4 - 1)\, v^2 + (\xi_3 + \xi_4)\frac{\delta z}{2} v \frac{\partial v}{\partial z}\right]\right.$$

$$\left. + (\xi_3 - \xi_4 - 1)\frac{(\delta z)^2}{4}\frac{\partial v}{\partial z} + \frac{\delta z}{2}(\xi_3 + \xi_4)\, v\right\}\frac{\partial^2 \rho}{\partial z^2}\,.$$

Stability criteria call for positive coefficients for the diffusion-like terms, i.e. the coefficients of $\frac{\partial^2 \rho}{\partial r^2}$, $\frac{1}{r}\frac{\partial \rho}{\partial r}$, and $\frac{\partial^2 \rho}{\partial z^2}$.

B. Momentum Transport Equation

(1) radial direction momentum equation

The differential equation for radial momentum transport is

$$\frac{\partial \rho u}{\partial t} + \frac{1}{r}\frac{\partial}{\partial r}(\rho u u r) + \frac{\partial}{\partial z}(\rho u v) = N_r - \alpha \frac{\partial p}{\partial r} + D(\bar{u} - u) + V_r\,, \qquad (12)$$

where

N_r = radial component of momentum source function

p = pressure

D = drag term

$\bar{u}$ = representative radial velocity component for other fields.

The radial component of the viscous term, denoted by V_r, is

$$V_r = \frac{4}{3}\mu\left(\frac{\partial^2 u}{\partial r^2} + \frac{1}{r}\frac{\partial u}{\partial r}\right) + \mu\frac{\partial^2 u}{\partial z^2} + \frac{2}{3}\frac{1}{r}\left[\mu\frac{\partial v}{\partial z} - u\frac{\partial \mu}{\partial r} - 2\frac{\mu u}{r}\right]$$

$$+ \frac{4}{3}\frac{\partial \mu}{\partial r}\frac{\partial u}{\partial r} + \frac{\partial \mu}{\partial z}\frac{\partial u}{\partial z} - \frac{1}{r}\frac{\partial}{\partial r}\left(\frac{2}{3}\mu r\frac{\partial v}{\partial z}\right) + \frac{\partial}{\partial z}\left(\mu\frac{\partial v}{\partial r}\right).$$

Differential Equation (12) can be approximated at the point $i + \frac{1}{2}$, j by

$$\frac{1}{\delta t}\left[{}^{n+1}(\rho u)^j_{i+e} - {}^{n}(\rho u)^j_{i+e}\right] + \frac{1}{r_{i+e}\delta r}\left[{}^{n}\langle\rho uur\rangle^j_{i+1} - {}^{n}\langle\rho uur\rangle^j_{i}\right]$$

$$+ \frac{1}{\delta z}\left[{}^{n}\langle\rho uv\rangle^{j+e}_{i+e} - {}^{n}\langle\rho uv\rangle^{j-e}_{i+e}\right]$$

$$= {}^{n}(N_r)^j_{i+e} - {}^{n+1}\alpha^j_{i+e}\left[{}^{n+1}p^j_{i+1} - {}^{n+1}p^j_i\right]/\delta r$$

$$+ {}^{n}D^j_{i+e}\left[{}^{n+1}\bar{u}^j_{i+e} - {}^{n+1}u^j_{i+e}\right] + {}^{n}(V_r)^j_{i+e}\ . \qquad (13)$$

Each term in Equation (13) needs to be expanded in a Taylor Series about some fixed reference, the most convenient in this case being the point $i + \frac{1}{2}$, j at time step n. Using the difference approximations for the various terms as in Chapter III, and proceeding on the same principles as the density transport equation, one can finally arrive at a modified equation for radial momentum transport as

$$\frac{\partial \rho u}{\partial t} + \frac{1}{r}\frac{\partial}{\partial r}(\rho uur) + \frac{\partial}{\partial z}(\rho uv) = N_r - \alpha\frac{\partial p}{\partial r} + D(\bar{u}-u)$$

$$+\left\{\frac{2}{3r}\left[\mu\frac{\partial v}{\partial z} - u\frac{\partial \mu}{\partial r} - 2\frac{\mu u}{r}\right] + \frac{4}{3}\frac{\partial \mu}{\partial r}\frac{\partial u}{\partial r} + \frac{\partial \mu}{\partial z}\frac{\partial u}{\partial z} - \frac{2}{3r}\frac{\partial}{\partial r}\left(\mu r\frac{\partial v}{\partial z}\right) + \frac{\partial}{\partial z}\left(\mu\frac{\partial v}{\partial r}\right)\right\}$$

$$+\left\{\frac{\delta t}{2}\left(\frac{\rho}{\rho+D\delta t}\right)(1-\xi_1+\xi_2)\left[\delta t Du^2 + (\xi_1-\xi_2-1)\rho u^2\right.\right.$$

$$\left.\left. + (\xi_1+\xi_2)\frac{\delta r}{2}\left(3u^2\frac{\partial \rho}{\partial r} + \rho u\frac{\partial u}{\partial r}\right)\right] + \frac{\delta t}{2}\rho\frac{\partial p}{\partial \rho'} + \frac{4}{3}\mu\right.$$

$$\left. + (\delta r)^2(\xi_1-\xi_2-1)\left[\frac{3}{4}u\frac{\partial \rho}{\partial r} + \frac{1}{2}\rho\frac{\partial u}{\partial r}\right] + \frac{\delta r}{2}(\xi_1+\xi_2)\rho u\right\}\frac{\partial^2 u}{\partial r^2}$$

$$+\left\{\frac{\delta t}{2}\left(\frac{\rho}{\rho+D\delta t}\right)\left[\delta t Du^2 + (\xi_1-\xi_2-1)\rho u^2 + (\xi_1+\xi_2)\frac{\delta r}{2}\left(3u^2\frac{\partial \rho}{\partial r} + \rho u\frac{\partial u}{\partial r}\right)\right]\right.$$

$$\left. + \frac{\delta t}{2}\rho\frac{\partial p}{\partial \rho'} + \frac{4}{3}\mu + (\delta r)^2(\xi_1-\xi_2-1)\left[\frac{3}{4}u\frac{\partial \rho}{\partial r} + \frac{1}{4}\rho\frac{\partial u}{\partial r}\right]\right.$$

$$\left. + \frac{\delta r}{2}(\xi_1+\xi_2)\rho u\right\}\frac{1}{r}\frac{\partial u}{\partial r}$$

$$+\left\{\frac{\delta t}{2}\left(\frac{\rho}{\rho+D\delta t}\right)(1-\xi_3+\xi_4)\left[(\xi_3-\xi_4-1)\rho v^2 + (\xi_3+\xi_4)\frac{\delta z}{2}\left(2v^2\frac{\partial \rho}{\partial z} + \rho v\frac{\partial v}{\partial z}\right)\right]\right.$$

$$\left. + \mu + (\delta z)^2(\xi_3-\xi_4-1)\left[\frac{1}{2}v\frac{\partial \rho}{\partial z} + \frac{1}{4}\rho\frac{\partial v}{\partial z}\right] + \frac{\delta z}{2}(\xi_3+\xi_4)\rho v\right\}\frac{\partial^2 u}{\partial z^2}\,. \qquad (14)$$

where

$$\xi_1 = \left(\beta_0\frac{\delta t}{\delta r}\right){}^n u_{i+1}^j + \theta_0\,\mathrm{sign}\left({}^n u_{i+1}^j\right)$$

$$\xi_2 = \left(\beta_0\frac{\delta t}{\delta r}\right){}^n u_{i}^j + \theta_0\,\mathrm{sign}\left({}^n u_{i}^j\right)$$

$$\xi_3 = \left(\beta_0\frac{\delta t}{\delta z}\right){}^n v_{i+e}^{j+e} + \theta_0\,\mathrm{sign}\left({}^n v_{i+e}^{j+e}\right)$$

$$\xi_4 = \left(\beta_0\frac{\delta t}{\delta z}\right){}^n v_{i+e}^{j-e} + \theta_0\,\mathrm{sign}\left({}^n v_{i+e}^{j-e}\right)\,.$$

Equation (14) neglects diffusion terms, which have as coefficients the gradients of the viscosity coefficient, since these are small compared to the other terms. Stability criteria call for positive coefficients for the diffusion-like terms, i.e. the coefficients of $\frac{\partial^2 u}{\partial r^2}$, $\frac{1}{r}\frac{\partial u}{\partial r}$ and $\frac{\partial^2 u}{\partial z^2}$. Only u diffusion has been considered here, since the density derivatives on the left hand side of Equation (14) can be removed using the density transport equation.

(2) axial direction momentum equation

The differential equation for axial momentum transport is

$$\frac{\partial \rho v}{\partial t} + \frac{1}{r}\frac{\partial}{\partial r}(\rho uvr) + \frac{\partial}{\partial z}(\rho vv) = N_z - \alpha\frac{\partial p}{\partial z} + D(\bar{v}-v) + V_z + \rho g \ , \quad (15)$$

where

N_z = axial component of momentum source function

$\bar{v}$ = representative axial velocity component for other fields.

The axial component of the viscous term, denoted by V_z, is

$$V_z = \mu\left(\frac{\partial^2 v}{\partial r^2} + \frac{1}{r}\frac{\partial v}{\partial r}\right) + \frac{4}{3}\mu\frac{\partial^2 v}{\partial z^2} + \frac{\partial \mu}{\partial r}\frac{\partial v}{\partial r} + \frac{4}{3}\frac{\partial \mu}{\partial z}\frac{\partial v}{\partial z}$$

$$+ \frac{1}{r}\left[\frac{\partial}{\partial r}\left(r\mu\frac{\partial u}{\partial z}\right) - \frac{2}{3}\frac{\partial}{\partial z}\left(\mu\frac{\partial}{\partial r}(ur)\right)\right] .$$

Differential Equation (15) can be approximated at the point $i,j+\frac{1}{2}$ by

$$\frac{1}{\delta t}\left[{}^{n+1}(\rho v)_i^{j+e} - {}^{n}(\rho v)_i^{j+e}\right] + \frac{1}{r_i \delta r}\left[{}^{n}\langle \rho uvr\rangle_{i+e}^{j+e} - {}^{n}\langle \rho uvr\rangle_{i-e}^{j+e}\right]$$

$$+\frac{1}{\delta z}\left[{}^{n}\langle\rho vv\rangle_i^{j+1} - {}^{n}\langle\rho vv\rangle_i^{j}\right] = {}^{n}(N_z)^{j+e} - {}^{n+1}\alpha_i^{j+e}\left[{}^{n+1}p_i^{j+1} - {}^{n+1}p_i^{j}\right]/\delta z$$

$$+ {}^{n}D_i^{j+e}\left[{}^{n+1}\bar{v}_i^{j+e} - {}^{n+1}v_i^{j+e}\right] + {}^{n}(V_z)_i^{j+e} + {}^{n+1}\rho_i^{j+e}\, g \,. \qquad (16)$$

Each term in Equation (16) needs to be expanded in a Taylor Series about some fixed reference, the most convenient in this case being the point $i,j+\frac{1}{2}$ at time step n. Using the difference approximations for the various terms as in Chapter III, and proceeding on the same principles as the density transport equation, one can finally arrive at a modified equation for axial momentum transport as

$$\frac{\partial \rho v}{\partial t} + \frac{1}{r}\frac{\partial}{\partial r}(\rho uvr) + \frac{\partial}{\partial z}(\rho vv) = N_z - \alpha\frac{\partial p}{\partial z} + D(\bar{v}-v) + \rho g$$

$$+\left\{\frac{\partial \mu}{\partial r}\frac{\partial v}{\partial r} + \frac{4}{3}\frac{\partial \mu}{\partial z}\frac{\partial v}{\partial z} + \frac{1}{r}\left[\frac{\partial}{\partial r}\left(r\mu\frac{\partial u}{\partial z}\right) - \frac{2}{3}\frac{\partial}{\partial z}\left(\mu\frac{\partial}{\partial r}(ur)\right)\right]\right\}$$

$$+\left\{\frac{\delta t}{2}\left(\frac{\rho}{\rho+D\delta t}\right)(1-\xi_1+\xi_2)\left[(\xi_1-\xi_2-1)\,\rho u^2 + (\xi_1+\xi_2)\frac{\delta r}{2}\left(2u^2\frac{\partial \rho}{\partial r} + \rho u\frac{\partial u}{\partial r}\right)\right]\right.$$

$$\left. + \mu + (\delta r)^2(\xi_1-\xi_2-1)\left(\frac{1}{2}u\frac{\partial \rho}{\partial r} + \frac{1}{4}\rho\frac{\partial u}{\partial r}\right) + \frac{\delta r}{2}(\xi_1+\xi_2)\rho u\right\}\frac{\partial^2 v}{\partial r^2}$$

$$+\left\{\frac{\delta t}{2}\left(\frac{\rho}{\rho+D\delta t}\right)\left[(\xi_1-\xi_2-1)\,\rho u^2 + (\xi_1+\xi_2)\frac{\delta r}{2}\left(2u^2\frac{\partial \rho}{\partial r} + \rho u\frac{\partial u}{\partial r}\right)\right]\right.$$

$$\left. + \mu + (\delta r)^2(\xi_1-\xi_2-1)\left(\frac{1}{2}u\frac{\partial \rho}{\partial r} + \frac{1}{4}\rho\frac{\partial u}{\partial r}\right) + \frac{\delta r}{2}(\xi_1+\xi_2)\rho u\right\}\frac{1}{r}\frac{\partial v}{\partial r}$$

$$+\left\{\frac{\delta t}{2}\left(\frac{\rho}{\rho+D\delta t}\right)(1-\xi_3+\xi_4)\left[(Dv^2-\rho gv)\,\delta t + (\xi_3-\xi_4-1)\,\rho v^2\right.\right.$$

$$+ (\xi_3+\xi_4)\ \frac{\delta z}{2}\left(3v^2\ \frac{\partial \rho}{\partial z} + \rho v\ \frac{\partial v}{\partial z}\right)\Bigg] + \frac{\delta t}{2}\ \rho\ \frac{\partial p}{\partial \rho'} + \frac{4}{3}\ \mu$$

$$+ (\delta z)^2\ (\xi_3-\xi_4-1)\left(\frac{3}{4}\ v\ \frac{\partial \rho}{\partial z} + \frac{1}{2}\ \rho\ \frac{\partial v}{\partial z}\right) + \frac{\delta z}{2}\ (\xi_3+\xi_4)\ \rho v\Bigg\}\ \frac{\partial^2 v}{\partial z^2}\ , \quad (17)$$

where

$$\xi_1 = \left(\beta_0\ \frac{\delta t}{\delta r}\right)\ {}^n u_{i+e}^{j+e} + \theta_0\ \text{sign}\left({}^n u_{i+e}^{j+e}\right)$$

$$\xi_2 = \left(\beta_0\ \frac{\delta t}{\delta r}\right)\ {}^n u_{i-e}^{j+e} + \theta_0\ \text{sign}\left({}^n u_{i-e}^{j+e}\right)$$

$$\xi_3 = \left(\beta_0\ \frac{\delta t}{\delta z}\right)\ {}^n v_{i}^{j+1} + \theta_0\ \text{sign}\left({}^n v_{i}^{j+1}\right)$$

$$\xi_4 = \left(\beta_0\ \frac{\delta t}{\delta z}\right)\ {}^n v_{i}^{j} + \theta_0\ \text{sign}\left({}^n v_{i}^{j}\right)\ .$$

Equation (17) neglects diffusion terms, which have as coefficients the gradients of the viscosity coefficient, since these are small compared to other terms. Stability criteria call for positive coefficients for the diffusion-like terms, i.e. the coefficients of $\frac{\partial^2 v}{\partial r^2}$, $\frac{1}{r}\frac{\partial v}{\partial r}$ and $\frac{\partial^2 v}{\partial z^2}$. Only v diffusion has been considered here, since the density derivatives on the left hand side of Equation (17) can be removed using the density transport equation.

C. Internal Energy Transport Equation

The differential equation for the transport of specific internal energy is

$$\frac{\partial \rho I}{\partial t} + \frac{1}{r}\frac{\partial}{\partial r}\ (\rho u I r) + \frac{\partial}{\partial z}\ (\rho v I) = -\ \frac{p}{r}\frac{\partial}{\partial r}\ (\alpha u r) - p\ \frac{\partial}{\partial z}\ (\alpha v) + Q$$

$$+ H\ (\bar{T}-T) + \frac{1}{r}\frac{\partial}{\partial r}\left(rk\alpha\ \frac{\partial T}{\partial r}\right) + \frac{\partial}{\partial z}\left(k\alpha\ \frac{\partial T}{\partial z}\right) + \mu\Phi + \Lambda\ , \quad (18)$$

where

Q = internal energy source function

H = energy exchange function

$\bar{T}$ = representative temperature of other fields

T = temperature of field

k = thermal conductivity

Λ = internal energy production due to momentum exchange

Φ = viscous dissipation term.

Differential Equation (18) can be approximated at the point i,j by

$$\frac{1}{\delta t}\left[{}^{n+1}(\rho I)_i^j - {}^{n}(\rho I)_i^j\right] + \frac{1}{r_i \delta r}\left[{}^{n}\langle \rho u I r\rangle_{i+e}^{j} - {}^{n}\langle \rho u I r\rangle_{i-e}^{j}\right]$$

$$+ \frac{1}{\delta z}\left[{}^{n}\langle \rho v I\rangle_{i}^{j+e} - {}^{n}\langle \rho v I\rangle_{i}^{j-e}\right] = -\frac{{}^{n}p_i^j}{r_i \delta r}\left[r_{i+e}\,{}^{n}(\alpha u)_{i+e}^{j} - r_{i-e}\,{}^{n}(\alpha u)_{i-e}^{j}\right]$$

$$- \frac{{}^{n}p_i^j}{\delta z}\left[{}^{n}(\alpha v)_i^{j+e} - {}^{n}(\alpha v)_i^{j-e}\right] + {}^{n}Q_i^j + {}^{n}H_i^j\left[{}^{n}\bar{T}_i^j - {}^{n}T_i^j\right]$$

$$+ \frac{1}{r_i(\delta r)^2}\left\{r_{i+e}\,{}^{n}(\alpha k)_{i+e}^{j}\,({}^{n}T_{i+1}^{j} - {}^{n}T_i^j)\right.$$

$$\left. - r_{i-e}\,{}^{n}(\alpha k)_{i-e}^{j}\,({}^{n}T_i^j - {}^{n}T_{i-1}^{j})\right\} + \frac{1}{(\delta z)^2}\left\{{}^{n}(\alpha k)_i^{j+e}\,({}^{n}T_i^{j+1} - {}^{n}T_i^j)\right.$$

$$\left. - {}^{n}(\alpha k)_i^{j-e}\,({}^{n}T_i^j - {}^{n}T_i^{j-1})\right\} + {}^{n}(\mu\Phi)_i^j + {}^{n}\Lambda_i^j \,. \qquad (19)$$

Each term in Equation (19) needs to be expanded in a Taylor Series about some fixed reference, the most convenient in this case being the point i,j at time step n. Using the difference approximations for the various terms as in Chapter III, and proceeding on the same principles as the density transport equation, one can finally arrive at a modified equation for internal energy transport as

$$\frac{\partial \rho I}{\partial t} + \frac{1}{r}\frac{\partial}{\partial r}(\rho u I r) + \frac{\partial}{\partial z}(\rho v I) = -\frac{p}{r}\frac{\partial}{\partial r}(\alpha u r) - p\frac{\partial}{\partial z}(\alpha v) + Q$$

$$+ H(\bar{T}-T) + \mu\Phi + \Lambda + \frac{\partial}{\partial r}(k\alpha)\frac{\partial T}{\partial r} + \frac{\partial}{\partial z}(k\alpha)\frac{\partial T}{\partial z}$$

$$+\left\{\frac{\delta t}{2}(1-\xi_1+\xi_2)\left[(\xi_1-\xi_2-1)\,\rho u^2 + (\xi_1+\xi_2)\frac{\delta r}{2}\left(2u^2\frac{\partial \rho}{\partial r} + \rho u\frac{\partial u}{\partial r}\right)\right]\right.$$

$$\left. + k\alpha\frac{\partial T}{\partial I} + (\xi_1-\xi_2-1)(\delta r)^2\left(\frac{1}{2}u\frac{\partial \rho}{\partial r} + \frac{1}{4}\rho\frac{\partial u}{\partial r}\right) + \frac{\delta r}{2}(\xi_1+\xi_2)\rho u\right\}\frac{\partial^2 I}{\partial r^2}$$

$$+\left\{\frac{\delta t}{2}\left[(\xi_1-\xi_2-1)\,\rho u^2 + (\xi_1+\xi_2)\frac{\delta r}{2}\left(2u^2\frac{\partial \rho}{\partial r} + \rho u\frac{\partial u}{\partial r}\right)\right] + k\alpha\frac{\partial T}{\partial I}\right.$$

$$\left. + (\xi_1-\xi_2-1)(\delta r)^2\left(\frac{1}{2}u\frac{\partial \rho}{\partial r} + \frac{1}{4}\rho\frac{\partial u}{\partial r}\right) + \frac{\delta r}{2}(\xi_1+\xi_2)\rho u\right\}\frac{1}{r}\frac{\partial I}{\partial r}$$

$$+\left\{\frac{\delta t}{2}(1-\xi_3+\xi_4)\left[(\xi_3-\xi_4-1)\,\rho v^2 + (\xi_3+\xi_4)\frac{\delta z}{2}\left(2v^2\frac{\partial \rho}{\partial z} + \rho v\frac{\partial v}{\partial z}\right)\right]\right.$$

$$\left. + k\alpha\frac{\partial T}{\partial I} + (\xi_3-\xi_4-1)(\delta z)^2\left(\frac{1}{2}v\frac{\partial \rho}{\partial z} + \frac{1}{4}\rho\frac{\partial v}{\partial z}\right) + \frac{\delta z}{2}(\xi_3+\xi_4)\rho v\right\}\frac{\partial^2 I}{\partial z^2}, \quad (20)$$

where

$$\xi_1 = \left(\beta_0 \frac{\delta t}{\delta r}\right) {}^{n}u^{j}_{i+e} + \theta_0 \ \text{sign}({}^{n}u^{j}_{i+e})$$

$$\xi_2 = \left(\beta_0 \frac{\delta t}{\delta r}\right) {}^{n}u^{j}_{i-e} + \theta_0 \ \text{sign}({}^{n}u^{j}_{i-e})$$

$$\xi_3 = \left(\beta_0 \frac{\delta t}{\delta z}\right) {}^{n}v^{j+e}_{i} + \theta_0 \ \text{sign}({}^{n}v^{j+e}_{i})$$

$$\xi_4 = \left(\beta_0 \frac{\delta t}{\delta z}\right) {}^{n}v^{j-e}_{i} + \theta_0 \ \text{sign}({}^{n}v^{j-e}_{i}) \ .$$

Equation (20) neglects diffusion terms which have as coefficients the gradients of the thermal conductivity, since these are small compared to the other terms. Stability criteria call for positive coefficients for the diffusion-like terms, i.e. the coefficients of $\frac{\partial^2 I}{\partial r^2}$, $\frac{1}{r}\frac{\partial I}{\partial r}$ and $\frac{\partial^2 I}{\partial z^2}$. Only I diffusion has been considered here, since the density derivatives on the left hand side of Equation (20) can be removed using the density transport equation.

BIBLIOGRAPHY

1. "Reactor Safety Study: An Assessment of Accident Risks in U. S. Commerical Nuclear Power Plants." WASH-1400. U. S. Atomic Energy Commission. U. S. Government Printing Office (1975).

2. H. A. Bethe, "The Necessity of Fission Power." Scientific American, 234 (1), 21-31 (1976).

3. J. F. Jackson, M. G. Stevenson, J. F. Marchaterre, R. H. Sevy, R. Avery and K. O. Ott, "Trends in LMFBR Hypothetical Accident Analysis." Proc. Fast Reactor Safety Meeting, CONF-740401-P3, Beverly Hills, California (April 1974).

4. L. W. Deitrich, E. W. Barts, A. DeVolpi, C. E. Dickerman, J. C. Eberhart, A. K. Fisher, W. F. Murphy and G. S. Stanford, "Fuel Dynamics Experiments Supporting FTR Loss-of-Flow Analysis." Proc. Fast Reactor Safety Meeting, CONF-740401-P2, Beverly Hills, California (April 1974).

5. A. B. Rothman, L. W. Deitrich, R. C. Doerner, A. E. Wright and C. E. Dickerman, "Review of TREAT Experiments in Support of Transient Overpower (TOP) Analysis for Fast Reactor Safety." Proc. Fast Reactor Safety Meeting, CONF-740401-P2, Beverly Hills, California (April 1974).

6. E. T. Weber, O. D. Slagle and C. A. Hinman, "Laboratory Studies on Melting and Gas Release Behavior of Irradiated Oxide Fuel." Proc. Fast Reactor Safety Meeting, CONF-740401-P2, Beverly Hills, California (April 1974).

7. M. G. Stevenson, W. R. Bohl, F. E. Dunn, T. J. Heames, G. Hoppner and L. L. Smith, "Current Status and Experimental Basis for the SAS LMFBR Accident Analysis Code System." Proc. Fast Reactor Safety Meeting, CONF-740401-P2, Beverly Hills, California (April 1974).

8. W. R. Bohl and M. G. Stevenson, "A Fuel Motion Model for LMFBR Unprotected Loss-of-Flow Accident Analysis." Proc. Conf. Mathematical and Computational Techniques for Analysis of Nuclear Systems, CONF-730414-P1, Ann Arbor, Michigan (April 1973).

9. F. H. Harlow and A. A. Amsden, "Numerical Calculation of Multiphase Fluid Flow," Journal of Computational Physics, 17 (1), 19-52 (1975).

BIBLIOGRAPHY (continued)

10. F. H. Harlow and A. A. Amsden, "Flow of Interpenetrating Material Phases." Journal of Computational Physics, 18, 440-464 (1975).

11. F. H. Harlow and A. A. Amsden, "A Numerical Fluid Dynamics Calculation Method for All Flow Speeds." Journal of Computational Physics, 8 (2), 197-213 (1971).

12. R. C. Mecredy and L. J. Hamilton, "The Effects of Nonequilibrium Heat, Mass and Momentum Transfer on Two-Phase Sound Speed." Int. Journal of Heat and Mass Transfer, 15, 61-72 (1972).

13. R. B. Bird, W. E. Stewart and E. M. Lightfoot, Transport Phenomena. John Wiley and Sons, Incorporated, New York (1960).

14. S. L. Soo, Fluid Dynamics of Multiphase Systems. Blaisdel, Waltham, Mass. (1967).

15. W. E. Ranz and W. R. Marshall, Jr., "Evaporation from Drops." Chemical Engineering Progress, 48, 141-146, 173-180 (1952).

16. J. E. Welch, F. H. Harlow, J. P. Shannon and B. J. Daly, "The MAC Method -- A Computing Technique for Solving Viscous, Incompressible, Transient Fluid-Flow Problems Involving Free Surfaces." Los Alamos Scientific Laboratory Report LA-3425 (1965).

17. C. W. Hirt, "Heuristic Stability Theory for Finite-Difference Equations." Journal of Computational Physics, 2, 339-355 (1968).

18. R. F. Warming and B. J. Hyett, "The Modified Equation Approach to the Stability and Accuracy Analysis of Finite-Difference Methods." Journal of Computational Physics, 14, 159-179 (1974).

19. G. G. O'Brien, M. A. Hyman and S. Kaplan, "A Study of the Numerical Solution of Partial Differential Equations." Journal of Mathematics and Physics, 29, 223 (1950).

20. Anthony A. Amsden and Francis H. Harlow, "KACHINA - An Eulerian Computer Program for Multifield Fluid Flows." LA-5680, Los Alamos, New Mexico (1974).

21. D. Lal and R. W. Carlson, "Two Dimensional Fuel Motion Analysis During Loss-of-Flow Accidents in a Liquid Metal Cooled Fast Breeder Reactor." Quarterly Progress Report submitted to the Energy Research and Development Administration. ORO-4958-5 (October 1976).

BIBLIOGRAPHY (concluded)

22. D. Lal and R. W. Carlson, "Two Dimensional Fuel Motion Analysis During Loss-of-Flow Accidents in a Liquid Metal Cooled Fast Breeder Reactor." Quarterly Progress Report submitted to the Energy Research and Development Administration. ORO-4958-7 (October 1977).

23. P. Szymanski, "Sur L'ecoulement Non Permanent Du Fluide Visqueux Dans Le Tuyau." Proceedings of the Third International Congress of Applied Mechanics, 1, 249-254, Stockholm (1930).

24. M. C. Jischke and R. T. Doty, "Linearized Buoyant Motion in a Closed Container." Journal of Fluid Mechanics, 71, 729-754 (1975).

25. D. Lal and R. W. Carlson, "Two Dimensional Fuel Motion Analysis During Loss-of-Flow Accidents in a Liquid Metal Cooled Fast Breeder Reactor." Quarterly Progress Report submitted to the Energy Research and Development Administration. ORO-4958-6 (January 1977).

26. W. C. Rivard, J. R. Travis, and M. D. Torrey, "Numerical Calculation of Two Phase Flow in a Shock Tube." Specialists Meeting on Transient Two Phase Flow, Toronto, Ontario (August 1976).

27. P. S. Roache, Computational Fluid Dynamics. Hermosa Publishers, New Mexico (1972).

28. A. R. Gourlay and J. L. Morris, "Hopscotch Difference Methods for Nonlinear Hyperbolic Systems." IBM Journal of Research and Development, 16, 349-353 (1972).

VITA

Dhunjishaw Lal was born in Bombay, India. He received his schooling in Bangalore, and graduated at the top of his class in the Indian School Certificate Examination conducted by the local examinations syndicate of the University of Cambridge.

In 1972 Mr. Lal received the degree of Bachelor of Science in Chemical Engineering from the Massachusetts Institute of Technology. He completed his Master of Science Degree in Nuclear Engineering at Georgia Tech in 1974, and began work for a doctoral degree. Mr. Lal was a graduate research assistant during his program of study at Georgia Tech, working on internal and sponsored research projects. His research on fuel motion in loss-of-flow accidents was funded by the Energy Research and Development Administration.

Mr. Lal is a member of the American Nuclear Society, and the American Society of Mechanical Engineers.